Studying the degradation of magnetosomes in tumour cells by magnetometry and XANES spectroscopy

Alicia Gascón Gubieda*, Lucía Gandarias*, Alicia Muela, Ana Abad, Maria Luisa Fernández-Gubieda, Ana García Prieto

Universidad del País Vasco / Euskal Herriko Unibertsitatea

Abstract

Magnetosomes are magnetic nanoparticles biosynthesistised by **magnetotactic bacteria**, such as *Masgnetospirillum gryphiswaldense* (MSR-1) (**Figure 1**), which synthesises magnetosomes of 40 nm in diameter and made of **magnetite (Fe3O4)**. Due to their biocompatibility and magnetic properties, they are currently being studied for several biomedical applications, such as magnetic hyperthermia and magnetic resonance imaging (MRI). However, very little is known about the fate of magnetosomes once they are inside cells, which is of high relevance if they are to be approved for clinical use. Our research group has combined the use of **3D cancer tumour models called spheroids** and 2D cell cultures with X-ray absorption near edge structure (**XANES**) and **magnetometry**, to describe how magnetosomes are degraded in cancerous cells.

Figure 1: Magnetotactic bacteria of the MSR-1 species with a magnetosome chain (red arrow) inside it.

Spheroids as tumour models

2D cell culture vs	3D spheroids
-Cells have the same access to nutrients and oxygen	-The interior of the spheroid has lower access to nutrients and oxygen (as in tumours)
-Cells are equally attached to a surface, but not strongly attached to each other	-Cells are attached to each other and generate an extracellular matrix (as in our organism)
-Cells do not generate an extracellular matrix	-Cells in the interior of the spheroid have lower division rates and often form a necrotic centre (as in tumours)
-Cells have the same cell division rate	-Attachment level and different rates of access to nutrients affect gene expression
-Cells express the same genes	

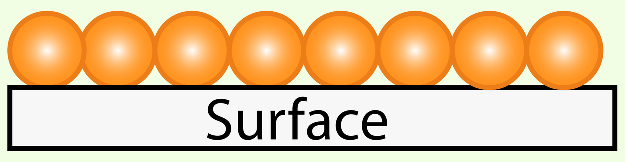

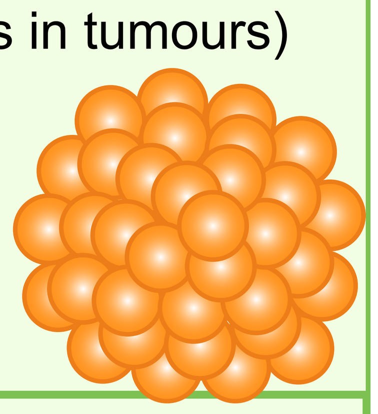

Spheroids share many characteristics with tumours

Generating spheroids

Steps for spheroid formation

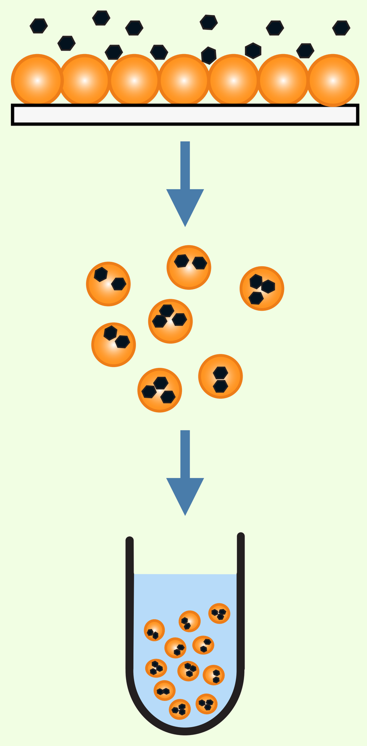

1. Incubate cells with magnetosomes for up to 2 hours
2. Collect cells in a suspension
3. Place cells in a 96-well low attachment plate with collagen in the medium, to stimulate attachment.

Cells and spheroids with magnetosomes

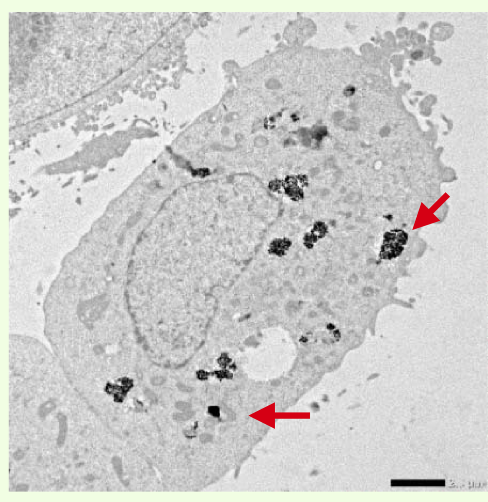

Figure 2: Human lung carcinoma cell (A549) with magnetosomes (red arrows point to some).

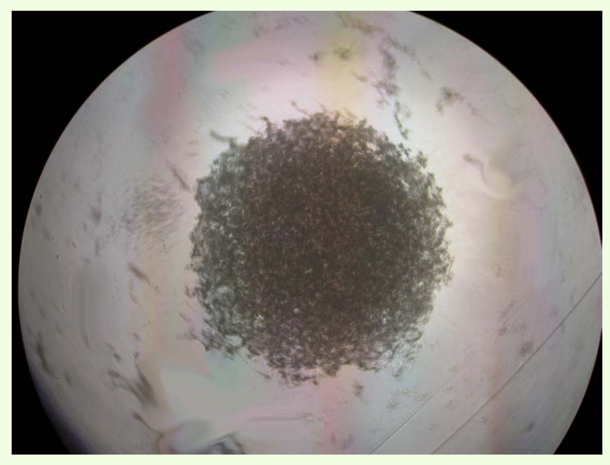

Figure 3: Spheroid of 80.000 human lung carcinoma cells (A549) with magnetosomes (1 mm in diameter).

Magnetometry

We have employed a superconducting quantum interference device (SQUID) to measure changes in the magnetic response of the magnetosomes in the spheroids, from the first day of internalisation, up to 18 days of internalisation. We have observed a decrease in the saturation magnetic moment, suggesting a degradation of the magnetite in the magnetosomes.

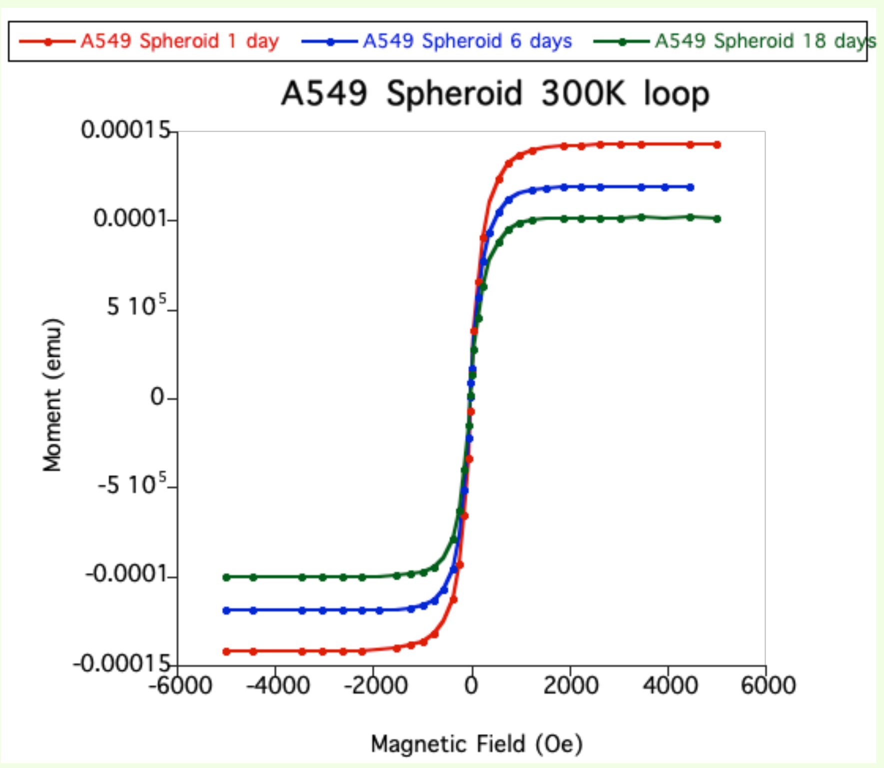

Figure 4: Magnetosome degradation measured by magnetometry (SQUID) in spheroids of lung carcinoma cells (A549) after 1 day, 6 days, and 18 days of magnetosomes internalisation. Measured at 300 K. Each loop represents one single spheroid.

XANES

Using X-ray absorption near edge structure (XANES, in CLAESS, ALBA; and BM23, ESRF) we have observed that cells can degrade magnetosomes, by oxidising magnetite into maghemite.

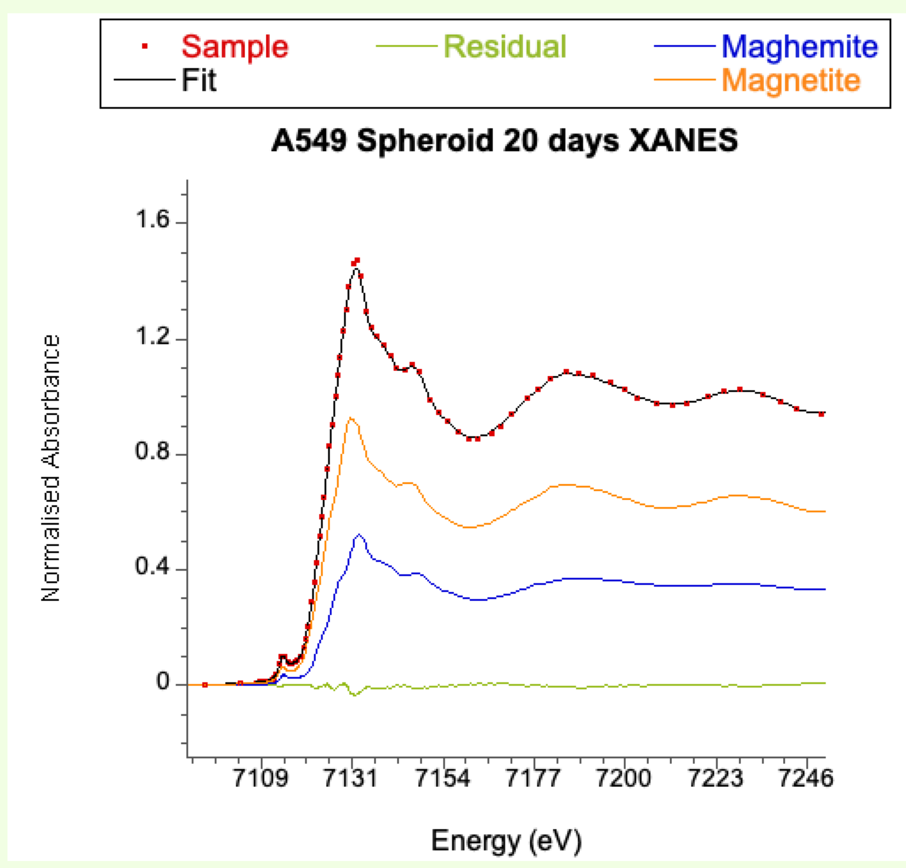

Figure 5: Changes in magnetosome composition after 13 days of internalisation in A549 cells, as measured by Fe K-edge XANES spectroscopy, fitted to the linear combination of magnetite (orange), and maghemite (dark blue).

Funding

MINISTERIO DE CIENCIA E INNOVACIÓN
AGENCIA ESTATAL DE INVESTIGACIÓN

"Personalización de la bacteria magnetotáctica para explorar su idoneidad para terapias específicas contra el cáncer" Proyecto PID2020-115704RB-C31 financiado por MCIN/ AEI /10.13039/501100011033

Superconductivity assisted change of the perpendicular magnetic anisotropy in V/MgO/Fe junctions

César González-Ruano[1]*, Diego Caso[1], Coriolan Tiusan[2,3], Michel Hehn[3], Farkhad G. Aliev[1].

[1]Departamento de Física de la Materia Condensada C-III, INC and IFIMAC, Universidad Autónoma de Madrid, Madrid, Spain
[2]Department of Physics and Chemistry, Center of Superconductivity Spintronics and Surface Science C4S, Technical University of Cluj-Napoca, Cluj-Napoca, Romania
[3]Institut Jean Lamour, Nancy Université, Vandoeuvre-les-Nancy Cedex, France

*cesar.gonzalez-ruano@uam.es
http://webs.fmc.uam.es/magnetrans.group/index.html

Abstract

Controlling the perpendicular magnetic anisotropy (PMA) in thin films has received considerable attention in recent years due to its technological importance. PMA based devices usually involve heavy-metal (oxide)/ferromagnetic-metal bilayers, where, thanks to interfacial spin-orbit coupling (SOC), the in-plane (IP) stability of the magnetization is broken. We have studied epitaxial V/MgO/Fe/MgO/Fe/Co junctions, where the soft Fe layer of the Fe/MgO/Fe/Co spin-valve part has competing in-plane and out-of-plane (OOP) magnetic anisotropies, and SOC is present at the V/MgO/Fe interface. In previous studies, we first observed a thousand-fold increase in tunneling anisotropic magnetoresistance below the critical temperature (T_C) of vanadium, supporting triplet Cooper pair formation [1]. Then we showed that under an in-plane rotation of an external magnetic field, new easy axes for the magnetization appear below T_C, directed in the above-T_C hard axes 45 degrees from the easy ones. We modelled our results in terms of the free energy of the system, which varies with the relative angle between the exchange field of the ferromagnet and the spin-orbit field by generating triplet Cooper pairs [2]. Now we demonstrate that the effective PMA is also enhanced below T_C. This produces a partial OOP magnetization reorientation without any applied field, and a reduction of the field required to induce a complete OOP transition (H_{OOP}). Our results suggest that the degree of effective PMA could be controlled by the junction lateral size in the presence of superconductivity and by an applied electric field [3]. Our experimental findings, supported by theoretical modelling and numerical simulations of the ferromagnet-superconductor interaction, open pathways to active control of magnetic anisotropies in the emerging dissipation-free superconducting spin electronics.

Sample description and experimental set-up

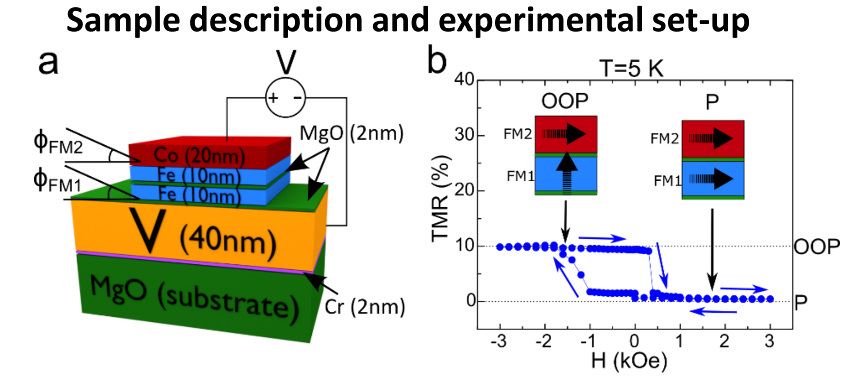

a Sketch of the junctions under study. Fe(10 nm) (FM1) is the soft ferromagnet undergoing magnetization reorientations, while Fe(10 nm)Co(20 nm) (FM2) is the hard layer. ϕ_{FM1} and ϕ_{FM2} are the angles of each FM layer magnetization with respect to the plane of the layers. Since the FM2 layer is normally fixed to act as a sensor, ϕ_{FM2} is assumed to be very close to 0. **b** depicts a typical TMR experiment where the field is applied in the OOP direction, showing the field-induced transition into the nonvolatile OOP state. The insets sketch the magnetization of the two FM layers in the P and OOP configurations of the spin valve stack.

The MTJs are fully epitaxial in order to have a well-defined magnetocrystalline anisotropy. They were grown by molecular beam epitaxy (MBE) in on (001) MgO substrates in the Institut Jean Lamour (Nancy, France). The measurements are performed inside a He^3 cryostat (minimum temperature is 0.3 K). The magnetic field is varied using a 3D vector magnet with H_{max} = 3.5 T.

Experimental results and discussion

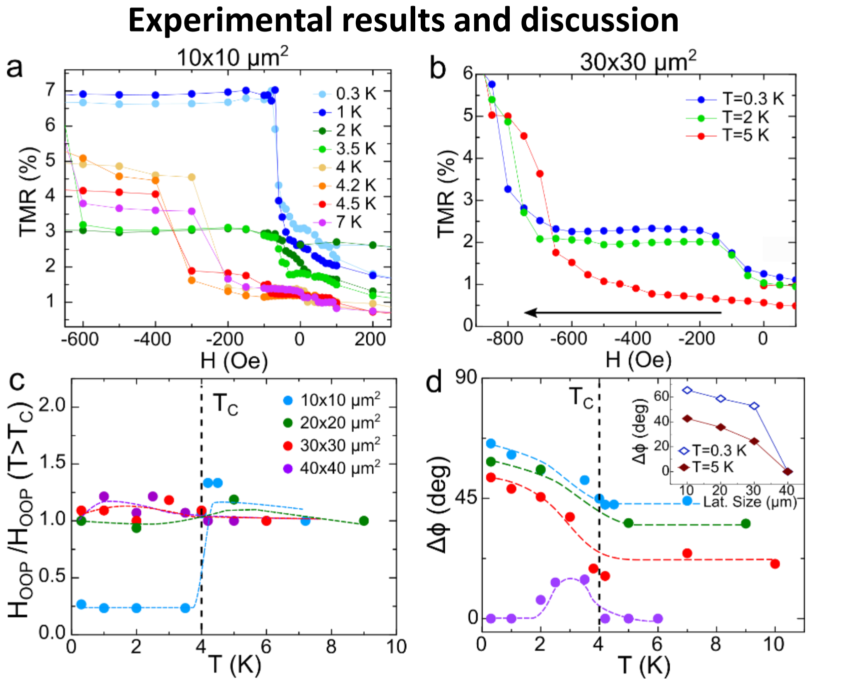

a Field induced OOP magnetization transition in a 10×10 µm² junction, from above to below T_C. A strong reduction of H_{OOP} takes place below T_C. **b** Shows a similar experiment in a 30×30 µm² junction, in this case with an incomplete OOP reorientation due to the higher in-plane shape anisotropy in larger junctions. **c** Temperature dependence of the normalized H_{OOP} field for junctions with four different lateral sizes. **d** Temperature dependence of the misalignment angle between the two FM layers ($\Delta\phi=\phi_{FM1}-\phi_{FM2}$) at zero field for the four different sized samples (same color legend as in **c**).

The decrease of $\Delta\phi$ above T_C with increasing lateral size points towards an equilibrium angle already existing in the normal state. When superconductivity develops below T_C, an additional magnetization reorientation is observed in all except the bigger samples. This behavior is attributed to the variation of the relative intensities of the competing surface (OOP) and shape (IP) anisotropies depending on the lateral size, which favors an OOP magnetization for the smallest junctions and an IP one for the biggest ones.

Microscopic model

In heterostructures consisting of superconducting and magnetic layers, the superconducting condensate is weakened as Cooper pairs leak into the magnetic regions. This leakage is more eficient when the spin-singlets are transformed into equal-spin triplet pairs polarized along the magnetization axis. In our system, Rashba SOC at the SC/FM interface allows for a generation of equal-spin triplets that depends on the orientation of the magnetization with respect to the interface. The free energy is calculated from a tight-binding Bogoliubov–de Gennes (BdG) Hamiltonian.

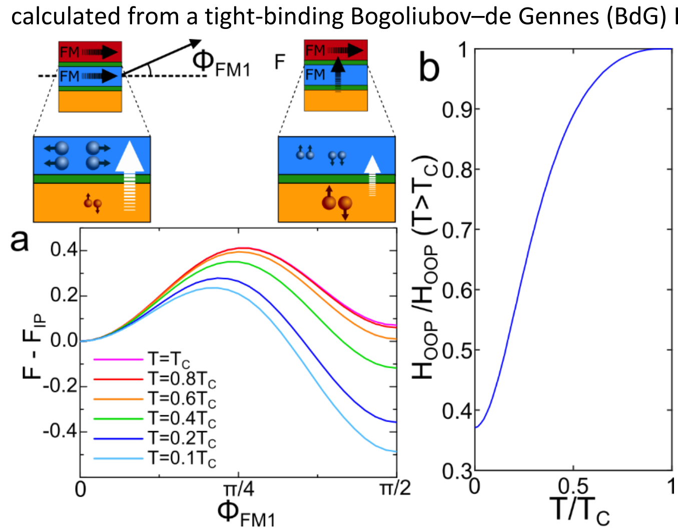

a When the magnetization of the soft ferromagnet is rotated from a parallel to an OOP alignment with respect to the hard ferromagnet, the SOC assisted conversion (white arrows) of singlet Cooper pairs (orange) into equal-spin triplets (blue) is at its minimum. The superconducting condensate is therefore stronger when the magnetization is OOP, decreasing the OOP free energy as the temperature drops below T_C. **b** The deepening of the OOP energy minimum causes a decrease in H_{OOP}, as observed in the experimental measurements.

Conclusions

Our experiments point towards the superconductivity induced modification of the perpendicular magnetic anisotropy. For the smallest junctions, H_{OOP} drops by an order of magnitude in the superconducting state. In all but the largest junctions, an increase in the OOP misalignment angle between the FM layers is observed below T_C without applied field, suggesting that superconductivity could affect the competition between the IP and OOP anisotropies. The results are consistent with the theoretical prediction of a free energy minimum for an OOP magnetization in SC/SOC/FM hybrids with competing (IP vs OOP) anisotropies below T_C. The interaction between superconducting vortices and magnetic stray fields or inhomogeneities has been accounted for by performing micromagnetic simulations, and could explain a weak increase of H_{OOP} below T_C in the largest junctions. Our results open a route to active manipulation of perpendicular magnetic anisotropy in the expanding field of dissipation-free superconducting electronics involving spin or spin polarized supercurrents.

Acknowledgements The work has been supported by Spanish Ministerio de Ciencia (RTI2018-095303-B-C55) and Consejería de Educación e Investigación de la Comunidad de Madrid (NANOMAGCOST-CM P2018/ NMT-4321). We thank Igor Zutic, Jaroslav Fabian, Alexandre Buzdin, Jacob Linder, Lina Johnsen and Niladri Banerjee for valuable discussions.

References

[1] I. Martínez et al; Physical Review Applied, **13**, 014030 (2020).
[2] C. González-Ruano et al; Physical Review B, **102**, 020405(R) (2020).
[3] C. González-Ruano et al; Scientific Reports, **11**, 19041 (2021).

Excitation and propagation of edge spin waves in ferromagnetic triangles

Diego Caso[1], and Farkhad G. Aliev[1]

[1]Departamento de Física de la Materia Condensada C-III, IFIMAC and INC, Universidad Autónoma de Madrid 28049, Madrid, Spain

Spin waves, being usually reflected by domain walls, could also be channeled along them. Recent studies allowed observation of spin waves along domain walls in rectangular, circular [1] and triangular dots in the ground or metastable states. Triangular dots could also present edge pinned inhomogeneous magnetic states, depending on the direction of the external magnetic field. These edge domain walls yield the interesting, and potentially applicable to real devices property of broadband spin wave confinement to the edges of the structure [2,3], with capabilities to be redirected at angles exceeding 100 degrees. It has been previously shown how these waves could be generalized for arbitrary shapes and propose few devices (such as edge spin wave interferometers, controllers or splitters) where edge spin waves could be implemented [3].

http://webs.fmc.uam.es/magnetrans.group/

Here we present simulation results obtained on the YIG based triangles where edge spin waves (ESWs) were propagated over the corner in 2 micron sized triangles with a fixed thickness of 85 nm. The superior vertex angle, studied in the range of 40-75 degrees, has been optimized in order to obtain a higher transmission coefficient over the vertex of the edge spin waves. Our simulations showed resonance increase of the ESW transmission for the angles close to 50 degrees. A slight excess of the transmission above one could be due to positive interference with SWs propagating directly from the microwave field source to the opposite edge. A generated upper vertex domain wall's topology seems to be key in understanding the efficiency of the ESW propagation. We have also investigated the ESW transmission along the out of plane profile of the triangle and optimized the applied bias field to maximize the effectiveness of the exchange energy channels that behave as a propagation route for the spin wave.

Sample's description

We are using **YIG triangles** due to their **low damping**, which enables long distance propagation of the spin waves (SWs), becoming a proof of concept for **larger devices**.

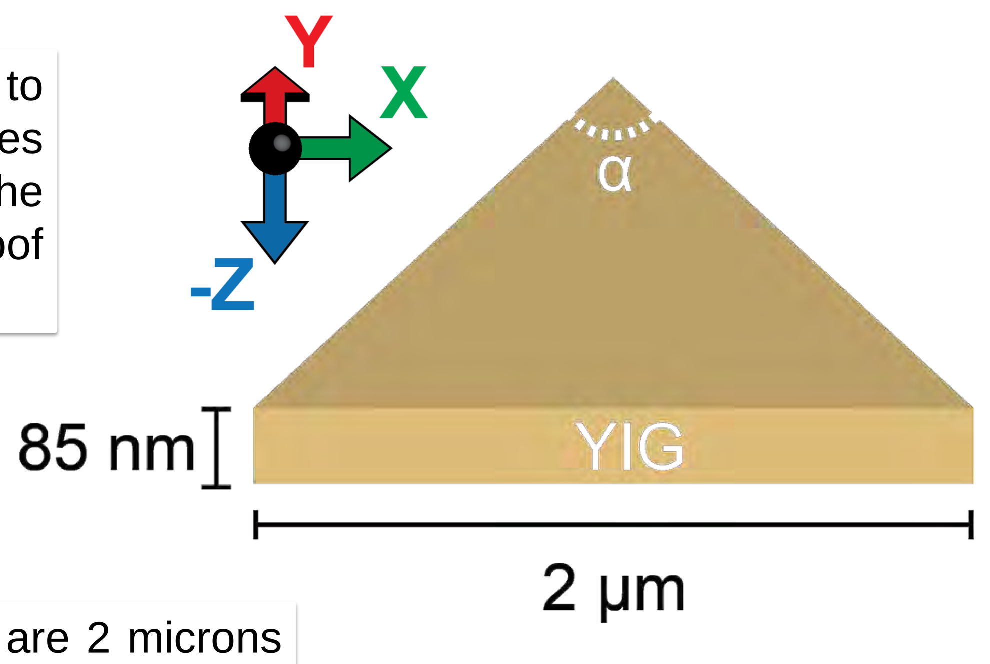

Typical dimensions of our triangles are 2 microns in its base and a fixed thickness of 85 nm.

Experimental set-up

1. To get the ground state magnetization distribution we apply bias field and relax the system.

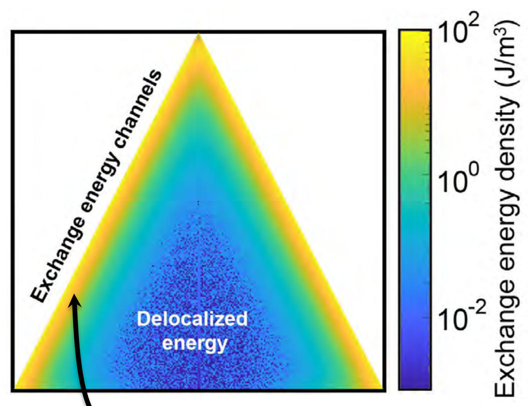

Excess of exchange energy on the edges with the applied field

The excess of exchange energy generates a easy pathway for the spin waves to propagate through.

2. A Sinc pulse is used to perturb the system. This is then followed by an analysis (FT) of the OOP magnetization component response to reconstruct the edge-related modes.

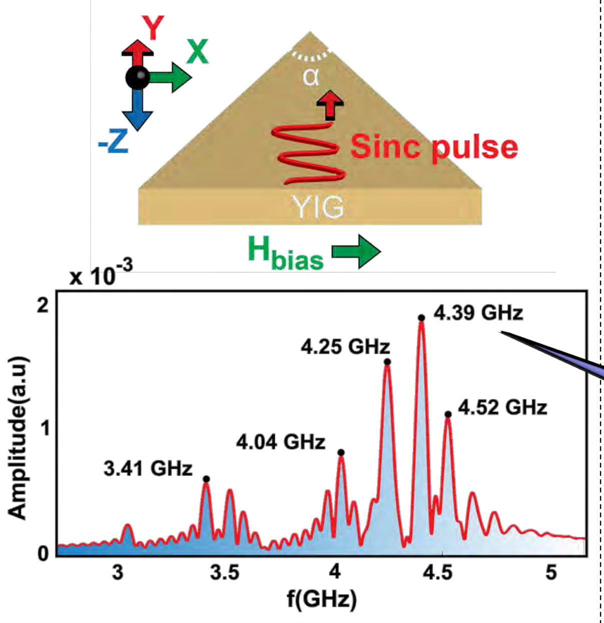

3. Microwave local excitation at the corner of the triangle is used to propagate edge spin waves (ESWs).

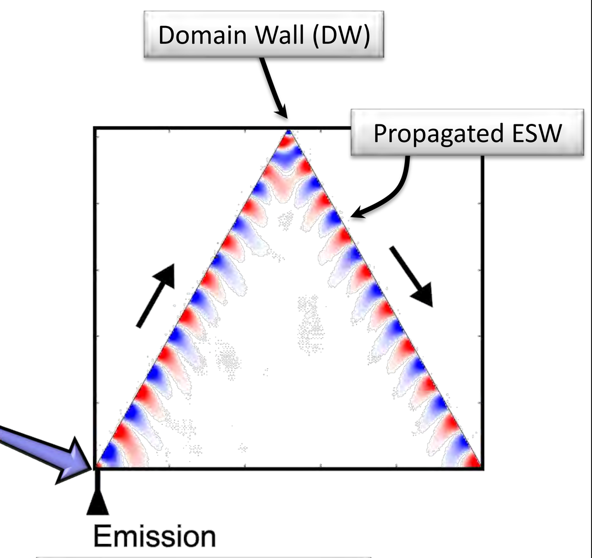

Optimization of the bias field

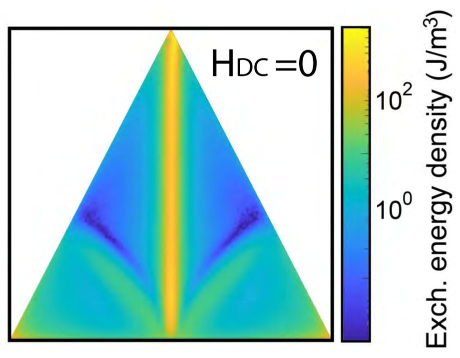

When there is no static field applied the system relaxes into a distribution with an accumulation of exch. energy in the middle of the triangle

Static field is applied parallel to the base of the triangle

The field distribution accumulates exchange energy on the sides, which could be used as channels to propagate the SWs.

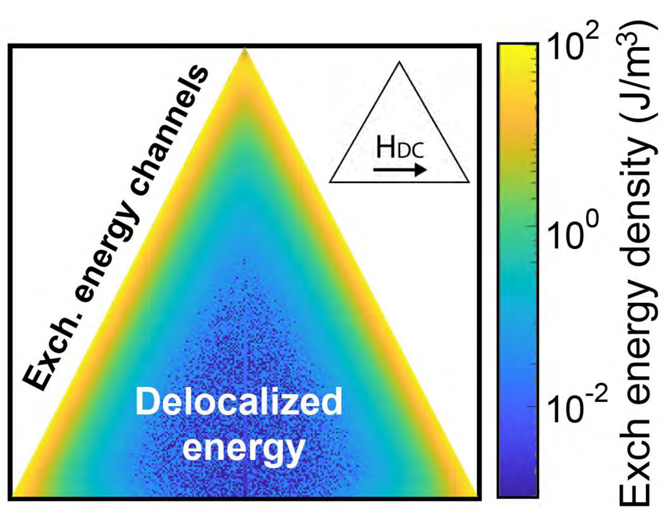

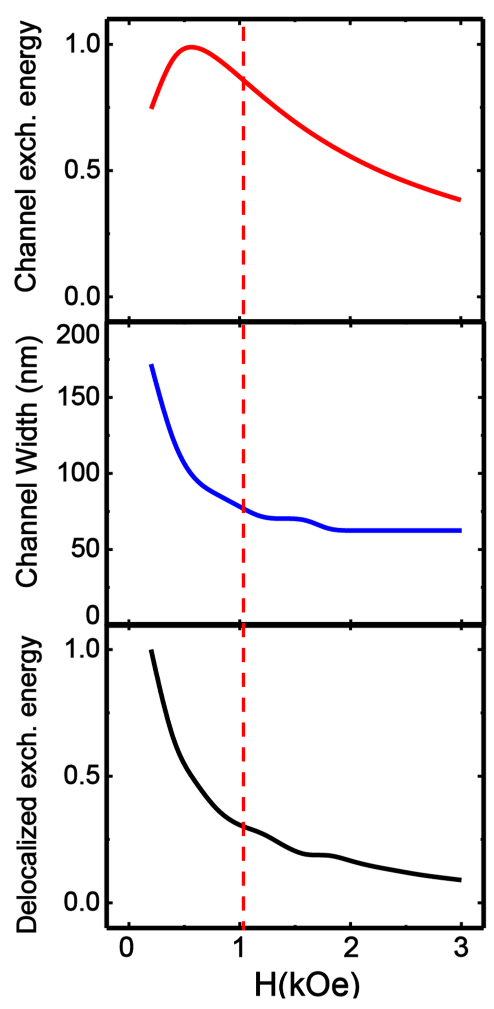

The applied field should have a balance between providing high exchange energy to the channels and low channel width and delocalized exchange energy. Fields close to **1 kOe** meet all three conditions.

Transmission of the ESW

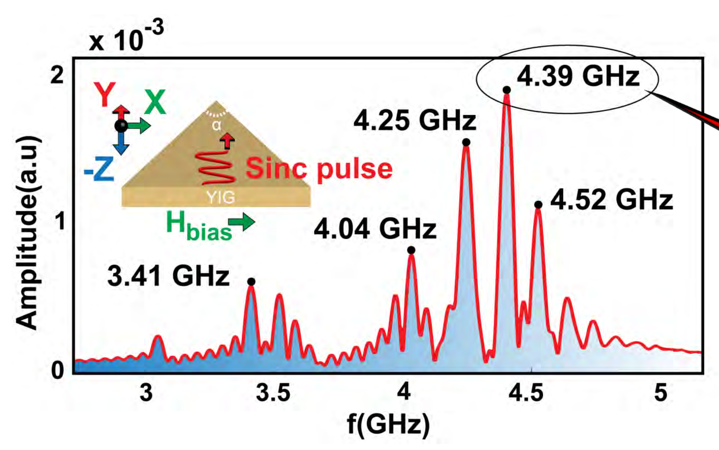

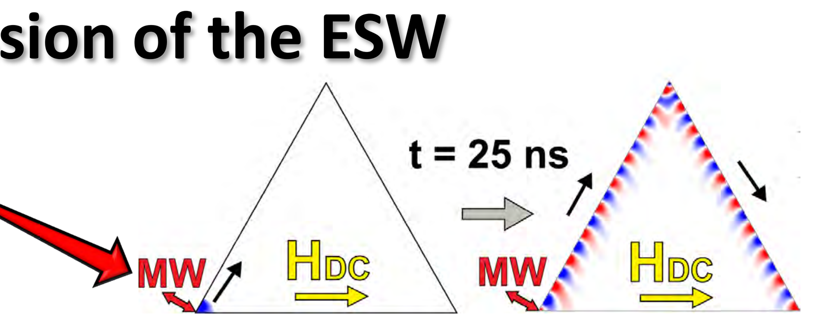

Bulk modes are used to excite the ESWs locally in the left corner of the triangle.

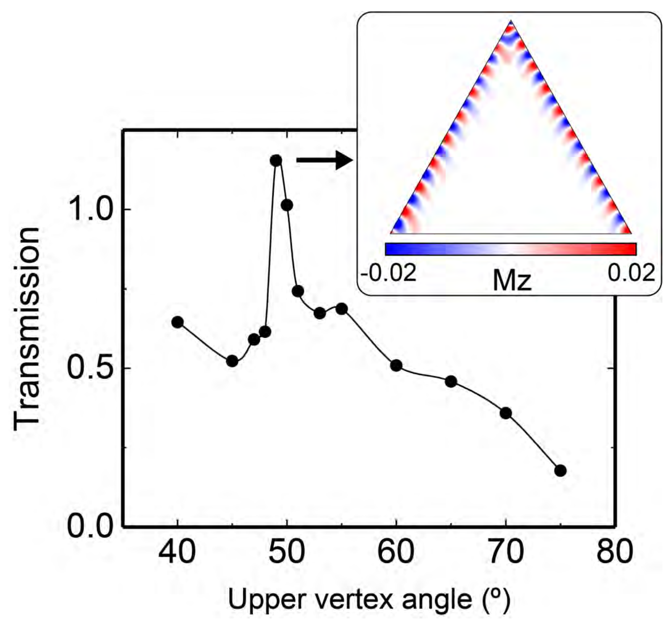

49-50 degrees is presented as a **high transmission range**. Even surpassing the T = 1 limit for 49 degrees.

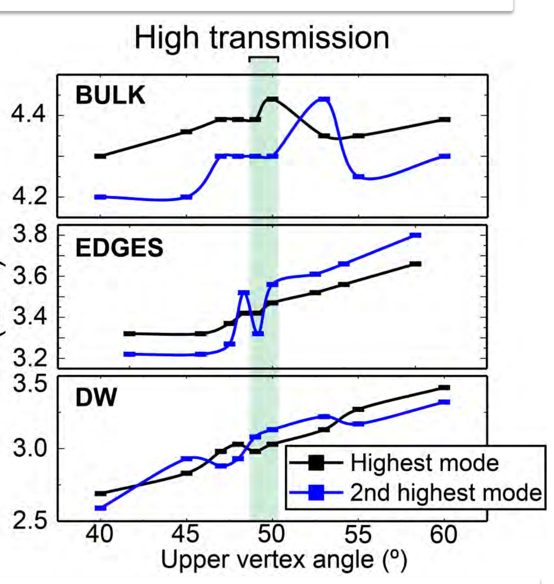

Some modes are localized in regions of the triangle. For the principal modes: **f(BULK) > f(EDGES) > f(DW)**

Effects at the DW

DW topology

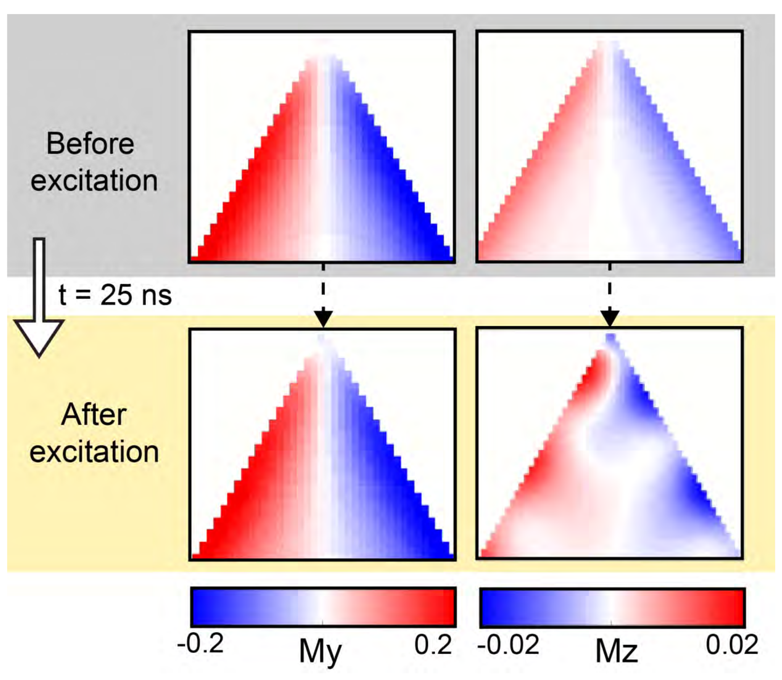

The low out-of-plane magnetization component characterizes the DW as a **Néel-type DW**

DW asymmetry

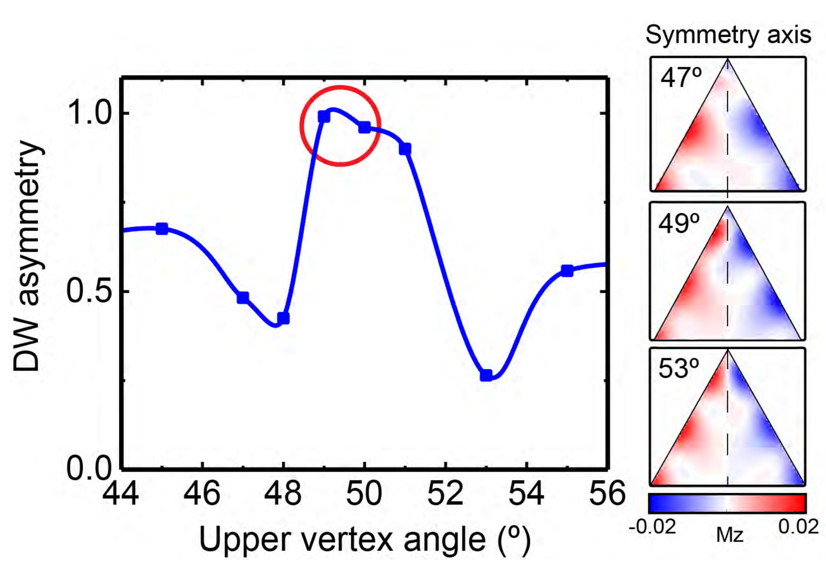

The angles of more assymetry match those of higher transmission, indicating that there is a **direct correlation between the topology of the DW and the efficiency of the ESW propagation**.

Phase shift

$$\Delta\phi = \phi_{left} - \phi_{right}$$

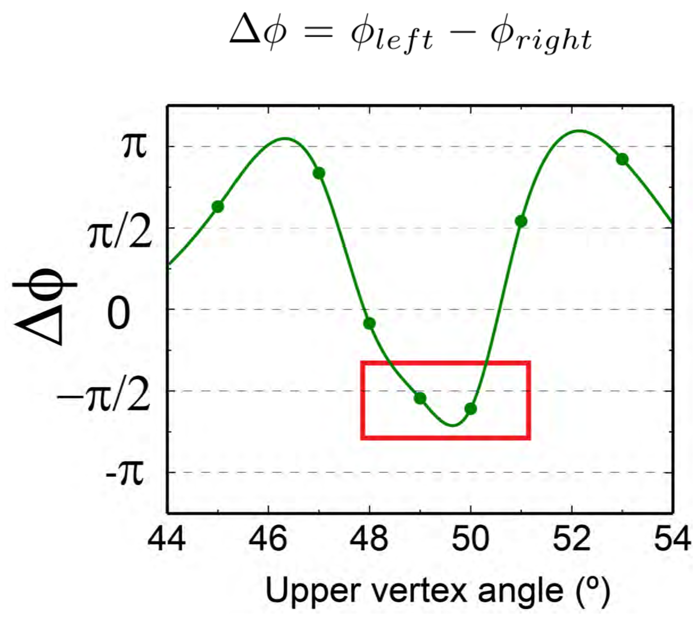

For the high transmission range (49-50 degrees) the two SWs are shifted almost exactly **π/2**.

This π/2 phase shift indicates the possibility of a **coupled resonant system.**

Overlapping of localized modes

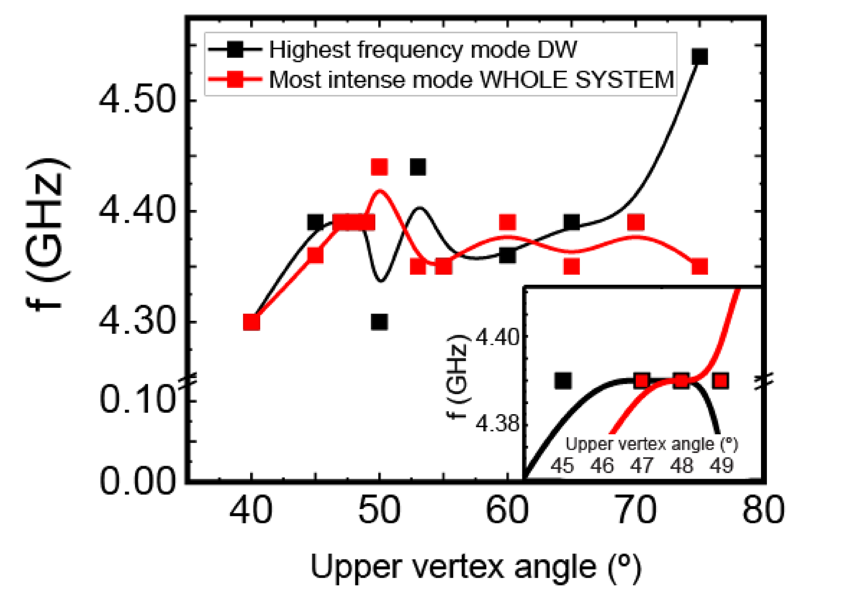

Indeed, in the high transmission range, there are some modes of the DW that overlap with the principal bulk modes, which means that they couple at the DW, possibly **improving the transmission**.

References

[1] F. G. Aliev, et al., Phys. Rev. B **84**, 144406 (2011).

[2] A. Lara, V. Metlushko, F. G. Aliev, J. Appl. Phys. **114**, 213905 (2013).

[3] A. Lara, J. Robledo, K.Y. Guslienko, F. G. Aliev, Scientific Reports, **7**, 5597 (2017).

The work has been supported by Spanish Ministerio de Ciencia (RTI2018-095303-B-C55) and Consejería de Educación e Investigación de la Comunidad de Madrid (NANOMAGCOST-CM P2018/ NMT-4321). DC acknowledges contract ref. S2018/NMT-4321 from CM.

instituto IMDEA nanociencia
EXCELENCIA SEVERO OCHOA
nanoscience and nanotechnology: small is different

Homogenisation of tumour heating in magnetic hyperthermia through exploitation of magnetisation dynamics of interacting particles

Jonathan Leliaert[1], Javier Ortega-Julià[2], and Daniel Ortega[2,3,4]

[1] Department of Solid State Sciences, Ghent University, Ghent, Belgium; [2] IMDEA Nanoscience, Madrid, Spain; [3] Condensed Matter Physics department, University of Cádiz (Cádiz) Spain; [4] INiBICA, Cádiz, Spain.
E-mail: javier.ortega@imdea.org

In this work we propose an equation that can be used to resolve the individual heat dissipation of interacting nanoparticles at nonzero temperature. The presented micromagnetic approach is scalable and can be implemented into more complex settings.

Derivation and validation of a new equation

In the micromagnetic framework, magnetisation dynamics are described by the Landau-Lifshitz-Gilbert (LLG) equation. From this framework, and building on a previous theoretical work[1], we present an equation that estimates the heat dissipation of individual interacting particles that perform field induced and thermal switching at non-zero temperature:

$$\frac{d\mathcal{E}}{dt} = \frac{\alpha\gamma M_s}{1+\alpha^2}\left(\mathbf{m}\times\mathbf{B}_{\mathrm{eff}}\right)^2 - M_s\mathbf{B}_{\mathrm{th}}\cdot\frac{d\mathbf{m}}{dt} \qquad \text{Eq. 1}$$

We integrated the LLG equation for different systems using the simulation tool Vinamax[2] to validate Eq. 1

Results

A system of two particles with 11 nm radius and separated 34 nm was simulated. Other parameters: M_s=800 kA/m, α=0,01 and anisotropies K_1=20 kJ/m^3 and K_2=75 kJ/ m^3. Simulations were performed at 300K with and without interparticle interactions. Fig. 1 shows that each particle starts heating as soon as the field is big enough to overcome the anisotropy barrier. Also, in the presence of interactions, both particles tend to homogenize their released heat at larger fields. Fig. 2 gives insight into this effect by showing the dissipated heat for the interacting particles as function of time. We can see that the low anisotropy particle makes a second step after switching, when the second particle switches. This effect can be explained by non-reversible intra-well dynamics induced by the first particle in the second, causing it to dissipate heat.

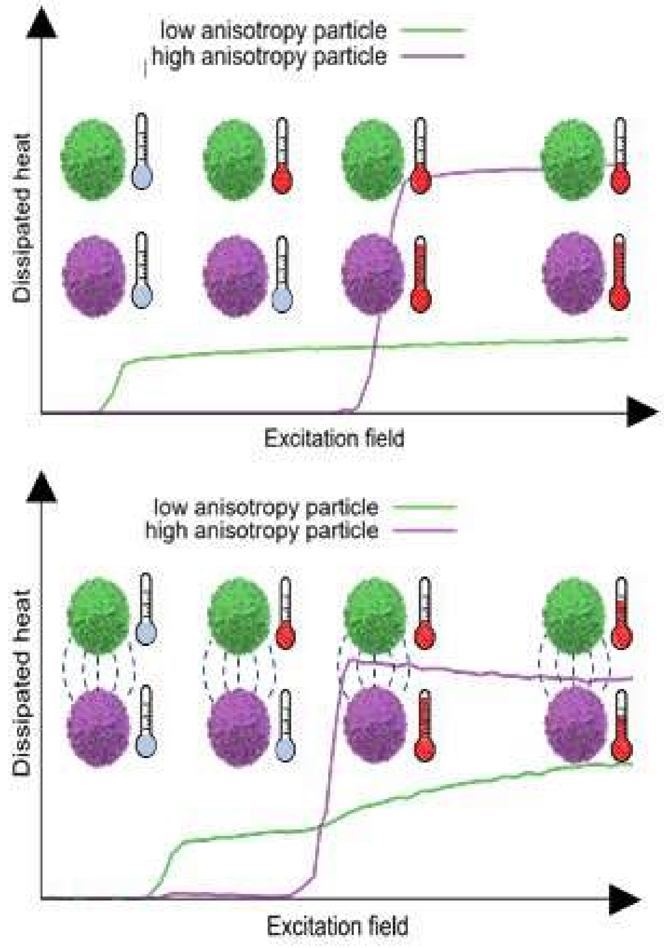

Fig. 1 Non-interacting (top) and interacting (bottom) particles.

Fig. 2 Evolution of dissipated heat as a function of time for two interacting particles. Highlighted, the second jump in the low anisotropy particle caused by its interaction with the high anisotropy one.

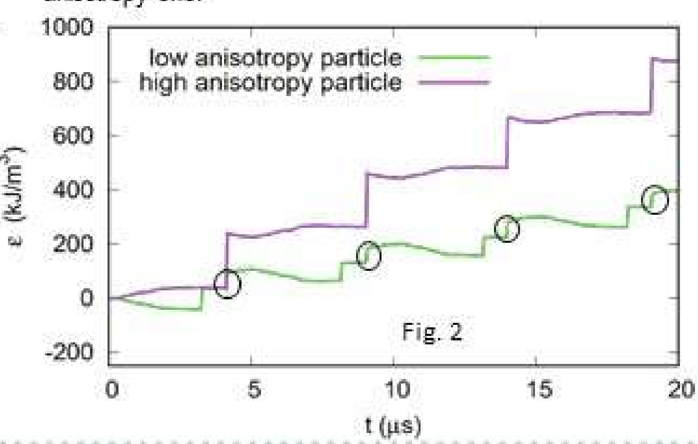

Conclusions

After assessing the equation for different model systems, we have found that the proportion of heat dissipated in each individual particle tends to become more uniformly distributed for larger fields. Furthermore, this method is easy to implement and it cost almost no extra computation time.

[1]C. Muñoz Menendez, et al. *Phys. Rev. B*, 2020, 102, 214412;
[2]J. Leliaert, et al. Med. Biol. Eng. Comput., 2015, 53, 309–317.

Structural and Magnetic Characterization of Nanostructured NiO prepared by Mechanical Milling

José Luis Garrido Álvarez, M.P. Fernández García, C. Echevarría-Bonet, D. Martínez Blanco, P. Gorria, J.A. Blanco

Departamento de Física, Universidad de Oviedo, 33007, Oviedo, Spain

INTRODUCTION

- ✓ Bulk NiO is an antiferromagnetic material [1] and its Néel temperature (523K) is the highest between all antiferromagnetic metallic monoxides.
- ✓ In 1956, Richardson and Milligan [2] discovered that the Néel temperature of NiO decreases as its size is reduced.
- ✓ Recently, Rinaldi-Montes *et al.* [3] studied the effects of the reduction size on the magnetic properties of NiO nanoparticles, with cubic crystallographic structure (Fm-3m). They observed that the antiferromagnetism in NiO nanoparticles can be broken under a critical diameter.

OBJECTIVES

- ✓ Synthesis of 6 NiO samples with different milling times (particle sizes).
- ✓ Investigate the relationship between milling time and the crystalline structure, microstructure and magnetic properties of our samples.

EXPERIMENTAL TECHNIQUES

Mechanical Milling

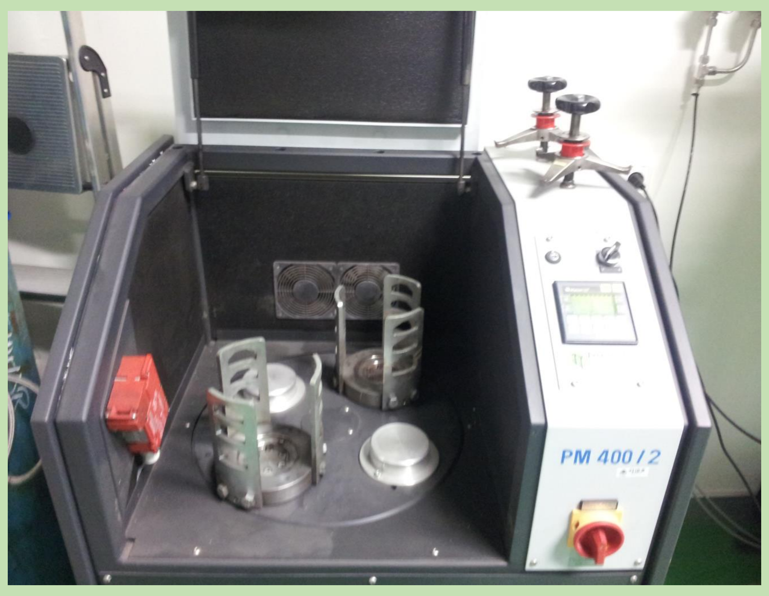

Our milling times were: 0 h (NiO0), 1 h (NiO2), 3 h (NiO4), 10 h (NiO6), 50 h (NiO8) and 100 h (NiO9)

X-Ray Diffraction

The diffraction patterns were measured using XRD with λ_{Cu} in the 2θ range 10°-140°.

Transmission Electron Microscopy

Vibrating-Sample Magnetometry

The hysteresis curves were measured at room temperature up to 20 KOe.

X-Ray Diffraction

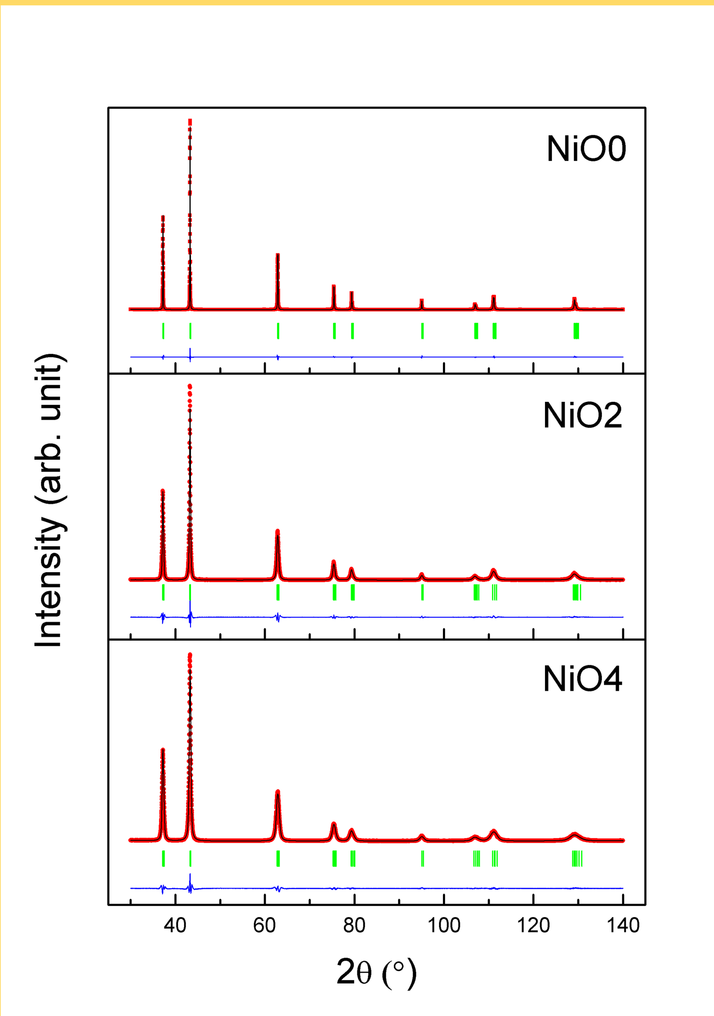

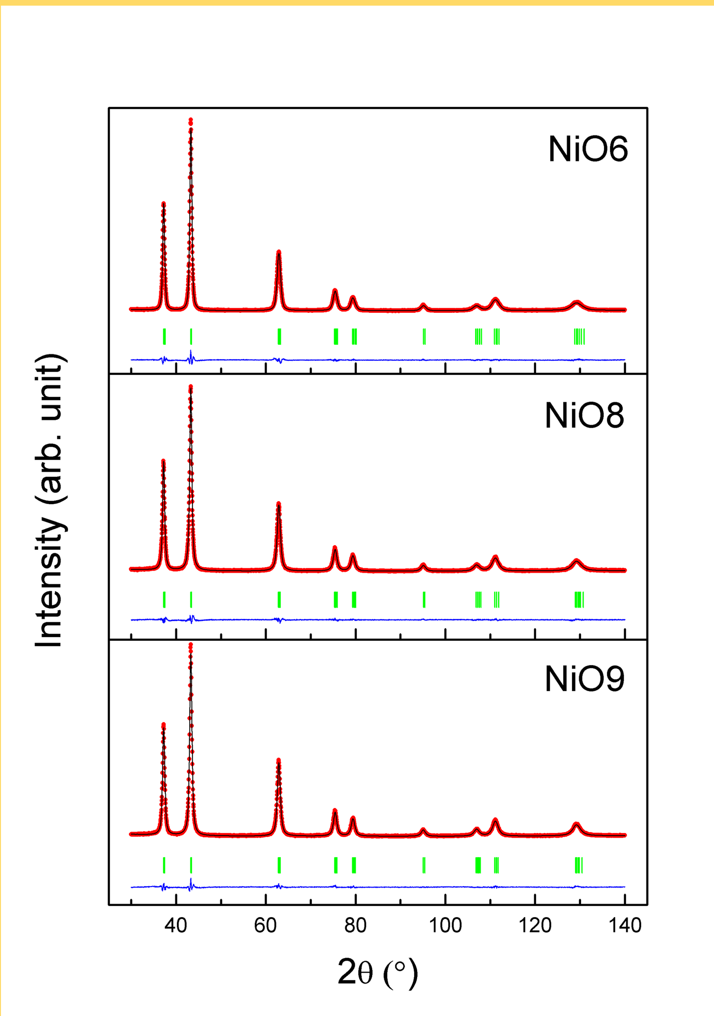

Not cubic, but rhombohedral structure (R-3m) !

Sample	a(Å)	c(Å)	$\langle D\rangle_V$(nm)	$Strain$(%)	χ^2	R_{Bragg}
NiO0 (0 h)	2.95539(1)	7.22695(1)	-	-	2.34	0.79
NiO2 (1 h)	2.95729(4)	7.2086(1)	-	-	4.65	1.67
NiO4 (3 h)	2.9600(1)	7.2023(3)	-	-	2.66	1.05
NiO6 (10 h)	2.9581(1)	7.1964(3)	-	-	2.20	1.12
NiO8 (50 h)	2.9563(1)	7.2043(4)	26.2	0.51	1.77	1.03
NiO9 (100 h)	2.9562(1)	7.2127(6)	18.2	0.39	1.65	1.28

We observed an enhancement in the width of the diffraction peaks as the milling time Increased.

Transmission Electron Microscopy

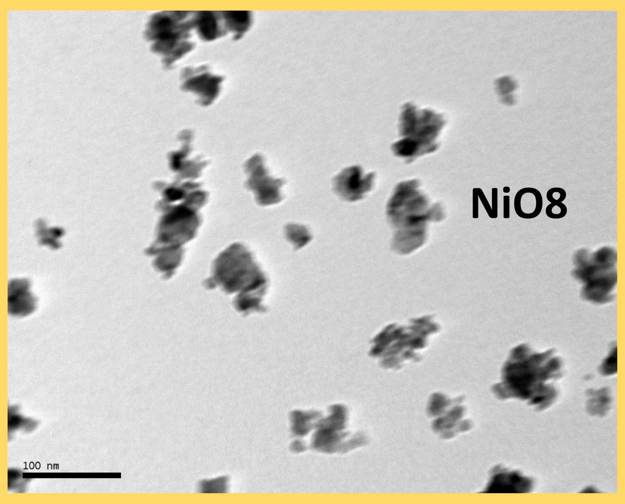

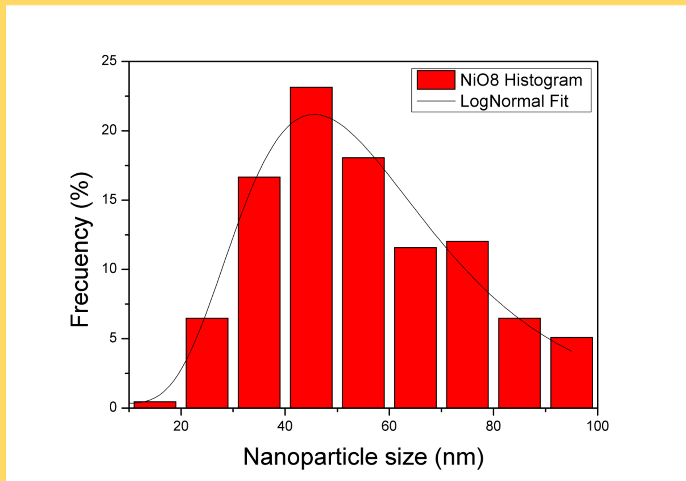

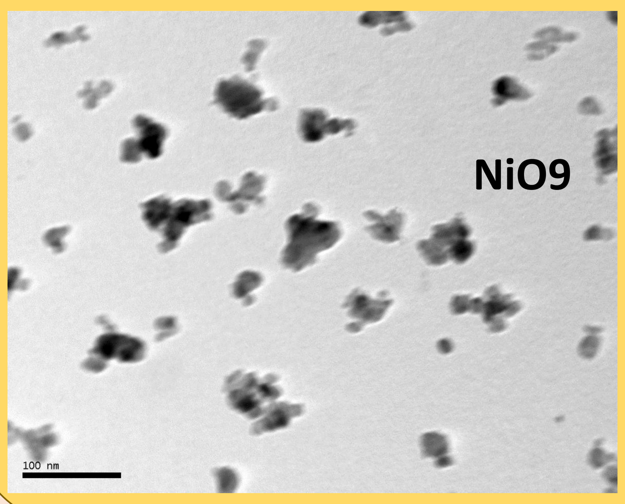

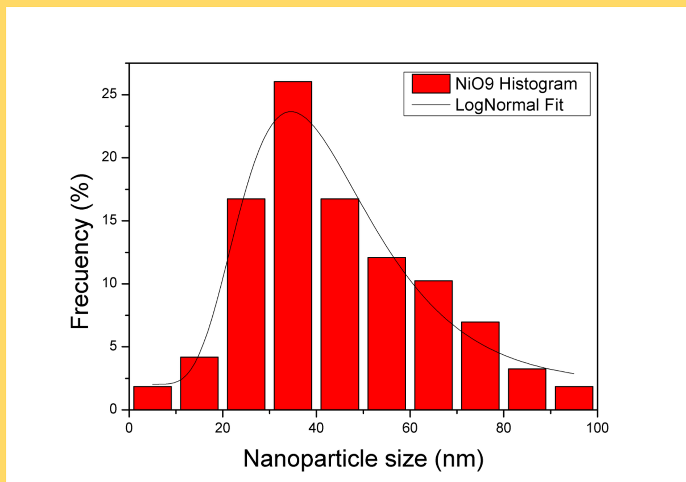

The relationship between $\langle D\rangle_V$ and D_m is given by the following equation:

$$D_m = \frac{4}{3}\langle D\rangle_V$$

These results differ from those obtained by XRD [37 (2) nm and 29 (2) nm], but they are within the same order of magnitude.

Sample	D_m(nm)	σ(nm)	R^2
NiO8 (50 h)	54.9	18.9	0.93
NiO9 (100 h)	44.5	19.5	0.94

Magnetic Measurements

Antiferromagnetic behaviour

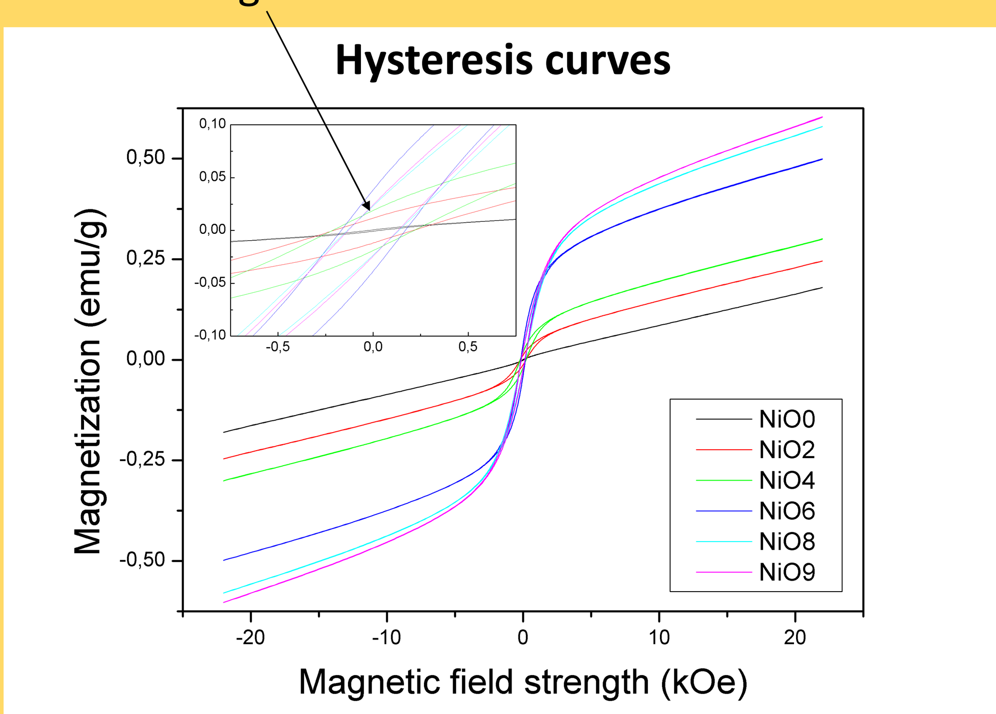

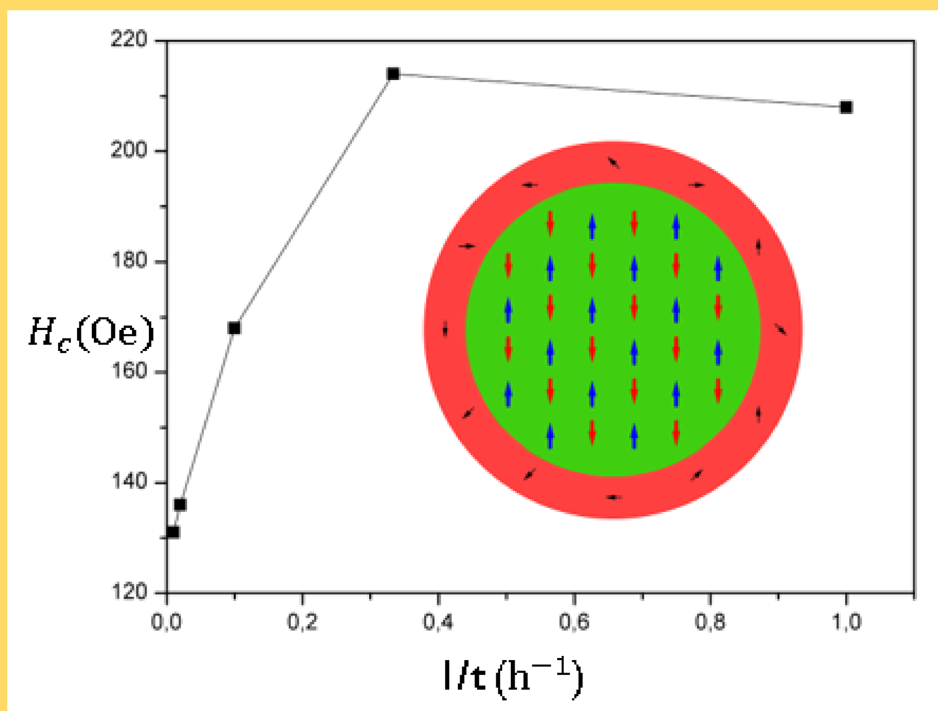

CONCLUSIONS

- ✓ Rietveld refinement didn't confirm the cubic crystalline structure (space group Fm-3m), but rhombohedral structure (space group R-3m) with lattice parameters $a = 2.957(2)$ Å and $c = 7.21(1)$ Å.
- ✓ The analysis of TEM images revealed that milling times of 50 h and 100 h lead to NiO NPs with mean diameters of 55(19) nm and 45(20) nm, respectively.
- ✓ Hysteresis curves confirmed the antiferromagnetic behavior of the samples. However, those obtained with milling times of 50 h and 100 h, also revealed the presence of a ferromagnetic contribution due to surface spin disorder.
- ✓ From the measurements of the coercive field, we could determine that the NiO NPs exhibit a transition from the multidomain regime into the monodomain one within the hours of milling time.

Bibliography

[1] L. Néel. *Physica*, 15:225, 1949.
[2] J. Richardson and W. Milligan. *Phys.Rev.*, 102:1289, 1956.
[3] N. Rinaldi-Montes *et al*. *Nanoscale*, 6:457, 2014.

Nanosensors with spin waves

J.D. Aguilera[a,b], P. de la Presa[b], P. Marín[b], M.C. Horrillo[a] and D. Matatagui[a]*

[a]SENSAVAN, Instituto de Tecnologías Físicas y de la Información (ITEFI), CSIC, 28006 Madrid, Spain
[b]Instituto de Magnetismo Aplicado (IMA), UCM-ADIF, 28230 Las Rozas, Spain
*d.m@csic.es

Abstract— *We built an innovative sensor based on the interaction between nanostructures and gases using spin waves to detect the induced magnetic changes. The device is sensitive to low (below 50 ppm) gas concentration of acetone, ammonia, carbon monoxide and benzene. When traces of these gases diluted in air pass through zinc ferrite nanoparticles, which are contained in a 2 mm diameter teflon tube, the magnetic properties of the nanostructures change. This change is detected by means of spin waves: due to the known dependence of their propagation on the external field [1], their frequency will shift as the properties of the nanoparticles change. These excitations propagate along the surface of a 2 µm thick epitaxial film made of YIG (Yttrium Iron Garnet), a ferrimagnetic insulator with a quite narrow magnetic resonance line. The frequency of the spin waves is detected by means of an oscillator circuit connected to a frequency counter. Before manufacturing the device, the computer simulations and calculations described in [2] were replicated in order to optimize its design.*

Introduction

Gas sensing is important for many applications: pollution control, medical care, food industry or homeland security. Magnetic gas sensors have certain advantages (fast response, absence of electrical contacts, tunable working temperature) which make them interesting candidates to replace previous techniques.

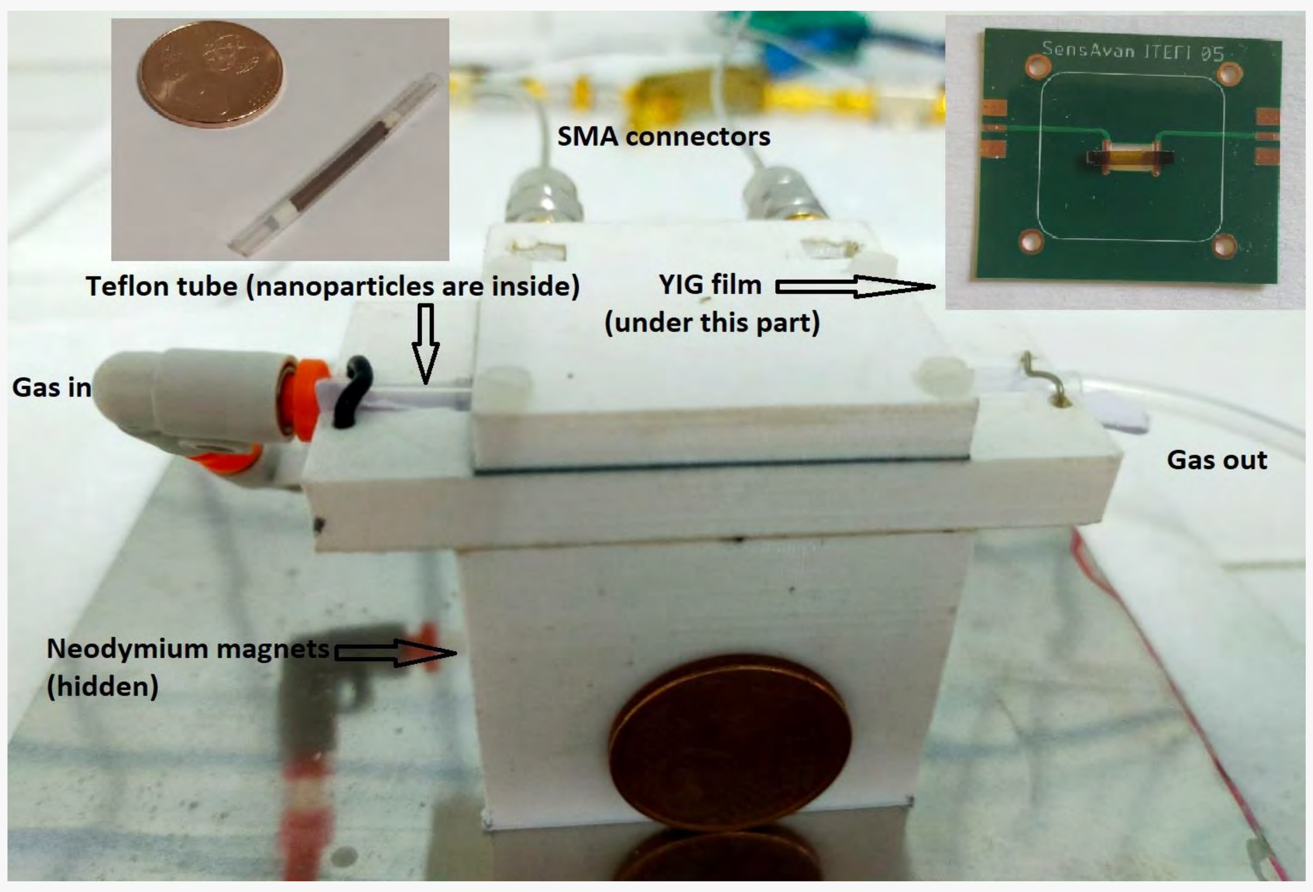

Results

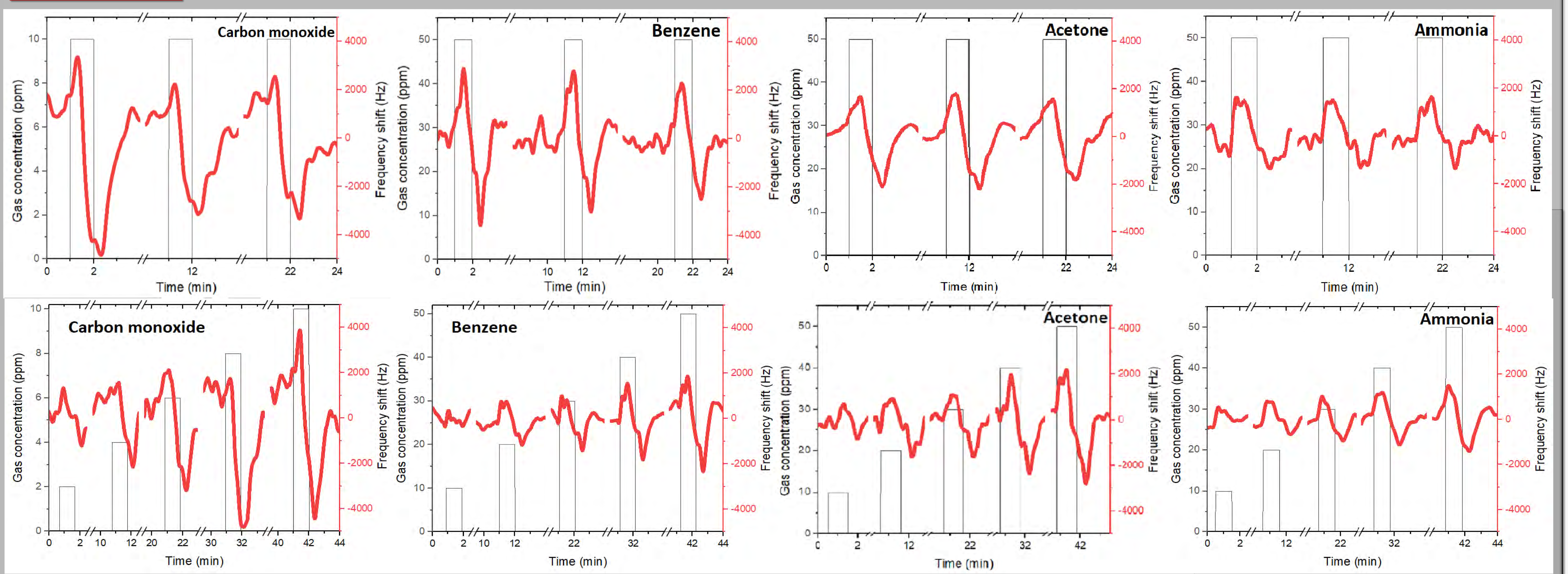

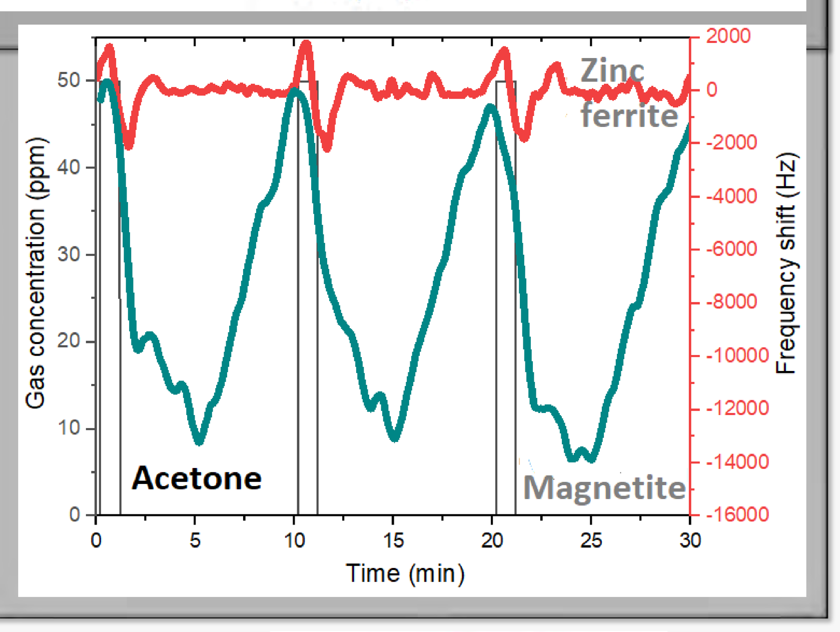

References

[1] J. R. Fragoso and D. Matatagui, "Bicapas de guías magnónicas para el procesamiento de señales", Universidad Nacional Autonoma de Mexico, 2016.

[2] M. Pozo-Gómez, J. Aguilera-Martín, P. de la Presa, C. Cruz, P. Marín, D. Matatagui, and M. Horrillo, "Modeling and simulation of a magnonic gas sensor to detected diseases in human breath", in 2021 13th Spanish Conference on Electron Devices (CDE), pp. 125-128, 2021.

Acknowledgements

The authors acknowledge the projects RTI2018-095856-B-C21 and RTI2018-095856-B-C22. D. M. acknowledges the financial support from the Fundación General CSIC via Programa ComFuturo.

Universitat de Girona
Departament de Física

Magnetic analysis: Fe-Co-Mn alloy produced by spark plasma sintering

K. Zaara[1,*], J.J. Suñol[1], V. Optasanu[2], M. Khitouni[3] , M.Chemingui[3]

1P2, EPS. Campus Montilivi s/n. University of Girona, 17003 Girona

2Labortory Carnot, Université de Bourgogne, 21078 Dijon, France

3Faculty of Sciences, University of Sfax, 3018 Sfax, Tunisia

YRinM 2021

Motivation

Fe-Co-based soft magnetic alloys possessing low coercivity, high electrical resistivity, good mechanical strength and elevated Curie temperature. They have attracted a pervading attention in different fields such as transformers, sensors, electromagnetic gadgets, data storage devices, etc. Spark plasma sintering (SPS) is a fast powder consolidation technique were the mechanical alloyed powders are compacted by heating and uniaxial pressing. The Fe-Co-Mn produced by mechanical alloying was also consolidated by spark plasma sintering SPS at 750°C and 1000°C under a pressure of 50MPa.

Preparation

Fe, Co, Mn elemental powders were weighted to give the desired compositions and milled in argon atmosphere by a high-energy planetary ball mill until 130h. Then, the as-milled powder was consolidated in vacuum atmosphere by SPS machine at 750 °C and 1000°C, using heating rate of 50°C/min, under a pressure of 50MPa.

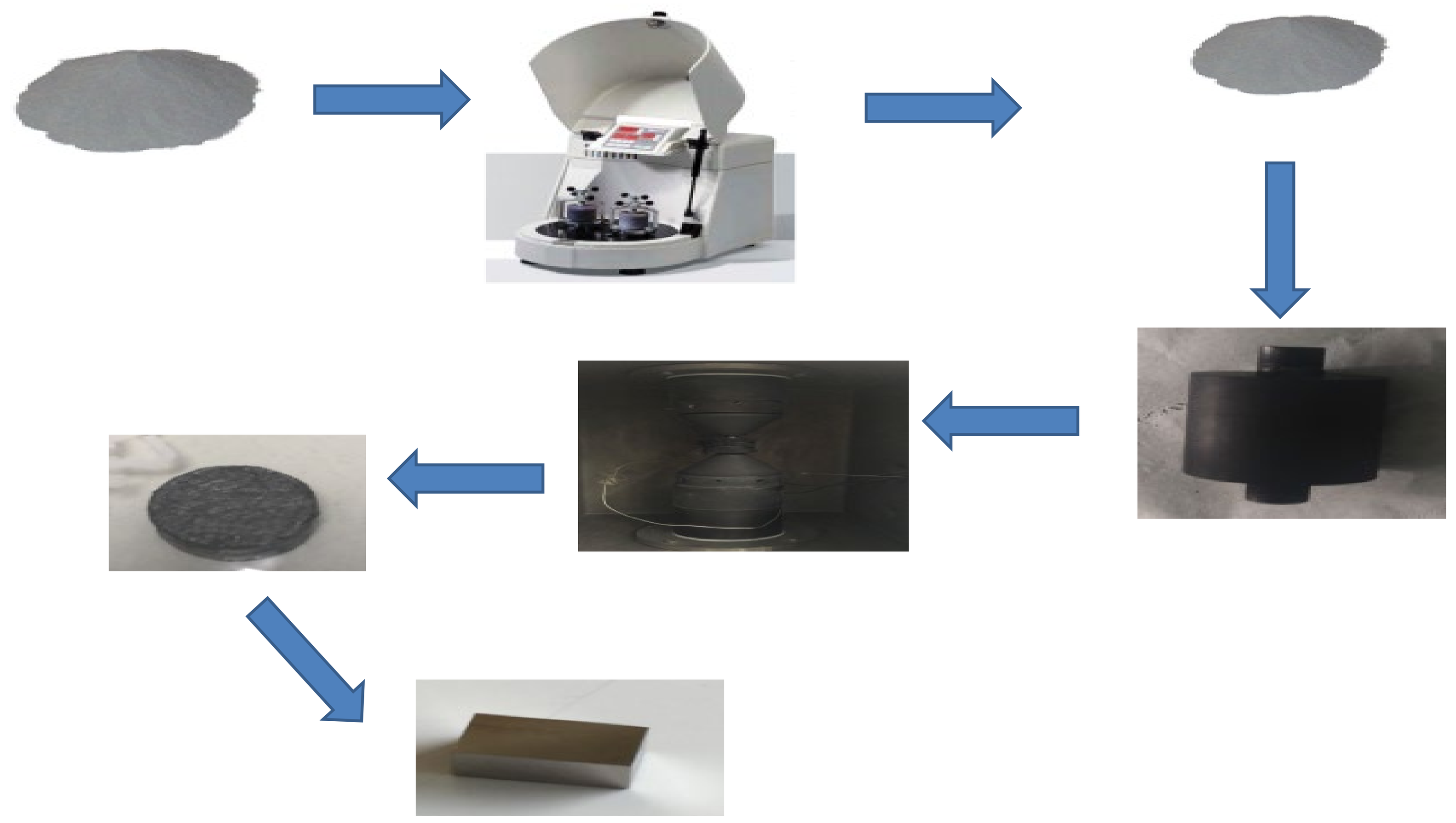

Morphological and microstructural characterization

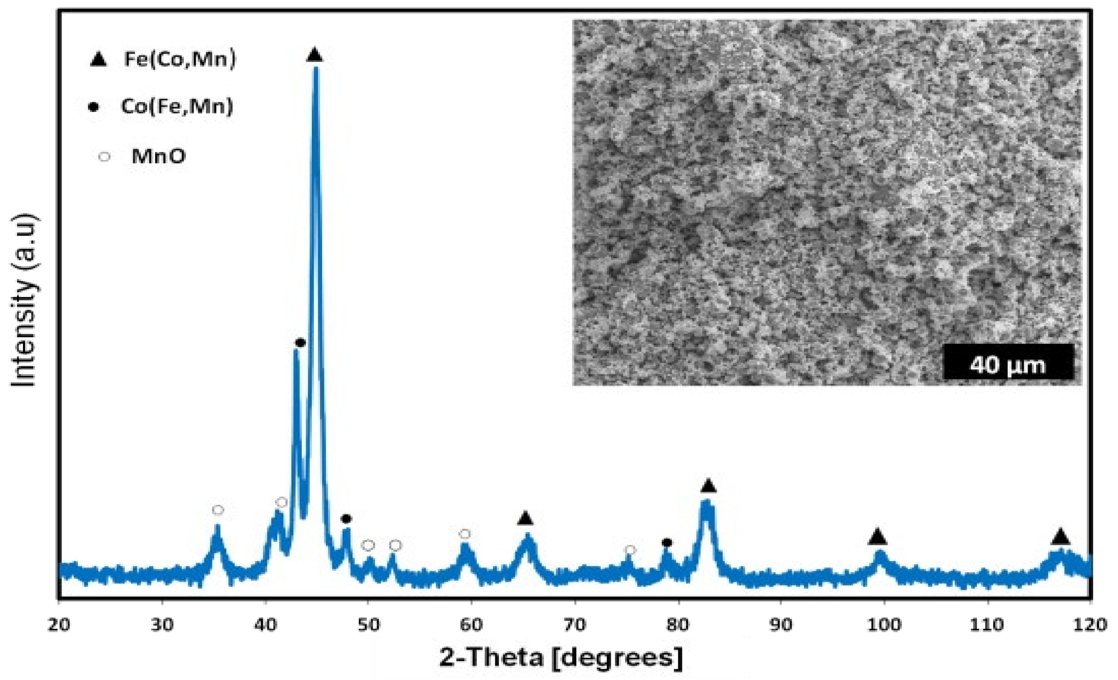

Fe-Co-Mn (MA for 130h)

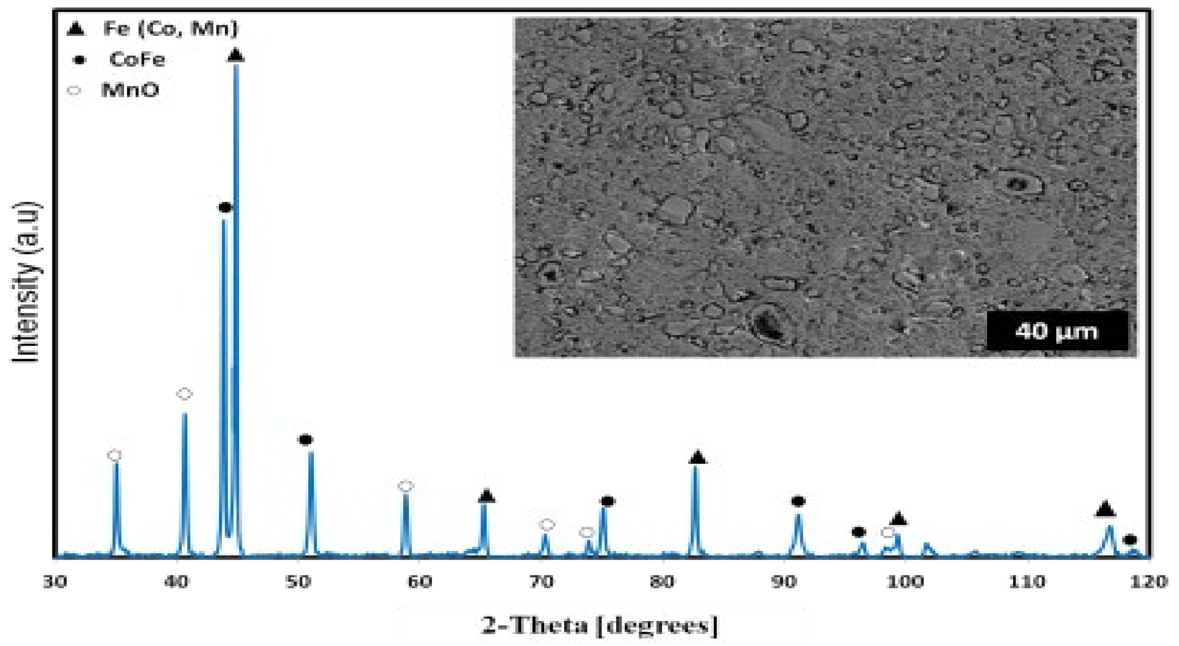

Fe-Co-Mn (SPS fat 750°C/50Mp)

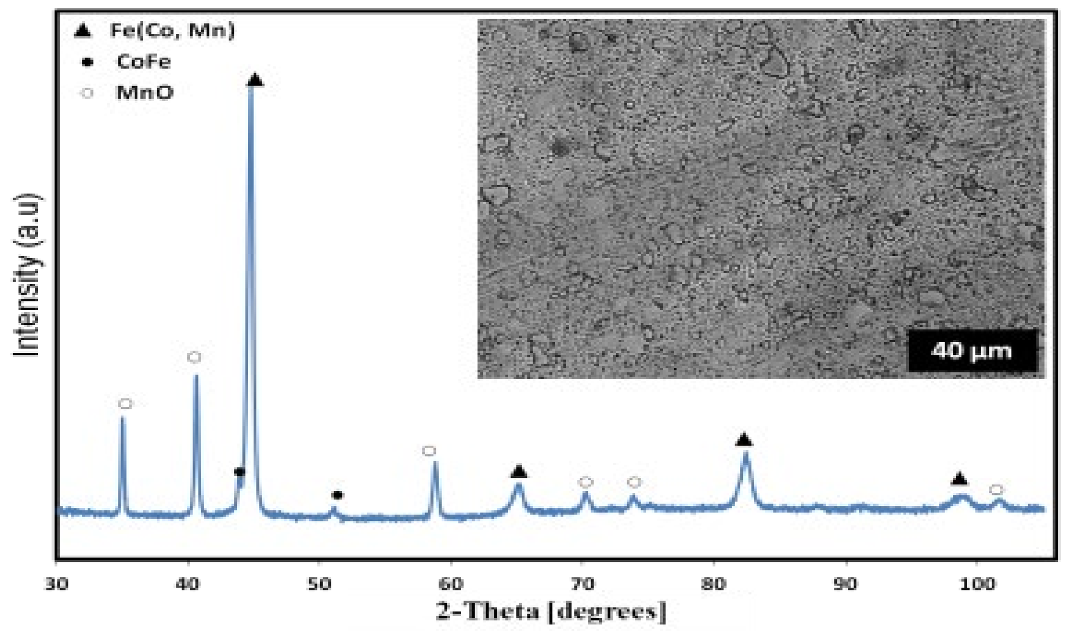

Fe-Co-Mn (SPS at 1000°C/50Mp)

Phase pourcentage	Fe(Co,Mn)	Co(Fe,Mn)	CoFe	MnO
Fe-Co-Mn (MA for 130h)	73.4	15.6	/	11
Fe-Co-Mn (SPS for 750°C)	44.6	/	24.4	31
Fe-Co-Mn (SPS for 1000°C)	91.4	/	6.9	1.7

Magnetic properties

Magnetic hysteresis plots

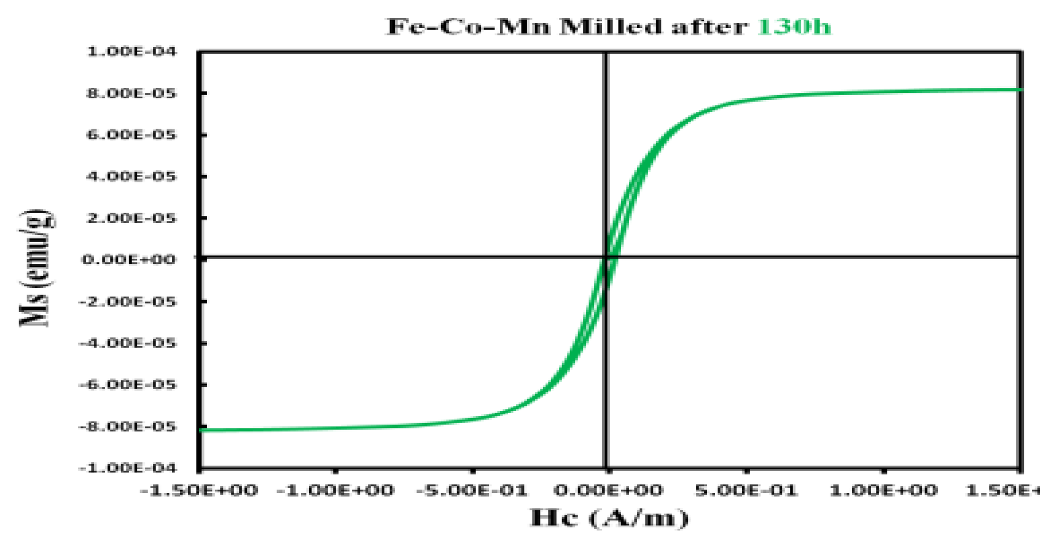

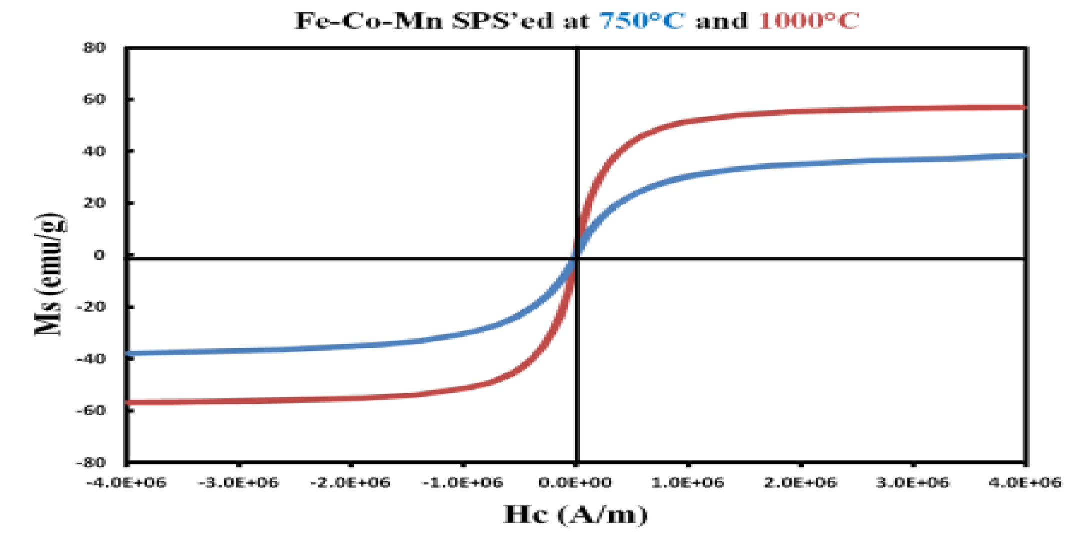

Saturation magnetization (Ms) and coercivity (Hc)

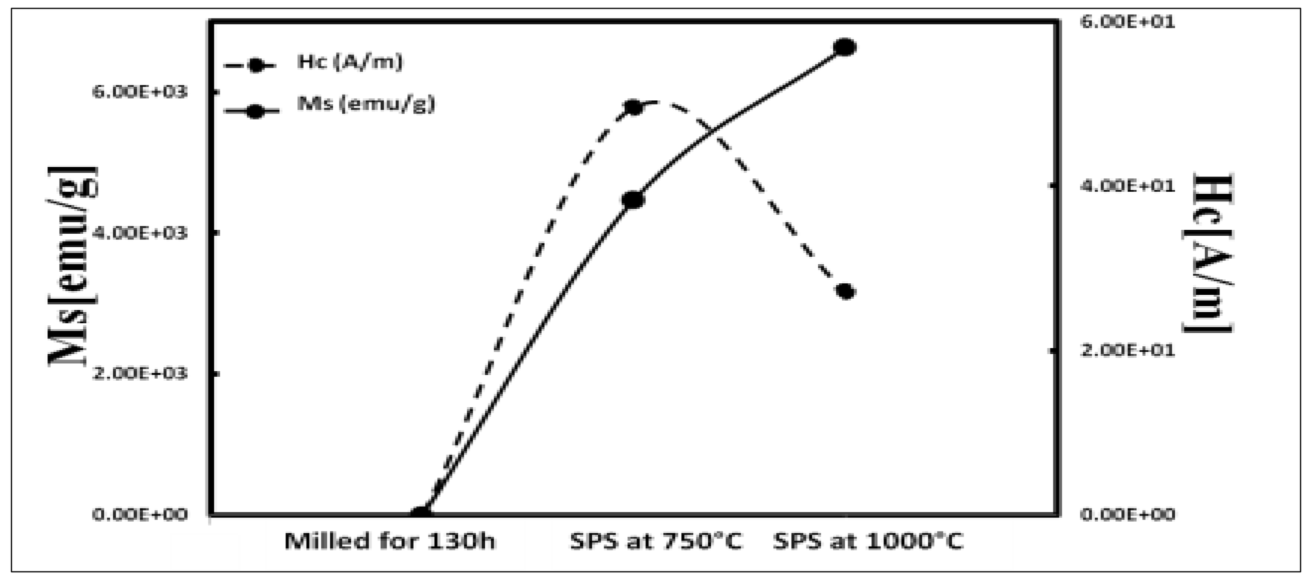

Squareness ratio (Mr/Ms)

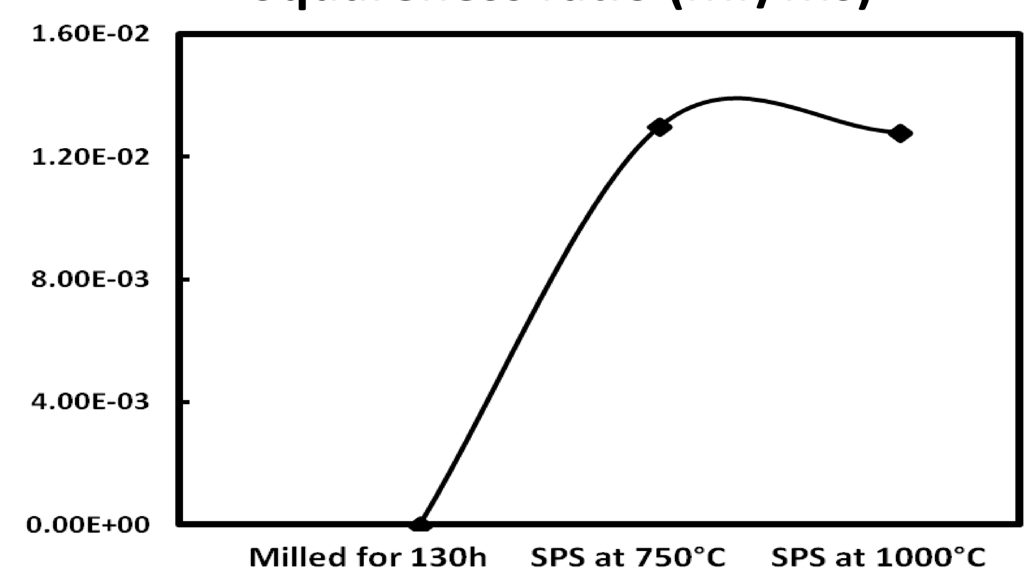

Conclusions

•SPS at 750°C/50Mp improves the magnetization saturation value from $8.23*10^{-5}$ to 38.36 emu/g, despite the fact that it increases the coercivity from $1.90*10^{-2}$ to $5.78*10^{+3}$. The appearance of the intermetallic CoFe and the increase of the MnO quantity modifies the magnetic beavior.

•SPS at 1000°C improves the magnetic softening by increasing of saturation magnetization to 56.92 emu/g and by a decrease in the coercivity and the squarness ratio to $3.17*10^{+3}$ and 0.0128 ,respectively .

•The magnetic softening of the obtained alloy after SPS at 1000°C is strongly linked to the minimization of the intermetallic and the MnO oxide phases.

PERMEABILITY VOLUME DISTRIBUTION IN AMORPHOUS MAGNETIC MICROWIRES: EXPERIMENT AND SIMULATION

Iu. Alekhina [a,b], V. Kolesnikova [b], V. Rodionov [b], V. Rodionova [b], N. Andreev [b,c], L. Panina [c], N. Perov [a,b]

[a] Lomonosov Moscow State University, 119991, Leninskie gory 1-2, Moscow, Russia
[b] Immanuel Kant Baltic Federal University, 236004, Nevskogo 14, Kaliningrad, Russia
[c] National University of Science and Technology MISiS, 119049, Leninsky Pr. 4, Moscow, Russia

YRinM 2021

ABSTRACT

Peculiarities of the magnetic properties of amorphous magnetic microwires have been the subject of numerous scientific works for decades. Mechanical stresses, which are induced during manufacture, lead to the appearance of magnetoelastic anisotropy and associated complex core-shell domain structure of the microwire, which depends on the magnetostriction of the particular alloy [1]. The fine micromagnetic structure of the wire affects its magnetic response, as it determines the magnetization mechanisms. Nevertheless, to define the micromagnetic structure, one has to use modified approaches, as its direct observation is limited. Several works devoted to microtomography using X-rays [2] described the obstacles, which primarily concern the sample dimensions restrictions. The magnetization reversal experiments allow conclusions about the internal structure by indirect investigations. A complete description of the micromagnetic structure and the mechanisms of magnetization reversal processes in the microwires requires not only a comprehensive experimental study but also their numerical simulation, taking the obtained experimental data into account. Thus, modelling of magnetization reversal on a microlevel is necessary for the understanding of the main features and crucial details of such processes and further prediction of the properties of the amorphous materials. In this work, the simulation of the microwires magnetization reversal by circular magnetic field was carried out to analyze the magnetization mechanisms and circular permeability distribution over the volume of the wire. The analysis of the results of the experimental investigations of impedance showed nonuniform permeability distribution over the cross-section of the microwire. The comparison of the experimental and simulation results showed possible mechanisms of the distribution non-uniformity.

SIMULATION METHODS AND PARAMETERS

Micromagnetic modelling was carried out using the OOMMF package [3].

Additional calculations were carried out with Matlab software.

Geometry and material parameters:

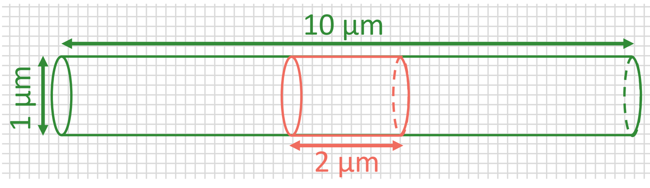

Cubic mesh with cell size 5nm (~exchange length)

Magnetoelastic anisotropy - uniaxial with the spatial distribution of anisotropy constant K_{me} and easy magnetization axis direction.

Wire type	Positive magnetostriction	Negative magnetostriction
λ_s	$2.5\cdot10^{-5}$	$-4.0\cdot10^{-6}$
M_s, kA/m	$1.25\cdot10^{6}$	$4.77\cdot10^{5}$
A, J/m	$8.0\cdot10^{-12}$	$4.8\cdot10^{-12}$
K_{me}, J/m^3 and EMA direction	$k_{me} = \frac{3}{2}\lambda_s\sigma_{ii}$	
	σ_{ii} from [4]	σ_{ii} from [5]

Magnetization reversal:

1st step: Equilibrium magnetization distribution in zero magnetic field (total energy minimization using conjugate gradients method).

1½ step: Equilibrium magnetization distribution in zero magnetic field in middle part of the wire – short sample with neglected demagnetizing field influence and preset domain wall. Used as initial magnetization distribution for 2nd step.

2nd step: Magnetization reversal under the applied circular magnetic field (solution of the Landau-Lifshitz-Gilbert equation using the Runge-Kutta methods).

Applied magnetic field have circular component only. Amplitude changes with radius as Bessel function (accounts skin-effect). Amplitude was set as 10 kA/m at the surface of the wire as relative parameter.

Magnetic field varies with 100 MHz frequency according to the harmonic law.

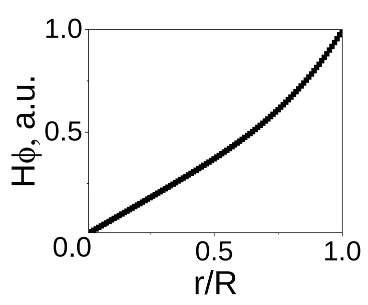

Permeability:

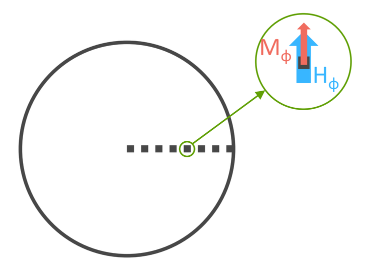

For every time moment the instant values of H_ϕ and M_ϕ can be obtained for every mesh cell.

Permeability

$\tilde{\mu}_\phi = \Delta M_\phi/\Delta H_\phi$

* Tilda marks the fact, that H_ϕ includes current field only

EXPERIMENT DETAILS

Samples:

1st series: $Co_{70}Fe_4B_{13}Si_{11}Cr_2$ microwires

d_m, µm	h_g, µm
8	2.8
22	1
28	2

2nd series: $Co_{69}Fe_4Cr_4Si_{12}B_1$ microwires with d_m = 90 µm

- Initial (without glass)
- Annealed at 200°C and 300°C
- Glass-coated

Methods:

Impedance – VNA Agilent FieldFox 9923A, HP4395A

Magnetization – VSM Lakeshore 7407, VSA

Analysis:

Impedance of cylindrical ferromagnetic wire in MHz frequency range in quasi-static approach [6]:

$$Z = -i\cdot 2\pi f\cdot L_e + R_{DC}\frac{ka}{2}\frac{J_0(ka)}{J_1(ka)}$$

$$k = \frac{1-i}{\delta},\ \delta = \frac{1}{\sqrt{\pi f \sigma \mu_0 \mu_\varphi}}$$

(Current frequency; External part of self-induction; DC resistance; 0 and 1st order Bessel functions; Wire radius; Conductivity)

Knowing the impedance, the value of the permeability averaged over the skin-layer can be restored.

Changing the layer thickness by f variations, permeability can be reconstructed layer by layer.

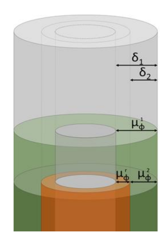

SIMULATION RESULTS

Positive magnetostriction | **Negative magnetostriction**

Equilibrium magnetization

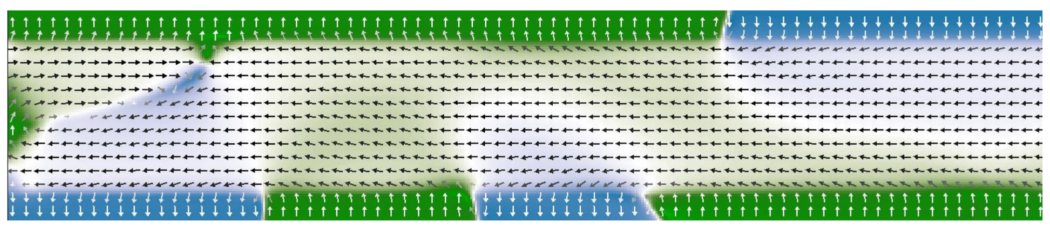

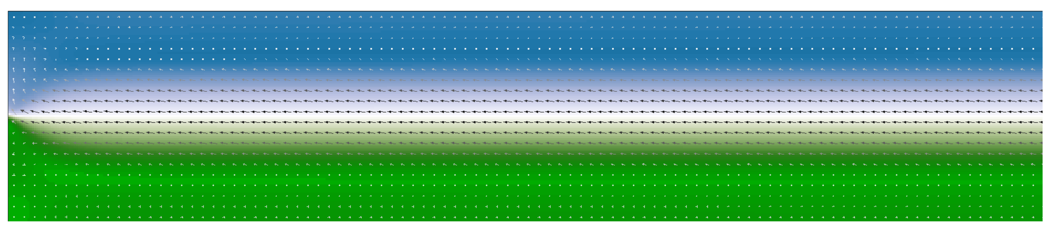

Positive magnetostriction:

- Axially magnetized core domain + radially magnetized near-surface shell
- Closure domain at the end of the sample, caused by demagnetizing field
- Domain structure of the radially magnetized shell

Negative magnetostriction:

- Axially magnetized core domain + circularly magnetized near-surface shell
- Pointed shape of the, caused by demagnetizing field
- Domain structure in the shell can be caused by defects

Magnetization reversal

Initial state: DW in the shell region (color marks y-component of magnetization)

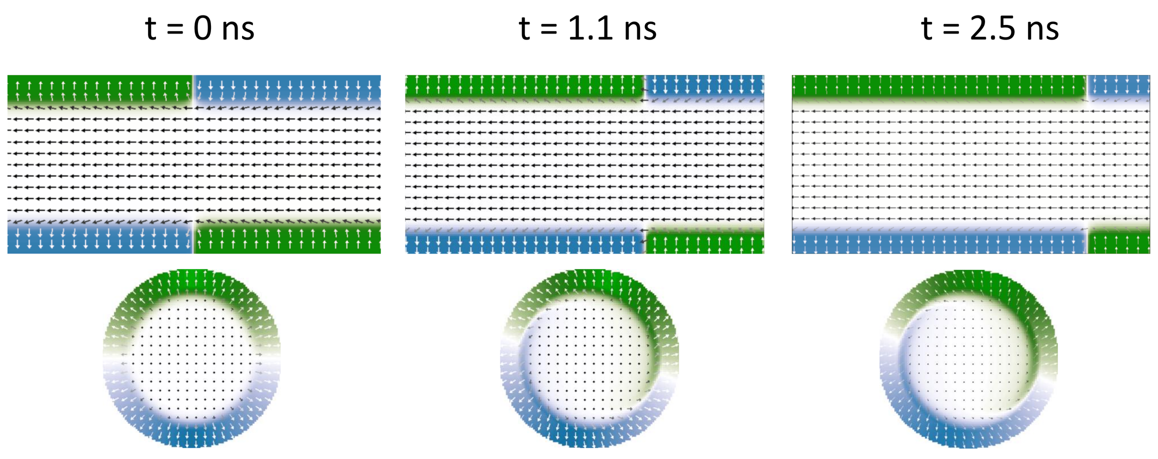

Initial state: DW in the shell region (color marks x-component of magnetization)

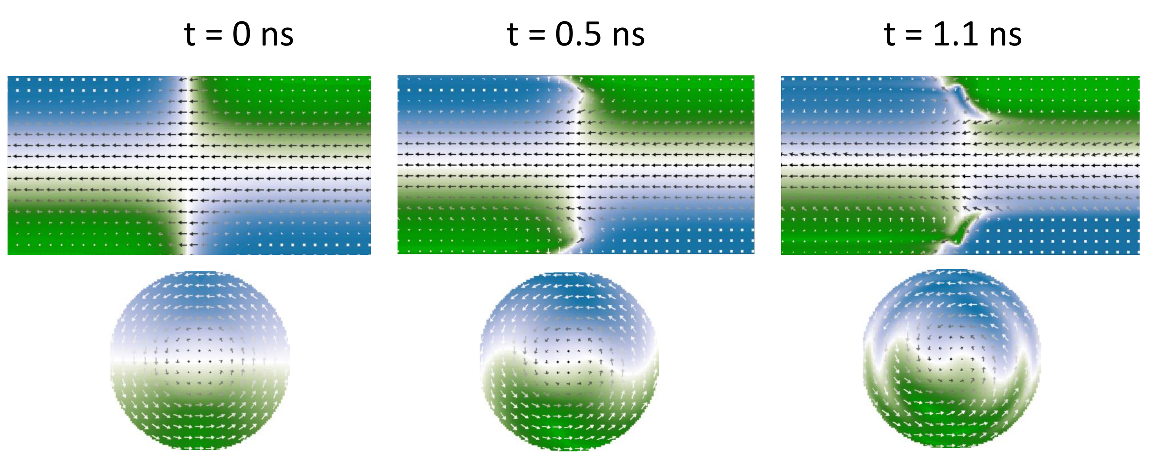

- Appearance of circular component of magnetization in the region of core-shell DW
- Shifting of the DW in the shell with enhancement of the circular magnetic field

- Appearance of radial component of magnetization, disturbance of radial magnetization
- Curved magnetic structures in the shell DW

Permeability

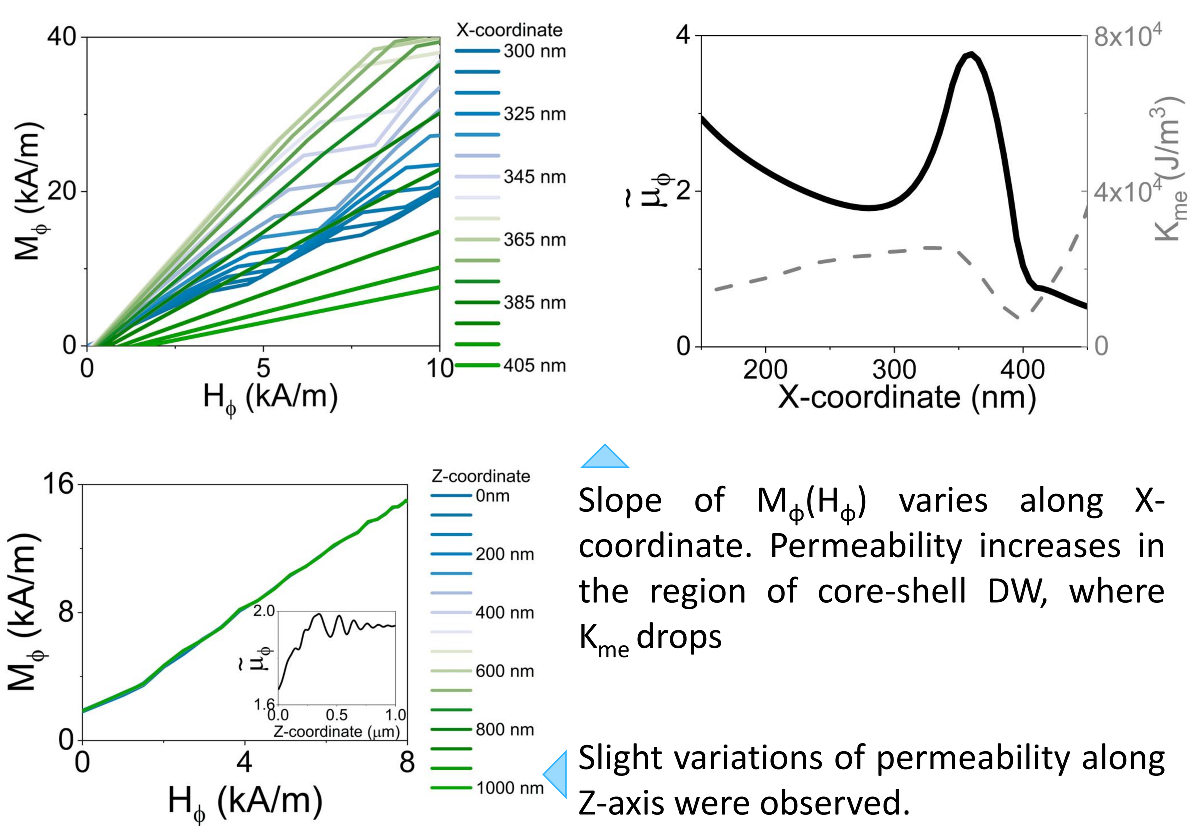

Slope of $M_\phi(H_\phi)$ varies along X-coordinate. Permeability increases in the region of core-shell DW, where K_{me} drops

Slight variations of permeability along Z-axis were observed.

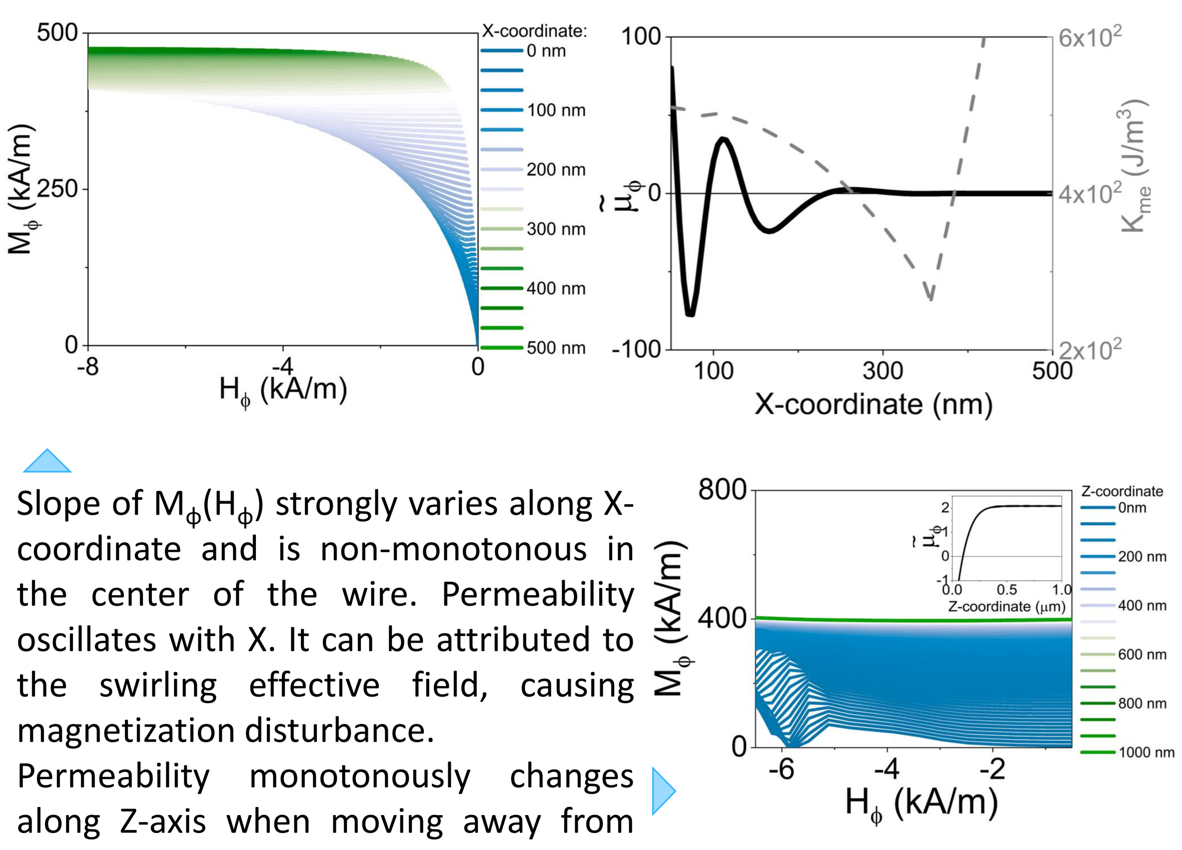

Slope of $M_\phi(H_\phi)$ strongly varies along X-coordinate and is non-monotonous in the center of the wire. Permeability oscillates with X. It can be attributed to the swirling effective field, causing magnetization disturbance.

Permeability monotonously changes along Z-axis when moving away from the DW.

EXPERIMENTAL RESULTS

1st series: Drop of permeability is obtained. Estimations of the core domain radius based on squareness coefficient show the presence of the domain wall between core domain and shell in this region.

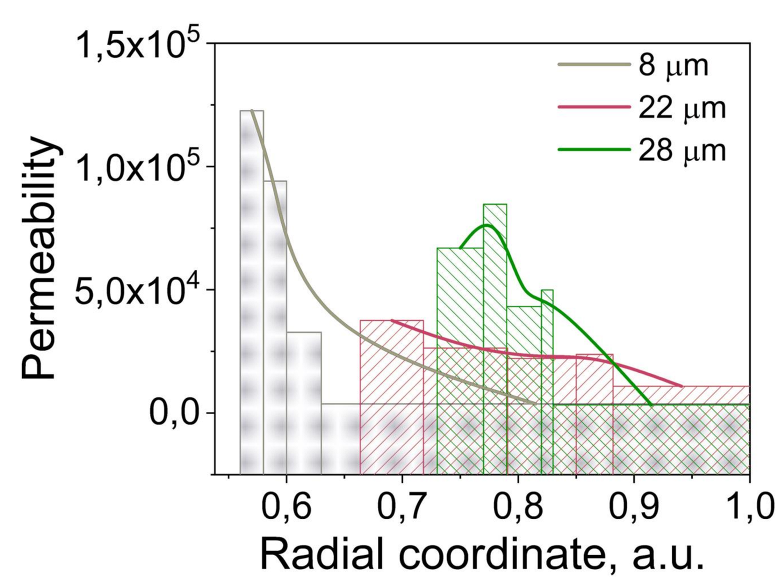

For details refer to

2nd series: oscillations of the permeability can be attributed to micromagnetic structure discontinuities. Peak can appear in the core domain/shell domain region. Oscillations can prove non-uniform magnetization process.

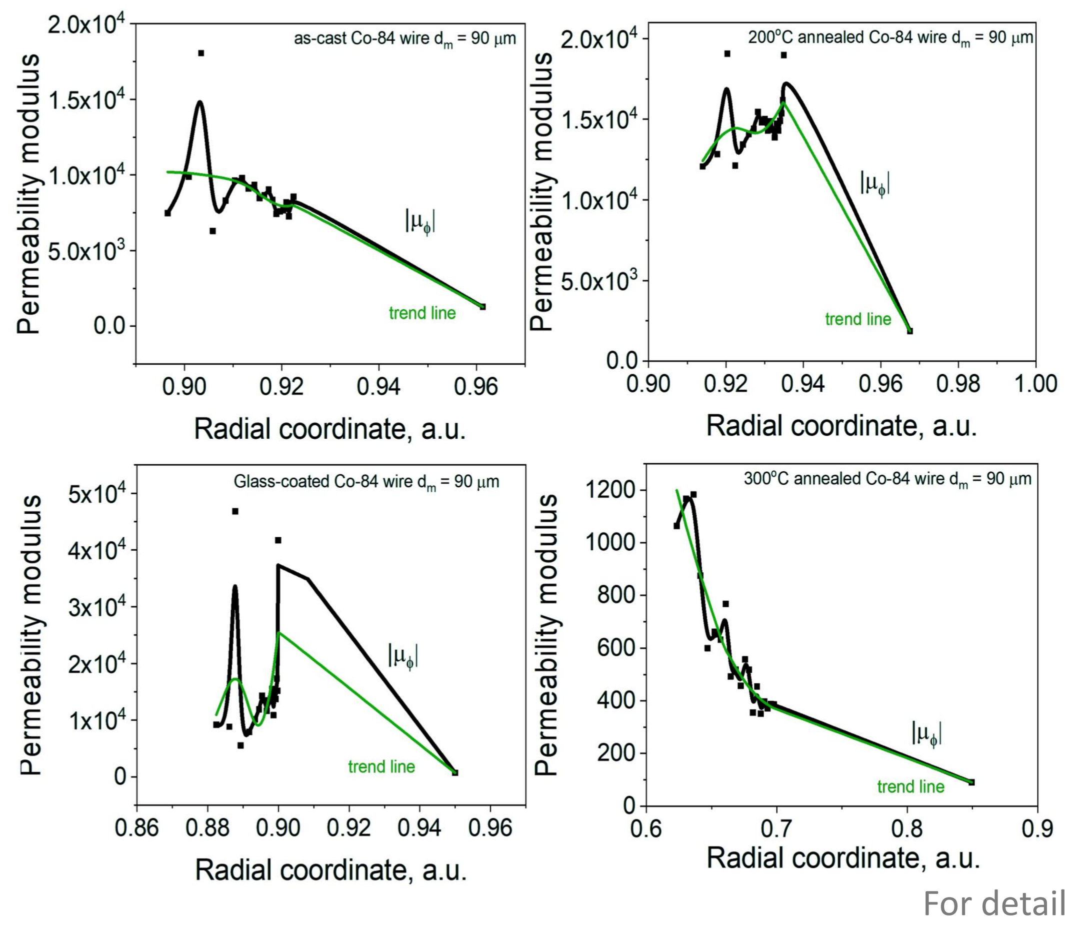

For details refer to

CONCLUSIONS

Magnetization reversal by circular magnetic field in amorphous microwires was simulated. The results obtained show, that non-uniform permeability distribution over the cross-section of the wire can be caused by the local peculiarities of micromagnetic structure. Higher permeability can be associated with local drop of anisotropy energy, as it was observed in the case of wires with positive magnetostrictions. Shell remagnetization by current was also observed. For samples with negative magnetostriction oscillations of permeability can be caused by swirling of the effective field, which can also account for the disturbance of shell DW.

[1] Vazquez M., Hernando A. Journal of Physics D: Applied Physics 29, 4 (1996)
[2] Donnely C. et al. Nature 547, 328 (2017)
[3] OOMMF User's Guide, Version 1.0 M. J. Donahue, D. G. Porter Interagency Report NISTIR 6376, NIST, Gaithersburg, MD (Sept 1999)
[4] Chiriac H. et al. PRB 52, 10104-10113 (1995).
[5] Antonov A.S. et al. Glass Physics and Chemistry 26, 353-358 (2000).

The work was financially supported by RFBR Grant 19-32-90089, 18-02-00137.

Contacts: Leninskiye gory 1-2, Moscow, Russia, 119991
Lomonosov Moscow State University, Faculty of Physics, Department of magnetism
+7 (495) 939-18-47
E-mail: ya.alekhina@physics.msu.ru

Incommensurate Magnetic Phases of the Multiferroic Compound $MnCr_2O_4$ Described with the Super-space Formalism

Miguel PARDO-SAINZ[1,2], Ayaka TOSHIMA[3], Gilles ANDRÉ[4], Juan BASBUS[5], Gabriel CUELLO[6], Takashi HONDA[7], Toshiya OTOMO[7], Katsuya INOUE[3], Yusuke KOUSAKA[2], Javier CAMPO[1,*]

[1]Instituto de Nanociencia y Materiales de Aragón (INMA), CSIC-University of Zaragoza, Zaragoza, Spain; [2] Osaka Prefecture University, Sakai, Japan; [3]Chirality Research Center and Institute for Advanced Materials Research, Hiroshima, Japan; [4]Laboratoire Léon Brillouin, Saclay, France; [5]Centro Atómico Bariloche, S. C. de Bariloche, Argentine; [6]Institut Laue-Langevin, Grenoble, France; [7]Institute of Materials Structure Science, Tsukuba, Japan

INSTITUTO DE NANOCIENCIA Y MATERIALES DE ARAGÓN

公立大学法人 大阪府立大学 Osaka Prefecture University

Introduction

❖ Nowadays, chromium-based normal spinel oxides ACr_2O_4 are one of the most studied materials in the condensed matter community due to the interplay between its magnetic, electric and structural properties [1,2].

❖ In particular, for $MnCr_2O_4$, the ground state magnetic structure is still controversial because the magnetic structures reported by different groups and investigated by independent techniques are inconsistent [1-3].

Super-space Group Formalism

❖ Incommensurate structure = basic structure + modulations:

$$\vec{M}_j(x_4) = \vec{M}_{j,0} + \sum_{n=1}^{\infty}\left[\vec{M}_{j,ns}\sin(2\pi n x_4) + \vec{M}_{j,nc}\cos(2\pi n x_4)\right]$$

❖ Symmetry operations: space group operations + phase shifts of modulations. Determined by the magnetic super-space group.

Methods

❖ The magnetic structure of this compound was reinvestigated by magnetization, specific heat and neutron diffraction at different temperatures.

❖ The results suggested that a new magnetic phase, not previously reported, is developed under 18 K.

❖ The magnetic phases in this sample were:

➢ Ferrimagnetic order below T_C = 45 K

➢ Conical spin order with propagation vector $\vec{k}_{S1}$= (0.62(1), 0.62(1), 0) below T_{S1} = 20 K

➢ Conical spin order with propagation vector $\vec{k}_{S2}$ = (0.660(3), 0.600(1), 0.200(1)) below T_{S2} = 18 K.

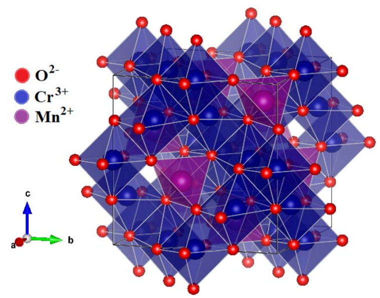

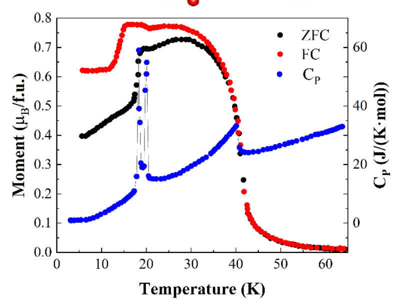

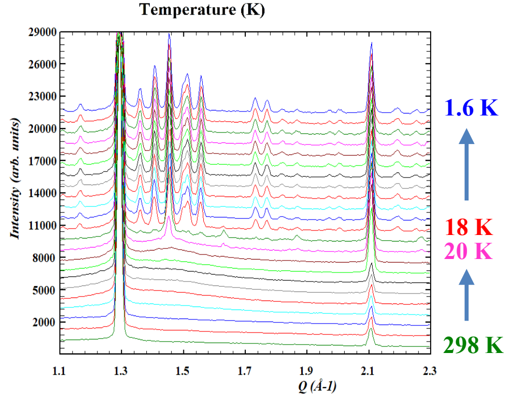

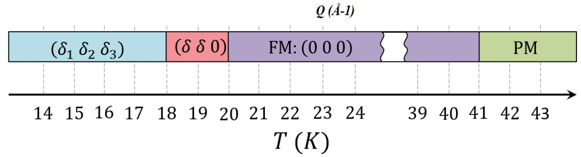

Results

❖ Using the super-space group approach [4], the symmetry of the nuclear and magnetic structures is determined:

Phase	Group	Irr. Rep	$\vec{k}$	$\vec{M}_{j,0}$	$\vec{M}_{j,s}$	$\vec{M}_{j,c}$
PM	Fd-3m (#227)	-	-	-	-	-
FiM	Imm'a' (#74.559)	mGM_4^+	(0 0 0)	$\langle 1\bar{1}0\rangle$	-	-
δ δ 0	Im'a'2(0,0,g)0ss (#46.1.12.4.m245.1)	$mGM_4^+ \oplus$ mSM2	(0.62 0.62 0)	$\langle 1\bar{1}0\rangle$	$\langle 110\rangle$	$\langle 001\rangle$
$\delta_1 \delta_2 \delta_3$	P1(a,b,g)0 (#1.1.1.1.m1.1)	$mGM_4^+ \oplus$ mGP1	(0.66 0.6 0.2)	$\langle 100\rangle$	$\langle 010\rangle$	$\langle 001\rangle$

❖ Electric polarization $\vec{P} \propto \vec{r}_{ij} \times (\vec{S}_i \times \vec{S}_j)$, also can be expressed as: $\vec{P} \propto \vec{k} \times \vec{M}_{j,0}$

❖ Non-zero value of polarization for transverse conical modulations:

➢ δ δ 0 phase: $\vec{P} \parallel \langle 001\rangle$

➢ δ_1 δ_2 δ_3 phase: $\vec{P} \parallel \langle 01\bar{3}\rangle$

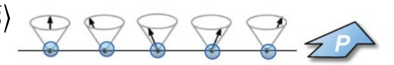

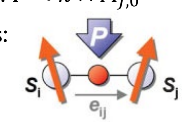

Conclusions

❖ New magnetic phase, not previously reported, identified under 18 K.

❖ Using SGF, symmetry of nuclear and magnetic structures is determined.

❖ Presence of transverse conical magnetic structures in lower-temperature phases implies existence of multiferroicity.

❖ Through simple theoretical calculations, we derive the macroscopic electric polarization vector for each magnetic phase.

References

[1] K. Dey et al., Journal of Magnetism and Magnetic Materials 435, 15 (2017).
[2] K. Tomiyasu et al., Phys. Rev. B 70, 214434 (2004).
[3] J. M. Hastings and L. M. Corliss, Phys. Rev. 126, 556 (1962).
[4] J. Rodríguez-Carvajal and J. Villain, Comptes Rendus Physique 20, 770 (2019).

CHARACTERIZATION OF Ni NANOPARTICLES INSERTED IN CARBONACEOUS MATERIAL WITH CONTROLLED POROSITY AND MORPHOLOGY

Mona Fadel[1], M.Paz Fernandez-Garcia[1], Fabian Suarez-Garcia[3], Julián Martin-Jimeno[3], David Martinez-Blanco[2], Alaa Adawy[2], P. Gorria[1]and J.A. Blanco[1]

1-Department of Physics, University of Oviedo, 33007, Oviedo, Spain 2- Scientific-Technical Services, University of Oviedo, 33006 Oviedo, Spain3- 3-National Institute of carbon CSIC, 33080, Oviedo, Spain

INTRODUCTION

Carbonaceous materials that include metallic nanoparticles (NPs) have attracted extensive interest during the last decades, especially those of metals like Ni and NiO in core/shell morphologies. To improve NiO properties for those applications, a correlated analysis of its microstructure and magnetic properties should be done. Nickel oxide is widely studied due to its importance in technological applications (i.e., catalysis, batteries, ceramics, etc) [1,2,3].

OBJECTIVES OF THE WORK

➢ Develop a simple procedure for the synthesis of an organometallic complex of 2-methylimidazole-nickel ('NiOF' in this work due to its similarity with MOF / ZIF).

➢ Synthesize five samples of 2-methylimidazole Nickel (NIOF) nanoparticles with carbonization temperatures between 400ºC and 600ºC Characterize their crystal structure and morphology by high resolution transition electron microscopy (HRTEM) and, X-ray diffraction (XRD).. Additionally, their magnetic properties were studied by SQUID magnetometer through ZFC-FC and M(H) curves ,

From the magnetic analysis, we suggest that each NPs can be described as consisting of a metallic Ni core, surrounded by very thin shell of NiO.

EXPERIMENTALAND MORPHLOLGY RESULTS

X-Ray Diffraction (XRD)

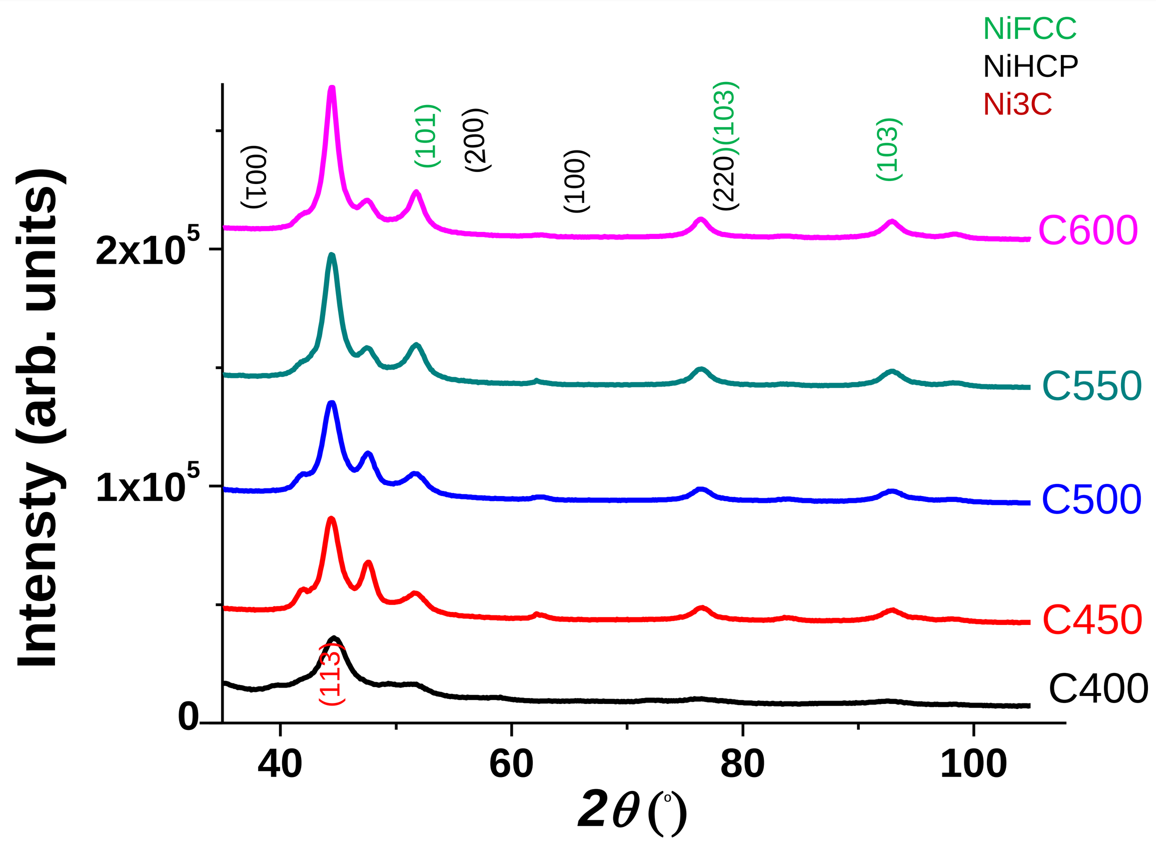

The samples exhibit two crystallographic phases of Ni: FCC and HCP. Additionally, at the lowest carbonization temperature Ni_3C was also detected. XRD peaks become narrower and symmetrical as the carbonization temperature raises, suggesting that the Ni-NPs mean diameter increases.

sample	D_{nm} (XRD)	D_{nm}(TEM)	M_s@300 K (emu/g-Ni)	M_s@5 K (emu/g-Ni)
C400	6	5(0.7)	7.3±0.05	39.8±0.7
C450	8	7(0.4)	22.3±0.11	160.3±3.5
C500	8	7(0.3)	22.4±0.03	51.7±0.5
C550	9	8(0.3)	24.4±0.03	50.6±0.4
C600	10	8(0.2)	28.3±0.022	101.2±0.8

High Resolution Transmission electron microscopy (HRTEM)

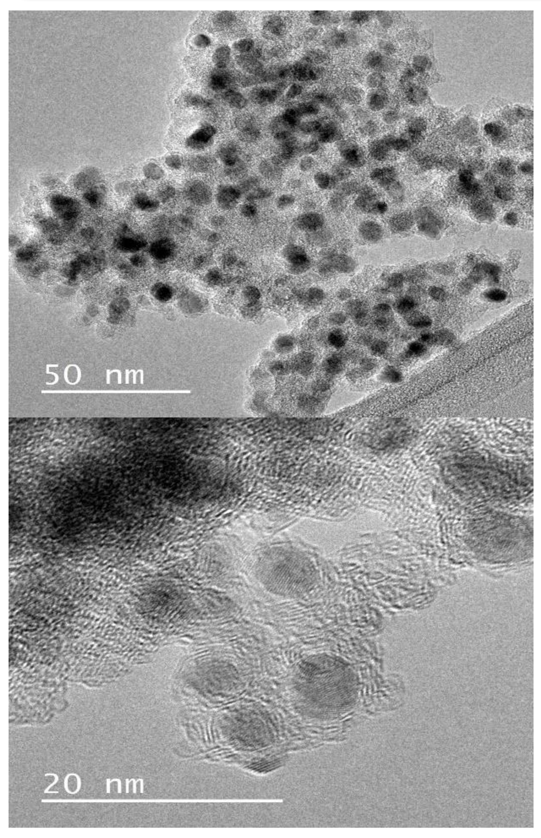

TEM images reveal that the NPs are randomly dispersed in the carbonaceous matrix and have a quasi-spherical shape with sizes ranging between 5 -10 nm.

HRTEM images of individual NPs showing interplanar distances ascribed to Ni-fcc, Ni-hcp , Ni_3C and NiO

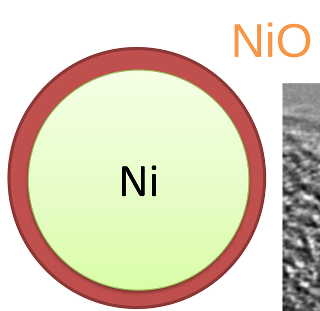

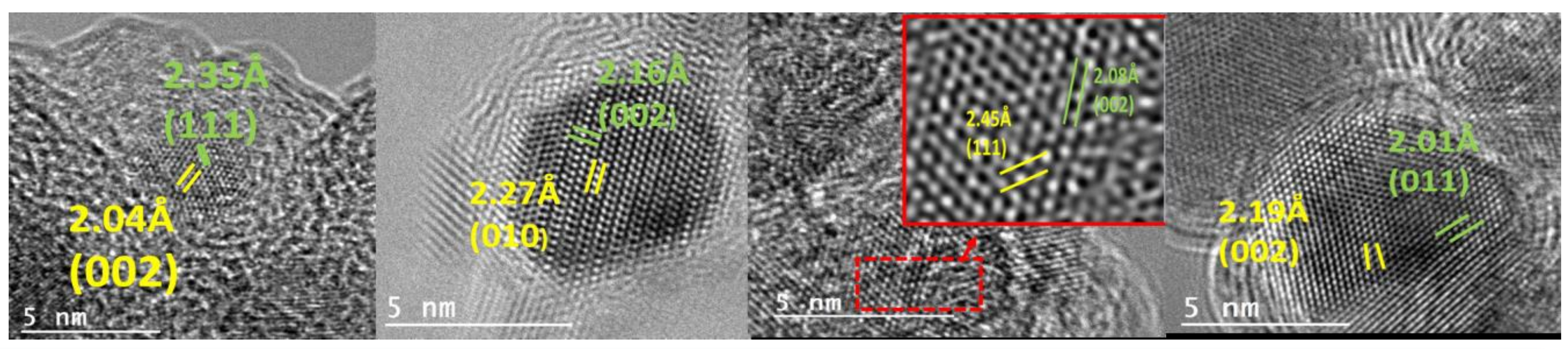

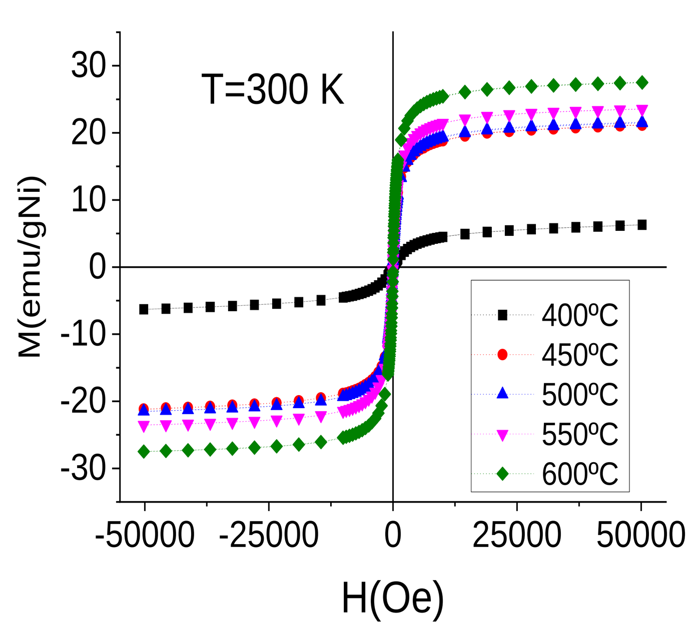

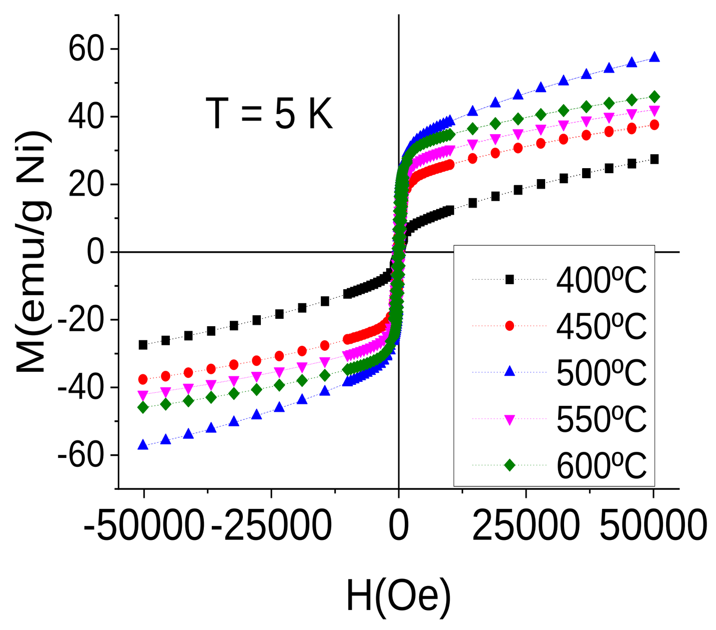

Magnetic characterization, *M(H,T)* curves

We observe that room temperature M_s values increase with the carbonization temperature because mean NP dimension also increases. The low M_s observed on sample C400 can be explained by the existence of antiferromagnetic Ni_3C phase.

The unsaturated magnetic behavior observed at low temperature, can be explained combining the existence of antiferromagnetic NiO and Ni_3C and the blocked character of NPs with small dimensions.

CONCLUSIONS

- NiOF samples were synthesized and carbonized at temperatures between 400 and 600 ºC.
- The samples exhibit a mixture of FCC and HCP Ni-phases. Additionally, Ni_3C was also detected on sample C400.
- As the carbonization temperature raises, the Ni-NPs mean diameter increases and thus, larger magnetic signals were measured (less surface to volume ratio).
- We corroborate the existence of thin shells of NiO at the surface of the Ni-NPs.

References: [1] M. Fernandez-Garcia, P. Gorria, M. Sevilla, M. P. Proenca, J. C. R Boada, A. B. Fuertes, J. A. Blanco, Enhanced protection of carbon-encapsulated magnetic nickel nanoparticles through a sucrose-based synthetic strategy, J. Phys. Chem. C 5 (115) (2011) 294-300. [2] J. Park, E. Kang, S. U. Son, H. M. Park, M. K. Lee, K. W. K. J. Kim, H. J. Noh, J. H. Park, C. J. Bae, J. G. Park, T. Hyeon, Alumina-supported nickel catalyst for liquid-phase reactions: an expedient and efficient heterogeneous catalyst for hydrogenation reactions, Adv. Mater. 17 (2005) 429. [3] J. Xiao, B. Chen, X. Liang, R. Zhang, Y. Li, NiO microspheres with tunable porosity and morphology effects for Co oxidation, Catalyst. Sci. Technol. 18 (2011) 1-999. [4] F. J. Martin-Jimeno, PhD thesis, 2018.

Acknowledgements: Authors acknowledge scientific contribution ; funding through research projects: FC-GRUPIN-IDI/2018/000185 and **RTI2018-094683-B-C52.**

Influence of Desing Parameters of Core@Shell Magnetic Nanoparticles in Magnetic Hyperthermia

Pelayo García Acevedo*, Ángela Arnosa Prieto, Yolanda Piñeiro and José Rivas

Applied Physics Department, NANOMAG laboratory, iMATUS Materials Institute of USC

pelayo.garcia.acevedo@usc.es

Introduction: Magnetic hyperthermia produced with Fe_3O_4 MNPs has been optimized in the last years, to produce an innovative technology (MAGFORCE) used for clinical applications in brain tumor treatments. It is based on the heat released by MNPs, when they are exposed to an alternating magnetic field, absorbing its magnetic energy, transforming it by relaxation processes (Néel and Brown) into thermal energy, thus acting as nanometric-scale heat sources. However, magnetic interactions (dipole interactions, exchange interactions, etc.), the composition and properties of the coating materials and the solvent viscosity can affect the magnetic hyperthermia performance of MNPs. The aim of this work is to study the effect of inorganic (SiO_2) and organic (PEG,PVA) shells in core@shell MNPs on magnetic hyperthermia proceses.

Core@Shell MNPs – Inorganic Shell $Fe_3O_4@SiO_2$

Synthesis: Microemulsion method

Code: M_8Si_2

D_{TEM} = 12.2 nm
D_{Core} = 8.2 nm
D_{Shell} = 2.0 nm

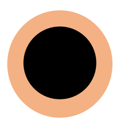

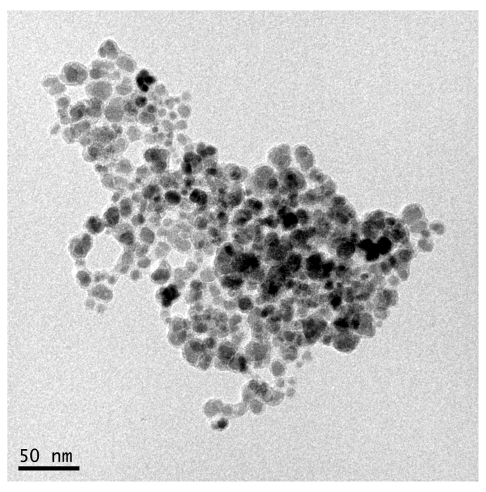

Code: M_8Si_5

D_{TEM} = 18.3 nm
D_{Core} = 8.1 nm
D_{Shell} = 5.1 nm

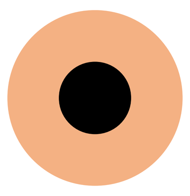

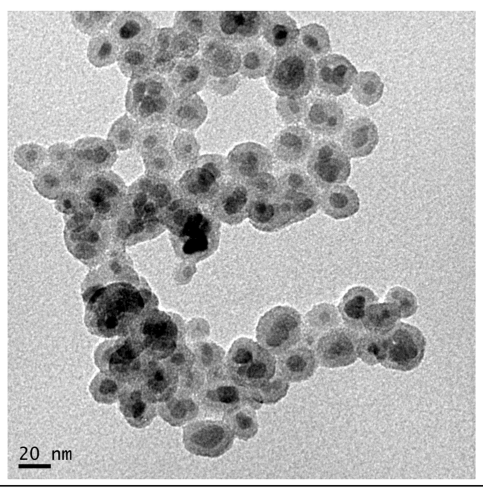

Code: M_8Si_{10}

D_{TEM} = 27.9 nm
D_{Core} = 8.1 nm
D_{Shell} = 9.9 nm

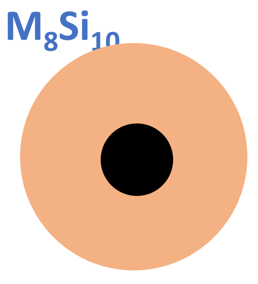

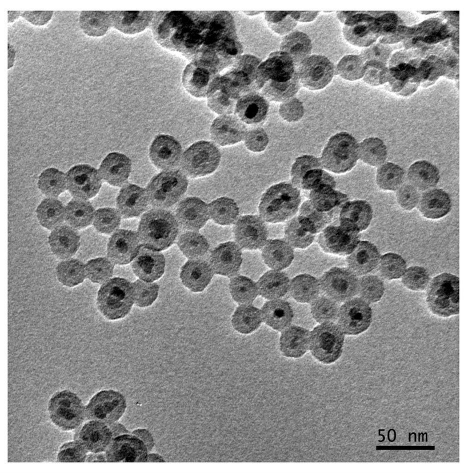

MNPs have been obtained with the same magnetic core but different shell thickness

Magnetic Characterization

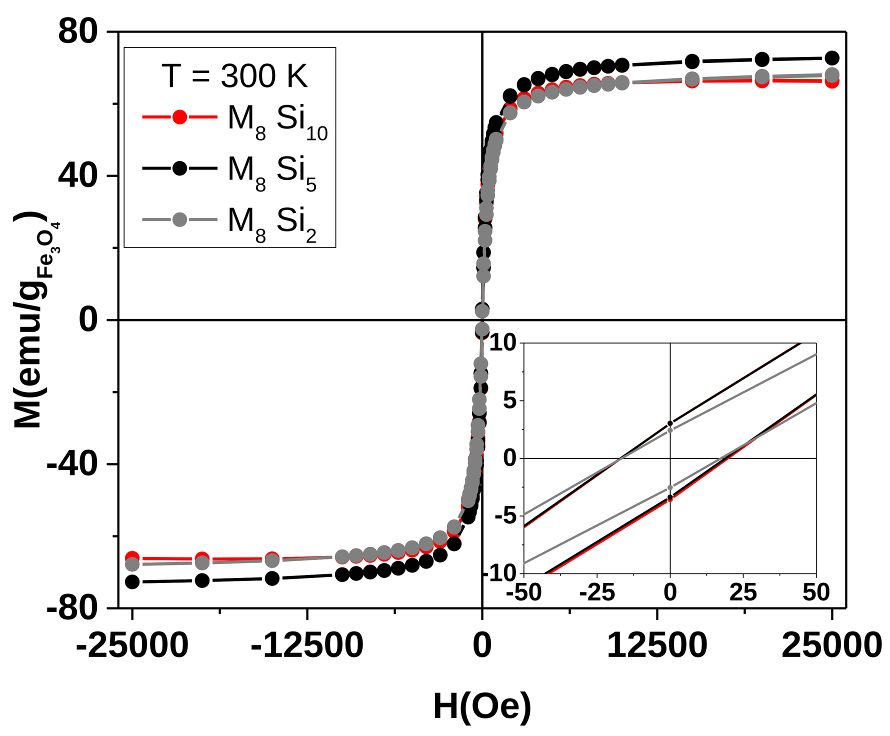

Sample	T (K)	M_s (emu/g)	M_R (emu/g)	H_C (Oe)
M_8Si_2	300	67.96	2.46	16.90
M_8Si_5	300	72.66	3.18	18.02
M_8Si_{10}	300	66.30	3.31	17.98

Saturation magnetization (M_S) values of 70 emu/g were obtained from the hysteresis loops at 300 K. In addition, the ZFC-FC measures allow us to demonstrate the superparamagnetic behavior of MNPs.

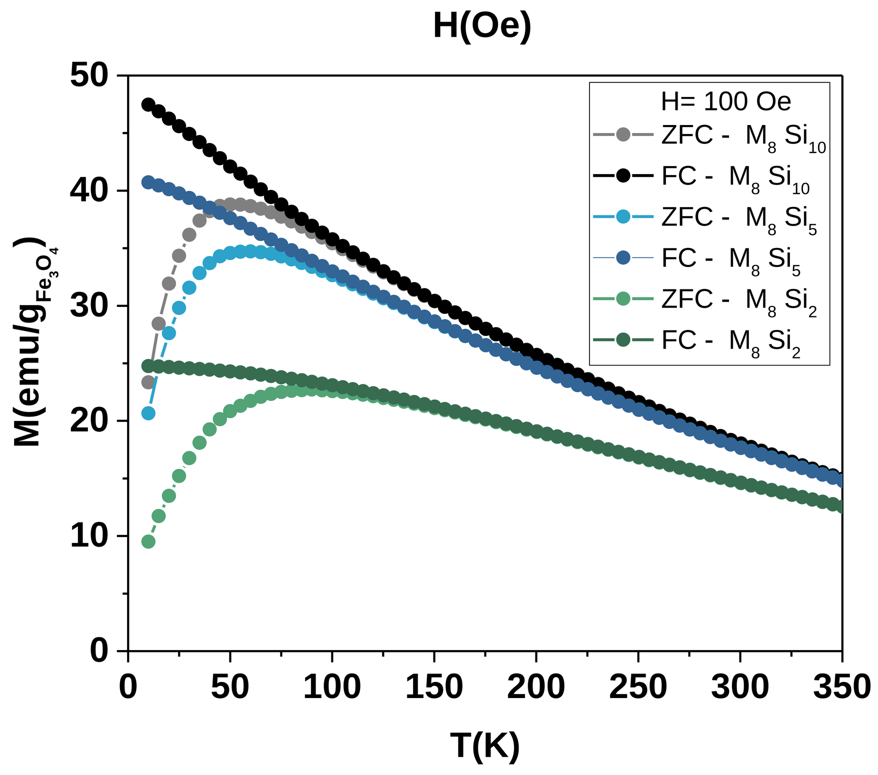

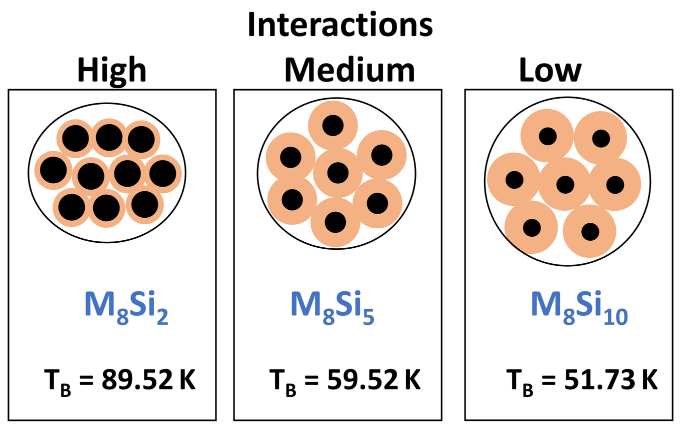

An increase in SiO_2 thickness leads to a decrease in the interaction between NPs and, therefore, a reduction in T_B

Magnetic Hyperthermia

Magnetic hyperthermia measurements were performed using a frequency of 293 KHz and a magnetic field of 30 mT for 3 minutes. The concentration used was 7 mg/ml

Sample	ΔT (ºC)	SAR (W/g)
M_8Si_2	6.4	32.97
M_8Si_5	4.8	29.20
M_8Si_{10}	4.4	23.04

Although the SiO_2 shell is ideal for reducing interactions between MNPs, it is clear that its poor heat conductivity negatively affects in magnetic hyperthermia processes

Core@Shell MNPs – Organic Shell Fe_3O_4@Polymer

Synthesis: Co-precipitation method

Fe_3O_4 Bare

D_{TEM} = 13.4 nm

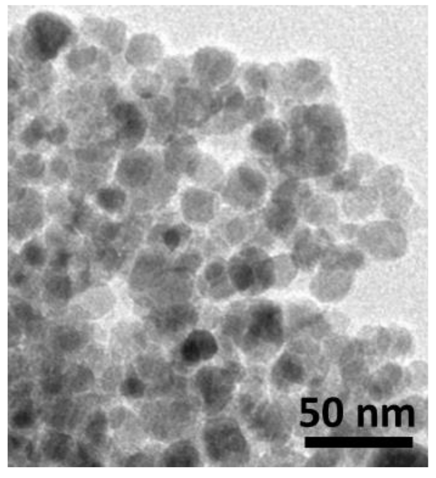

Fe_3O_4@PEG

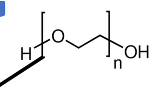

D_{TEM} = 13.4 nm

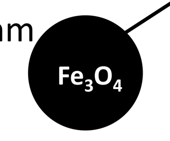

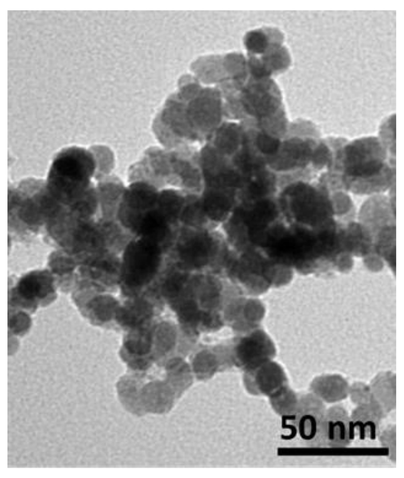

Fe_3O_4@PVA

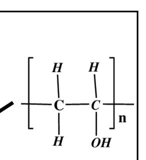

D_{TEM} = 9.1 nm

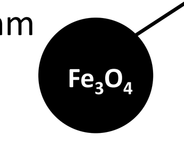

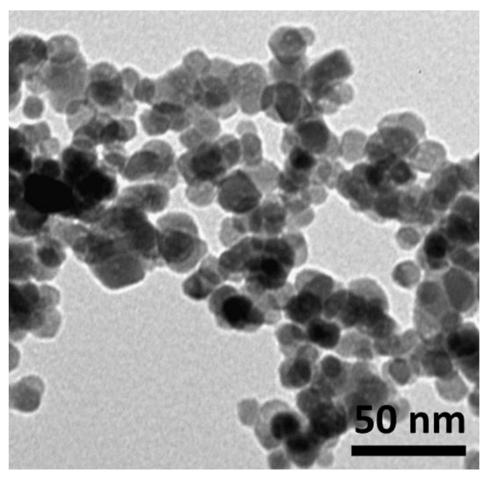

Magnetic Characterization

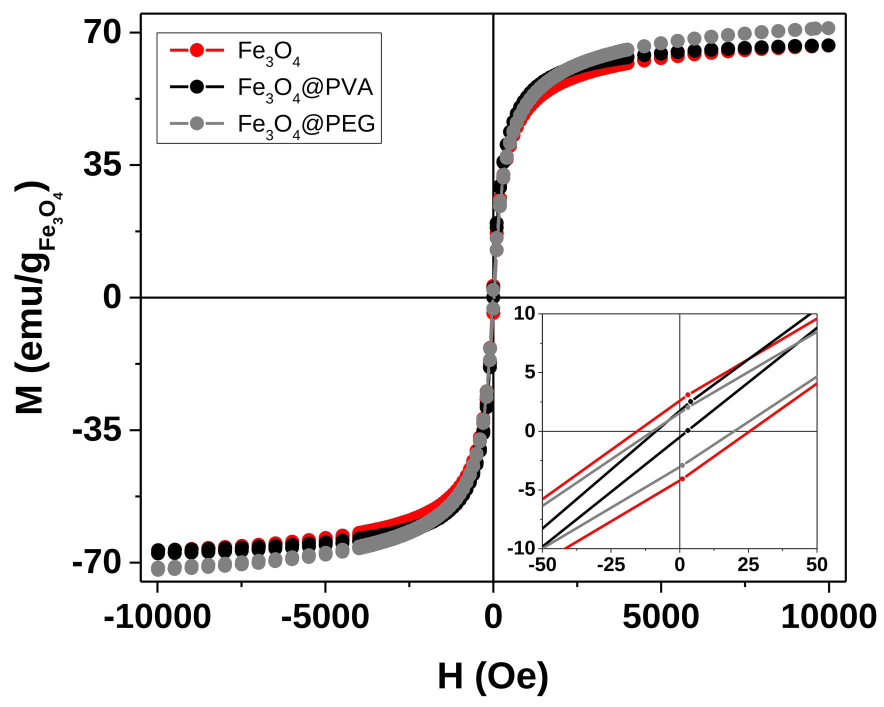

Sample	T (K)	M_s (emu/g)	M_R (emu/g)	H_C (Oe)
Fe_3O_4	300	66.97	3.38	20.44
Fe_3O_4@PVA	300	67.08	1.13	5.48
Fe_3O_4@PEG	300	71.51	2.31	14.73

Magnetization values similar to $Fe_3O_4@SiO_2$ MNPs were obtained

Magnetic Hyperthermia

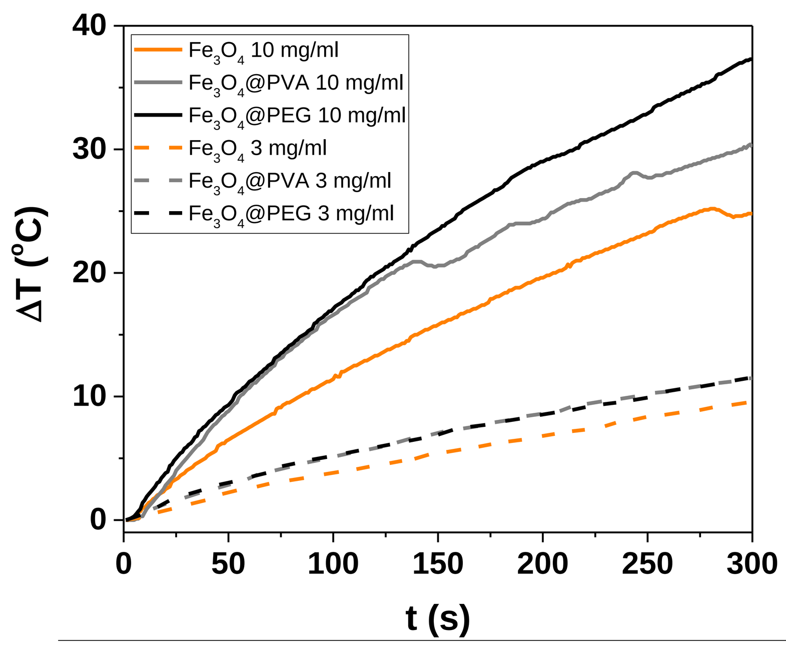

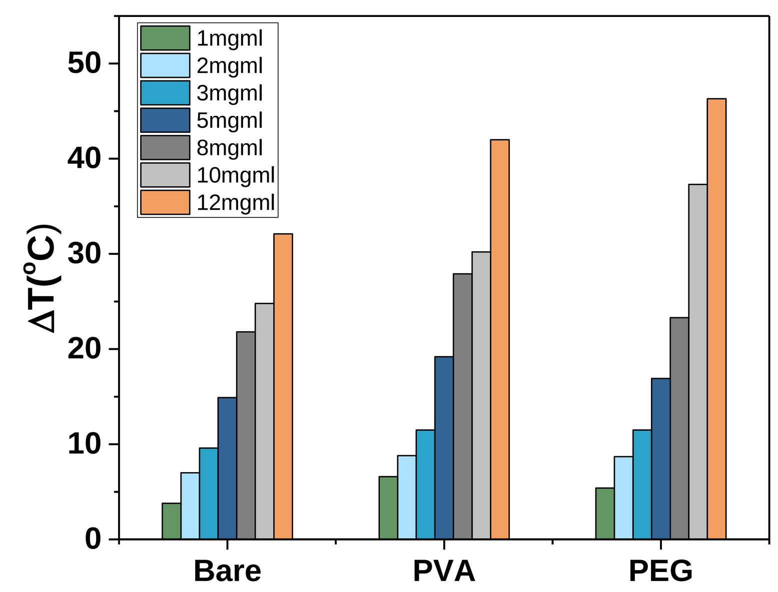

ϕ(mg/ml)	ΔT (ºC) (t = 300 s)			SAR (W/g)		
	Bare	Fe_3O_4@PVA	Fe_3O_4@PEG	Bare	Fe_3O_4@PVA	Fe_3O_4@PEG
1	3.8	6.6	5.4	55.74	83.60	83.60
2	7.0	8.8	8.7	69.61	62.65	111.38
3	9.6	11.5	11.5	60.28	88.10	97.37
5	14.9	19.2	16.9	63.88	66.66	77.77
8	21.8	27.9	23.3	53.67	74.45	72.72
10	24.8	30.2	37.3	55.31	69.14	82.58
12	32.1	42.0	46.3	59.82	98.93	93.18

Higher temperature increases and improved SAR values are observed in polymer functionalized MNPs. In addition, the SAR values obtained are much higher than in the $Fe_3O_4@SiO_2$ MNPs, showing the relevance of the organic coatings in magnetic hyperthermia.

Conclusion: In this work, the effects of different SiO_2 (inorganic) and polymer (organic) coatings in magnetic hyperthermia processes on Fe_3O_4 MNPs have been studied. It has been observed that the SiO_2 shell despite being suitable for reducing interactions between MNPs, however, negatively affects magnetic hyperthermia processes due to its poor thermal conductivity (SAR_{max} = 32.97 W/g). On the other hand, organic coatings (PEG, PVA) have been shown to improve heat generation in magnetic hyperthermia compared to bare Fe_3O_4. It has been observed how all MNPs reach the 47ºC necessary for the thermal ablation of cancer cells. In addition, higher SAR values have been observed than in $Fe_3O_4@SiO_2$ MNPs: SAR_{max} = 69.61 W/g for Fe_3O_4 MNPs, SAR_{max} = 98.93 W/g for Fe_3O_4@PVA and SAR_{max} = 111.38 W/g for Fe_3O_4@PEG.

This work was supported by the European Commission under the BOW project (FETPROACT-EIC-05-2019, Grant 952183) and partially supported by the Spanish Ministry of Science and Innovation (PID2020-112626RB-C21), Modalities «Research Challenges» and «Knowledge Generation» and the Regional Consellería de Innovación Program for the Grupos de Referencia Competitiva 2021 – GRC2021 of Xunta de Galicia.

5th Young Researchers in Magnetism 2021

Low temperature magnetic force microsocopy characterization of adjustable 3D ferrimagnetic multilayers based on NdCo+GdCo trilayers

Rodriguez-Rodriguez, G.*,[1], Hermosa-Muñoz, J.[2,3], Hierro-Rodriguez, A.[2,3], Delgado-Garcia, R.[1], Martín, JI [2,3], Quiros, C [2,3], Velez, M.[2,3], Colino Garcia, J.M.[1]

[1] INAMOL y Depto. de Física Aplicada, Universidad de Castilla-La Mancha, Campus de la Fábrica de Armas, Avd. Carlos III s/n, 45071, Toledo

[2] Depto. Física, Universidad de Oviedo, 33007 Oviedo, Spain

[3] CINN (CSIC – Universidad de Oviedo), 33940 El Entrego, Spain.

* gabriel.rrodriguez@uclm.es

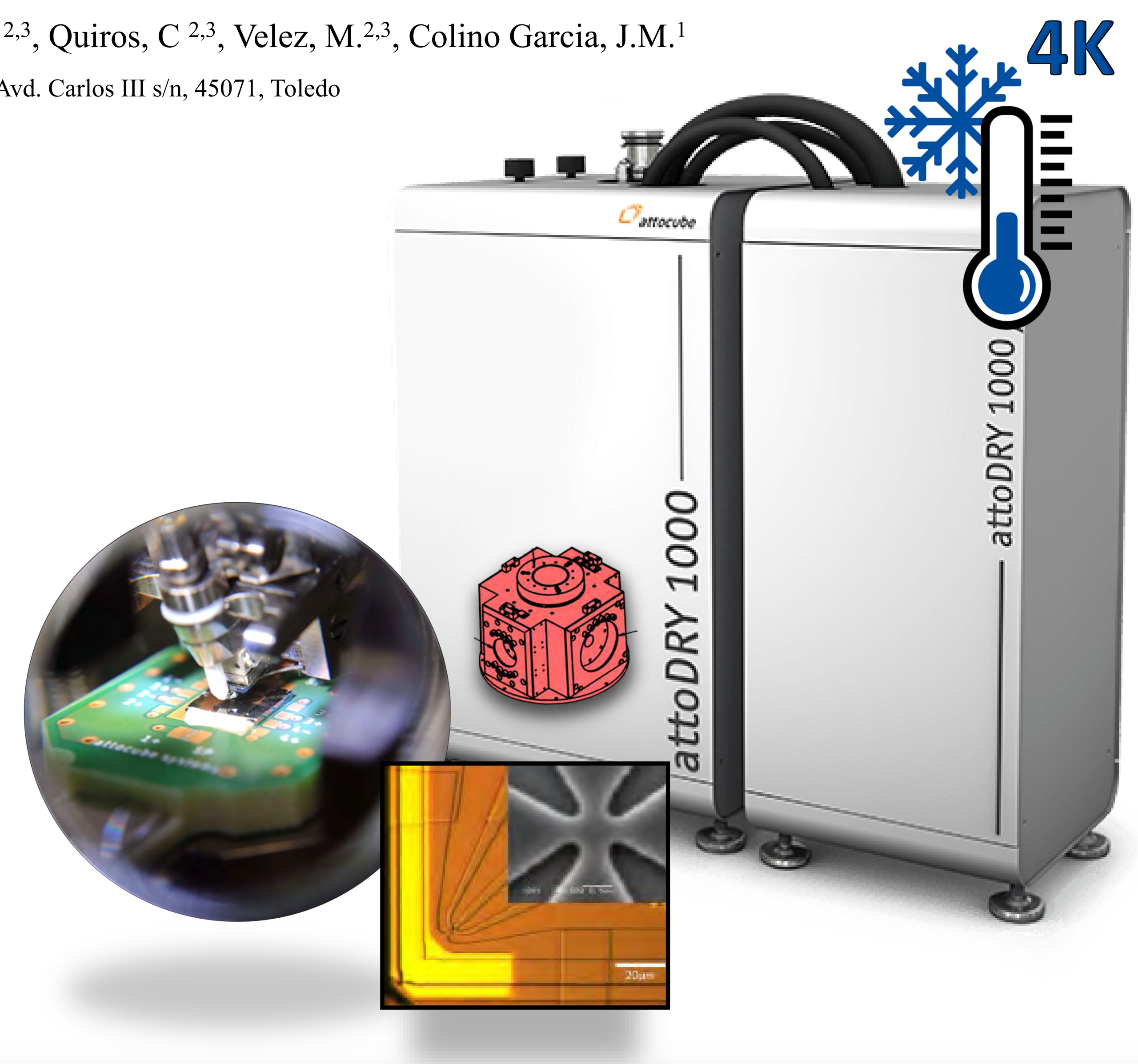

Multilayered systems allow us to tune the desired magnetic behavior of the entire structure by precisely adjusting material properties, thicknesses, and magnetic interactions such as exchange and magnetostatics for the involved materials. This capability is extremely useful to build advanced spintronic devices or magnetic recording media. Ferrimagnetic materials such as Gd-Co alloys exhibit adjustable magnetization, offering the possibility of controlling features such as spin-wave modes, skyrmion nucleation or fast domain wall motion [2]. In addition, temperature dependence of all these properties increases the interest of this kind of systems.

A GdCo/NdCo/GdCo trilayered system has been designed to support an exchange spring at the top layer as ferrimagnetic GdCo alloys present a soft magnetic behavior with weak PMA [2] [Figure 1], so the middle NdCo layer with its high anisotropy (one order of magnitude larger than GdCo layer) can create a pattern of stripe domains with alternating up-down magnetization orientation, that can be used to control the configuration in the neighbouring GdCo layers via interfacial exchange and magnetostatic interactions.

Low temperature MFM under variable field shows the results of the anisotropy, exchange and magnetostatic interactions across the entire GdCo/NdCo/GdCo trilayer: Stripe pattern reconfiguration along the entire hysteresis loop (mainly induced by the NdCo mid-layer) and the collapse of the top PMA stripe pattern above B_z=800mT.

Macroscopic sample characterization

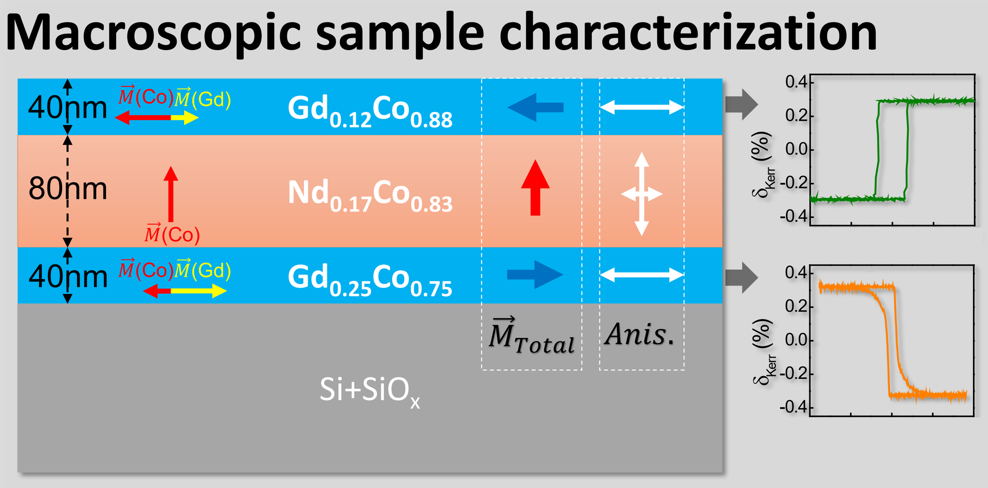

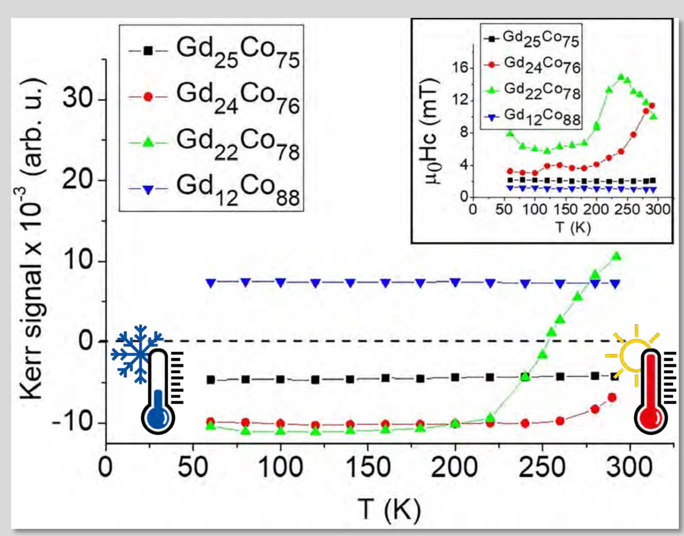

Hybrid Ferri/Ferromagnetic samples, macroscopic magnetic behavior (hysteresis loops) and thermal behavior (H_c and M_s) of the ferrimagnetic layer (GdCo) for several stoichiometric ratios.

Experimental system

Closed circuit He cryostat

- **4K + Sample heater**
- Low noise, **optimized for SPM**
  - AFM/**MFM**
  - SHPM: Scanning Hall Probe Microscopy
- Magnetotransport
  - Up to 8 extra custom channels

3D Vector magnet

- XY plane= 2T
- Z= 5T

Sample conditioning and characterization

- Nanosensors PPP-MFMR tip @76kHz
- Same free oscillation amplitude for each field.
- Initial sample demagnetization at 4K

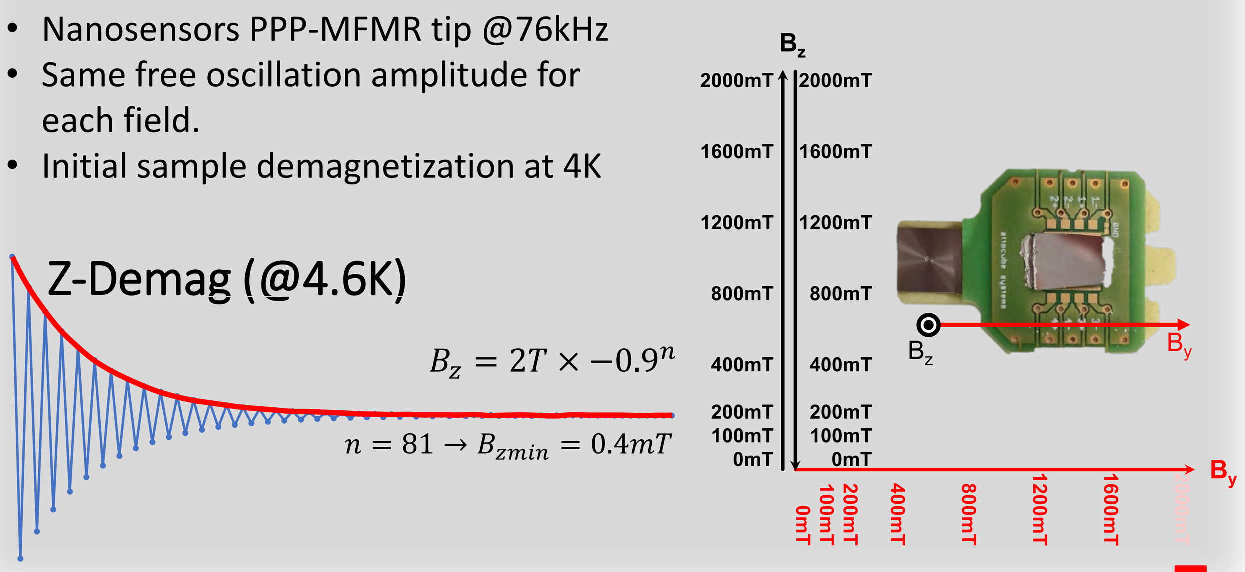

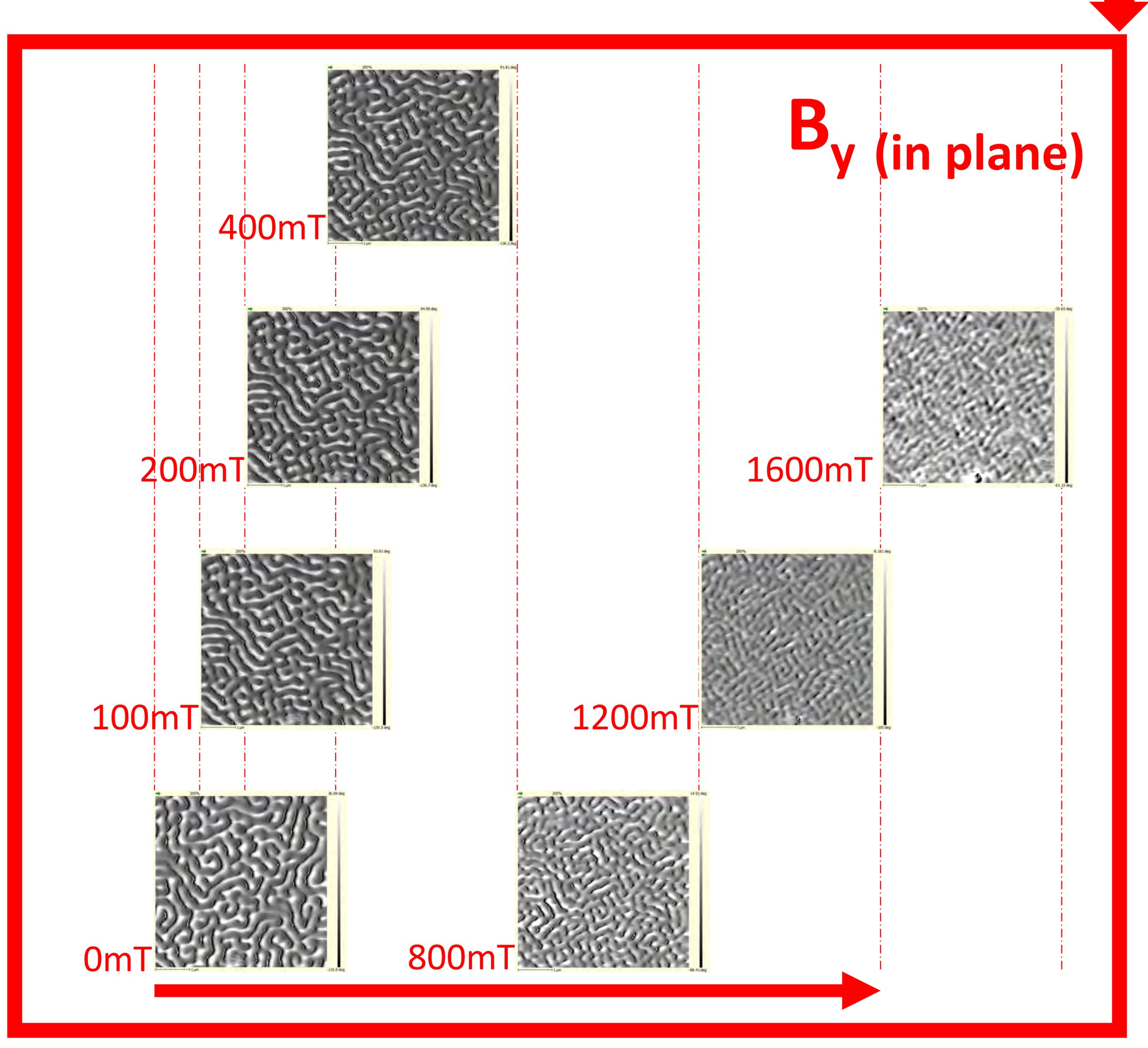

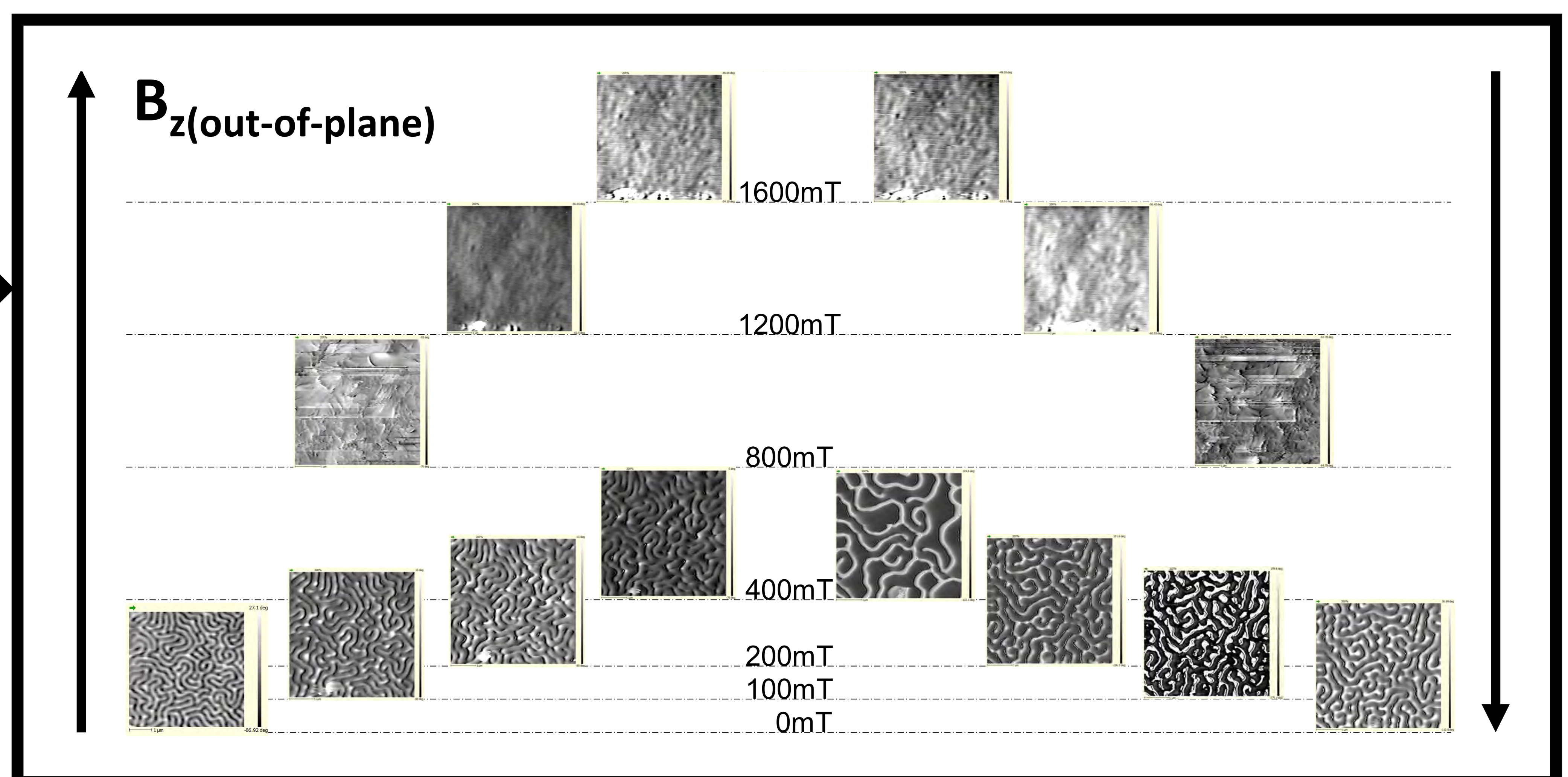

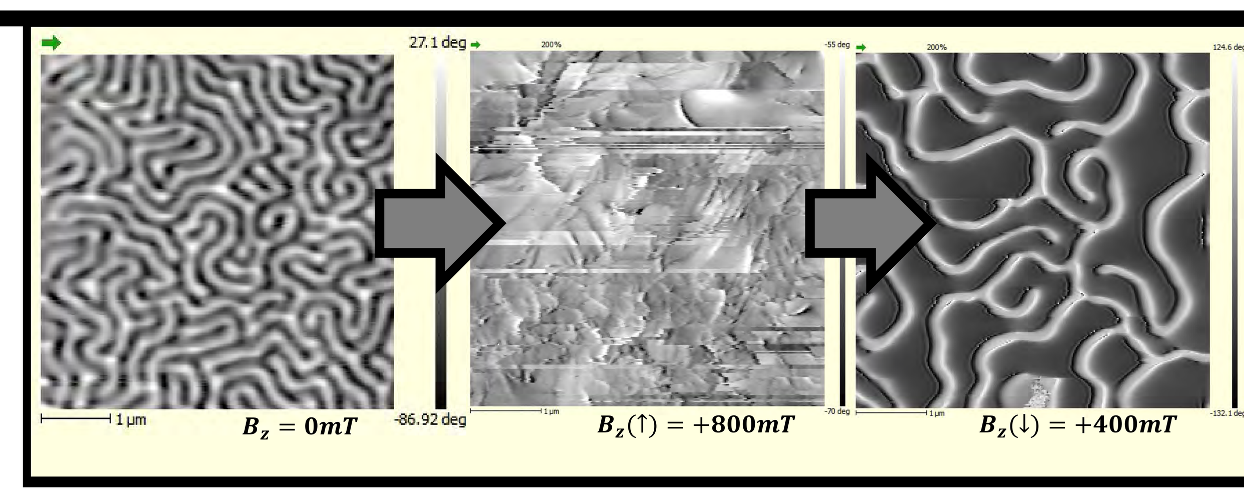

Conclusions

- MFM measurements at 4K and external applied field achieved.
- Stripe domains associated to NdCo's PMA persist even at large in-plane fields along the easy GdCo magnetization axis.
- In the out-of-plane direction, once NdCo reaches saturation at 800mT, the system adopts an in-plane GdCo-driven behavior. Beyond 1.2T magnetization seems to be fully saturated.

References

1. Hermosa-Muñoz, J., et. Al., Adjustable 3D magnetic configuration in ferrimagnetic multilayers with competing interactions visualized by soft X-ray vector tomography, *Condensed Matter Materials Science*, University of Cornell (2021), arXiv:2109.04064 [cond-mat.mtrl-sci] https://arxiv.org/abs/2109.04064v1
2. J. Hermosa et Al. Magnetic textures and singularities in ferri/ferromagnetic multilayers, *Journal of Magnetism and magnetic materials*, **Vol. 539**, 168384 (2021); https://doi.org/10.1016/j.jmmm.2021.168384
3. Hierro-Rodriguez, A et Al. Fabrication and magnetic properties of nanostructured amorphous Nd-Co films with lateral modulation of magnetic stripe period. *J. Phys. D: Appl. Phys.* **46** 345001 (2013) https://doi.org/10.1088/0022-3727/46/34/345001

Acknowledgements

This work has been supported by Spanish MICINN under ref: PID2019-104604RB/AEI/10.13039/501100011033.

Rafael Delgado Garcia thanks the UCLM and the Diputación de Toledo for his research grant.

INSTITUT JEAN LAMOUR

www.ijl.univ-lorraine.fr

Spin-charge interconversion in 111-oriented epitaxial Pt thin films

Anadón, Alberto[1], Gudín, Adrián[2], Arnay, Iciar[2], Guerrero, Ruben[2], Petit-Watelot, Sebastien[1], Camarero, Julio[2,3], Perna, Paolo[2], Rojas-Sanchez, Juan-Carlos[1]

1 *Institut Jean Lamour, Nancy, France* 2 *IMDEA nanociencia, Madrid, Spain.* 3 *DFMC, Instituto "Nicolás Cabrera" & IFIMAC, Universidad Autónoma de Madrid, Madrid, Spain.*

Objective: More efficient devices.

MRAM devices (SOT-MRAM)

- CMOS-compatible
- Very large endurance (> $5x10^{10}$)
- Non-volatile and very energy efficient
- Ultra-fast switching

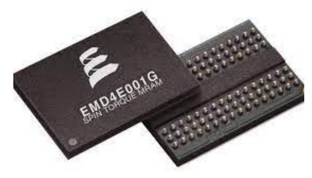

Spin-based computing: Spin logic and Nanooscillators

- Spin torque nano oscillators and spin neural networks
- New possibilities of mimicking "neural" functionalities with much lower area and energy

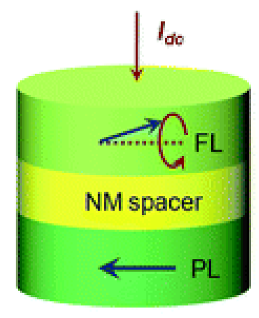

Direct conversion: SHE

$$J_s \propto \theta_{SH}(J_c \times \hat{m})$$

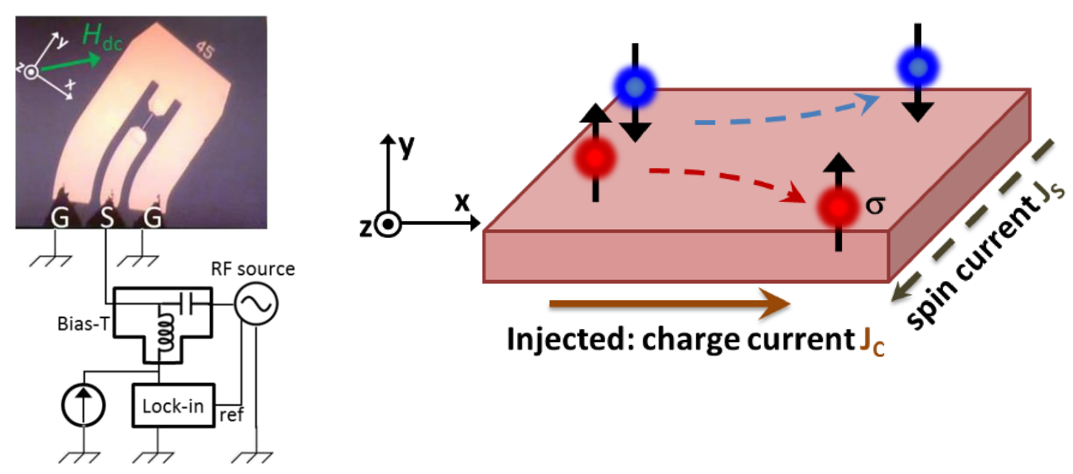

Inverse conversion: ISHE

$$J_c \propto \theta_{SH}(J_s \times \hat{\sigma})$$

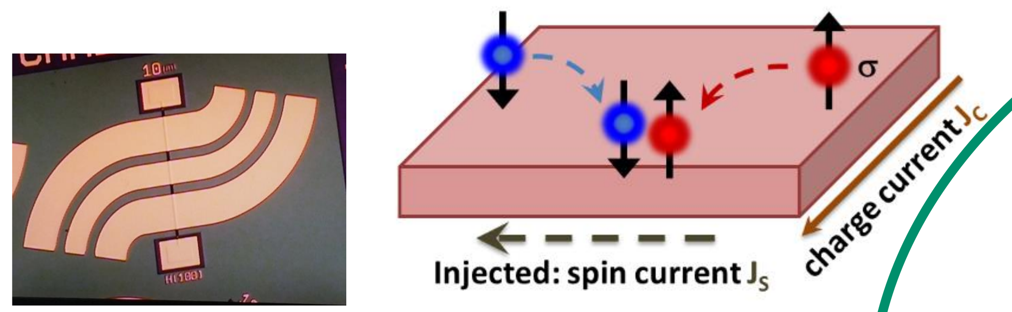

Epitaxial Al_2O_3//Pt/Co/AlO_x

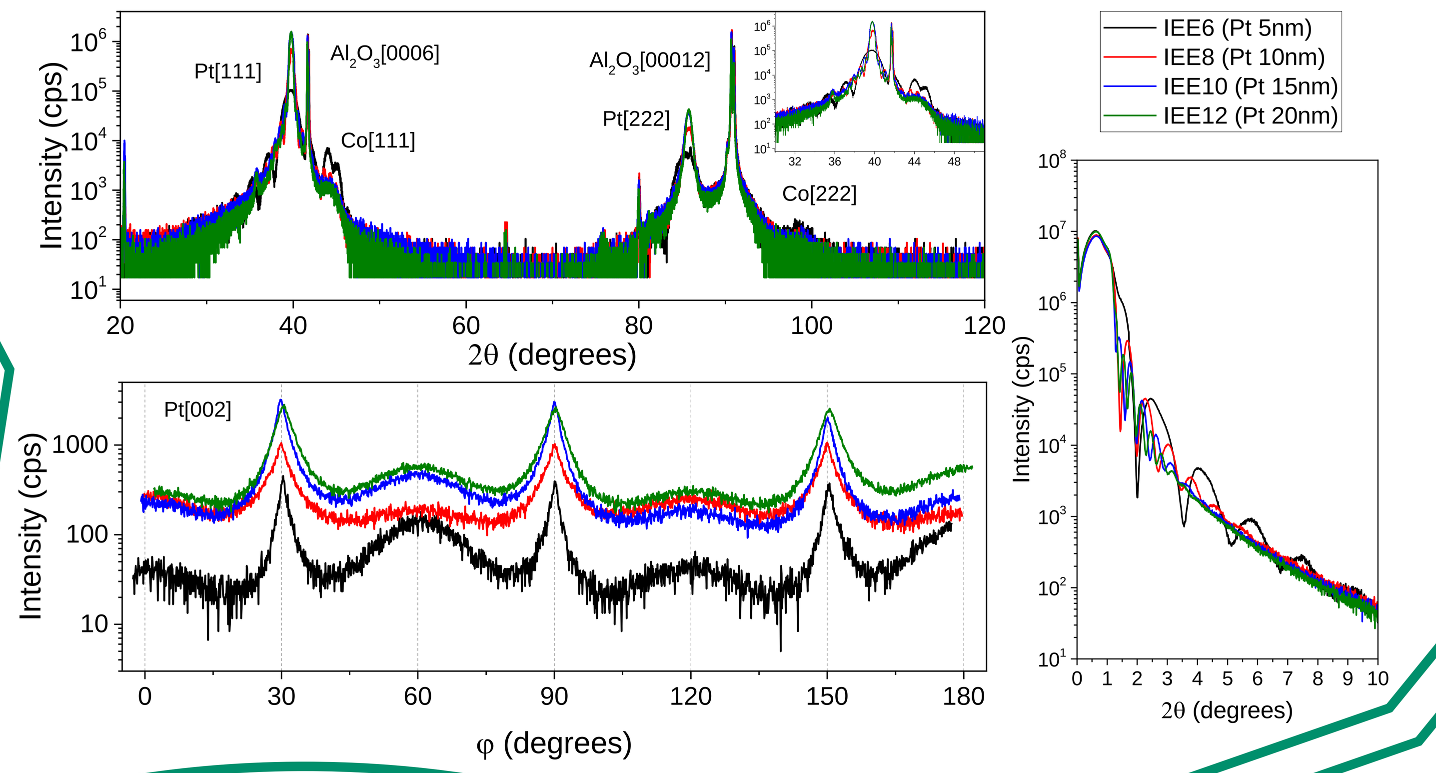

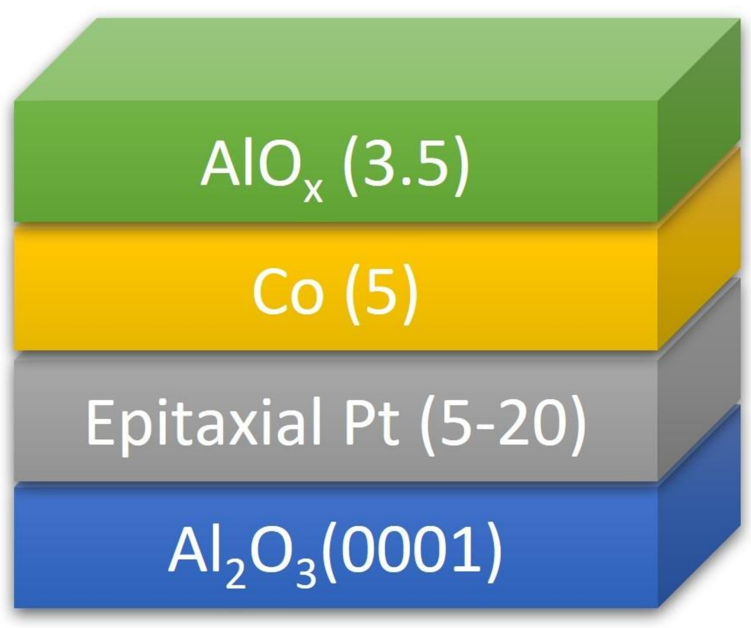

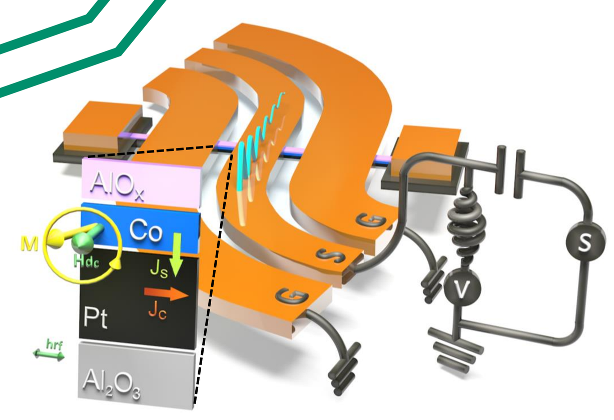

Spin-pumping FMR

- Spin-to-charge current conversion due to spin-orbit couping at FMR condition

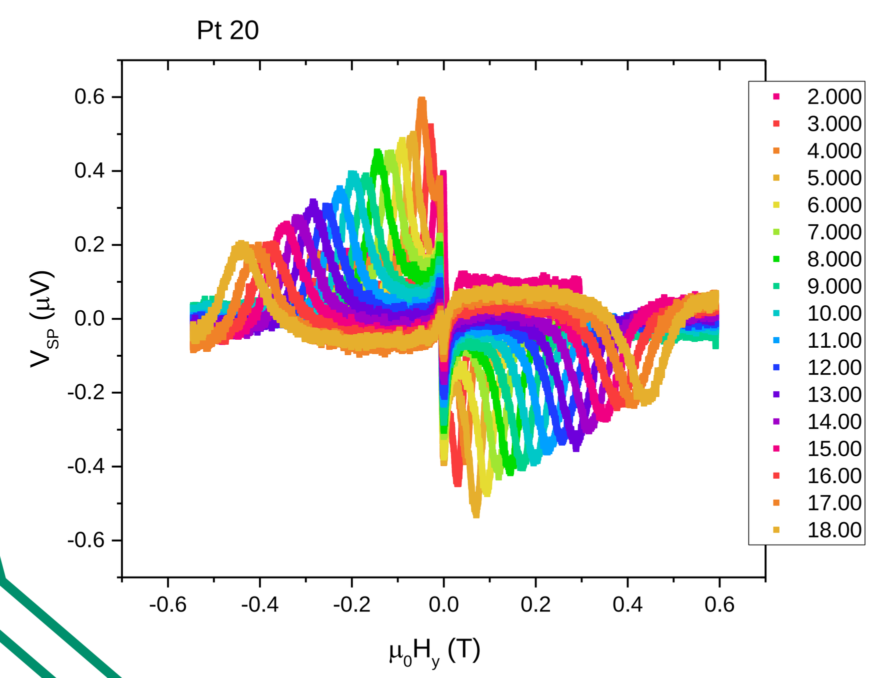

Spin-torque FMR

- Charge-to-spin current current conversion due to spin-orbit coupling at FMR condition

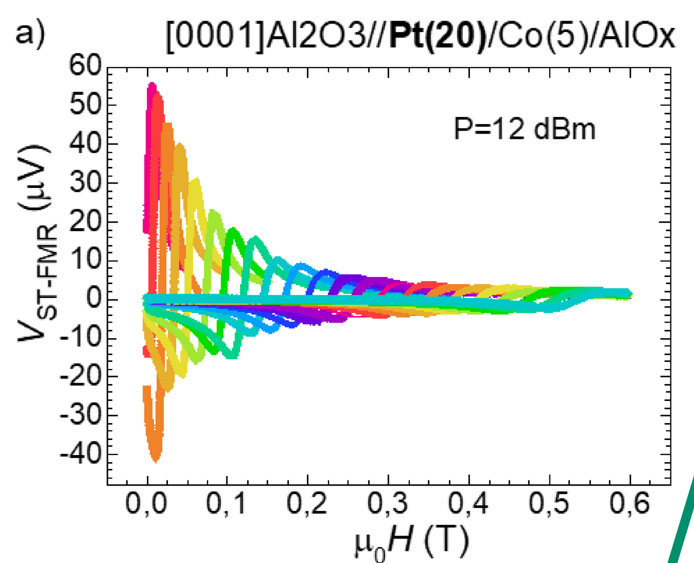

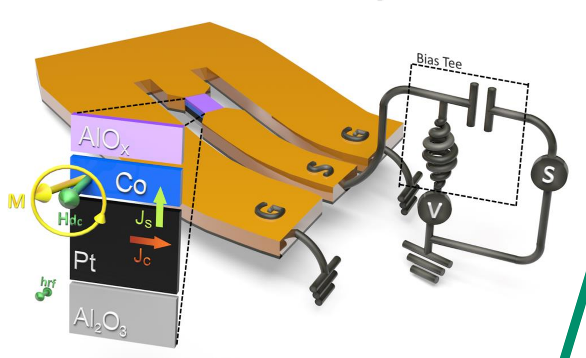

Spin Seebeck effect

- Spin-to-charge current conversion due to spin-orbit coupling at the HM from the thermal spin current

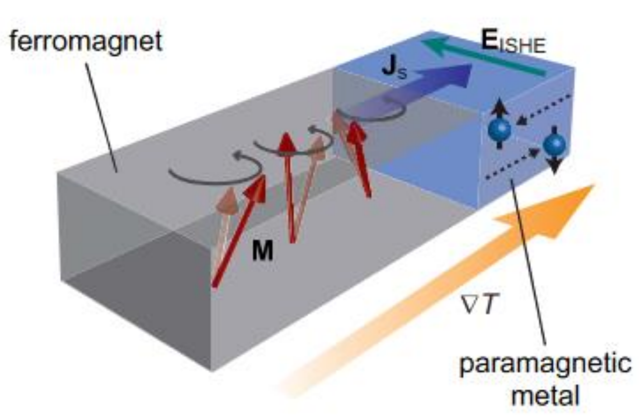

Journal of Applied Physics **111**, 103903 (2012)

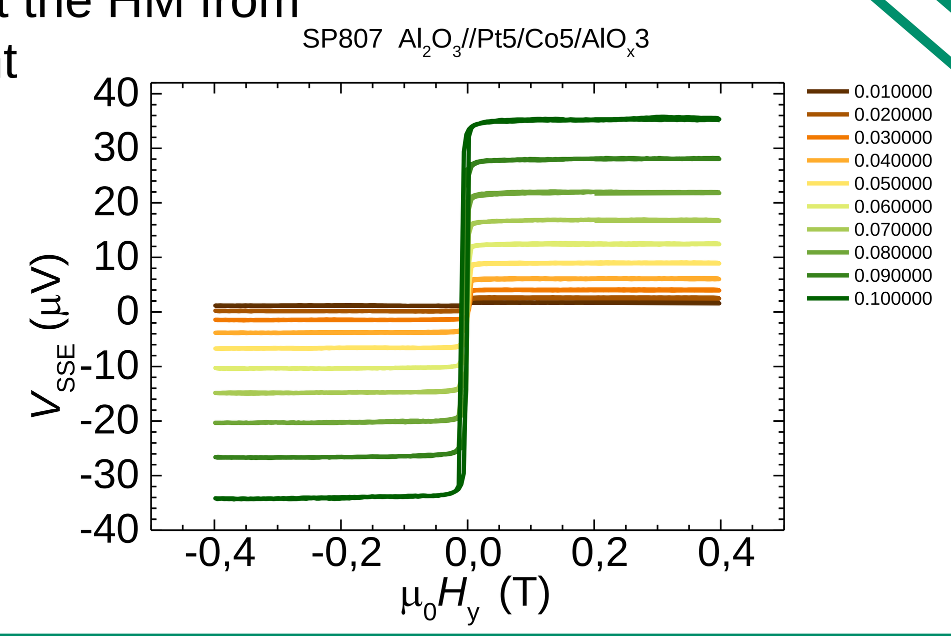

Summary

- Different results in literature present different conclusions for the spin coversion in epitaxial Pt as a function of the crystallographic direction.
- We have prepared epitaxial Al_2O_3//Pt/Co/AlO_x stacks with varying Pt thickness between 5 and 20 nm.
- We have estimated the spin conversion in the system by means of three different techniques for two different directions in all the samples.

Related recent publications:

[1] 1. Thompson, R. et al Phys. Rev. Appl. 15, 1 (2021). https://doi.org/10.1103/PhysRevApplied.15.014055

[2] **A. Anadón** et al. APL Materials, **9**(6), 061113 (2021). https://doi.org/10.1063/5.0048612

*alberto.anadon@univ-lorraine.fr

FUN-SOC:FEST
Project: TOPTRONIC Topological spin-orbitronics

SCAN ME

INSTITUT JEAN LAMOUR

www.ijl.univ-lorraine.fr

CNRS UNIVERSITÉ DE LORRAINE

Spin current generation from incoherent magnon excitation in the multifunctional ferrimagnet $Ga_{0.6}Fe_{1.4}O_3$

Alberto Anadon[1*], Elodie Martin[1], Suvidyakumar Homkar[2], Benjamin Meunier[2], Heloise Damas[1], Christophe Lefevre[2], Francois Roulland[2], Carsten Dubs[3], Olivier Copie[1], Rafael Ramos[4], Daniele Preziosi[2], Sébastien Petit-Watelot[1], Nathalie Viart[2], and Carlos Rojas-Sanchez[1]

1 Institut Jean Lamour, Nancy, France, France. 2 IPCMS, Strasbourg, France. 3 INNOVENT e.V. Technologieentwicklung, Jena, Germany. 4 CIQUS, Departamento de Química-Física, Universidade de Santiago de Compostela, Spain

Objective: Efficient energy Harvesting with multifunctional properties

Efficient spin current generation

- Ferromagnetic insulators for ultra low energy applications
- High spin current generation for efficient MRAMs
  - Non-volatile and very energy efficient
  - Ultra-fast switching

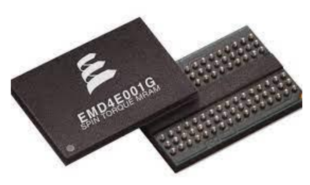

Spin-based Energy Harvesting

- Based on Thermo-spin phenomena like the Spin Seebeck effect
- New possibilities on condensed matter devices to take advantage of heat with no moving parts and high efficiency
- Multiple material functionalities could bring new possibilities in device design

Thermo-spin effects

Spin Seebeck effect (SSE)

- Thermal spin current generation ($\mathbf{J_s} \propto \nabla T$)
- Inverse spin Hall effect

$$J_c \propto \theta_{SH}(J_s \times \hat{\sigma})$$

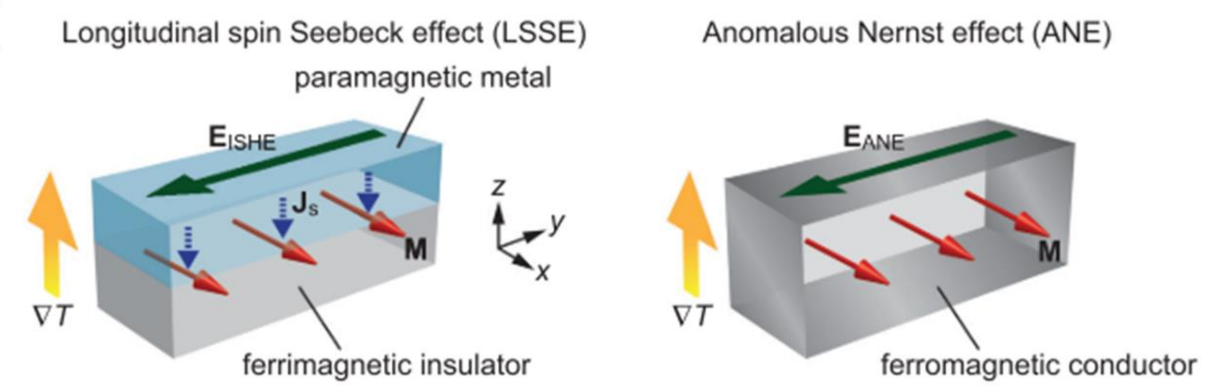

Ken-ichi UCHIDA. Proc. Jpn. Acad., Ser. B 97 (2021)

Anomalous Nernst effect (ANE)

- field pointing in-plane of sample stage
- fields up to 0.7 T applicable

$$E_{ANE} \propto (\boldsymbol{M} \times \nabla T)$$

$Ga_{0.6}Fe_{1.4}O_3$, a multifunctional material

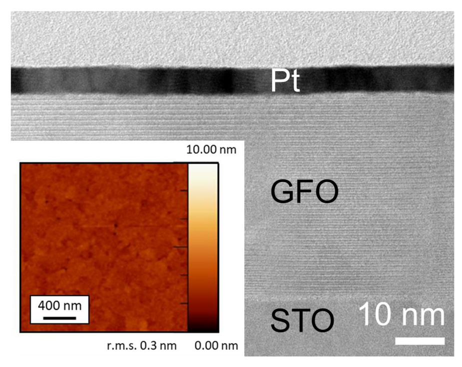

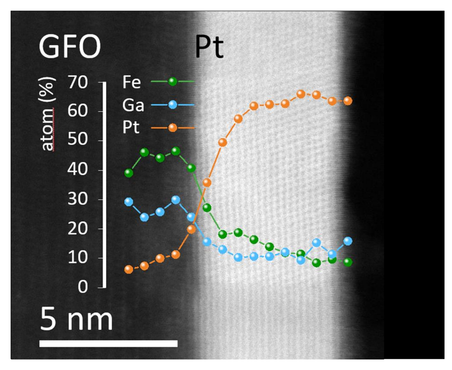

- Low interfacial
- no interdiffusion
- GFO is oriented along its [001] and Pt [111]
- Layer by layer (Laue)

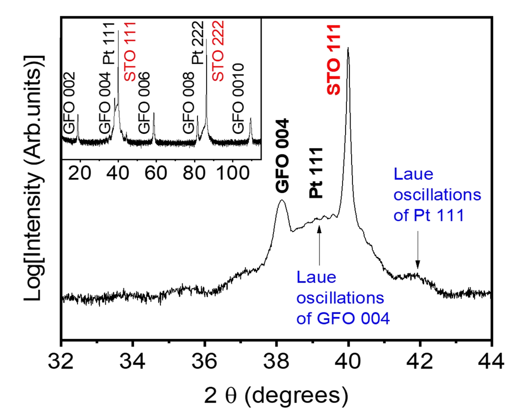

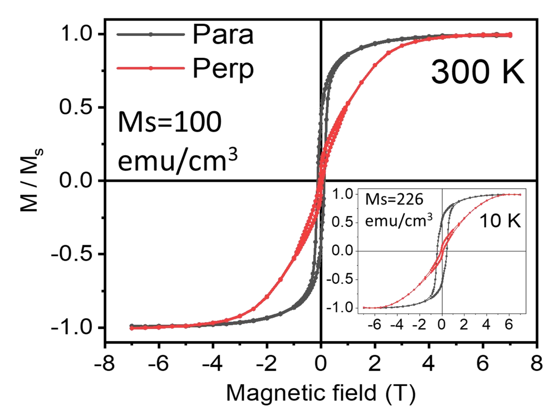

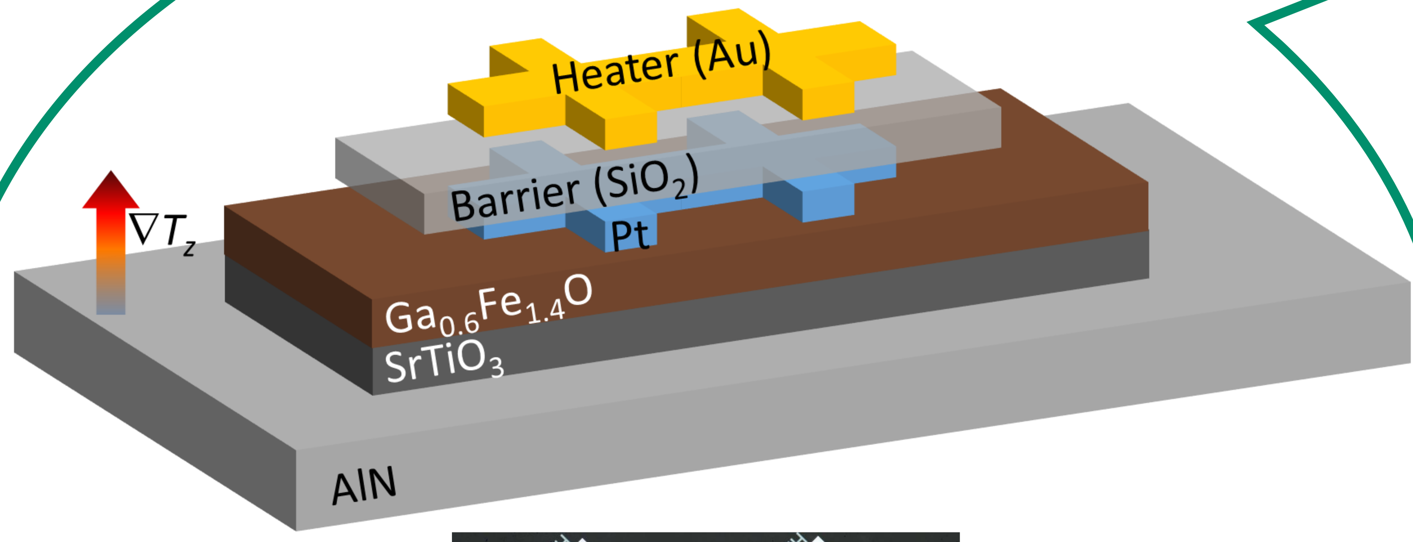

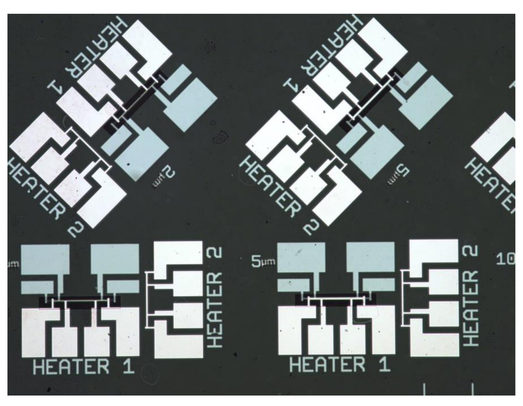

Spin current generation in GFO

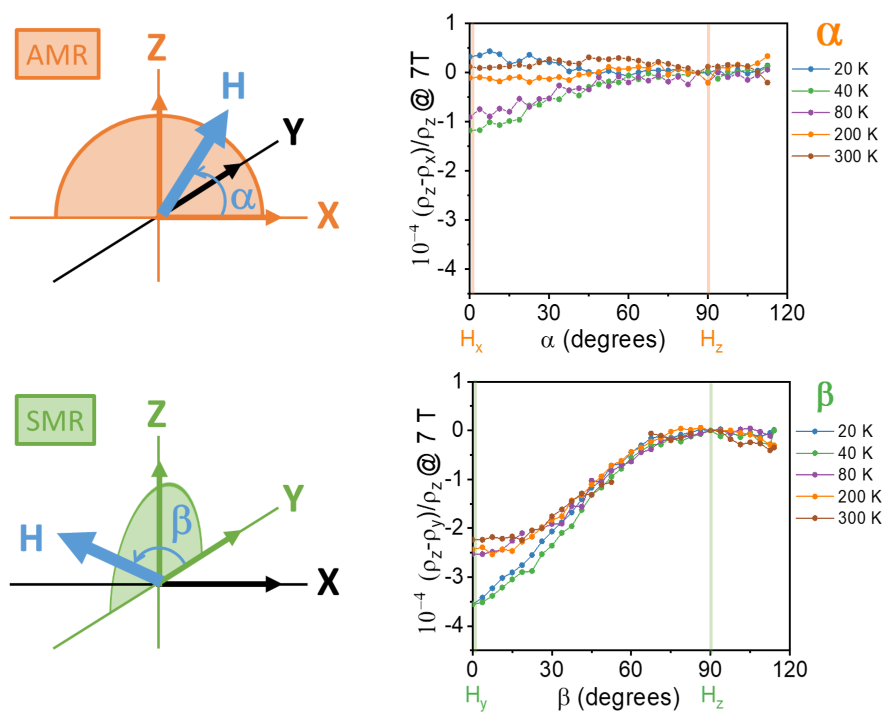

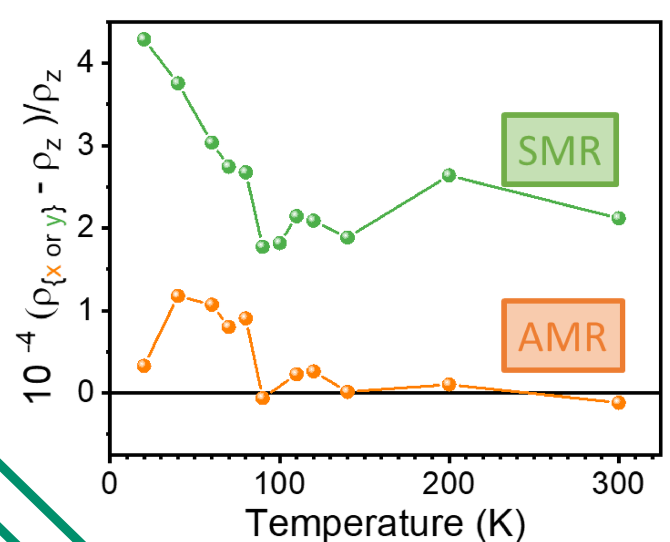

Similar magnitude than YIG/Pt and YIG/Pd

ACS Appl. Electron. Mater. 2021, 3, 10, 4433–4440

Parameters estimation

Temperature calibration

Pt temperature

Heater temperature

$R_{Pt}(T) \rightarrow \alpha_{Pt} = 1.77 \cdot 10^{-3}\ K^{-1}$ $R_{Au}(T) \rightarrow \alpha_{Au} = 1.28 \cdot 10^{-3}\ K^{-1}$

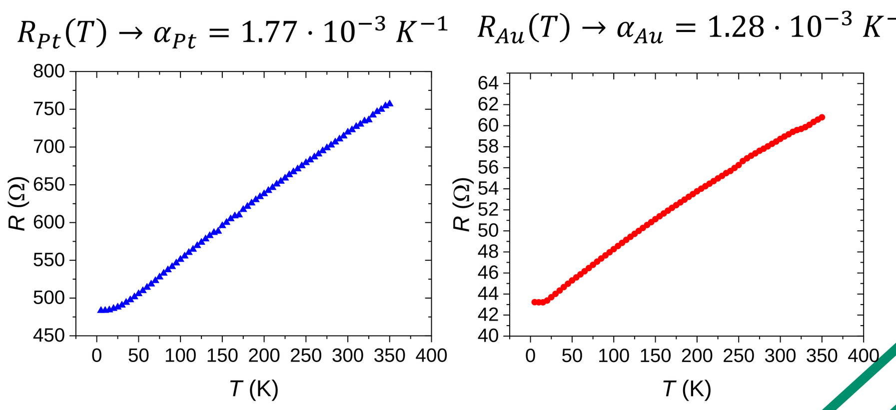

Estimation of temperature profile in the system

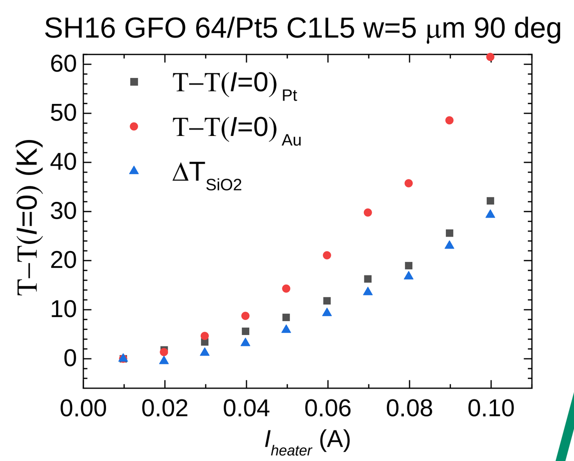

Benchmarking: Comparison with YIG/Pt

YIG

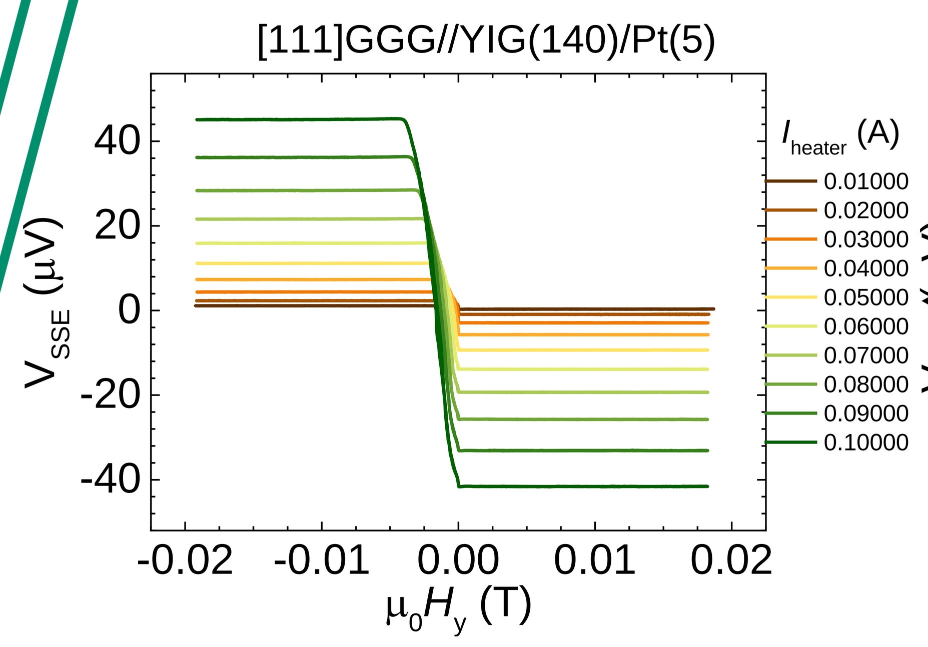

GFO

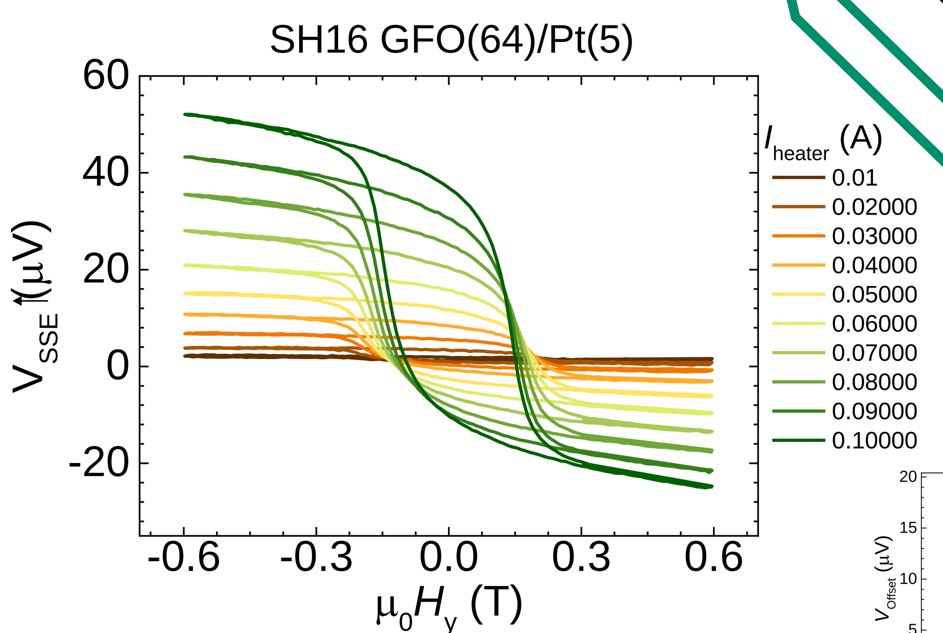

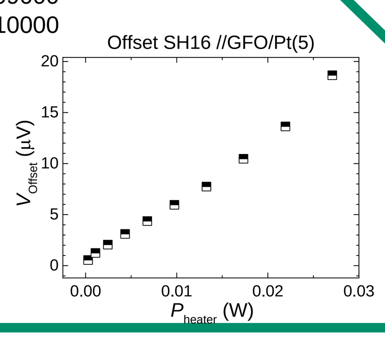

Similar magnitude than YIG/Pt, but offset dependence on temperature gradient

Related recent publications:

[1] S. Homkar, **A. Anadón**, et al ACS Applied Electronic Materials **3** (10), 4433-4440 2021 https://doi.org/10.1021/acsaelm.1c00586

[2] **A. Anadón** et al. APL Materials, **9**(6), 061113 (2021). https://doi.org/10.1063/5.0048612

*alberto.anadon@univ-lorraine.fr

Project: TOPTRONIC Topological spin-orbitronics

Project: MISSION Magnetoelectric oxides for spin-orbitronics

SCAN ME

From Magnetically Soft to Hard FeNi Nanowires: in the Search of the Cosmological $L1_0$-FeNi Phase

Alonso J. Campos-Hernández*, Ester M. Palmero, Alberto Bollero

Group of Permanent Magnets and Applications, IMDEA Nanoscience, 28049, Madrid, Spain

*alonsojose.campos@imdea.org

Introduction

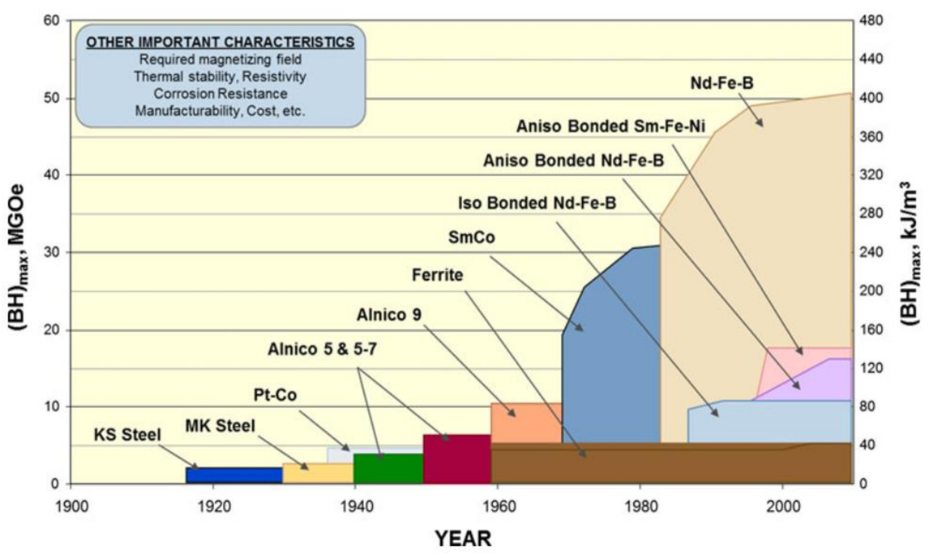

M.J. Kramer et al., *JOM* **64** (2012) 752

Tetrataenite, chemically ordered $L1_0$-FeNi naturally formed only in some meteorites over millions of years in cosmos, is a promising candidate for the substitution of the strongest rare-earth permanent magnets existing nowadays, as it could reach a value of $(BH)_{max}$ of 40 MGOe [1-3].

The synthesis of experimental Fe-Ni model systems (e.g. thin films, nanostructures…) may provide invaluable information towards the artificial synthesis of the $L1_0$-FeNi phase in feasible timescales.

Synthesis

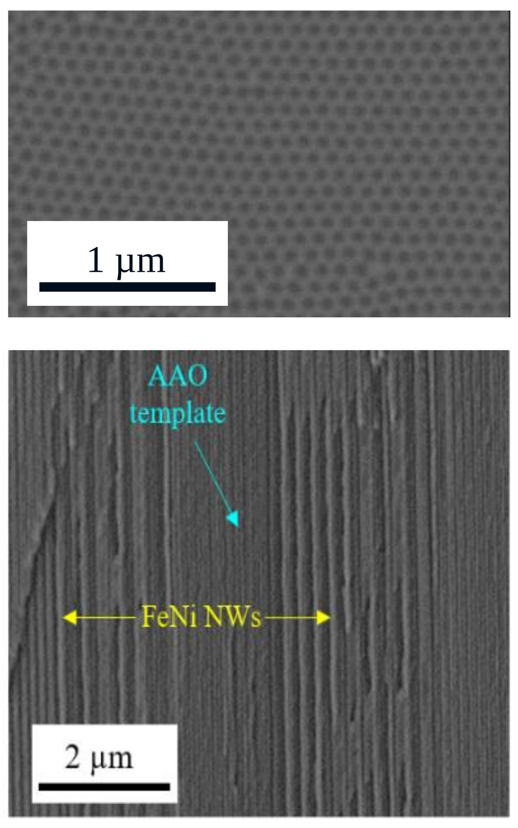

FeNi nanowires (NWs) were synthesized by electrochemical route under variable conditions, to be used as model structures for the study of the Fe-Ni system.

The 40 nm-diameter NWs were synthesized by potentiostatic electrodeposition into anodized aluminum oxide (AAO) templates using three aqueous electrolytes of varying Fe content and electrodeposition potentials, allowing for tailoring the properties of the nanowires.

Compositional and crystallographic structure analysis

- EDX chemical composition analysis of the samples shows an anomalous co-deposition [4], where Fe deposits in ratios higher than its electrolyte molar fraction, varying with both the applied potential and the electrolyte composition.
- XRD measurements show a mixture of *fcc* and *bcc* crystallographic phases.
- Interestingly, the $Fe_{0.51}Ni_{0.49}$ nanowires show biphasic *bcc-fcc* crystallographic structure, while for pure Fe nanowires a *fcc* structure (characteristic of γ-Fe) is observed and the Fe-rich $Fe_{0.80}Ni_{0.20}$ nanowires show a *bcc* crystallographic structure.

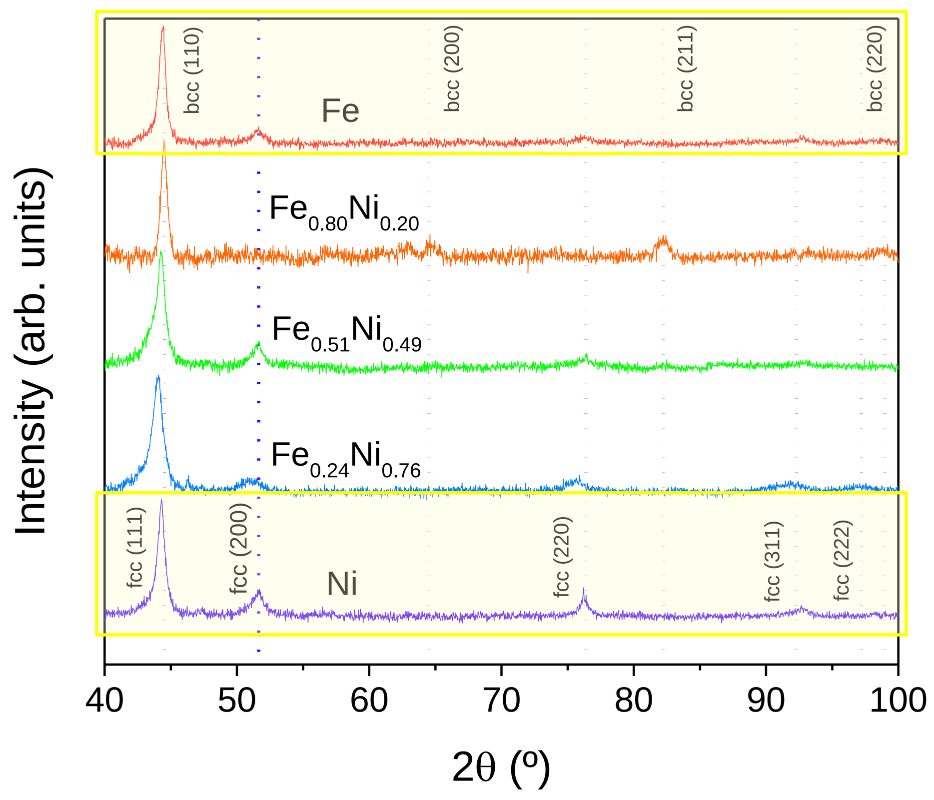

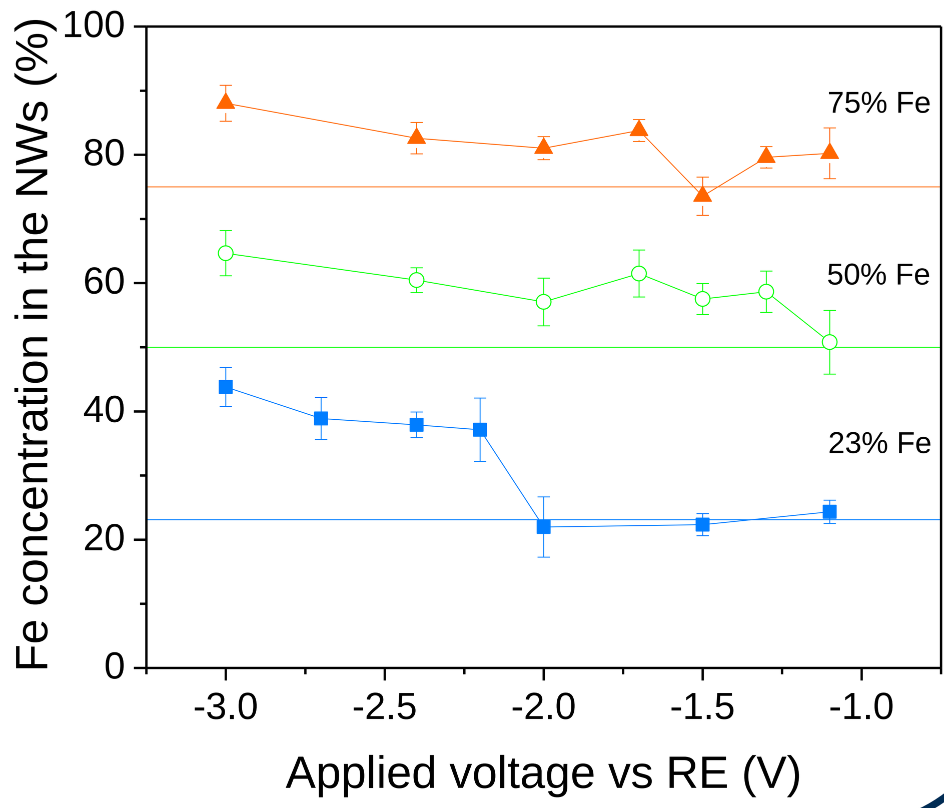

Magnetic characterization

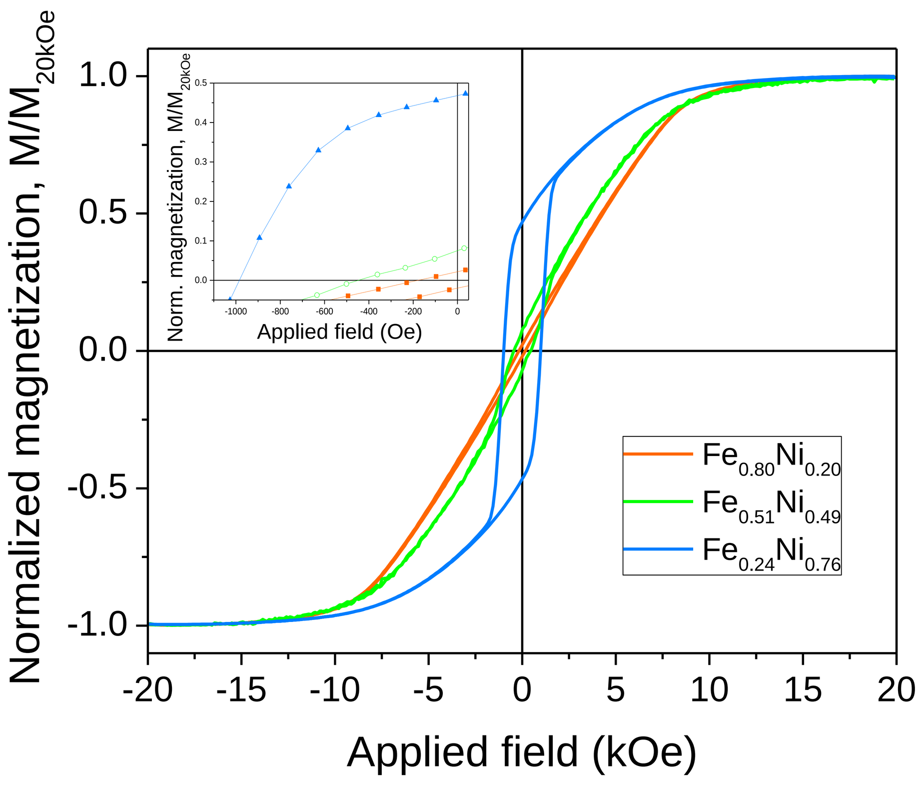

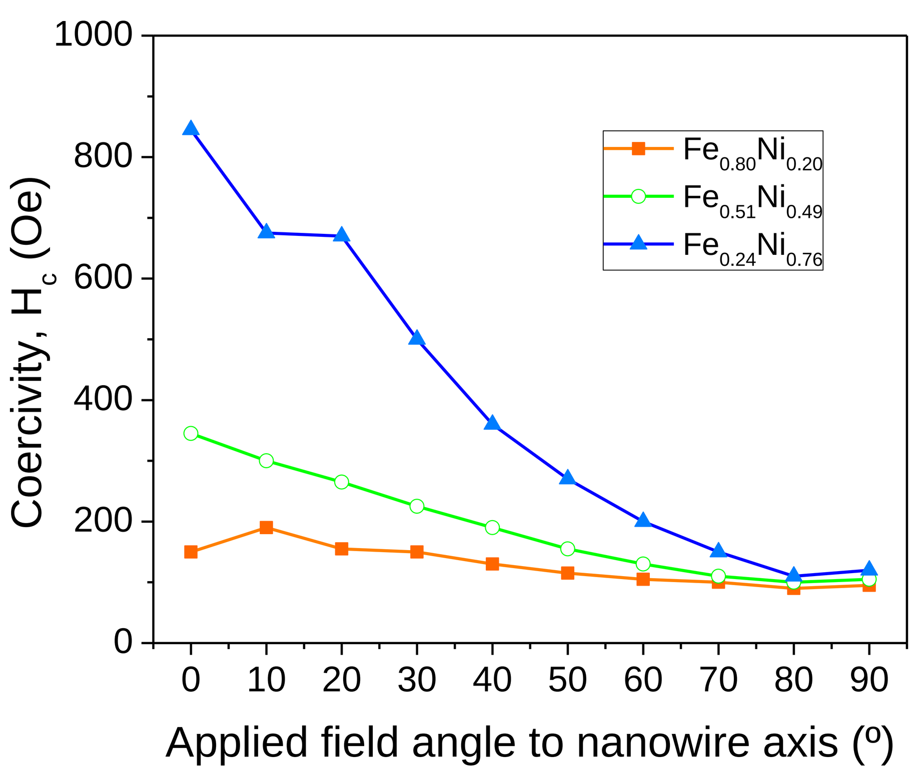

- The hysteresis loops measured at room temperature by VSM show a wide range of coercivities, from 0.1 to almost 1 kOe. The nanowires with the highest coercivity are those corresponding to the non-anomalous region of the $Fe_{23}Ni_{77}$ electrolyte.
- VSM measurements performed by applying the magnetic field at different angles to the nanowires' axis allowed for the determination of the magnetization reversal mechanisms [5].
- All studied arrays of FeNi nanowires show transverse domain wall magnetization reversal with magnetocrystalline anisotropy energy K_u of the order of 10^4 J m^{-3}.

Conclusions

- Arrays of FeNi nanowires proved to be a highly tuneable system with respect to both composition and crystallographic structure, which can be modified by changing the electrolyte stoichiometry and the deposition potential.
- Consequently, a wide range of magnetic hardness can be achieved with a magnetization reversal process via transverse domain wall mechanism.
- Establishment of a proper correlation between composition, crystallographic structure and magnetic properties in FeNi nanowires will provide insight into the possibility of forming the $L1_0$-FeNi phase in this experimental model system and, moreover, will contribute to the future synthesis of the ordered phase in other systems.

Acknowledgements

Authors acknowledge financial support from EU M-ERA.NET and MICINN through the projects *COSMAG* (PCI2020-112143) and *NEXUS* (PID2020-11521RB-C21).
A.J.C.-H. acknowledges support from "La Caixa" Foundation under the Doctoral INPhINIT Incoming program (fellowship reference LCF/BQ/DI20/1178002).

References

[1] L. H. Lewis *et al., J. Phys.: Condens. Matter* **26** (2014) 064213
[2] N. Bordeaux *et al., Acta Mater.* **103** (2016) 608-615
[3] M-ERA.NET Project "COSMAG": www.cosmag.eu
[4] H. Nakano *et al., Mat. Tran.* **45** (2004) 3130-3135
[5] L.G. Vivas *et al.*, *Phys. Rev. B* **85** (2012) 035439

EUROPEAN UNION STRUCTURAL FUNDS · GOBIERNO DE ESPAÑA · MINISTERIO DE CIENCIA, INNOVACIÓN Y UNIVERSIDADES · EXCELENCIA SEVERO OCHOA 2017 - 2021 · Comunidad de Madrid · M-era.Net · COSMAG · "la Caixa" Foundation

Controlling the Self-Assembly of Multicore Iron Oxide Nanoparticles to Enhance Magnetic Properties for Biomedical and Environmental Applications

A. Gallo-Cordova[1]*, J.G. Ovejero[1], S. Veintemillas-Verdaguer[1], P. Tartaj[1], M.P. Morales[1]

[1] Institute of Materials Science of Madrid, ICMM-CSIC, Sor Juana Inés de la Cruz 3, 28049 Madrid, Spain

CSIC CONSEJO SUPERIOR DE INVESTIGACIONES CIENTÍFICAS

YRinM 2021

PURPOSE

The polyol process is a well-known synthesis method in which the media can serve not only as a solvent but also as a reducing agent and surfactant allowing the control of particles growth. With this process it is possible to perform a controlled aggregation of small particles to produce flower-like nanostructures with high magnetic moment per particle. Previous studies on this matter have failed into deepen on the formation mechanism of this kind of structure under synthesis with mixed solvents (POLYOL/AMINE).

AMINE EFFECT

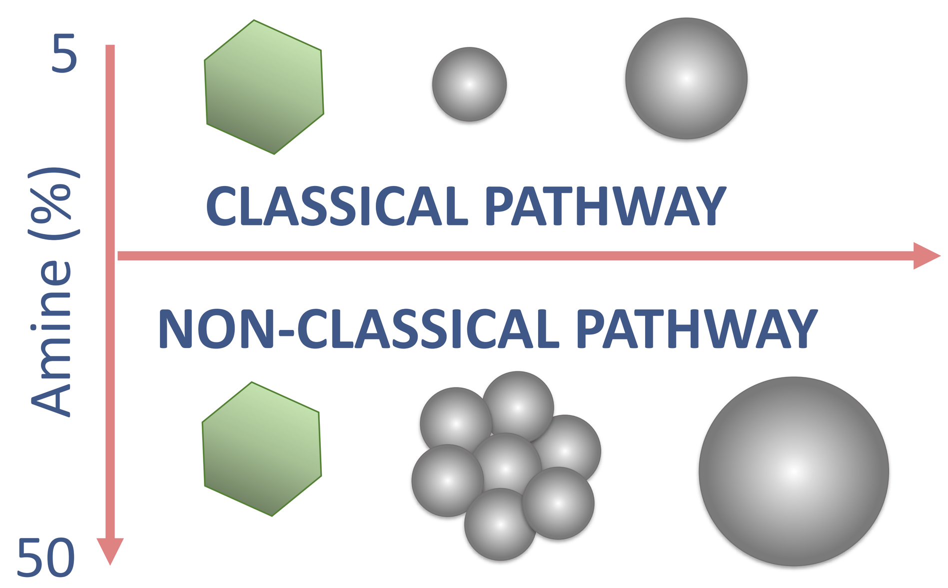

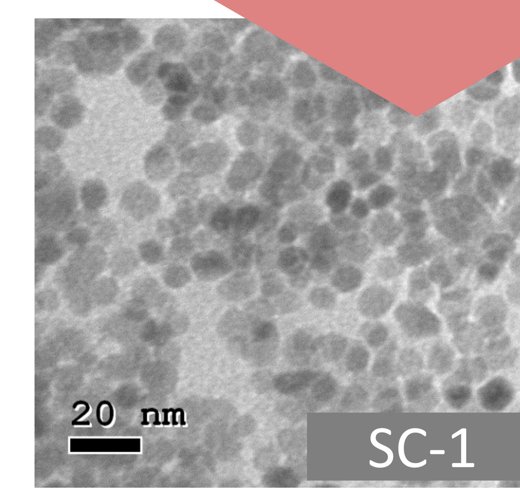

Amine determines the formation mechanism

PROPOSED NON-CLASSICAL MECHANISM

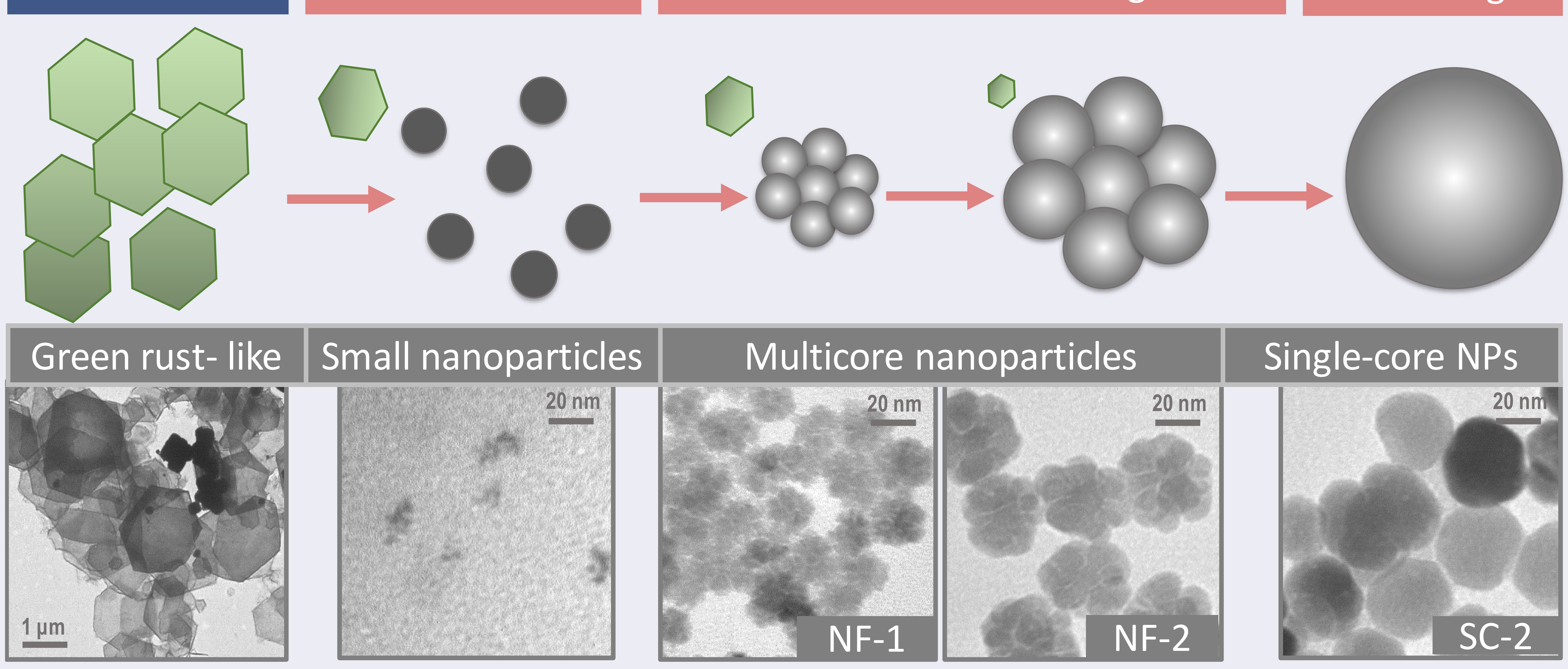

Sample	TEM size (nm)	XRD size (nm)
NF-1	23 ± 5	8.1
NF-2	35 ± 5	20.1
SC-2	31 ± 4	33.5

XRD size matchess TEM size when sintered

ENVIRONMENTAL CATALYSIS

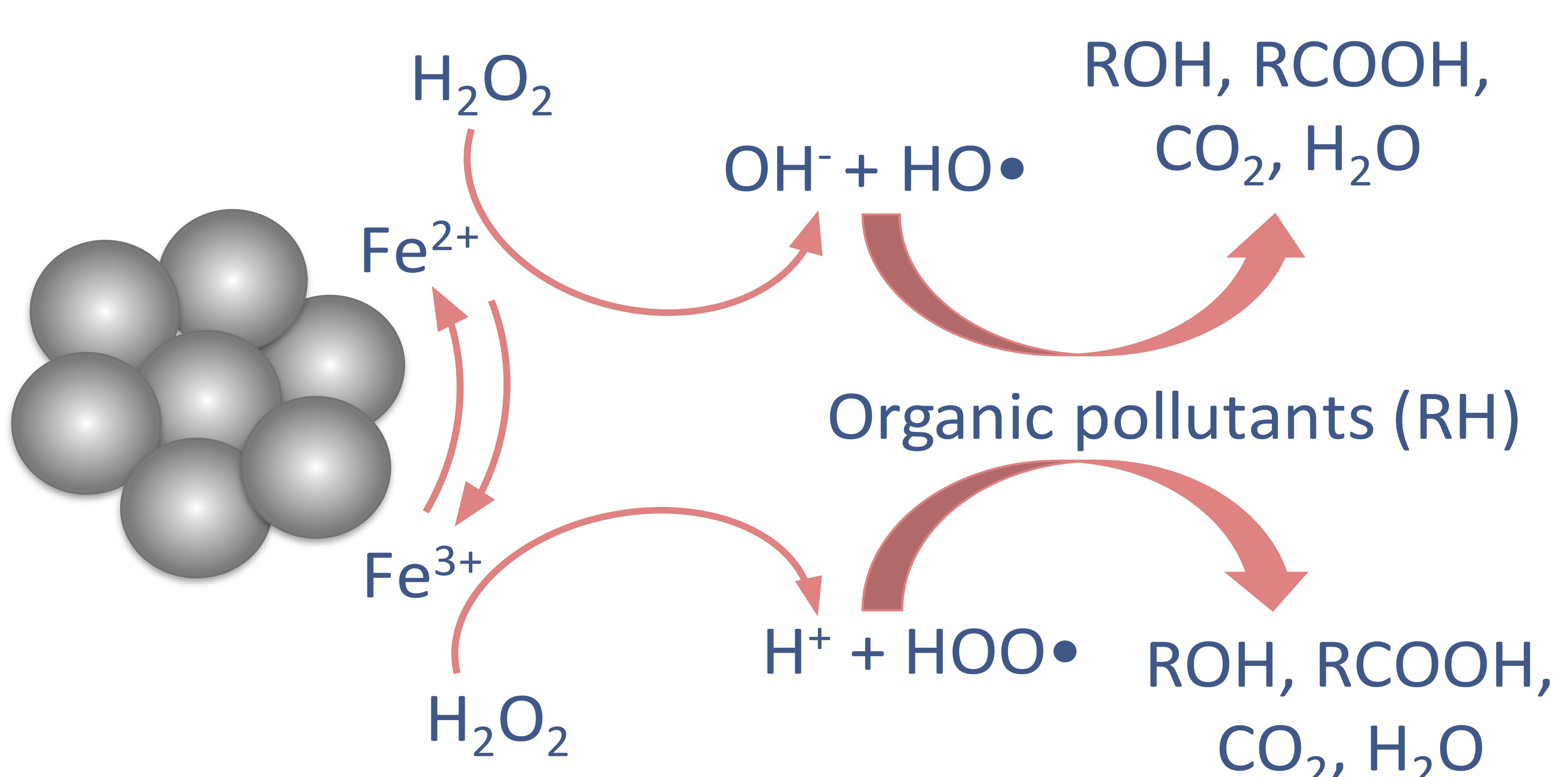

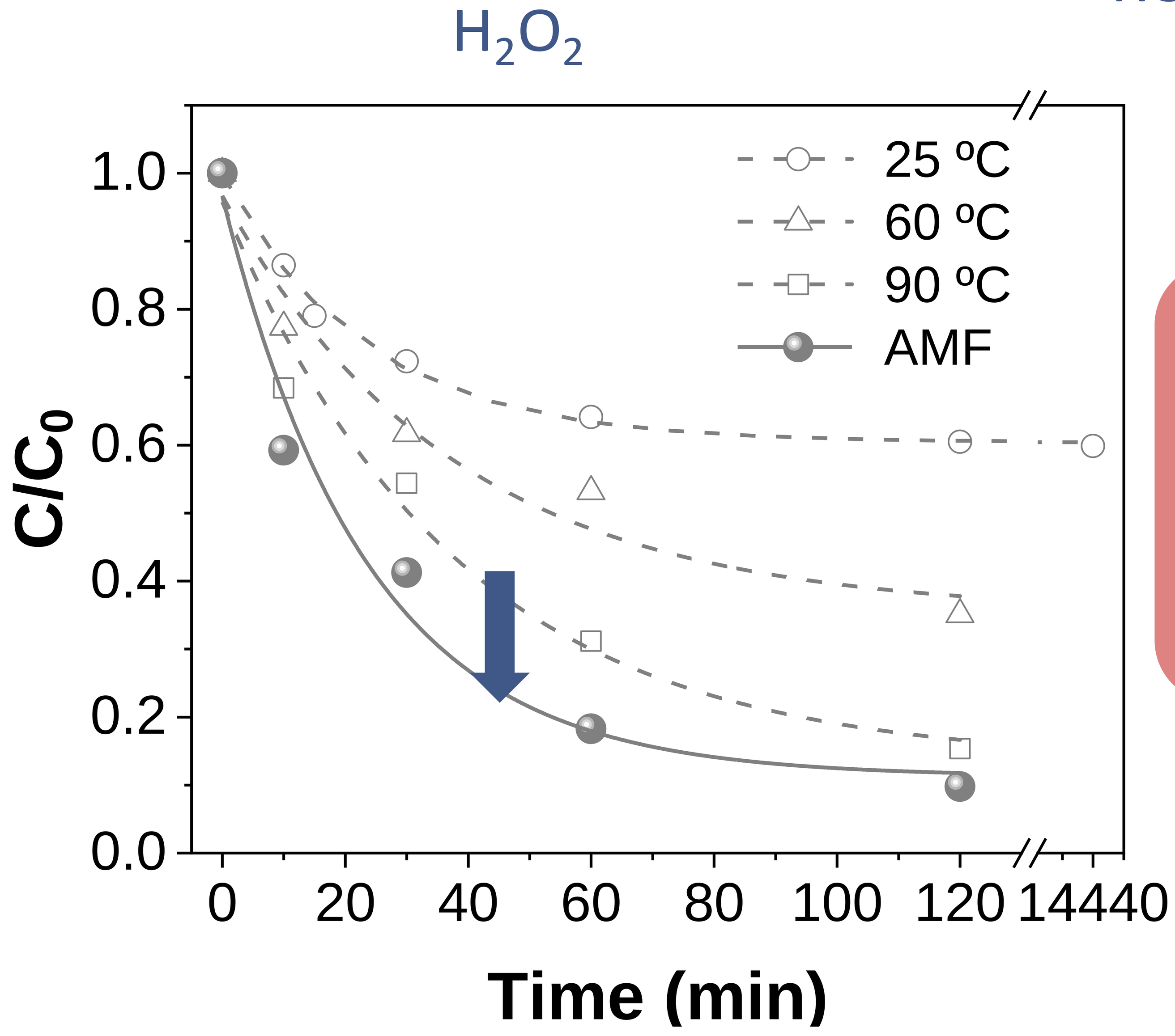

AMF improves degradation of landfill leachate

HYPERTHERMIA

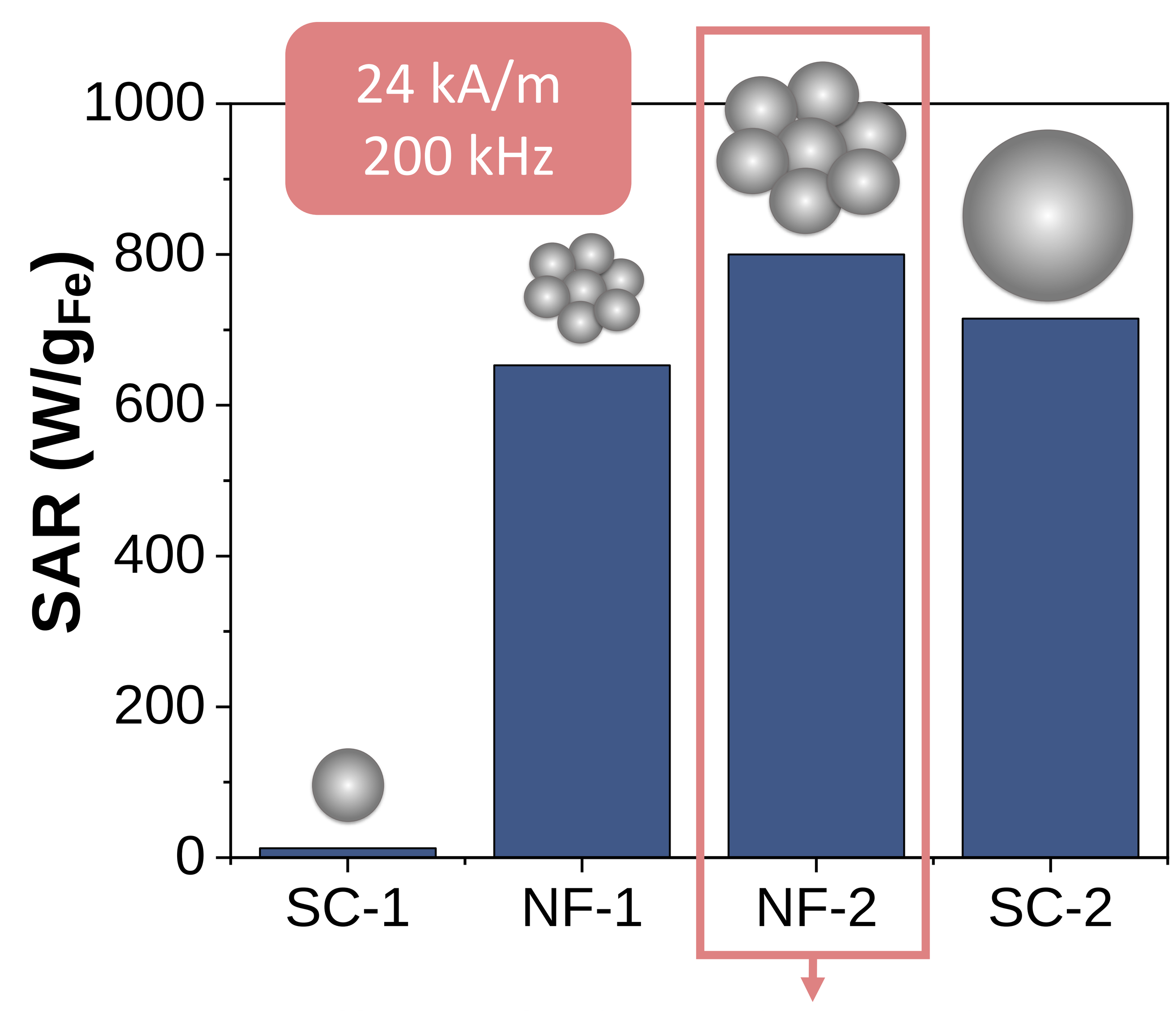

Most efficient for hyperthermia therapy

CONCLUSIONS

- Here, the formation of iron oxide nanoflowers occurs through a non-classical crystallization pathway and can easily transform into large single core nanoparticles.
- A change in amine concentration can induce a crystallization crossover to a classical pathway.
- Nanoflowers configuration with cooperative magnetic effects benefits magnetic hyperthermia and environmental catalysis.

REF:
A.Gallo-Cordova, *et al. J. Clean. Prod.* 308 (2021) 127385.
A.Gallo-Cordova, et al. *J. Colloid Interface Sci.* 608 (2022) 1585-1597.

***Correspondence**
Email: alvaro.gallo@csic.es
Tel: 913349000 ext. 131268

icmm Instituto de Ciencia de Materiales de Madrid

MaMBIO

Synthesis and Characterization of Magnetocaloric Ni-Co-Mn-Ti Heusler Alloys

Aun N. Khan, Luis M. Moreno-Ramírez, Jia Yan Law, Victorino Franco

Dpto. Física de la Materia Condensada. ICMS-CSIC. Universidad de Sevilla, P.O. Box 1065, Sevilla 41080, Spain

ABSTRACT

Magnetocaloric (MC) materials have found potential applications in magnetic refrigeration devices. Amongst the various MC materials, all-d-metal **Heusler alloys** have shown improved mechanical properties when compared to the most famous magnetocaloric Heusler alloys, such as Ni-Mn-In or Ni-Mn-Sn. In this poster, we demonstrate the influence of processing parameters on the microstructural and magnetocaloric properties of out-of-stoichiometry bulk $\mathbf{Ni_{36}Co_{14}Mn_{35}Ti_{15}}$ Heusler alloy by varying the annealing temperatures and using different fabrication techniques, such as arc melting and suction casting.

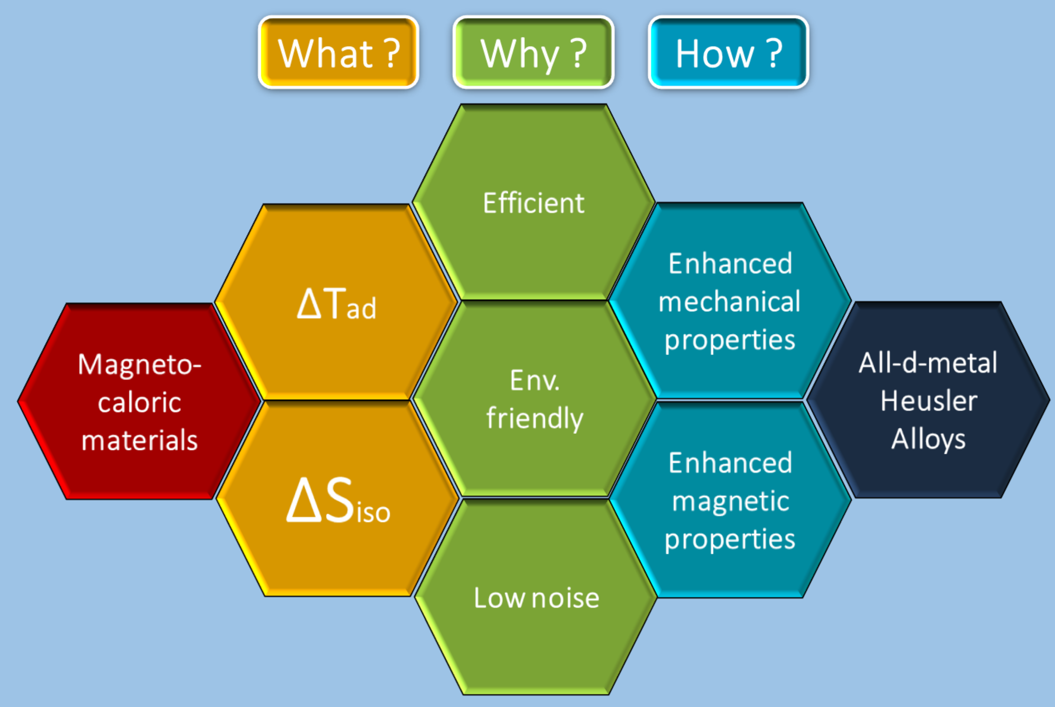

Influence of Annealing Temperatures

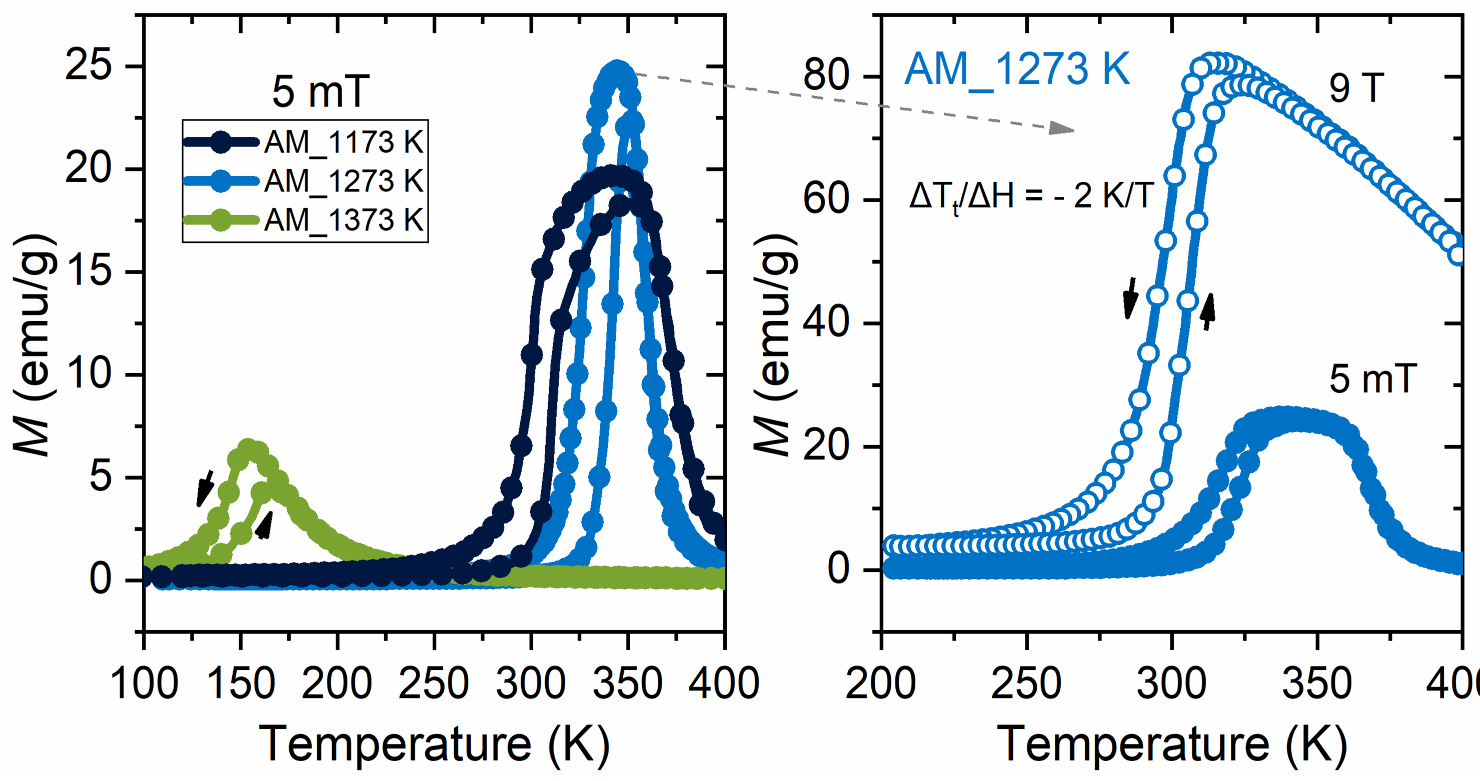

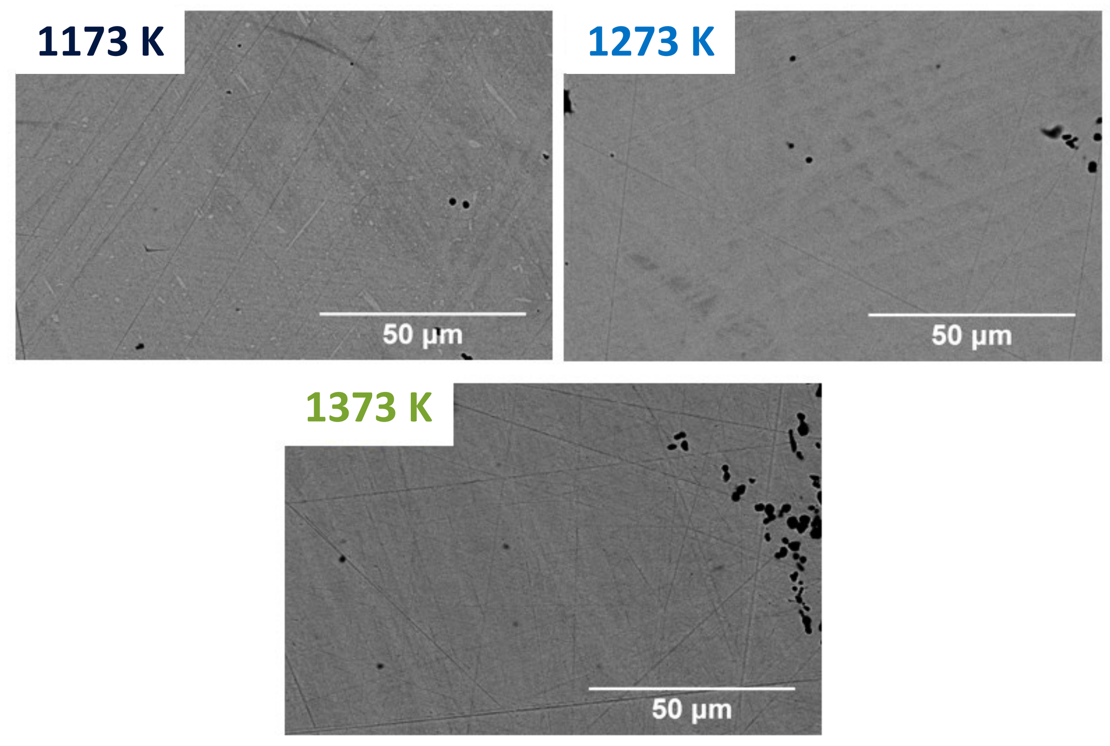

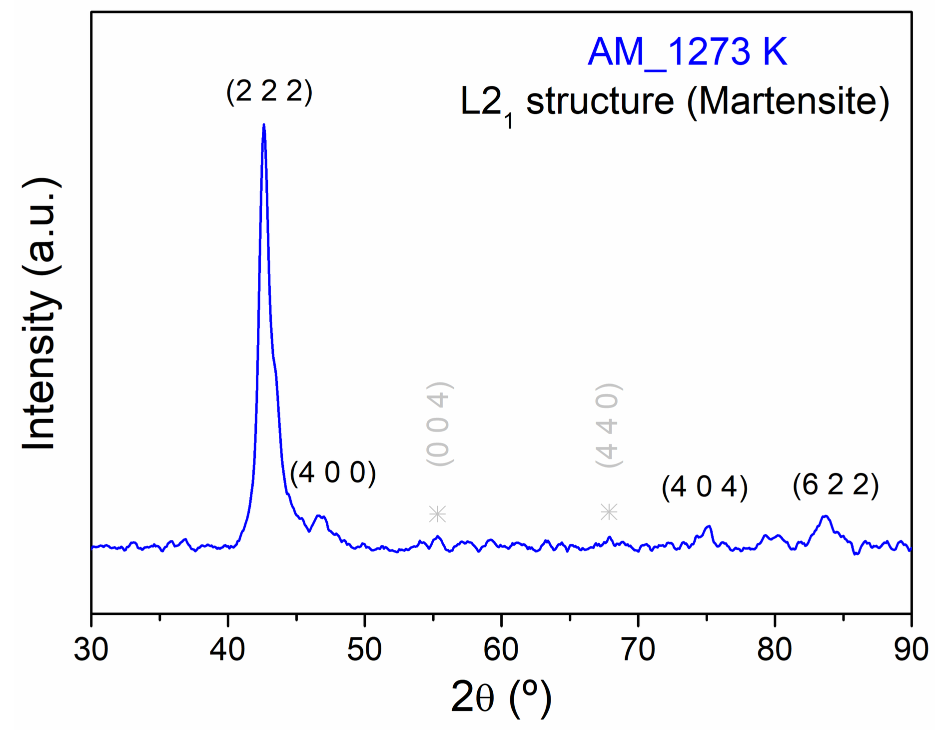

- Martensitic transition is optimized for arc melted (AM) sample annealed at 1273 K
- Annealed samples at 1173 K and 1373 K with higher inhomogeneities
- Presence of $L2_1$ martensitic structure
- No secondary phases

Influence of Fabrication Techniques

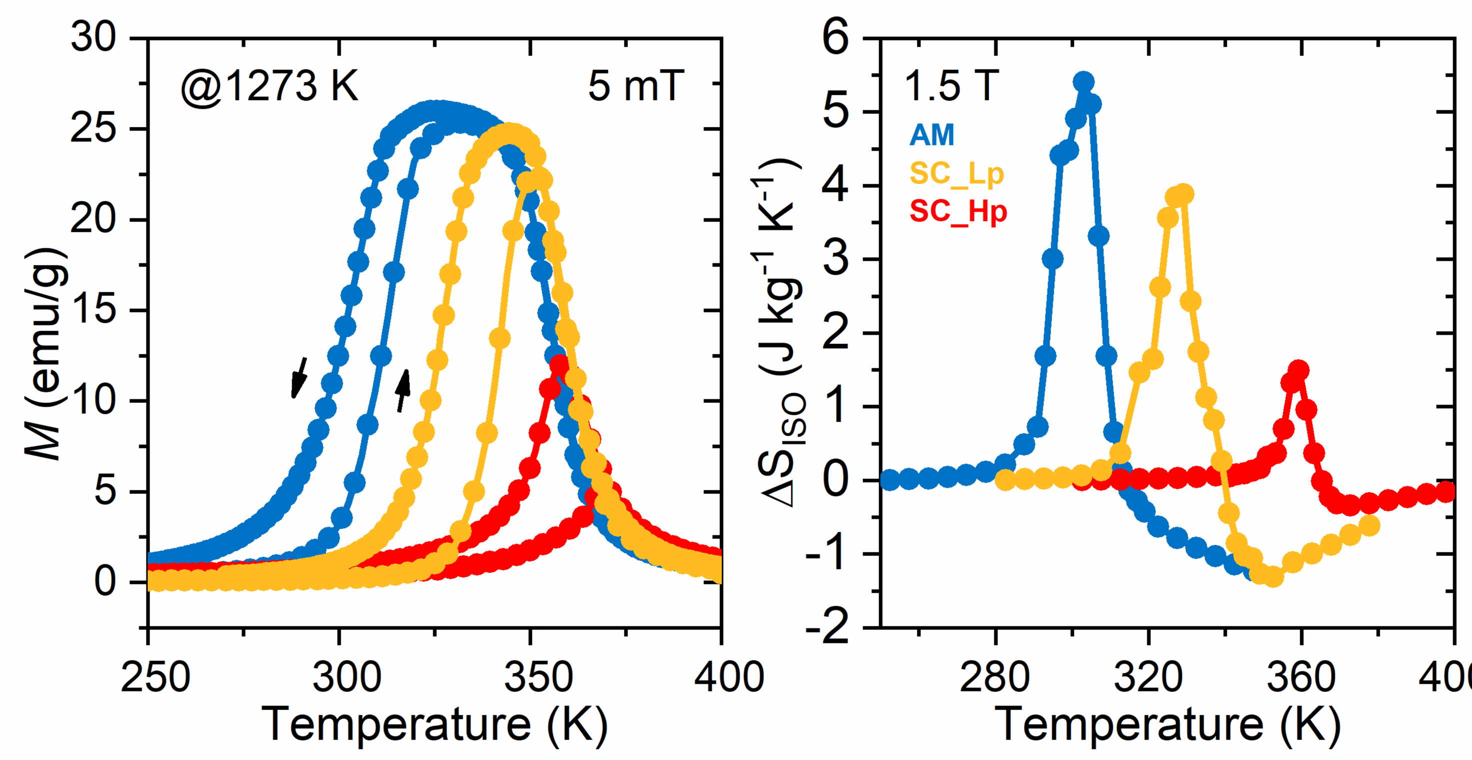

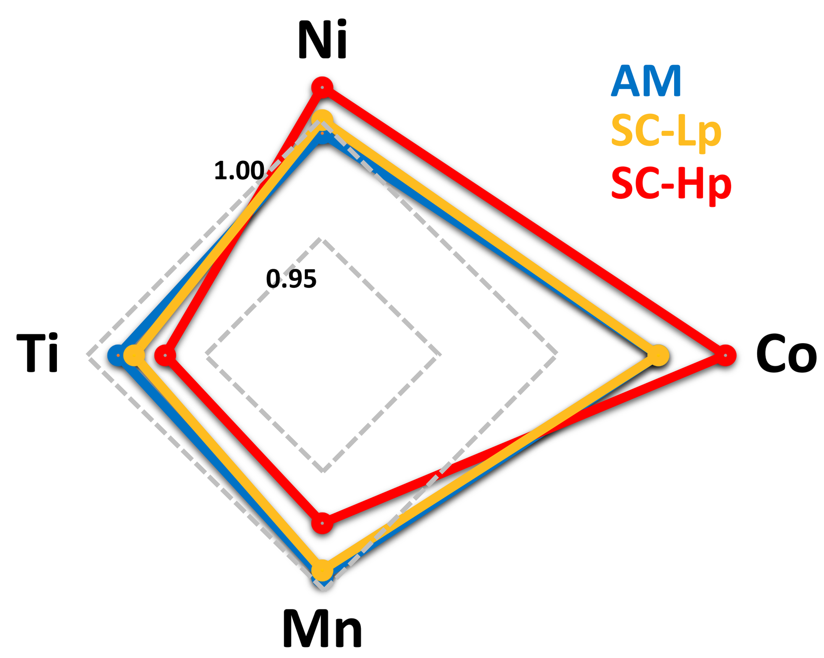

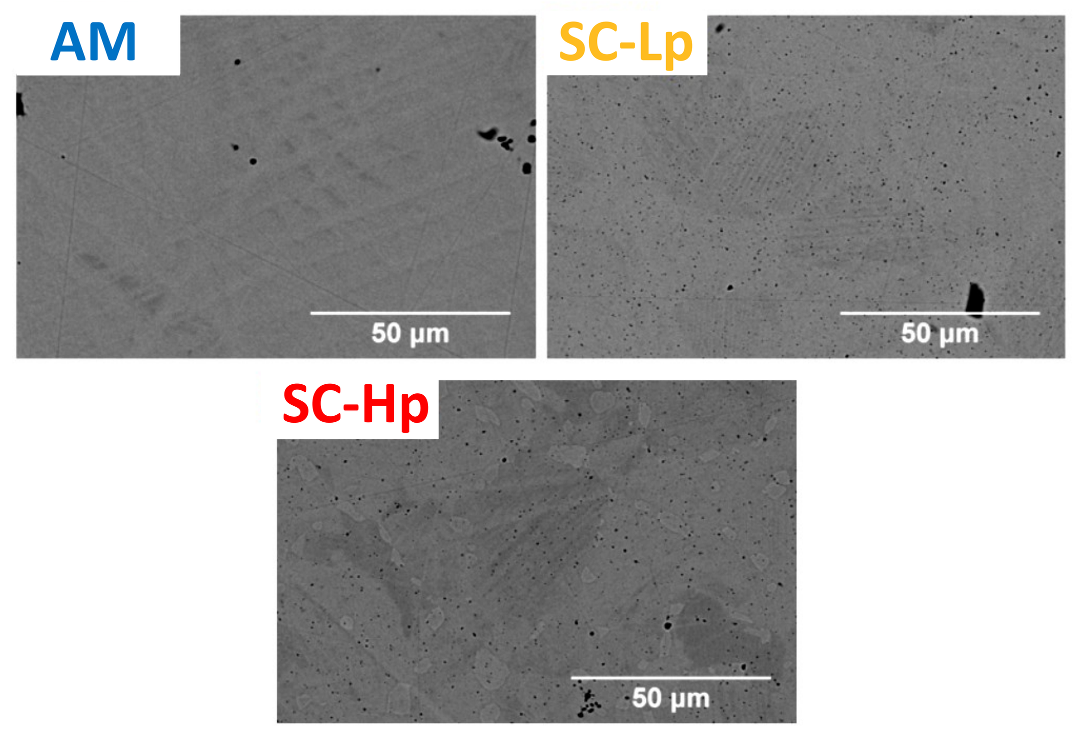

- AM sample shows the highest magnetization and magnetocaloric effect (MCE) followed by suction cast sample synthesized at low arc power (SC-Lp)
- Significant deviations from nominal composition are observed for suction cast sample synthesized at high arc power (SC-Hp)
- Larger inhomogeneities are found for SC samples

CONCLUSIONS

- AM sample optimally annealed at 1273 K shows the highest MCE in comparison to the SC samples.
- EDS analysis reveals that the composition for AM sample is in good agreement with the nominal composition of the alloy.
- Inhomogeneities increases the hysteresis of martensitic transformation.

ACKNOWLEDGEMENTS

Work supported by AEI/FEDER-UE (PID2019-105720RB-I00), Air Force Office of Scientific Research (FA8655-21-1-7044), US/JUNTA/ FEDER-UE (grant US-1260179), and Junta de Andalucía (P18-RT-746). Aun N. Khan thanks the Ministry of Science and Innovation of Spain for the FPI scholarship (grant PID2019-105720RB-100). Luis M. Moreno-Ramírez acknowledges a postdoctoral fellowship from Junta de Andalucía and European Social Fund (ESF).

REFERENCES

1. A. Taubel. *et al.*, "Tailoring magnetocaloric effect in all-d-metal Ni-Co-Mn-Ti Heusler alloys: a combined experimental and theoretical study," *Acta Materialia* 201 (2020) 425-434.
2. Z. Y. Wei *et al*. "Realization of multifunctional shape-memory ferromagnets in all-d-metal Heusler phases", *Applied Physics Letters* 107 (2015) 022406.

UNIÓN EUROPEA
Fondo Social Europeo
El FSE invierte en tu futuro

MINISTERIO DE CIENCIA E INNOVACIÓN

instituto IMdea nanociencia

EXCELENCIA SEVERO OCHOA

nanoscience and nanotechnology: small is different

Exploring the ratchet effect in chemically modulated cylindrical nanowires

Claudia Fernández-González*[1,2], Alba Berja[3], Lucía Aballe[4], Michael Foerster[4], Miguel Ángel Niño[4], Carolina Martín-Rubio[5], Ruy Sanz[5], Arantzazu Mascaraque[2,6], Lucas Pérez[1,2,6] and Sandra Ruiz-Gómez[4]

[1] IMDEA Nanociencia, Campus de Cantoblanco, 28049 Madrid, Spain [2] Dpto. de Física de Materiales, Universidad Complutense de Madrid, 28040 Madrid, Spain
[3] Instituto de Cerámica y Vidrio (CSIC), 28049, Madrid, Spain [4] Alba Synchrotron Light Facility, CELLS, E-08280, Bellaterra, Spain
[5] Instituto Nacional de Técnica Aeroespacial – INTA, 28850, Torrejón de Ardoz, Madrid, Spain
[6] Surface Science and Magnetism of Low Dimensional Systems. UCM, Unidad Asociada al IQFR-CSIC

*claudia.fernandez@imdea.org

Motivation

Our recent work:

Local changes in composition introduced in nanowires (NWs) can act as pinning sites for the domain walls (DWs)[1].
DWs can be moved by applying external magnetic or electric fields[2].

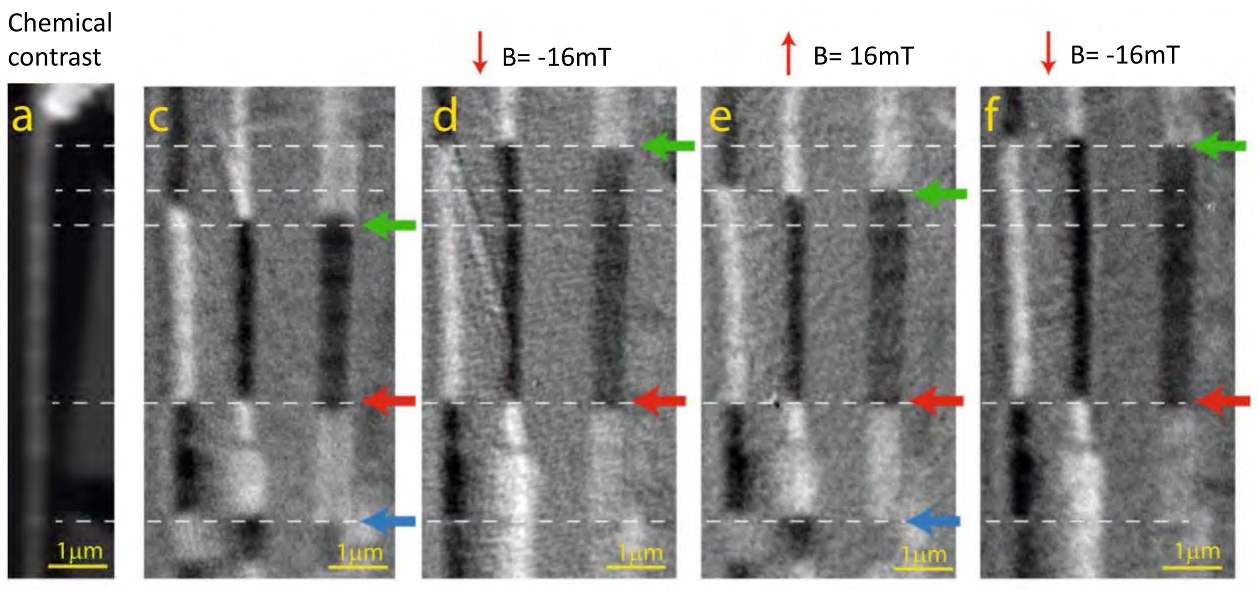

Next objectives:

Synthesize chemical ratchets along the length of the nanowire to generate different energy landscapes for domain walls (DWs) with the aim of create an asymmetric DW propagation.

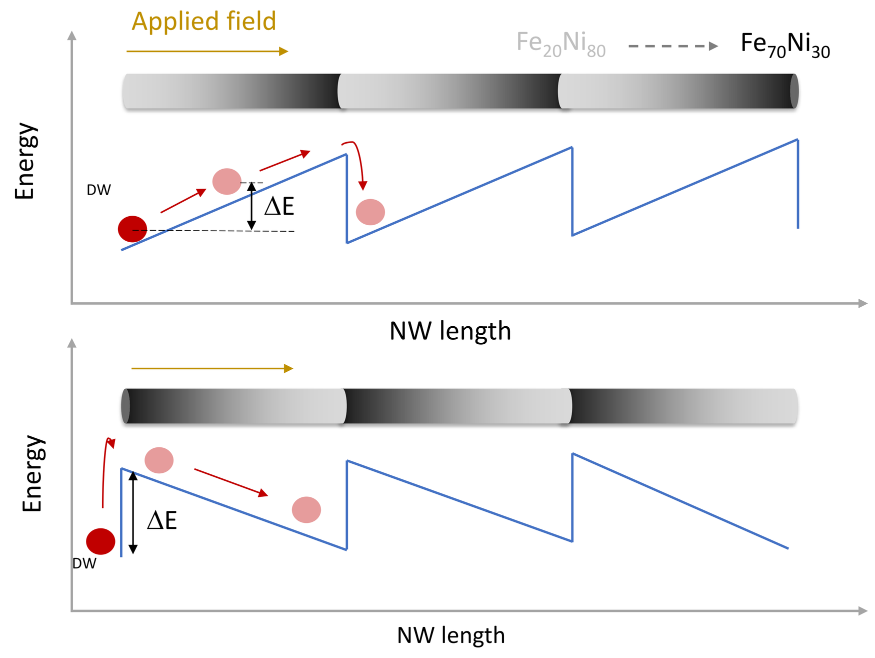

Synthesis

Template assisted electrodeposition:

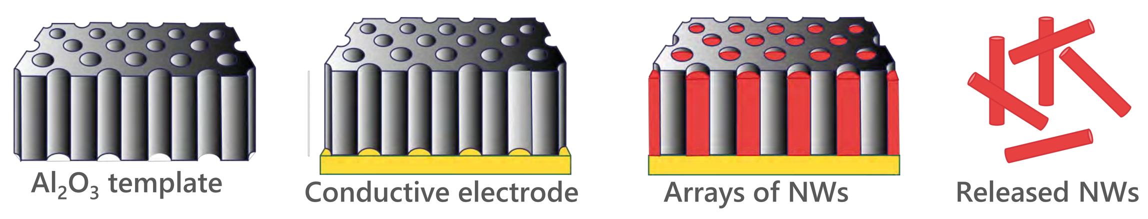

We can control the composition by changing the applied voltage

Fe-Ni ratio calibration

Electrodeposition procedure

CHEMICAL RATCHET

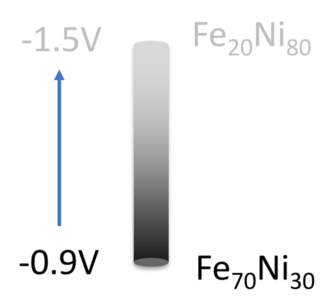

Characterization

Chemical structure

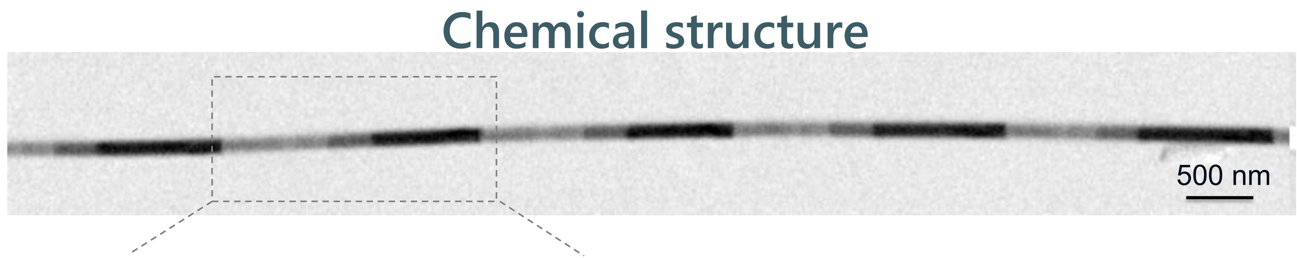

Nanowires composed by chemical gradients of 2μm in length.

Magnetic configuration

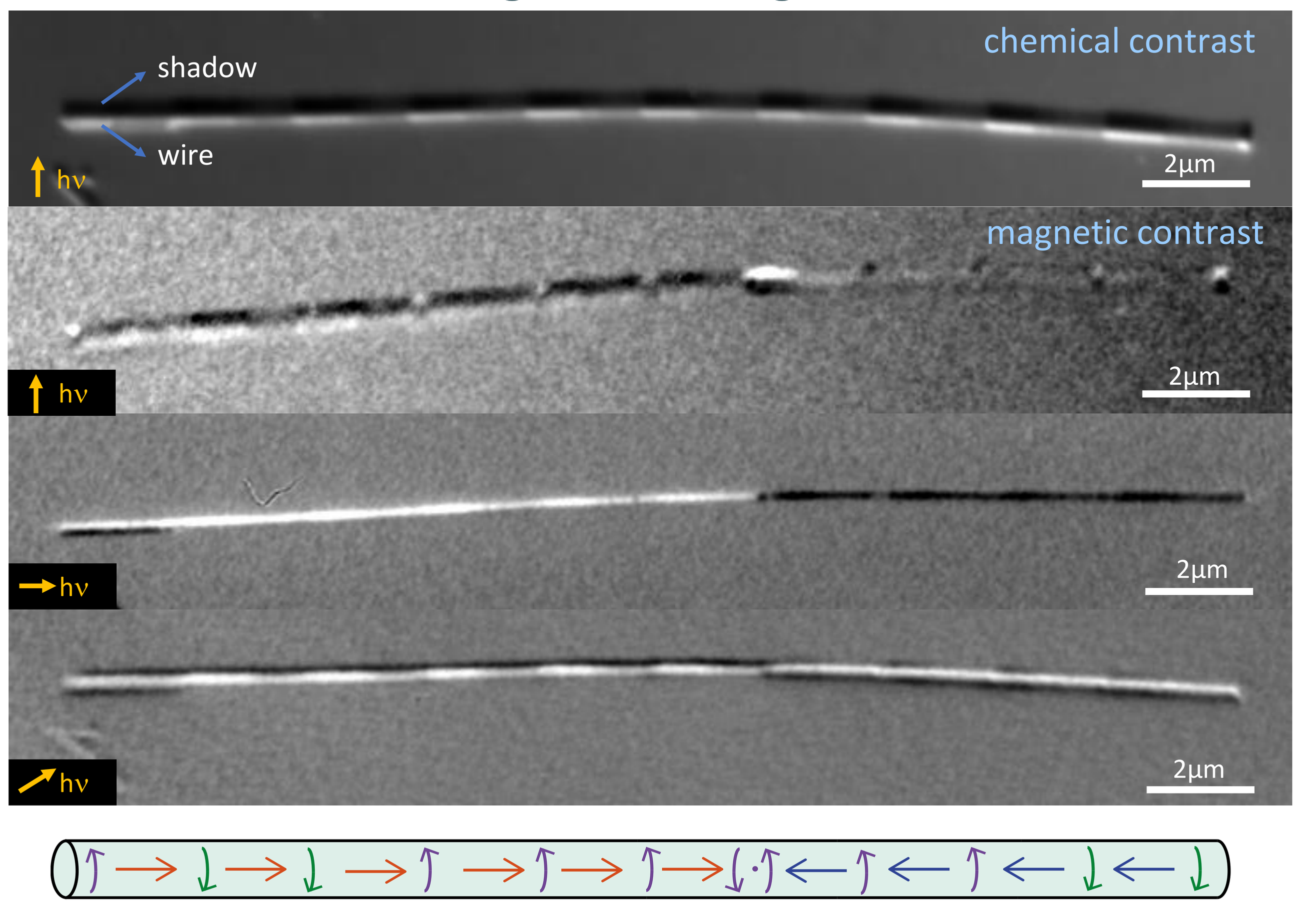

- Longitudial magnetization with curling component at the end of each ratchet.
- Bloch Point DW separates domains with opposite magnetization

Magnetic behaviour

SINGLE NANOWIRES

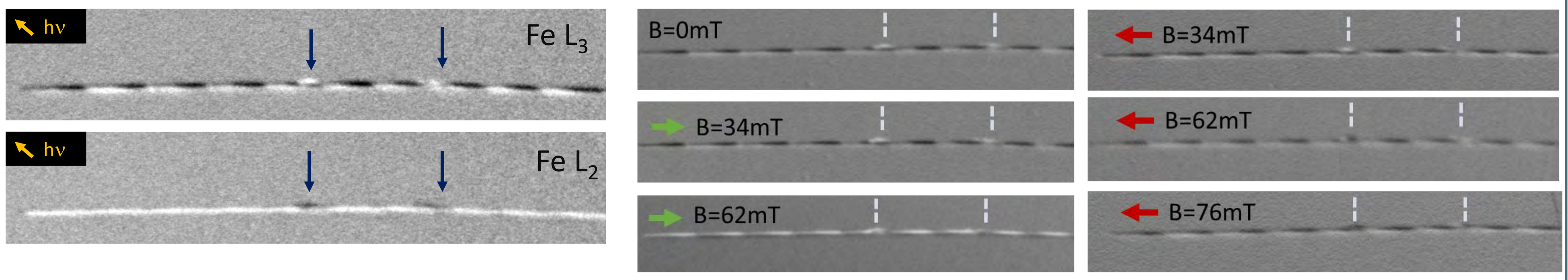

- Asymmetric response to external magnetic field pulses

HIGLY ORDERED NANOWIRE'S ARRAYS

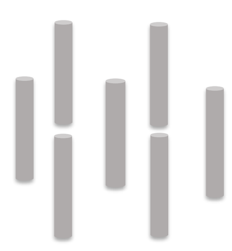

Py

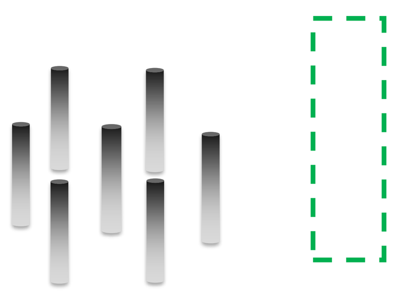

Ratchet 2μm

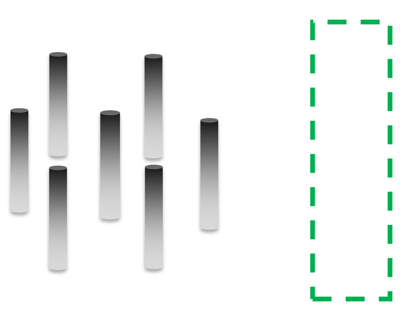

Ratchet 1μm

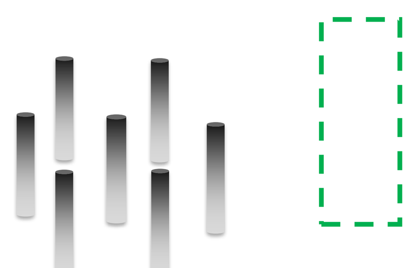

Ratchet 4μm

Conclusions and prospective

The results up to now show that:

- Introducing changes in Fe/Ni ratio along the length of the nanowires creates an asymmetric magnetic response under magnetic applied fields.
- Different switching field values were found in single nanowires.
- Shorter ratchet's lengths increase the magnetic interaction field in arrays of NWs while longer ratchets decrease them.

Next steps on this work:

- Study the domain wall dynamics under electrical current and pulsed magnetic fields.

References and acknowledgements

[1] S. Ruiz-Gómez et al. Nanoscale. (2020) 17880-17885.
[2] S. Ruiz-Gómez et al. Sci. Rep. (2018) 16695.

This project is partially supported by Comunidad de Madrid through project NANOMAGCOST-CM P2018/NMT-4321

Hydrothermal synthesis of iron oxide nanoparticles for biomedical applications.

Daniel Arranz [1,3,4*], Jose María Alonso [1,2], Rosa Weigand [3], Patricia de la Presa [4]

[1]Instituto de Magnetismo Aplicado Salvador Velayos (UCM-ADIF-CSIC), A6 km.22'5 Las Rozas (Madrid), [2]Instituto de Ciencia de Materiales, CSIC, C/Sor Juana Inés de la Cruz s/n, 28049 Madrid, Spain [3]Dpto. de Óptica, [4]Dpto. de Física de Materiales, Facultad de Ciencias Físicas, Universidad Complutense de Madrid, Avda. Complutense s/n, 28040 Madrid, Spain.

daniarra@ucm.es

UNIVERSIDAD COMPLUTENSE MADRID

INSTITUTO DE MAGNETISMO APLICADO
LABORATORIO SALVADOR VELAYOS UCM ADIF

Iron salt precursors used

Partial Fe oxidation

$Fe(II)Cl_2 \cdot 4H_2O \rightarrow Fe_2(III)Fe(II)O_4 \rightarrow Fe_3O_4$ (Magnetite)

$Fe(III)Cl_3 \cdot 6H_2O \rightarrow Fe_2(III)O_3 \rightarrow \alpha\text{-}Fe_2O_3$ (Hematite)

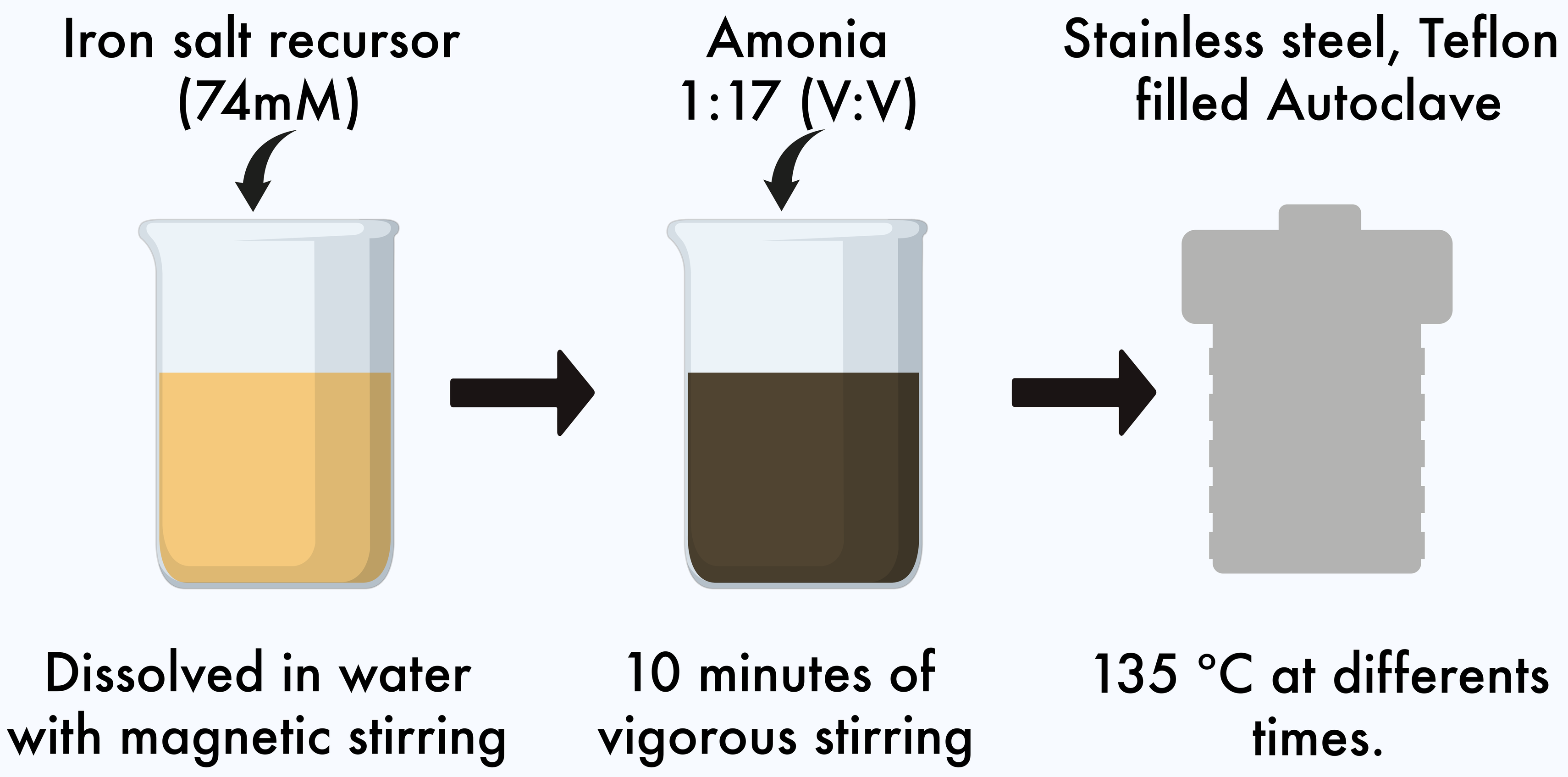

Characterization

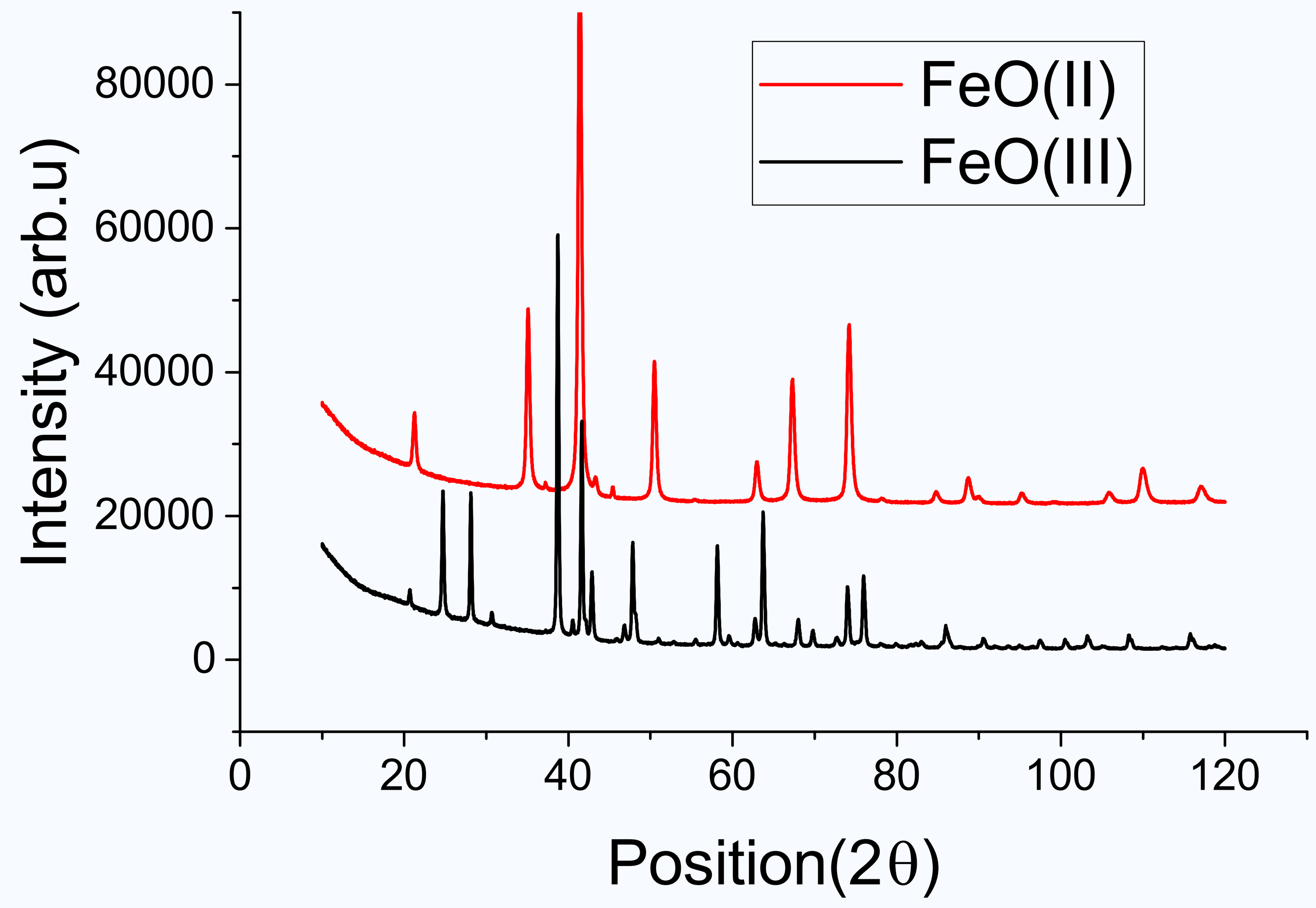

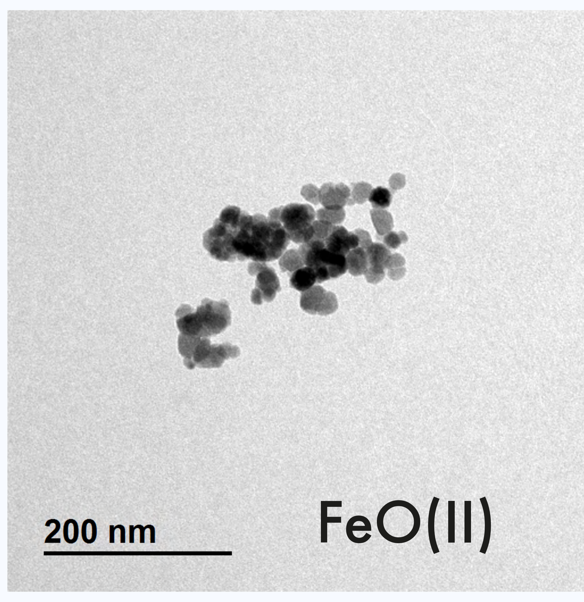

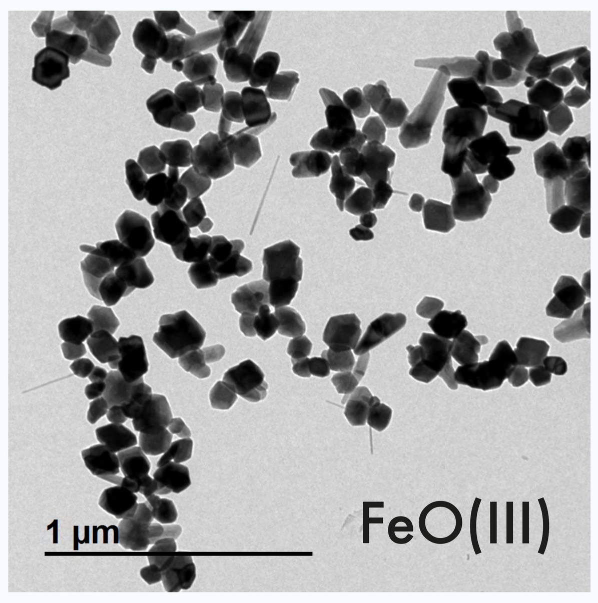

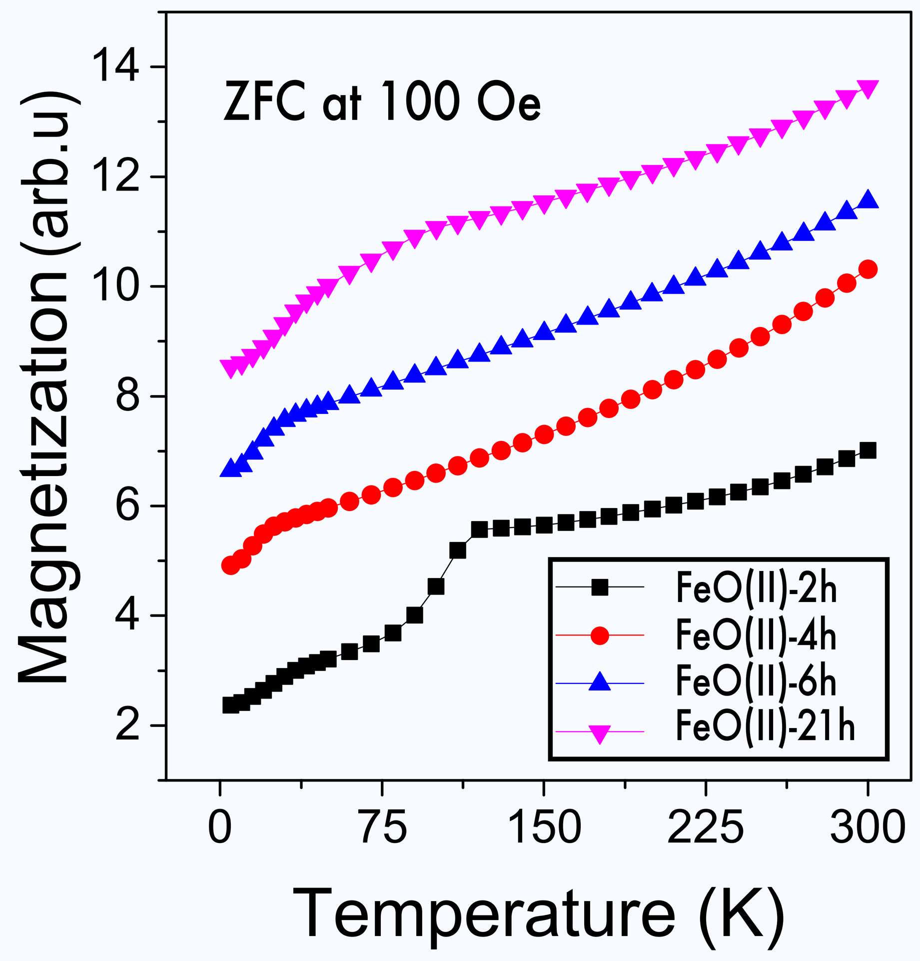

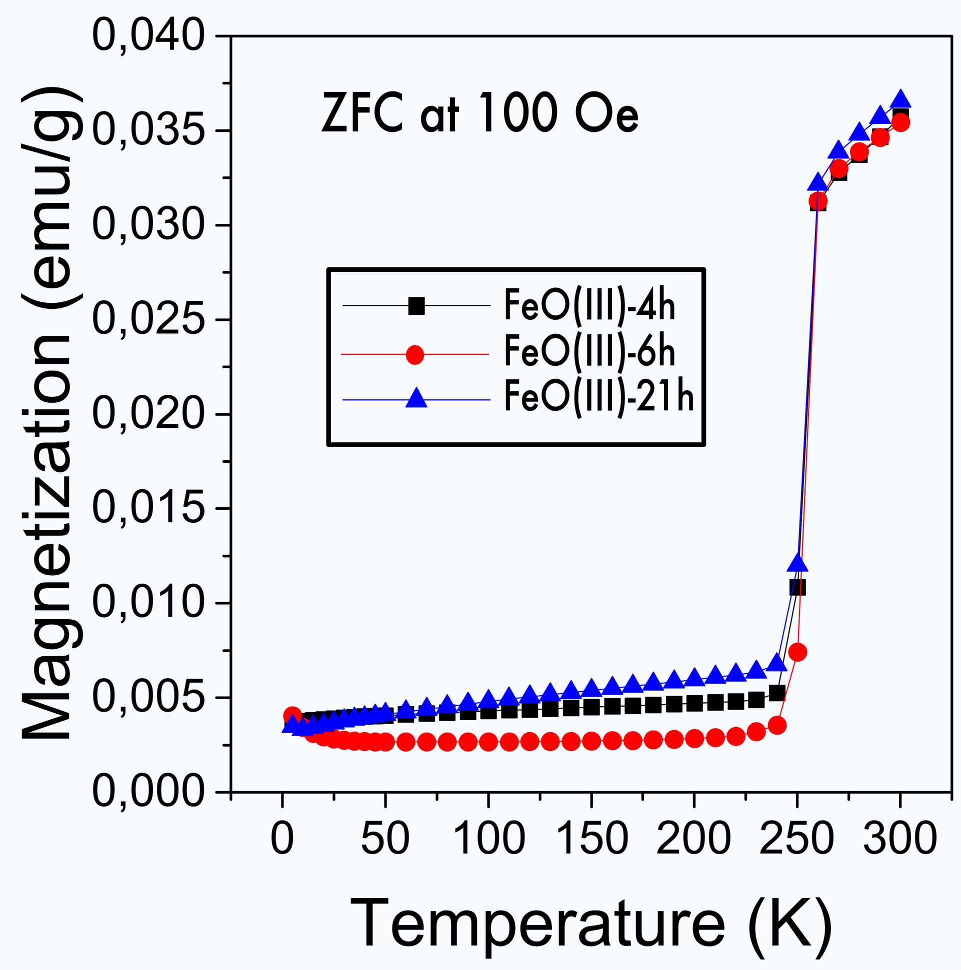

	Hc 5 K (300 K)	Ms 5 K (300 K)	Transition T	<D> TEM
FeO(II)-2h	470 (67) Oe	94 (89) Oe	Verwey at 110 K	29±6 nm
FeO(II)-4h	274 (39) Oe	85 (79) Oe	15 K	31±7 nm
FeO(II)-6h	301 (30) Oe	86 (80) Oe	15 K	26±5 nm
FeO(II)-21h	297 (24) Oe	76 (66) Oe	30 K	25±5 nm
FeO(III)-4h	80(192) Oe	Antiferromagnetic	Morin a 250 K	117±24 nm
FeO(III)-6h	270 (226) Oe	Antiferromagnetic	Morin at 250 K	123±21 nm
FeO(III)-21h	154 (191) Oe	Antiferromagnetic	Morin at 250 K	-

Photothermal Results

20 μL of NPs are introduced in a thin capilar. The NPs are irradiated with a λ=1047 nm laser operating in the second biological window.

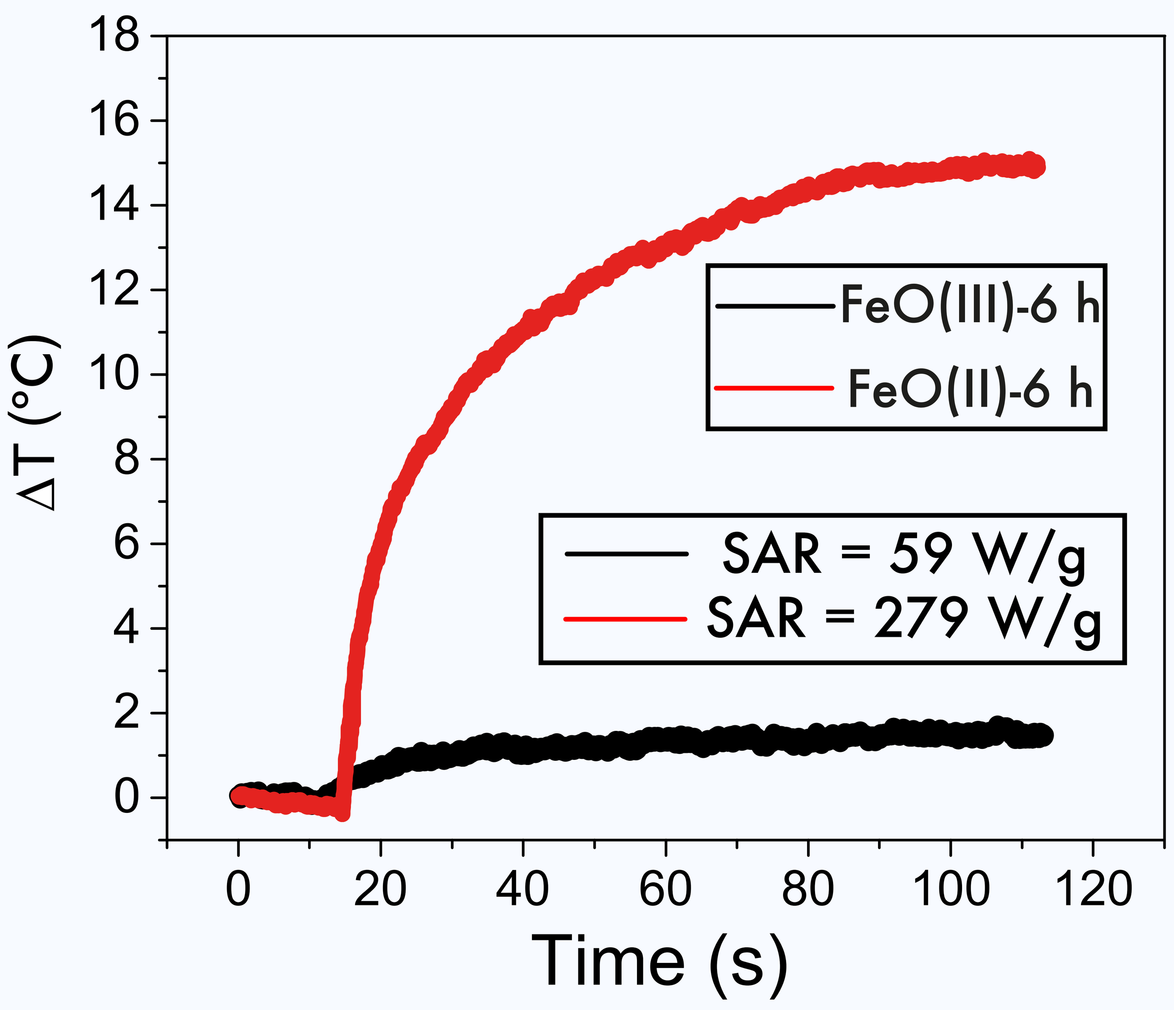

Summary

- Characterization shows different iron oxide phases with different sizes, depending on the salt precursor.
- Differences in the magnetic results suggests that the time in the autoclave plays a notable role on the sample crystallization.
- In previous works, hematite NPs (30 nm) showed a higher heating performance (ΔT = 10 °C and SAR = 300 W/g). This suggests that smaller hematite NPs are required for a higher heating efficency.

YRinM 2021

CEMAG Club Español de Magnetismo

Universidad del País Vasco / Euskal Herriko Unibertsitatea — FACULTY OF SCIENCE AND TECHNOLOGY, UNIVERSITY OF THE BASQUE COUNTRY — YRinM 2021 — GMMMT.NET research group on magnetism & magnetic materials

Magnetic Hyperthermia of Magnetotactic Bacteria doped with Terbium and Gadolinium

Danny Villanueva-Alvaro[1,*], Lucía Gandarias[2], Elizabeth M. Jefremovas[3], Javier Alonso[3], Luis Fernández-Barquín[3], Alicia Muela[2], Ana García-Prieto[4], MªLuisa Fdez-Gubieda[1,5].

[1] *Dpto. Electricidad y Electrónica, Universidad del País Vasco (UPV/EHU), 48940 Leioa, Spain*
[2] *Dpto. Inmunología, Microbiología y Parasitología, Universidad del País Vasco (UPV/EHU), 48940 Leioa, Spain*
[3] *Dpto. Ciencias de la Tierra y Física de la Materia Condensada, Universidad de Cantabria (UC), 39005 Santander, Spain.*
[4] *Dpto. Física Aplicada, Universidad del País Vasco (UPV/EHU), 48013 Bilbao, Spain.*
[5] *Basque Center for Materials Applications and Nanostructures (BCMaterials), 48940 Leioa, Spain.*

*** dannyyosmar.villanueva@ehu.eus**

Introduction

Magnetotactic bacteria (MTB) are non-pathogenic self-propelled microorganisms with the ability to biomineralize magnetic nanoparticles (called magnetosomes) and organize them inside forming one chain along their longitudinal axis. This special property allows them to orientate and navigate along the geomagnetic field lines and be guided by external magnetic fields [1,2]. One of the best known strain is the ***Magnetospirillum gryphiswaldense*** **MSR-1** because it is relatively easy to culture and dope to tune their magnetic properties. MSR-1 strain syntesizes high chemical purity nanoparticles with a truncated cubo-octahedral shape, uniform size distribution and magnetite (Fe_3O_4) composition. The properties and characteristics of the MSR-1 make them unique for biomedical applications, such as **magnetic hyperthermia,** due to an optimal chain configuration which maximizes the hysteresis losses [3]. In this work, we have succesfully cultured and doped MSR-1 with Tb^{3+} and Gd^{3+}, and have analyzed their performance as magnetic hyperthermia agents for cancer treatment.

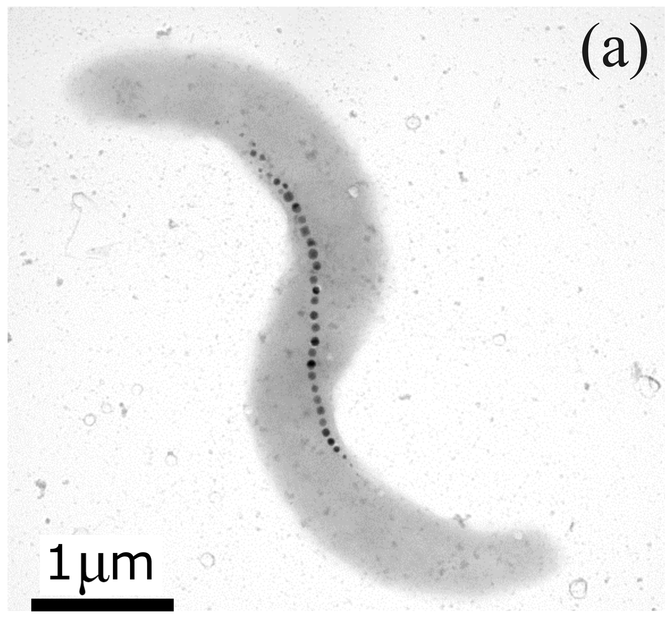

Figure 1: (a) TEM image of *M. gryphiswaldense* and **(b)** Cryo-TEM of extracted magnetosomes.

As hyperthermia agents

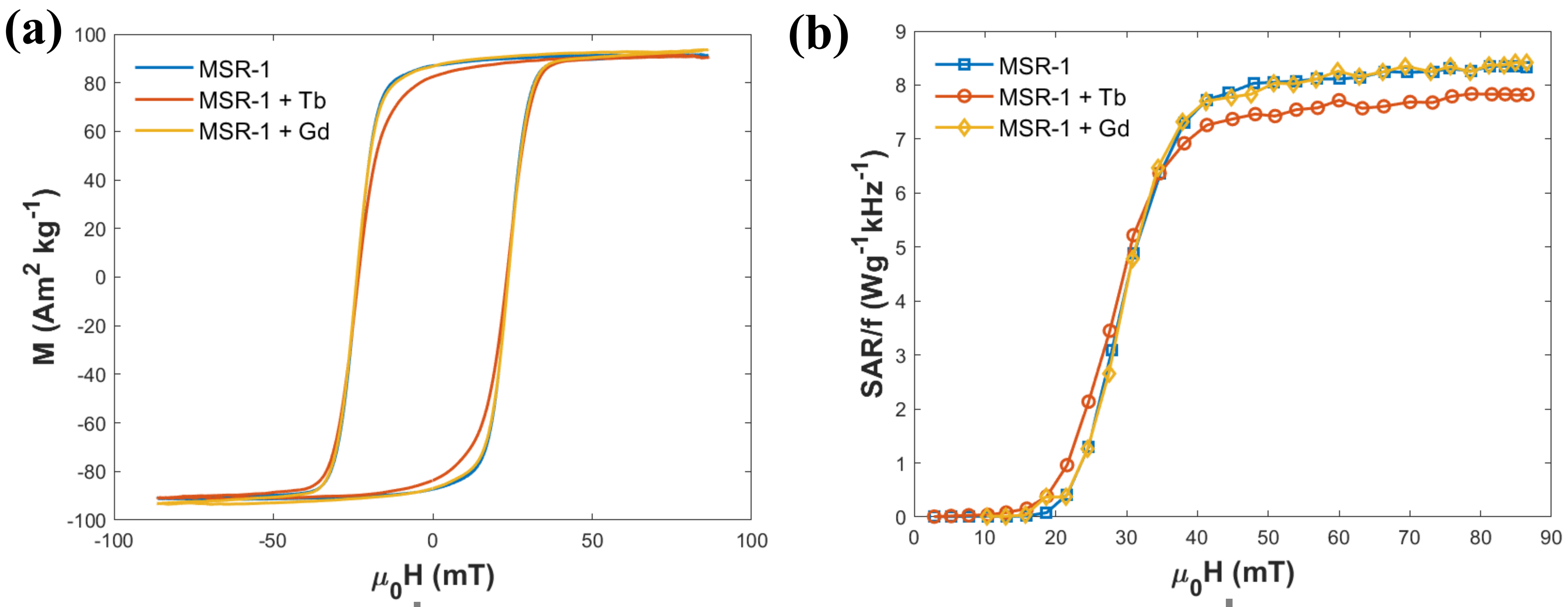

Figure 2: (a) Room temperature AC hysteresis loops measured at 133 kHz. (b) SAR normalized by the frecuency for undoped and Tb and Gd doped bacteria.

SAR curve follows the tendency reported in previous studies for undoped MTBs [3,4]:
→ Negligible below 20 mT and increases rapidly between 20 and 40 mT until saturation.

Area hysteresis loops →

$$SAR\left(\frac{W}{g}\right) = \frac{f}{c}\oint \mu_0 M_t \mathrm{d}H_t$$

	Amplitude (mT)	Frecuency (kHz)	SAR/f ($Wg^{-1}kHz^{-1}$)	References
MSR-1	38	133	7.4	This work
MSR-1+Tb	38	133	6.9	"
MSR-1+Gd	38	133	7.3	"
MSR-1	38	300	7.7	[3]
magnetosomes of MSR-1	38	310	4.4	[4]
magnetosomes of AMB-1	80	183	2.2	[5]
magnetosomes of AMB-1+Co	80	183	2.7	[6]

Table 1: SAR values of some MTB and isolated magnetosomes dispersed in water. It has been considered that SAR values reach the saturation between 300 - 400 Oe.

Conclusions

- High saturation SAR values are reached even for doped MTBs with Tb and Gd **(Table 1)**
- By accepting **Hergt criteria** ($H.f<5*10^9$ $Am^{-1}s^{-1}$), the maximum SAR values are complying with the health safety limits, for a magnetic field with f=133 kHz and μ_0H=46.5 mT.

References:

[1] M.L. Fdez-Gubieda, *et al*. J. Appl. Phys. 128, 070902 (2020).
[2] E. Alphandéry. Drug Discovery Today 25, 8,1444 -1452 (2020).
[3] D. Gandia, *et al*. Small, 15, 1902626 (2019).
[4] A. Muela, *et al*. J. Phys. Chem. C 2016, 120, 42, 24437–24448
[5] E. Alphandéry, et al. J. Nanobiotechnol. 17 , 126 (2019).

Acknowledgements:

Project PID2020-115704RB-C31: "Personalización de la bacteria magnetotáctica para explorar su idoneidad para terapias específicas contra el cáncer" , funding by MCIN/ AEI /10.13039/501100011033.

MINISTERIO DE CIENCIA E INNOVACIÓN — AGENCIA ESTATAL DE INVESTIGACIÓN

Magnetic response to bending strain in epitaxial ferrite thin films on mica

Darla Mare a), Zheng Ma a), c), Vassil Skumryev b), c), Florencio Sánchez a), Nico Dix a), Marti Gich a)

a) Institut de Ciència de Materials de Barcelona (ICMAB-CSIC), Campus UAB, Bellaterra 08193, Barcelona, Spain
b) Institució Catalana de Recerca i Estudis Avançats (ICREA), Barcelona 08010, Spain
c) Universitat Autònoma de Barcelona, Departament de Física, Bellaterra 08193, Spain

Motivation

Controlling magnetic anisotropy through strain, for tuneable ferromagnetic resonance (FMR) devices to be voltage-controlled with magnetic-piezoelectric interfaces. ε-Fe_2O_3 is appealing because it shows FMR in the mm-wave range (i.e. relevant to 5G and beyond) and a **magnetostructural transition at 500 K with an increase of H_c and significant magnetostriction[1].**

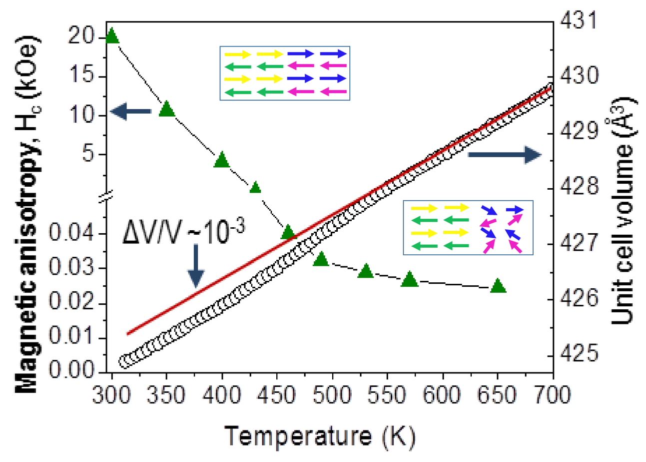

Garcia-Muñoz et al. *Chem. Mater.*, 2017[1].

Goal

Testing if magnetic anisotropy can be controlled by strain in epitaxial ε-Fe_2O_3 films with a simple approach: Using flexible ε-Fe_2O_3 films grown on mica by PLD, which can be bent and placed between 2 straws, keeping their curvature, to be magnetically characterized in a SQUID magnetometer.

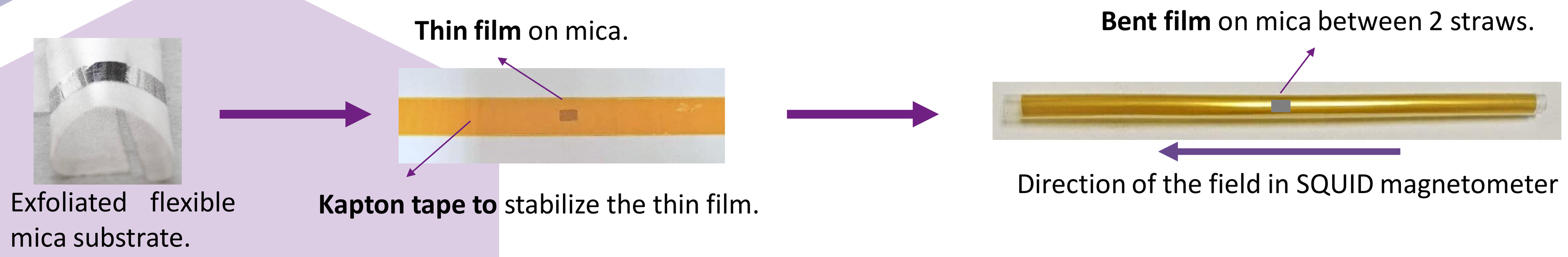

Exfoliated flexible mica substrate. **Thin film** on mica. **Kapton tape to** stabilize the thin film. **Bent film** on mica between 2 straws. Direction of the field in SQUID magnetometer

Epitaxial flexible ferrite films

Magnetite $FeFe_2O_4$

- Inverse spinel (cubic)[2]
- Magnetic easy axis <111> (above 120 K)

Fd-3m *a* = 8.3941 Å

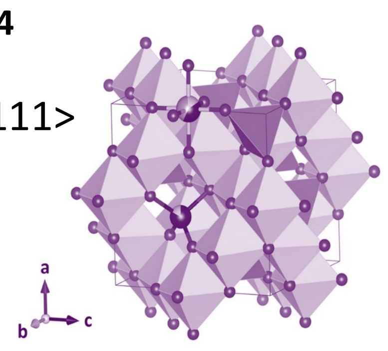

ε-Fe_2O_3

- Orthorhombic
- Polar space group[3]
- Magnetic easy axis along *a*

Pna2$_1$ *a* = 5.098 Å, *b* = 8.785 Å, *c* = 9.468 Å

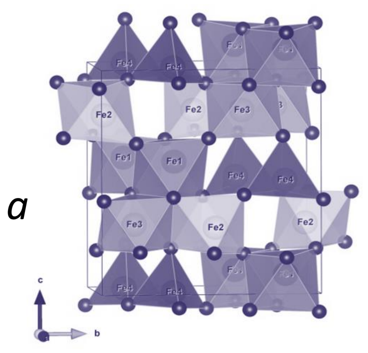

High resolution XRD θ-2θ scan

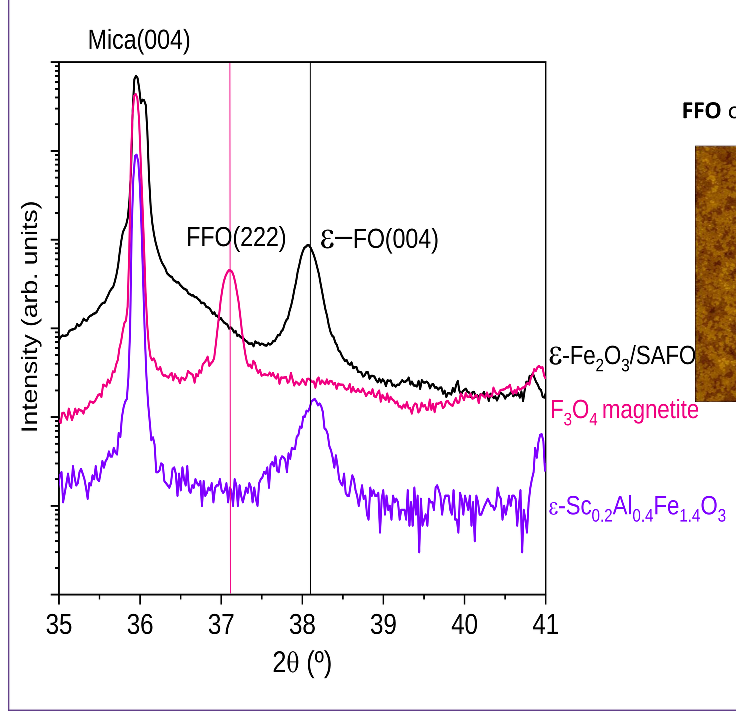

Atomic force microscopy images

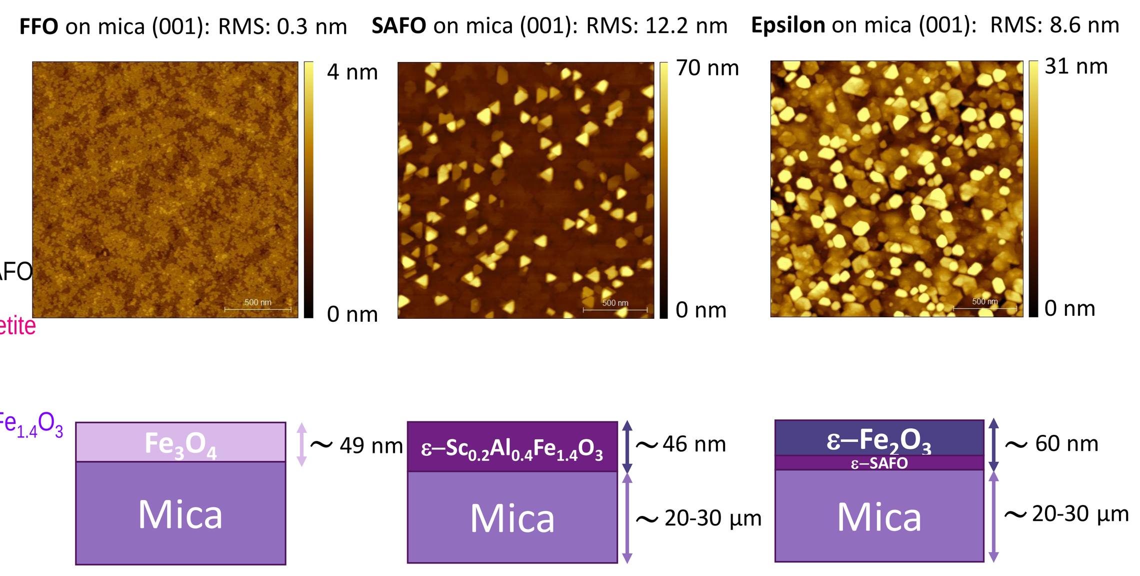

Measurement system

A **double straw system** is used for measurement. The inner radius of the sample holder (plastic straw) commonly used in SQUID measurements supports the bent film on one side and a second straw with its outer radius on the other. The mechanical deformation of the bent thin film/substrate is considered to be elastic. Magnetite films grown on mica, for which strain effects on magnetization were already reported[4], are used to assess the measurement system.

Order of the measurements

Maximum **strain**:

$$\epsilon = \pm\frac{d}{2r} \quad d \sim 20-30\,\mu m,\ r \sim 2.5\,mm$$

$$\epsilon = \pm 0.5\%$$

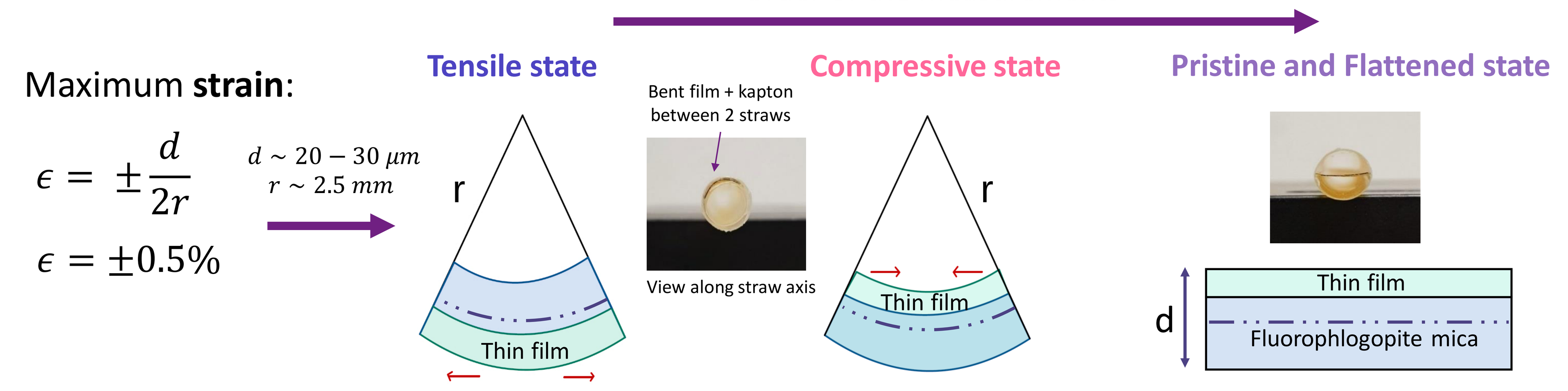

In-plane magnetization *vs* field for different strain states of the magnetite films on mica. Black loops correspond to the unstrained films.

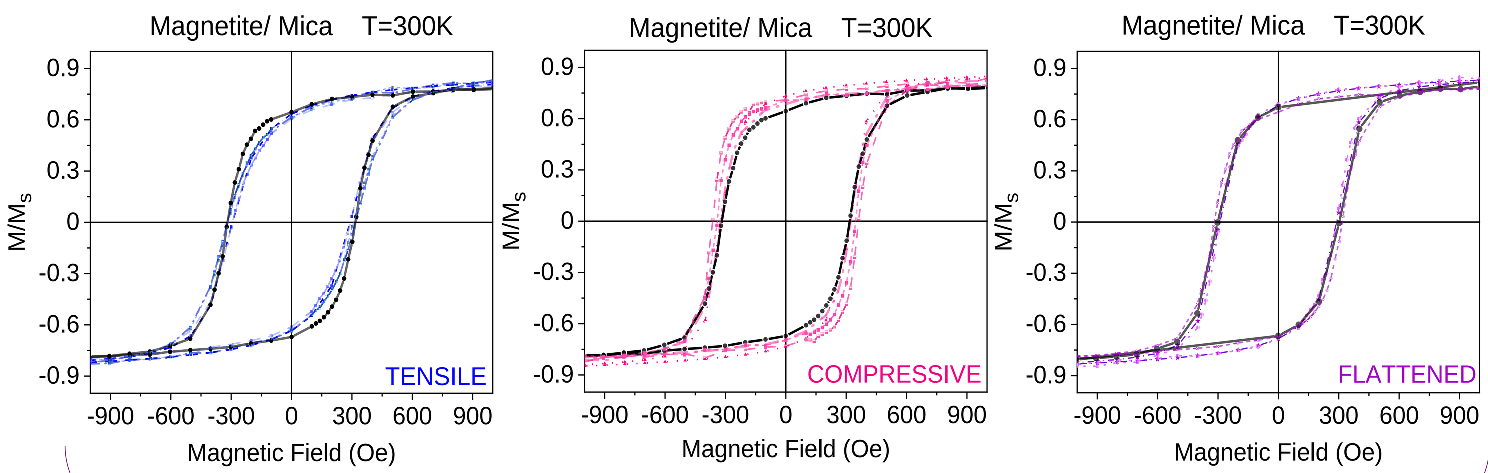

Difference in the shapes of the hysteresis loops in the compressive and tensile states.

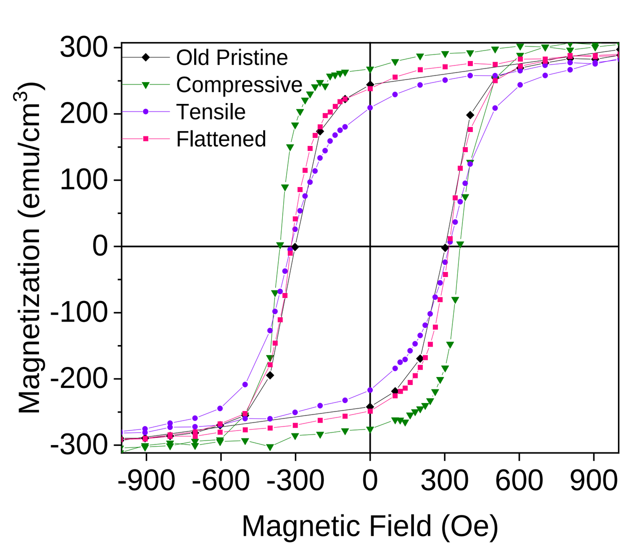

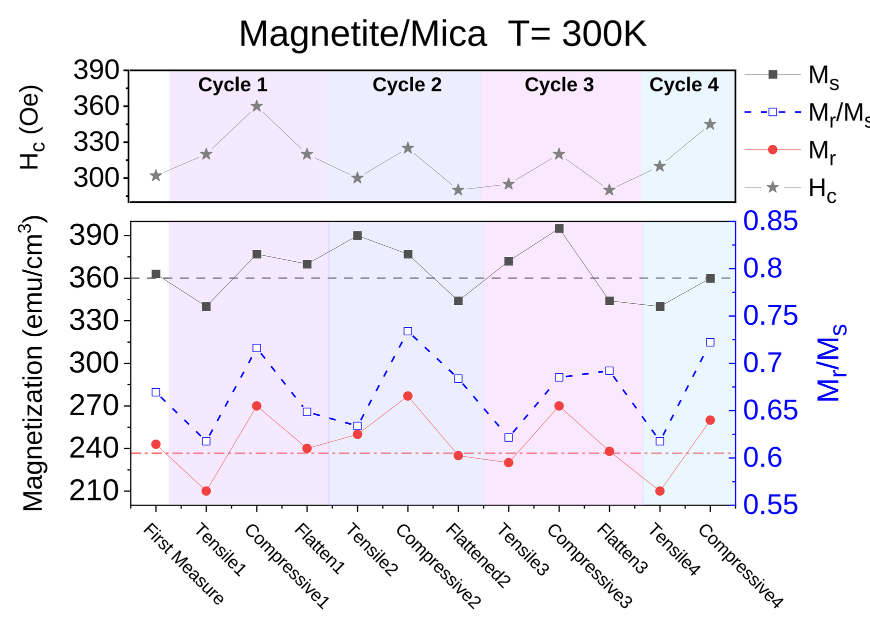

The measurements were repeated in four times cycles. The maximum values of magnetization and M_r/M_s occur in compression, being minimum in tensile state. This suggests that the compressively strained state favours the orientation of the easy magnetization direction (111) along the direction of the applied field.

Characterization of ε-Fe_2O_3 films

Pure ε-Fe_2O_3

- ε-Fe_2O_3 (eFO) is a multiferroic with large spontaneous magnetostriction.
- High H_c ~6500 Oe at 300 K.
- No changes of H_c under different strain states.

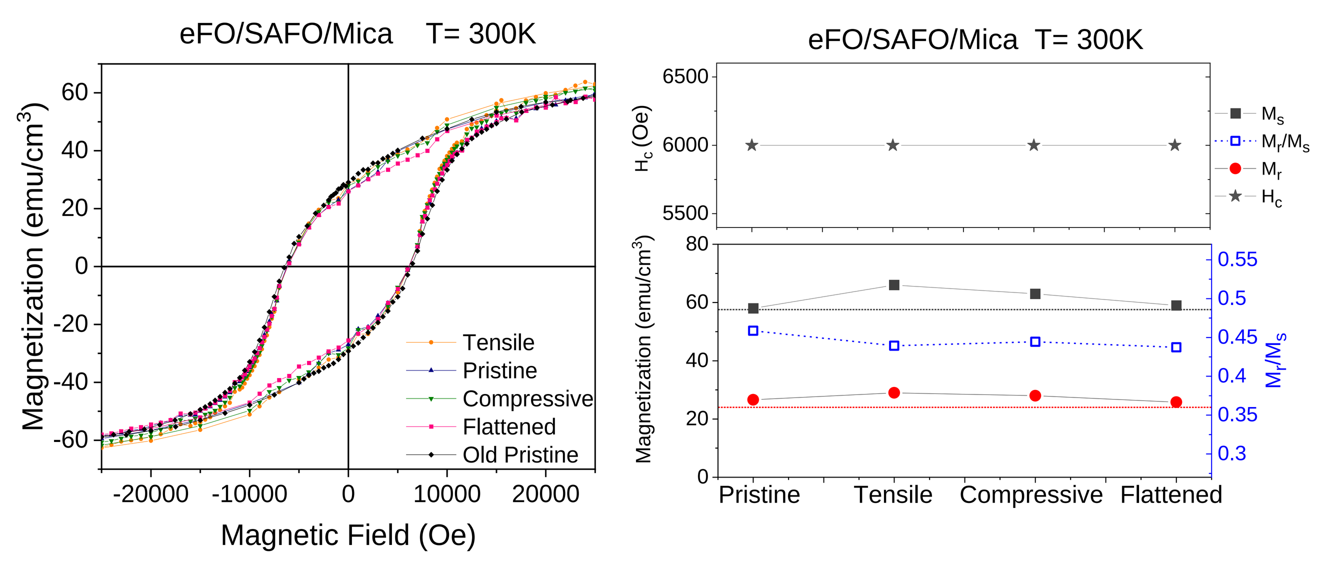

Doped ε-Fe_2O_3

- ε-$Sc_{0.2}Al_{0.4}Fe_{1.4}O_3$(SAFO) is used as a buffer layer to grow ε-Fe_2O_3.
- Low H_c ~1600 Oe at 300 K.
- Good candidate to detect strain effects on magnetic anisotropy.

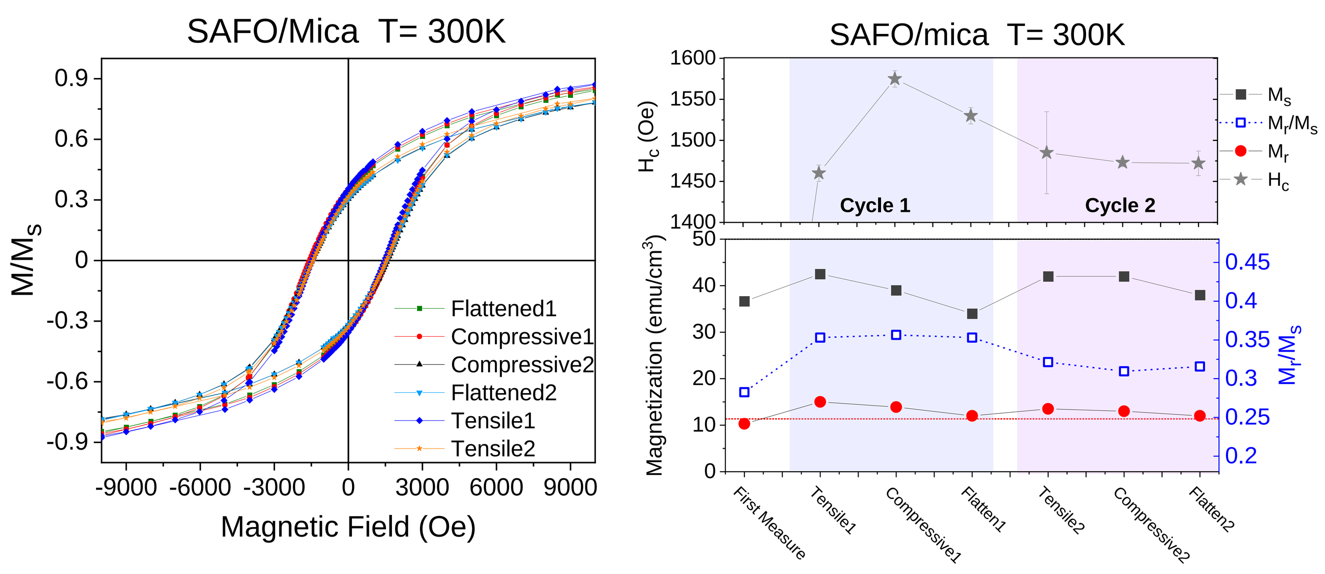

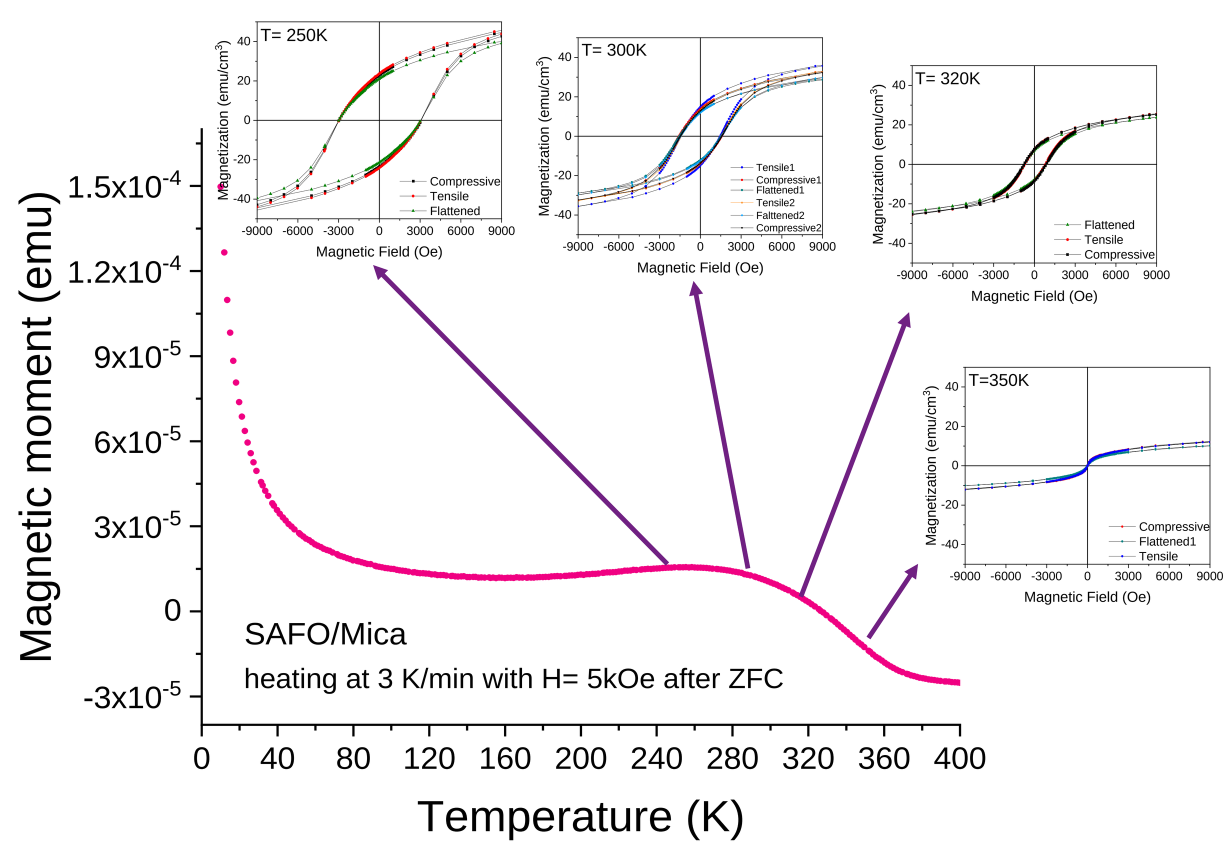

High temperature transition

- Magnetic transition at 370 K.
- H_c and M decrease while approaching 370 K, as in[1].
- No significant strain-induced changes in hysteresis loops.

Conclusions

- Magnetite Fe_3O_4 thin films show clear changes in the coercive field and remnant/saturation magnetization under different bending strains.
- ε-Fe_2O_3 thin films only show weak or no significant variation of magnetic properties with strain although reported otherwise in literature[5].

Next steps

- Growth and characterization of epsilon iron oxide on piezoelectric substrates.
- Better understanding of the structure of epsilon thin film system on different substrates.
- FMR characterization using a Vector Network Analyzer.

References:

1. J. L. García-Muñoz *et al.*, Chem. Mater. **(2017),** 29, 22, 9705–9713.
2. M.E. Fleet, Acta Cryst. **(1981),** B37, 917-920.
3. M. Gich *et al.*, Journal of App. Physics **(2005),** 98, 044307.
4. P. Wu *et al.*, ACS Appl. Mater. Interfaces **(2016),** 8, 49, 33794–33801.
5. T. Amrillah *at al.*, ACS Appl. Mater. Interfaces **(2021),** 13, 14, 17006–17012.

Acknowledgements:

Severo Ochoa Programme for Centres of Excellence in R&D (FUNFUTURE CEX2019-000917-S).
European Research Council FeMiT project: ERC-CoG 819623.

3D Skyrmionic configurations in soft magnetic nanodots

Starring

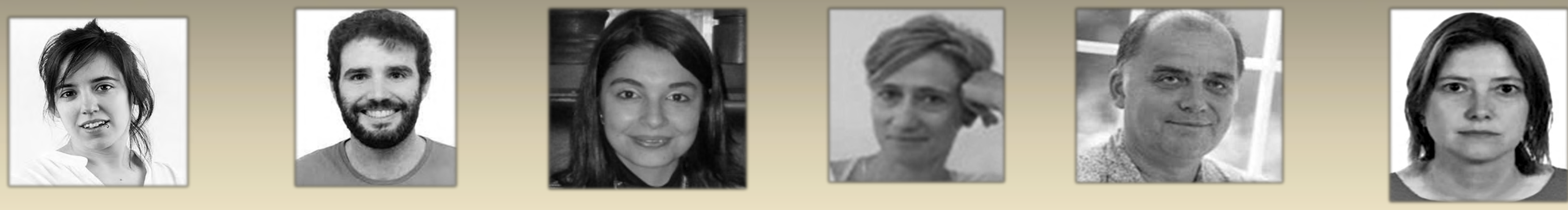

E. Berganza* J.A. Fernandez –Roldán M. Jaafar A. Asenjo K. Gusliyenko O. Chubykalo-Fesenko

Previously, on soft magnetic nanodots …

Magnetic Force Microscopy image of demagnetized permalloy nanodots.

Vortex or skyrmion?

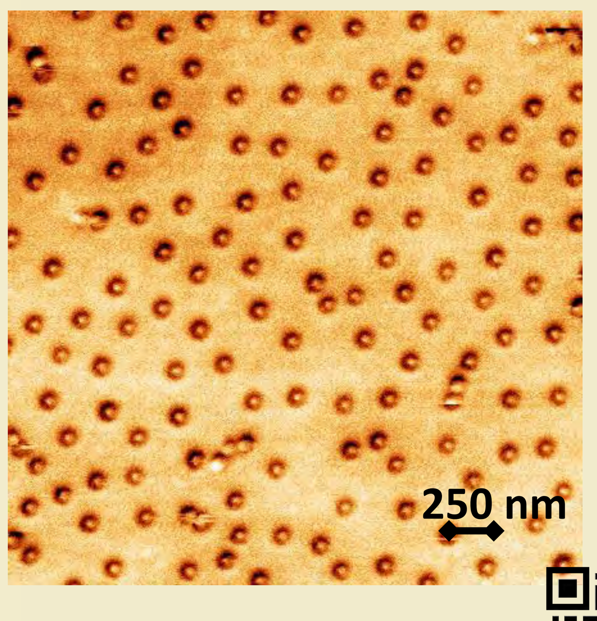

Fabricated by Hole-Mask-Colloidal Lithography

… but their phase diagram is well known …

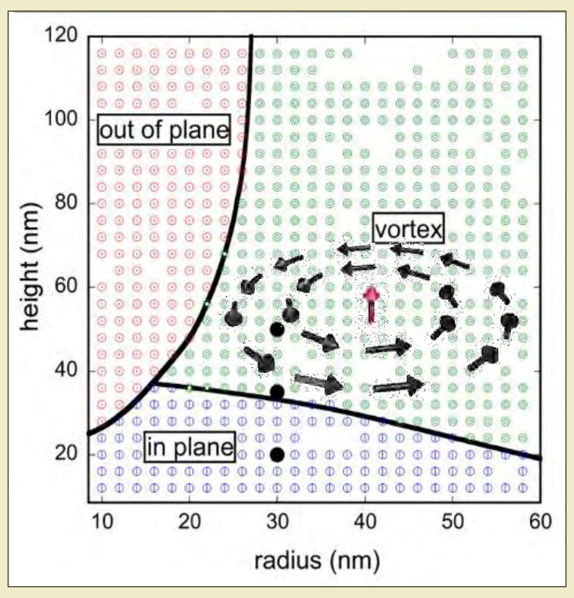

Sample features:
$Ni_{80}Fe_{20}$
r = 30 nm, h = 30 nm
dome-shaped

Core displacement was monitored under in-situ applied field:

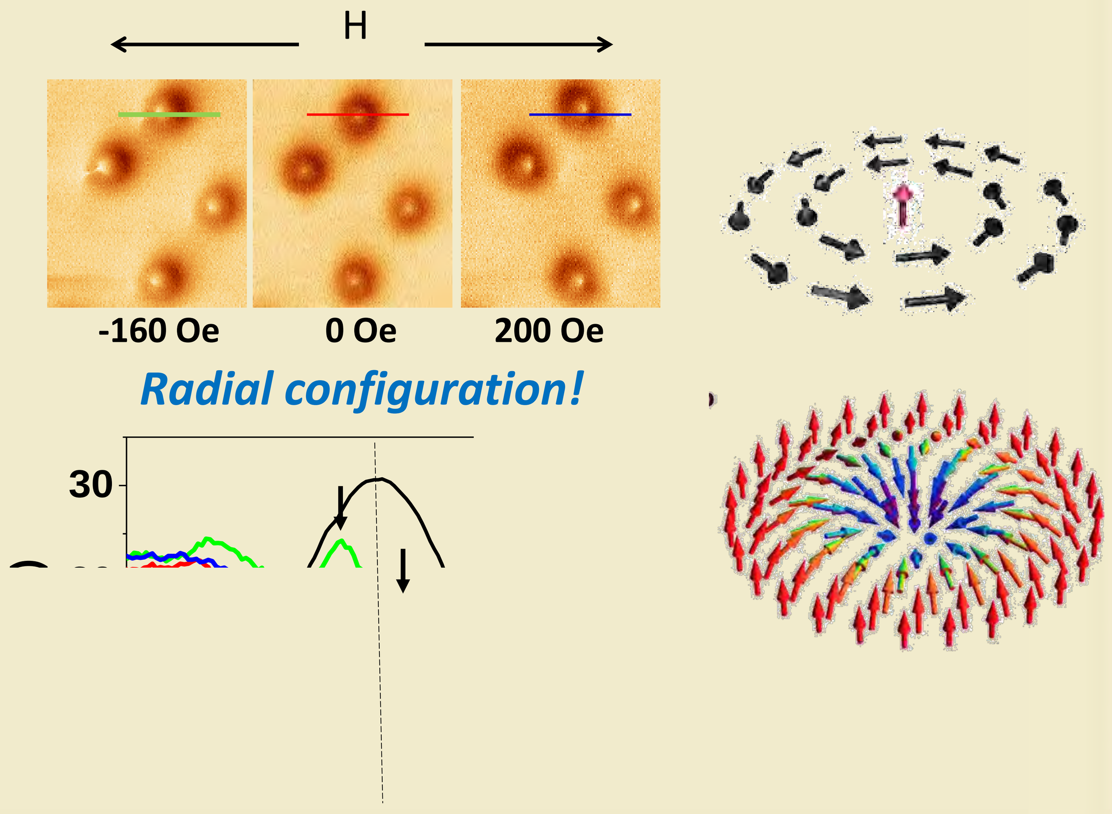

Radial configuration!

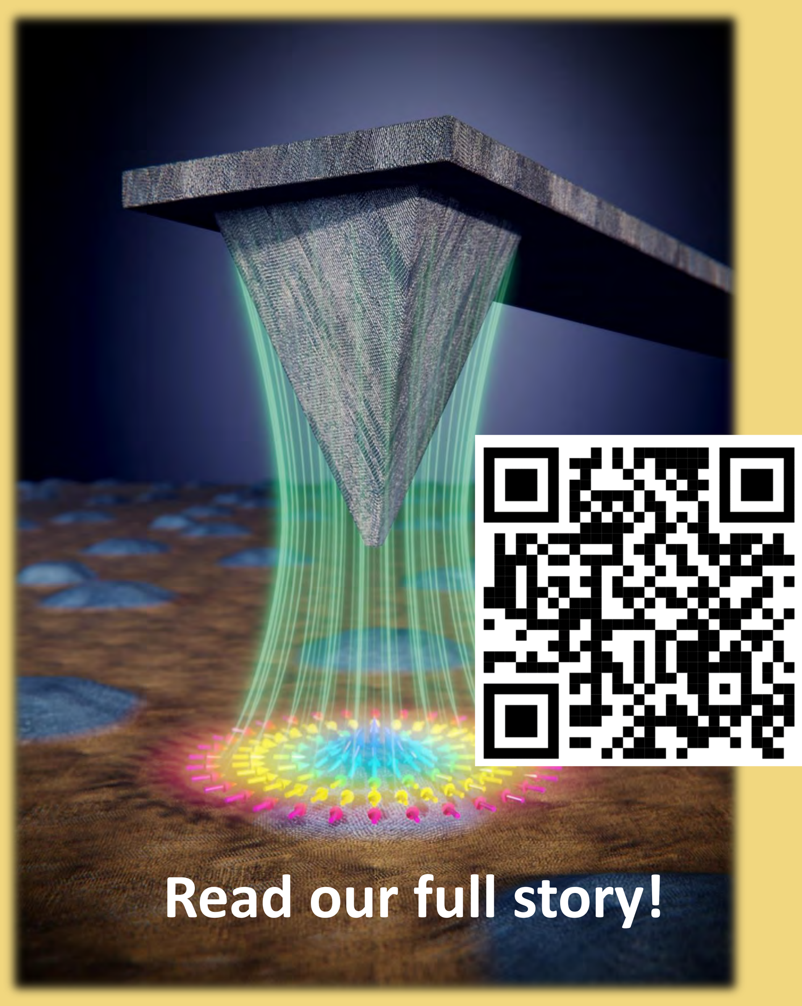

After some micromagnetic simulations…

Can topologically non-trivial configurations be stabilized in soft magnetic nanodots?

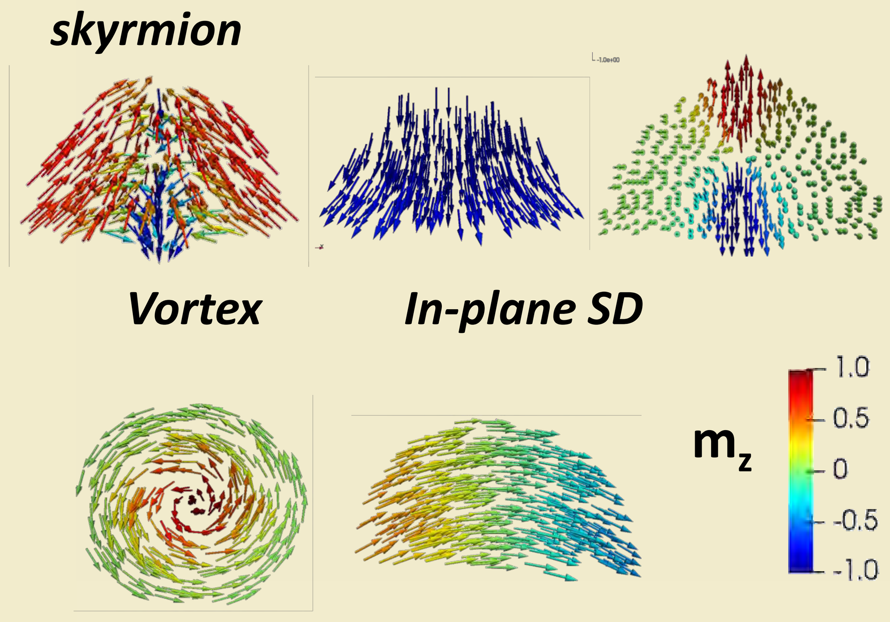

Energy values for different metastable configuration

Sk Fl Bl V IP

…some controversy and clarifications

Wait, but can we really call this a skyrmion?

2D skyrmion

Thin films and B20 crystals

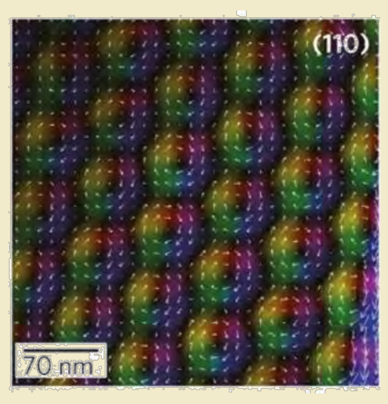

Topology: S= 1
Size: d < 100 nm
Chirality: yes
DMI: Yes

Skyrmion-Bubble

Thin films

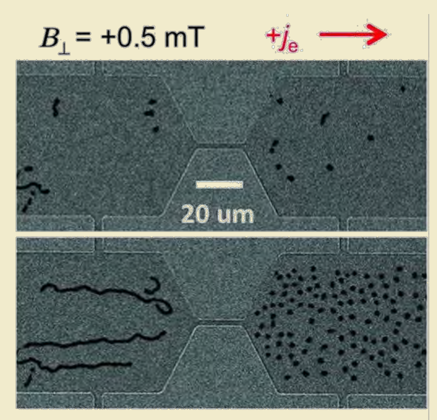

Topology: S= 1
Size: d ≈ 1 µm
Chirality: yes
DMI: Yes

3D skyrmion

Thick nanodots

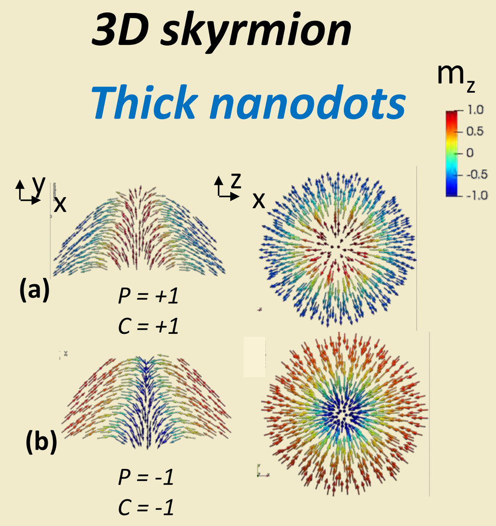

Topology: S < 1,
Size: d = 60 nm
Chirality: yes
DMI: no

What could be favoring the stabilization of 3D skyrmions?

- **Size and confinement**

Phase diagram of 3D skyrmions for Py hemispherical nanodots

Calculated total energies for different nanodot geometries

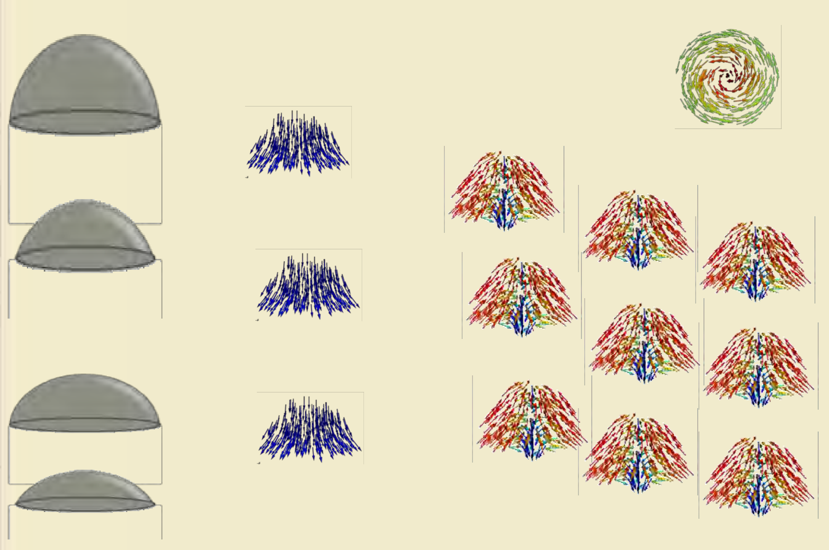

- **Curvature**

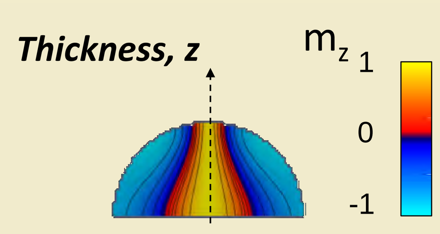

2D topological charge calculated according to the expression:

$$Q = -\frac{1}{4\pi}\int_S \vec{m}\cdot\left(\frac{\partial\vec{m}}{\partial x}\times\frac{\partial\vec{m}}{\partial y}\right)dxdy$$

2D topological charge along z thickness

Maximum topological charge value for dots of different dimensions

Coming soon!!

3D quasi-skyrmions in thick planar and dome-shape nanodots

*eider.eguiarte@kit.edu

Study of Dipolar Collective Properties in Binary Random Assemblies of Magnetic Oxide Nanoparticles

E.H. Sánchez* [1], M. Vasilakaki[2], S.S. Lee[3], P.S.Normile[1], G. Muscas[4], M. Murgia[1], M.S. Andersson[5], G. Singh[6], R. Mathieu[5], P. Nordblad[5], P.C. Ricci[4], D. Peddis[7], K.N. Trohidou[2], J. Nogués[8], J.A. De Toro[1]

[1] Instituto Regional de Investigación Científica Aplicada, Universidad de Castilla-La Mancha, Ciudad Real, Spain; [2] Institute of Nanoscience and Nanotecnology, Greece; [3] Institute of Bioengineering and Nanotechnology, The Nanos, Singapore; [4] Dipartimento di Física, Universita degli Studi di Cagliari, Monserrato, Italy; [5] Department of Engineering Sciences, Uppsala University, Sweden; [6] Department of Materials Science and Engineering, Norwegian University of Science and Technology, Norway; [7] Dipartimento di Chimica e Chimica Industriale, Universita degli Studi di Genova, Italy; [8] Catalan Institute of Nanoscience and Nanotechnology (ICN2), CSIC and BIST, Barcelona, Spain.

*Elena.hsanchez@uclm.es

Objectives

- To study and tune the magnetic properties of dense binary assemblies with different proportions of low and high anisotropy oxide nanoparticles.
- In particular, to assess the effect of strong dipolar interactions on coercivity, exchange bias and blocking temperature.

Experimental

• Mix nanoparticles preparation

Pure maghemite and Co-doped maghemite (23% of metal ions) nanoparticles, both 6.8 nm in diameter, were synthesized by a thermal decomposition route.[2] The two batches were mixed in different concentrations. The particles were collected and the oleic acid surfactant covering the particles was removed to yield several powders with different proportions of pure and Co-doped maghemite particles.

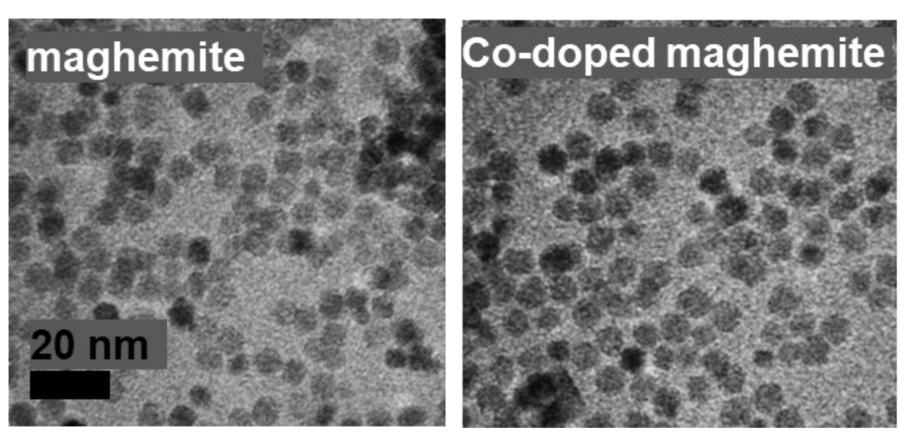

• Binary random compacts (BRCs) preparation

The BRCs were prepared with different proportions of low- and high-anisotropy bare nanoparticles (pure and Co-doped maghemite particles). The NPs powders were pressed into dense discs. The percentage by weight of Co-doped maghemite particles were 0, 10, 20, 30, 50 65, 85 and 100%. High resolution SEM and compositional mapping were used to verify the uniform mixing of the two types of NPs down to the nanoscale.

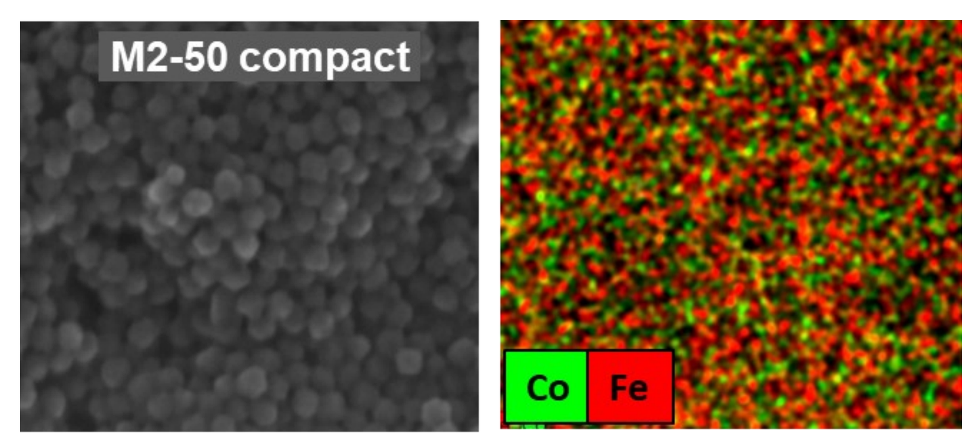

EXPERIMENTAL RESULTS

The changing proportion of particles with different magnetic moments led to a variation in the average interparticle dipolar interaction across the series. The particles mixed had significantly different effective anisotropy. The dipolar interactions were strong enough to fully couple the two types of NPs at low fields. ZFC curves showed a single collective freezing temperature. On the other hand, this temperature increases with decreasing interparticle interactions, pointing out that the collective blocking temperature is however mainly determined by the (increasing) average local anisotropy. In fact, the non-linear dependence could be due to the competition between increasing average anisotropy and decreasing interactions.

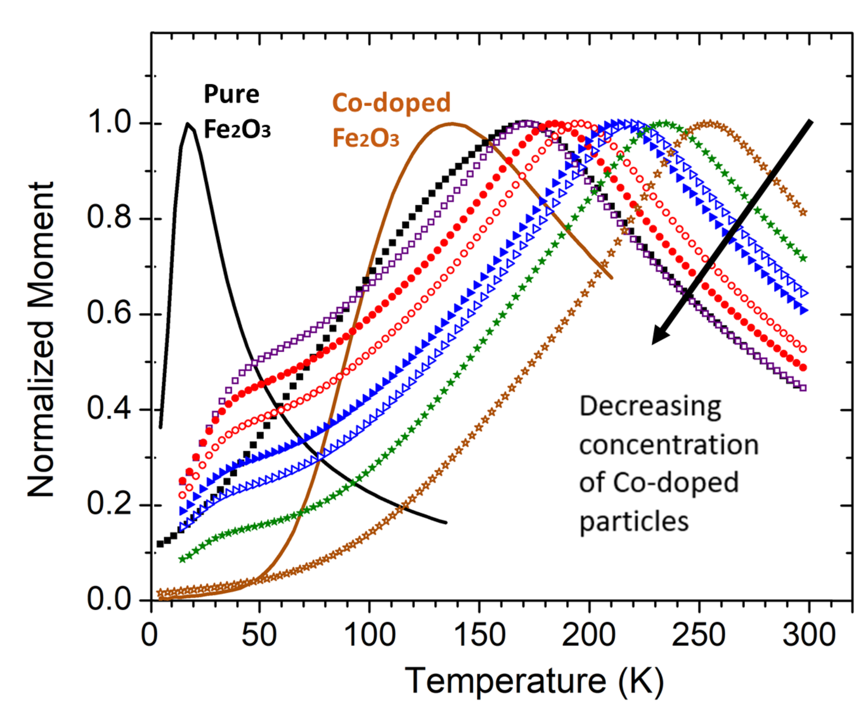

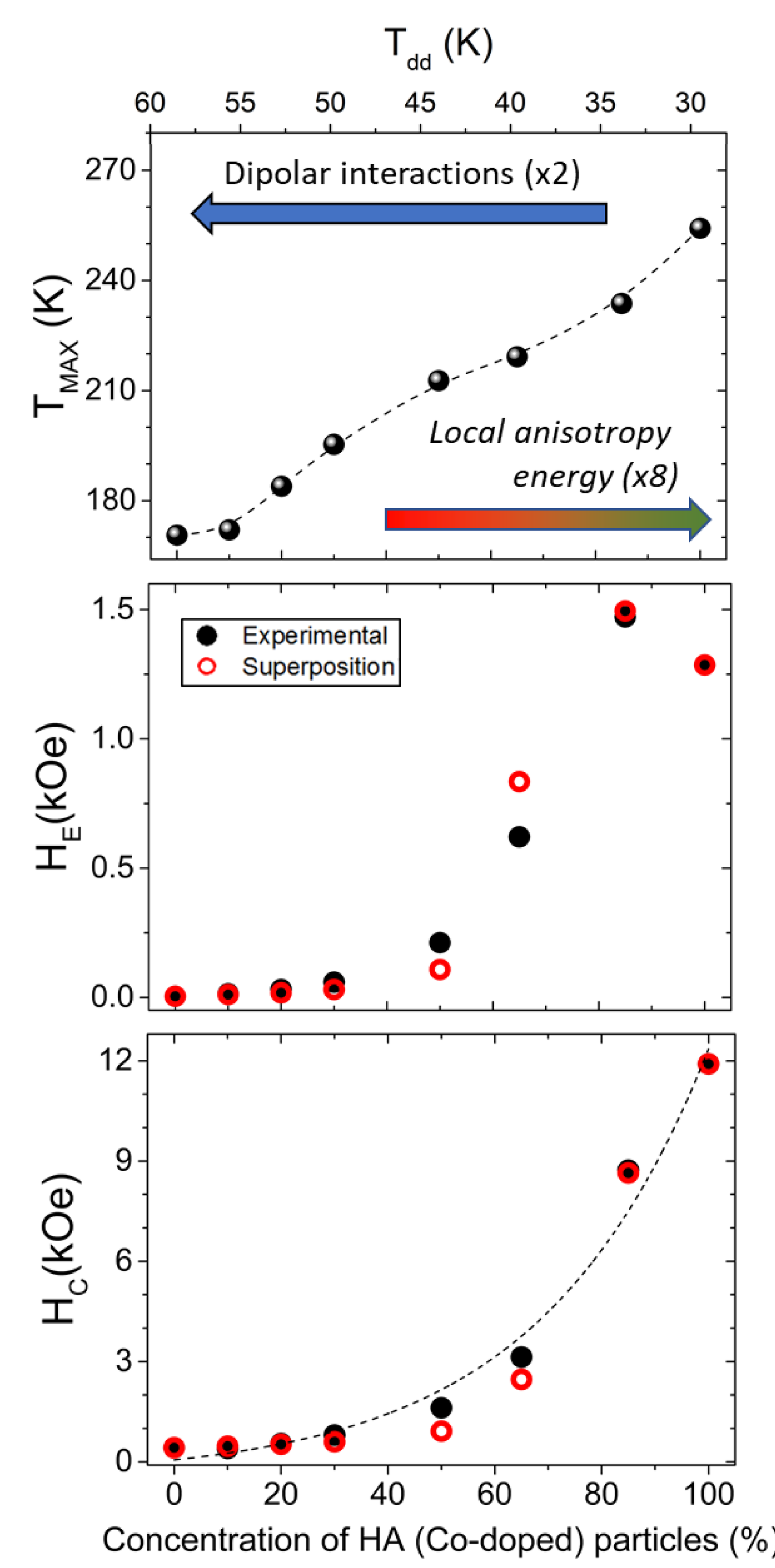

The high anisotropy contrast between the two particles populations led to de-coupled hysteresis loop similar to the weighted superposition of the pure systems. Although influenced by interparticle interactions, the magnetization reversal process was dominated by single particle anisotropy.[1]

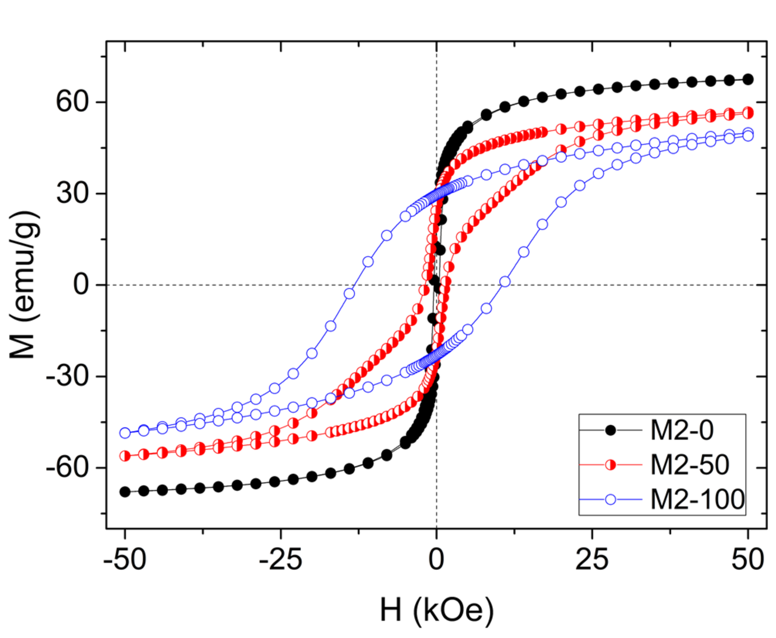

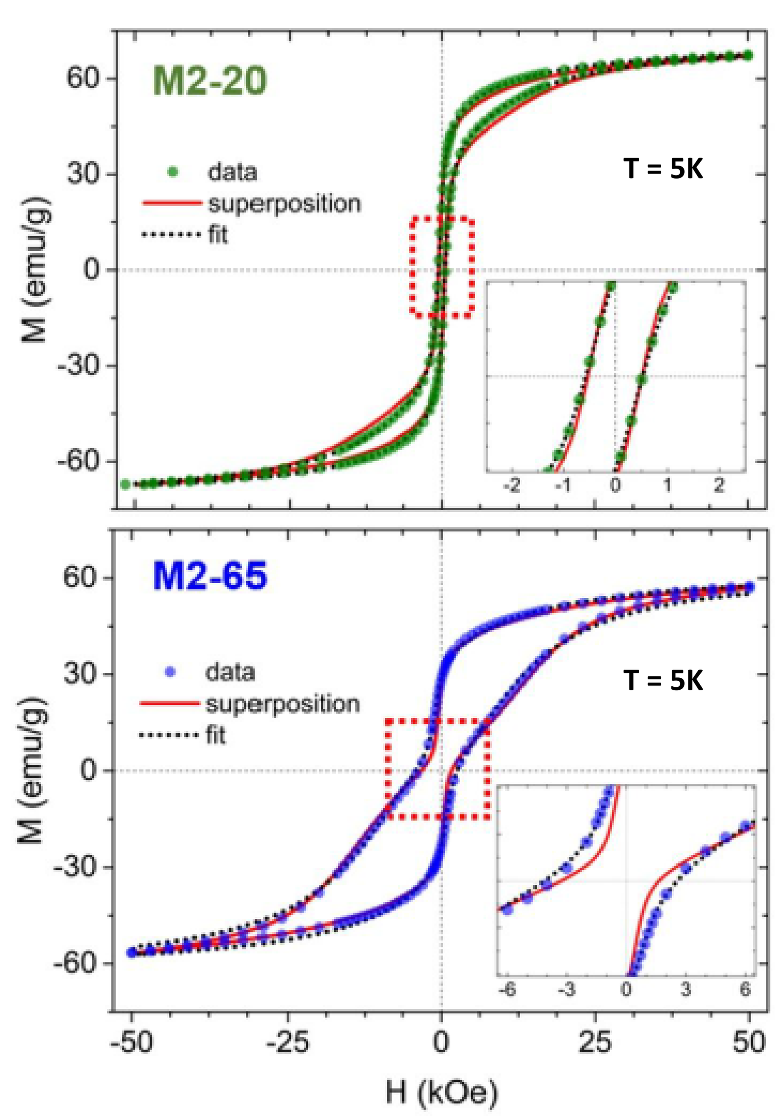

Hysteresis loops of 50% and 65% samples showed significant deviations at low fields from the calculated weighted superpositions of the end members loops. Dipolar interactions produced an increase in the coercivity field of the BRCs. This is understood in terms of the harder particles delaying the switching of the softer particles, which determines the coercivity value in these decoupled-like loops.

Remarkably, the exchange bias in the BRCs deviates from the superposition values, and it does it with different sign depending on the concentration. This is in contrast with maghemite NPs, where interparticle interactions had little effect on the exchange bias. [3]

Summary

- We have demonstrated the synthesis of nanoscale-homogeneous dense mixtures of nanoparticles, which allows to taylor the magnetic properties of such compacts.
- Despite the high anisotropy difference between the mixed particles, the systems present a collective blocking at low fields.
- The mixing produces an increase in coercivity with respect to the simple addition of (unmixed) populations (superposition loops).

Bibliography

[1] E. H. Sánchez et al., Chemistry of Materials 32, 969 (2020)
[2] J.A. De Toro et al., Chemistry of Materials 29, 8258 (2017)
[3] M.S. Andersson et al., Nanotechnology 26, 475703 (2015)

Acknowledgments

This work was financed by project MAT2015-65295-R (MINECO).

GOBIERNO DE ESPAÑA MINISTERIO DE ECONOMÍA, INDUSTRIA Y COMPETITIVIDAD

UCLM

Electric current effects in sensors based on anisotropic magnetoresistance

G. Gestoso[1], D. de Cos[2], M.L. Fdez-Gubieda[1,3], A. García-Arribas[1,3].

[1]*Basque Center for Materials, Applications and Nanostructures, BCMaterials, Spain*
[2]*Departamento de Física, Universidad del País Vasco UPV/EHU, Spain*
[3]*Departamento de Electricidad y Electrónica, Universidad del País Vasco UPV/EHU, Spain*

INTRODUCTION

Magnetic sensors based on the anisotropic magnetoresistance effect (AMR) are of great interest nowadays due to their numerous applications. One possible application is the detection of magnetic nanoparticles [1], since these sensors present a high sensitivity to slight magnetic field variations. However, one of the challenges posed by magnetoresistance-based sensors is the difficulty to obtain accurate numerical results when predicting their magnetic response [2].

MODELIZATION

The mulstiscale modelling process consists of three steps (depicted in the figures below):

I. Calculation, by micromagnetic simulations, of the magnetization configuration in the sensor for different values of an external magnetic field.
II. Solving a classical electrodynamic problem of current transport based on the magnetic state obtained in the previous point using Finite Element Method (FEM).
III. Calculate magnetic field generated by the current distribution in the sensor.

The results from each study condition the other one and is solved in an auto-consistent way to reach convergence criteria.

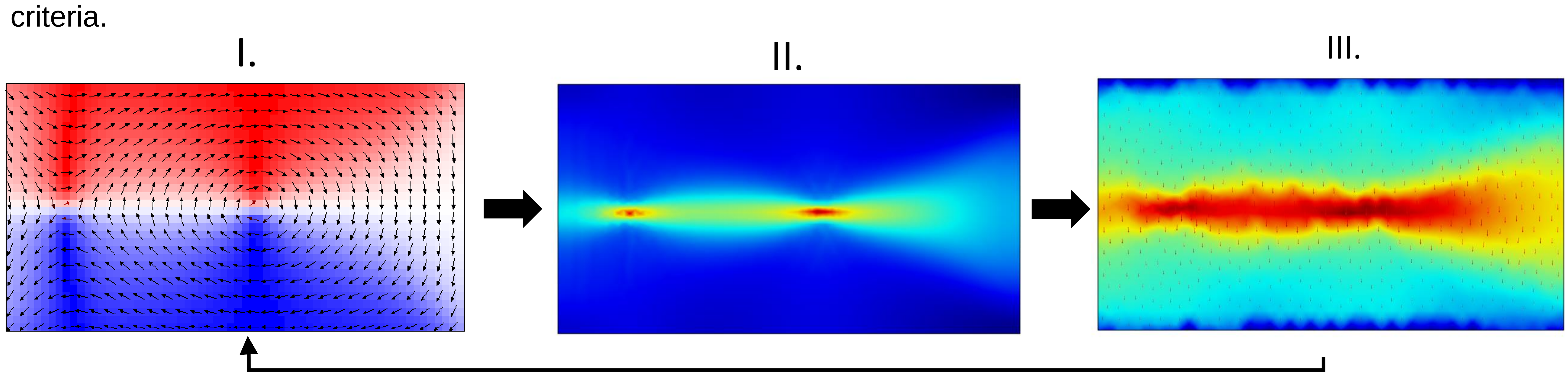

RESULTS

The electric current passing through an AMR sensor **is not uniform due to the resistivity dependence of the magnetization state**. As a result, we can obtain:

- The field generated by the electric current flowing through the sensor can generate asymmetries in the magnetoresistance (ΔR vs H) curve (Figure (A)).
- The described effect is heavily influenced by the sensor geometry, especially near the contacts, where the highest current accumulation takes place (Figure (B)).

The sensitivity of the sensor is $25\ m\Omega$ per kA/m versus 39 $m\Omega$ per kA/m when the effect produced by the current is considered, in a test sample consisting of a 10 nm thick Permalloy thin film with an elliptical shape (320 x 160 nm).

(A)

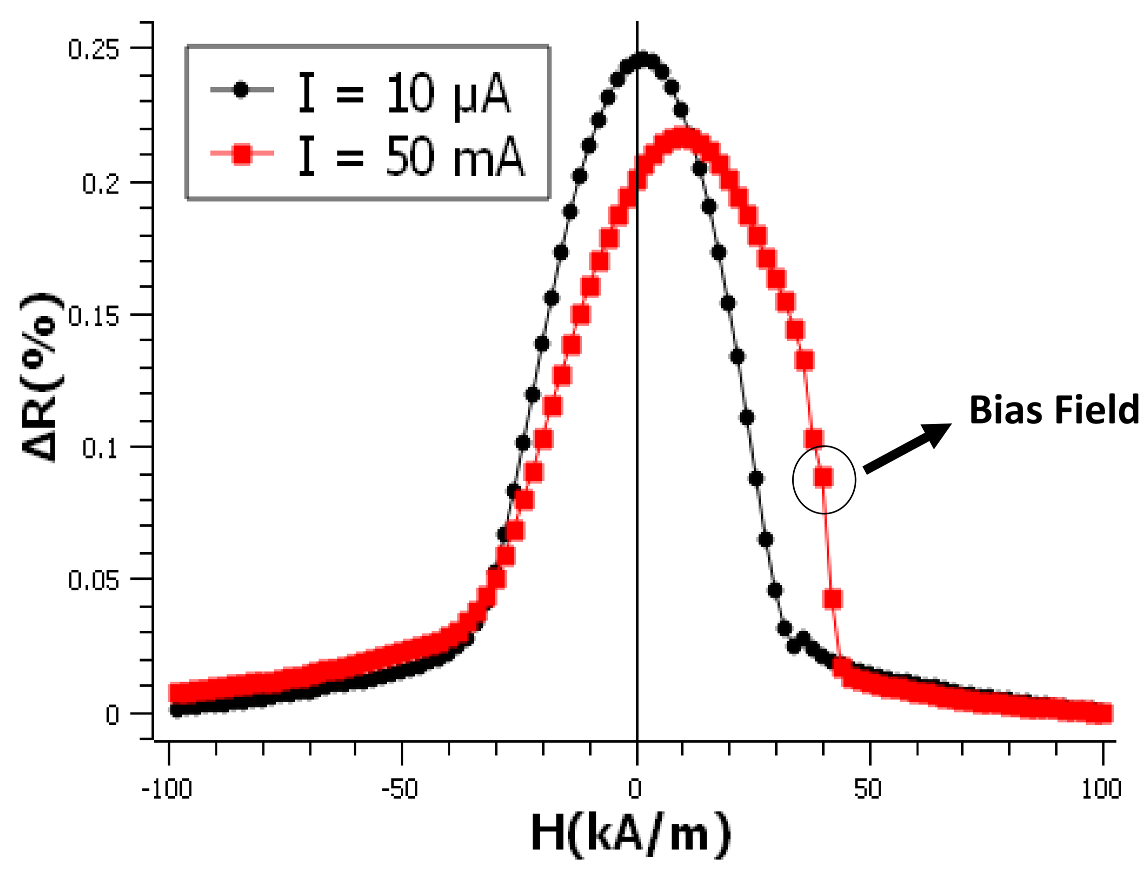

(B)

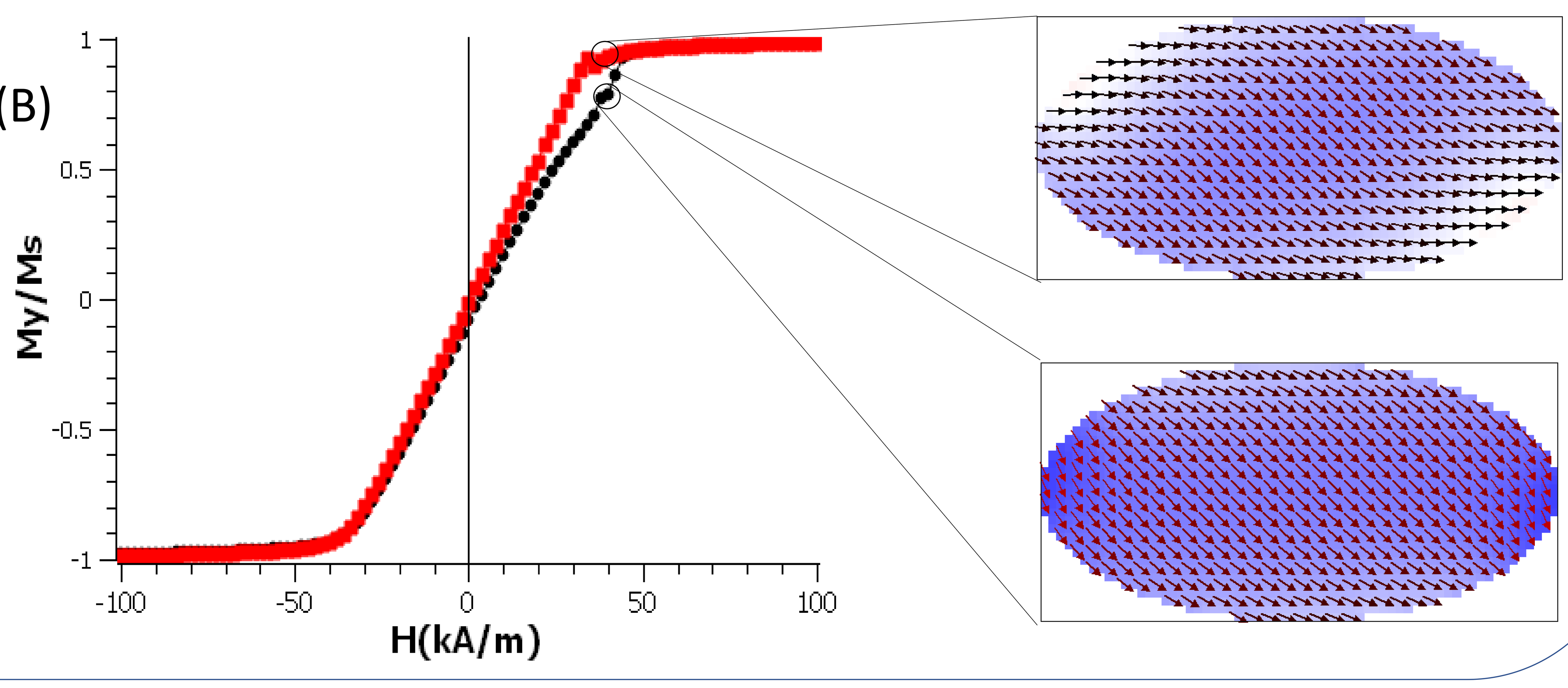

CONCLUSIONS

- Considering the effect of the field generated by the current provides more realistic results.
- Magnetization affects electric current and electric current affects the magnetization.
- The effect of the electric current improves the sensitivity of the sensor.

REFERENCES

[1] L. K. Quynh et al., Journal of Electronic Materials, 2019, 997–1004.

[2] M. Ferreira Velo et al, Journal of Magnetism and Magnetic Materials, 167945, 2021.

High Anomalous Nernst Effect on magnetic multilayers with Perpendicular Magnetic Ansotropy

G. Lopez-Polin[1], H. Aramberri[2], J. Marques-Marchan[1], J.I. Cerda[1], B. Weintrub[3], K.I. Bolotin[3], A.Asenjo[1].

[1] Instituto de Ciencia de Materiales de Madrid (CSIC), 28049 Madrid (Spain)
[2] Luxembourg Institute of Science and Technology, 4362 Esch-sur-Alzette (Luxembourg)
[3] Freie Universitat Berlin, 14195 Berlin (Germany)

Materials with Perpendicular Magnetic Anisotropy (PMA) are very convenient to maximize the Anomalous Nernst Effect (ANE). We have explored the ANE of Co/Pt sputtered multilayers, which show high PMA [1] and studied the dependence of the ANE with the magnetization. We performed Magnetic Force Microscope (MFM) images of the structures while applying the thermal gradient and measuring the Nernst voltage.

Deposition of Co/Pt Multilayers

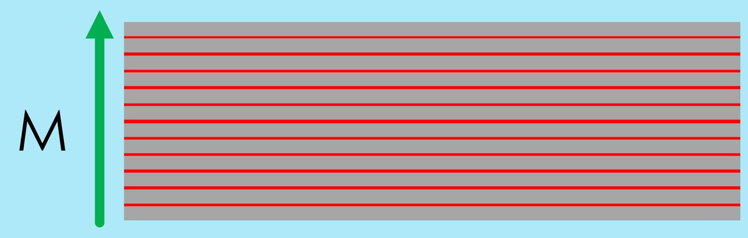

Alternative sputtering deposition of Pt and Co

10x[Co(0.6nm)/Pt(1.8nm)]

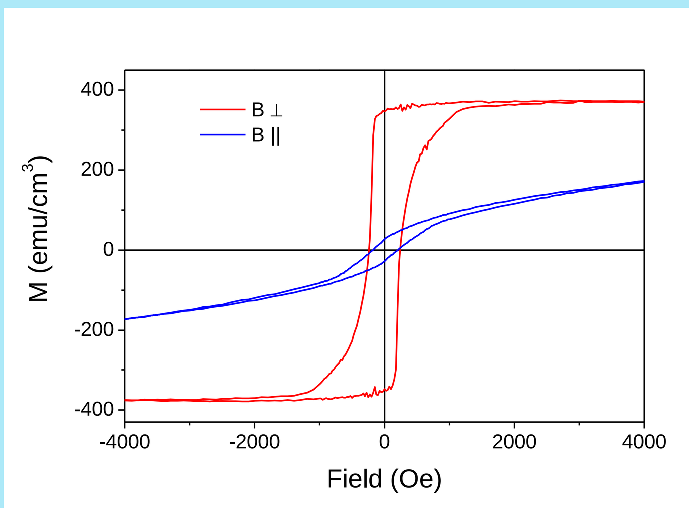

MFM image

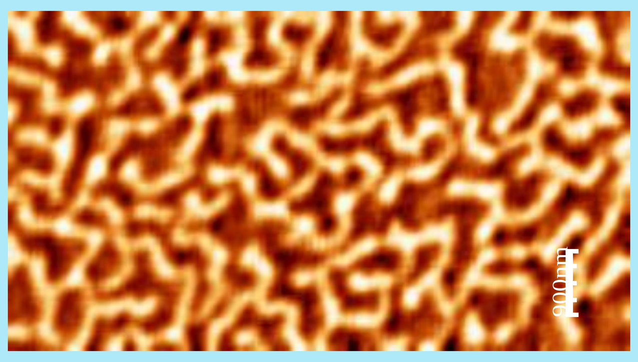

High anisotropic magnetic behavior: Remanence is mainly out of plane.

Fabrication of Co/Pt devices

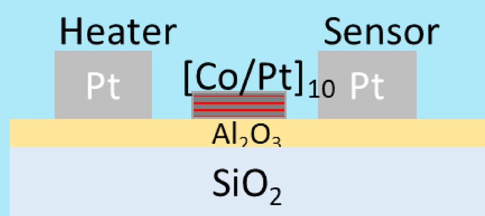

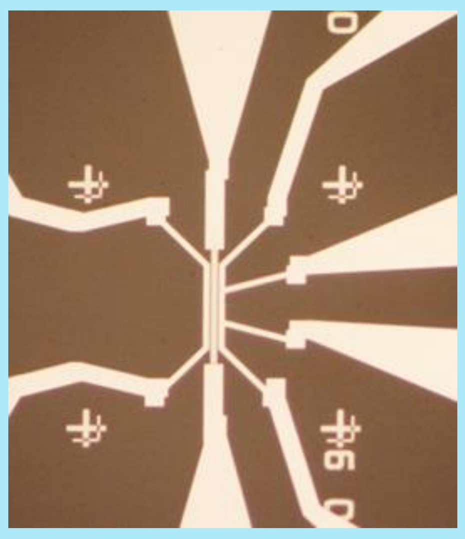

Topography

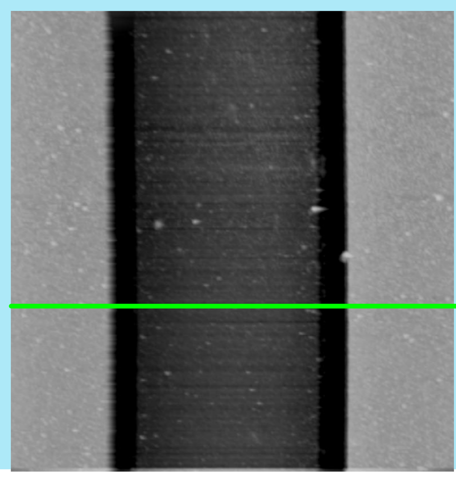

Magnetic signal (MFM)

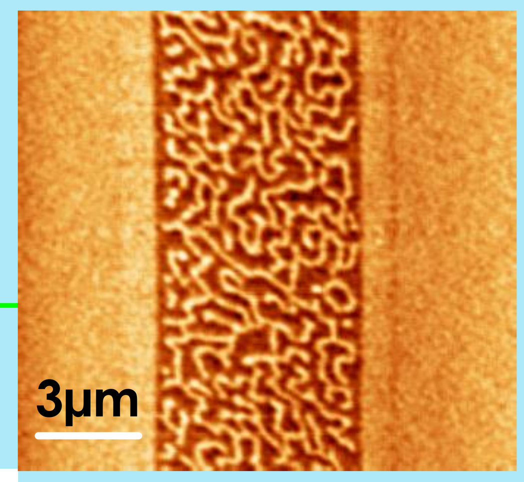

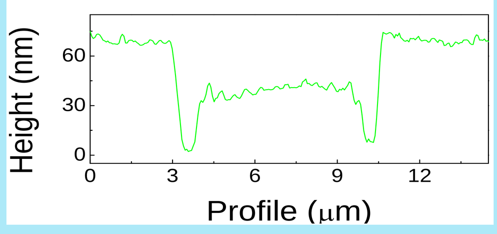

The device was microfabricated by electron beam lithography.

Wormlike magnetic domain structure of the Co/Pt multilayer (m~0)

Anomalous Nernst effect

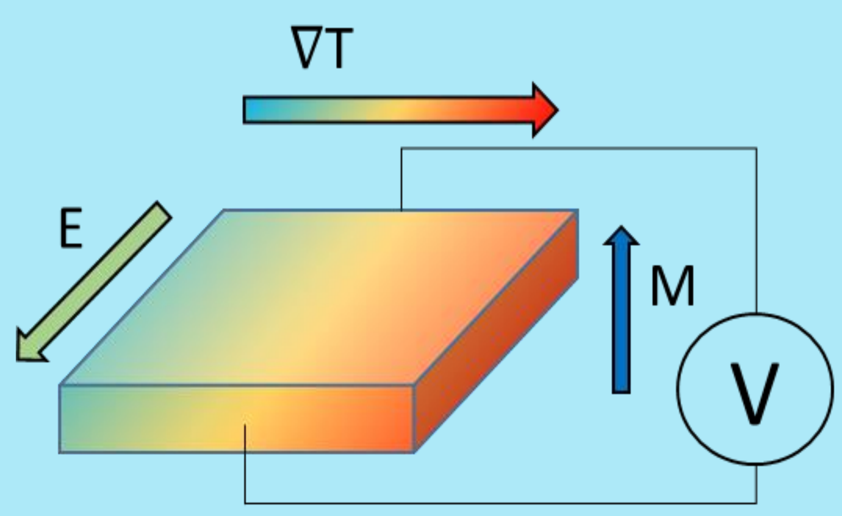

A thermal gradient perpendicular to the magnetization of a magnetic sample produces an electric field perpendicular to both.

ANE has attracted interest during the last years for applications in energy harvesting [2,3].

ANE of Co/Pt multilayers

Nernst voltage vs magnetic field and temperature gradient:

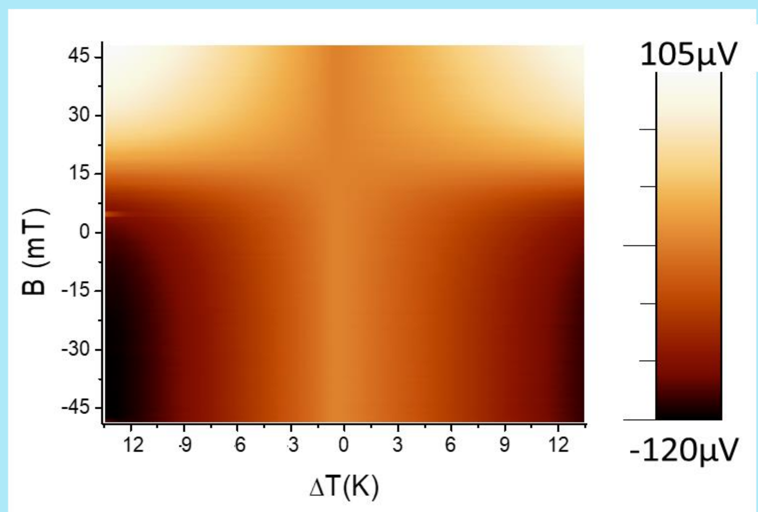

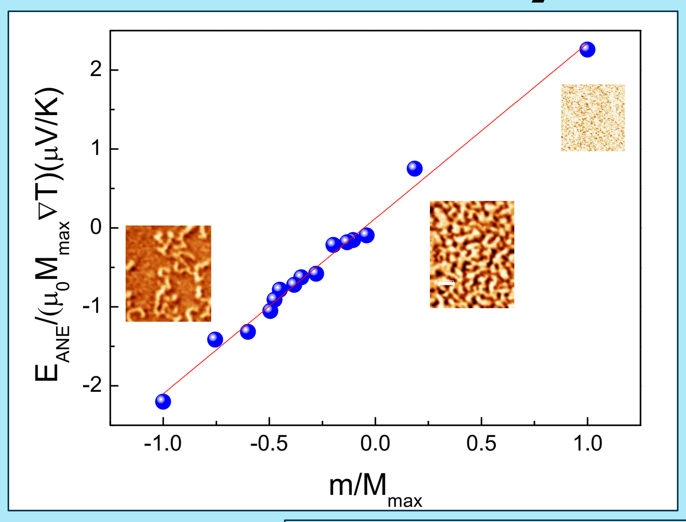

Voltage obtained vs magnetization of the sample as measured by MFM

Hysteresis loop of the Nernst voltage vs field :

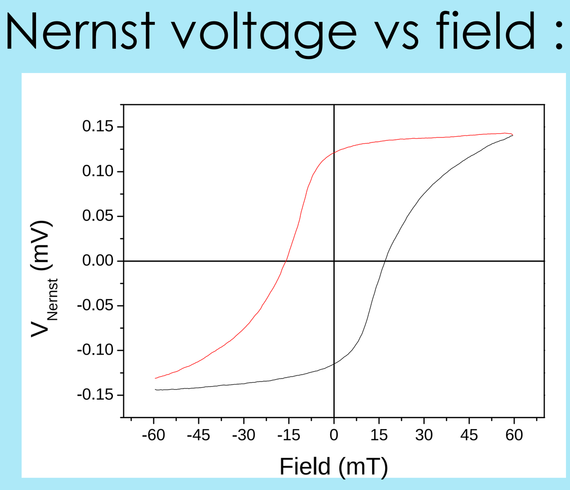

Voltage and current vs thermal gradient:

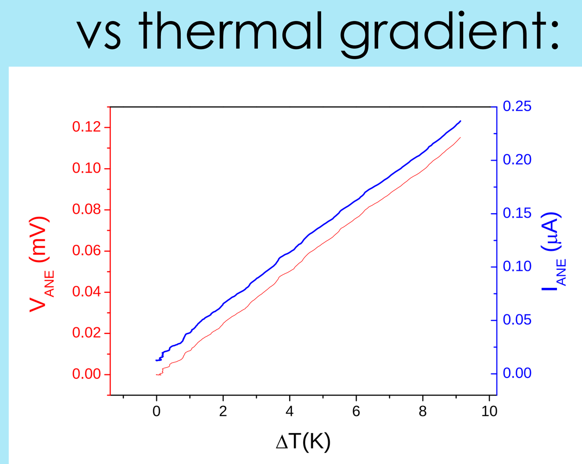

High sensitivity

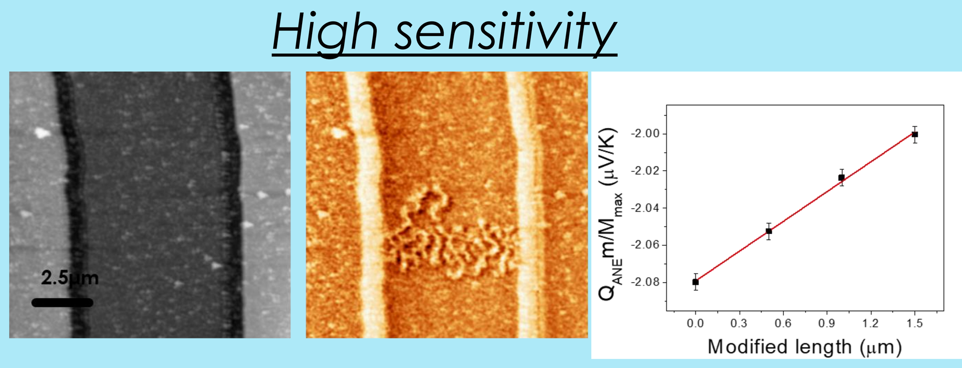

Measuring differences in ANE Voltage of submicron modified areas

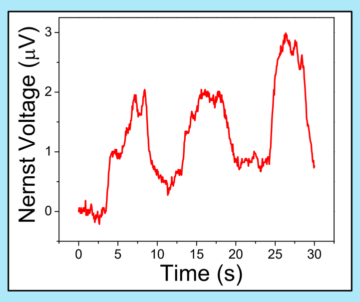

Detecting finger's heat at room temperature

References

[1] S. Hashimoto et al. *Journal of Applied Physics* 66, 4909 (1989)

[2] M. Mizuguchi & S. Nakatsuji , *Sci Technol Adv Mater,* 20:1, 262 (2019)

[3] A. Sakai et al. Nature, 581(7806), 53-57 (2020).

[4] B. He et al., Joule, https://doi.org/10.1016/j.joule.2021.08.007 (2021)

Conclusions

- We found a high ANE coefficient of ~0.9µV/K for $10x[Co_{0.6}/Pt_{1.8}]$, which, despite being smaller, is in the same order of magnitude of the maximum ever observed in other materials [4] but with the advantage of having a magnetization with a well-defined direction.

- We fabricated devices with high sensitivity to the field and to the temperature.

Enhancing the magnetocaloric response of high-entropy metallic-glass by microstructural control

Hangboce Yin[1,2], Jia Yan Law[2], Yongjiang Huang[1], Hongxian Shen[1], Sida Jiang[3], Shu Guo[1], Victorino Franco[2], Jianfei Sun[1]

hbcyin@hit.edu.cn; hbcyin@us.es

[1] School of Materials Science and Engineering, Harbin Institute of Technology, 150001-Harbin, China
[2] Dpto. Física de la Materia Condensada, ICMS-CSIC, Universidad de Sevilla, 41080-Sevilla, Spain
[3] Space Environment Simulation Research Infrastructure, Harbin Institute of Technology, 150001-Harbin, China

Publication of this work

Non-equiatomic high-entropy alloys (HEAs), the second-generation multi-phase HEAs, have been recently reported with outstanding properties that surpass the typical limits of conventional alloys and/or first-generation equiatomic single-phase HEAs [1-3].

Non-equiatomic $(Gd_{36}Tb_{20}Co_{20}Al_{24})_{97}Fe_3$ microwires, with Curie temperature up to 108 K, overcome the typical low temperature limit of rare-earth-containing HEAs (80 % increase) [4]. In this work [5], we further optimize their magnetocaloric response by microstructural control using the current annealing technique. The precipitation of nanocrystals within the amorphous matrix leads to a phase compositional difference that increases with current density, whereby within a certain range, the working temperature span broadens and simultaneously offers relative cooling power values that are at least 2-fold larger than many reported conventional magnetocaloric alloys, both single amorphous phase or multi-phase character (amorphous and nanocrystalline), while keeping a large ΔS_M. This demonstrates that microstructural control is a feasible way, in addition to appropriate compositional design selection, to optimize the magnetocaloric effect of HEAs.

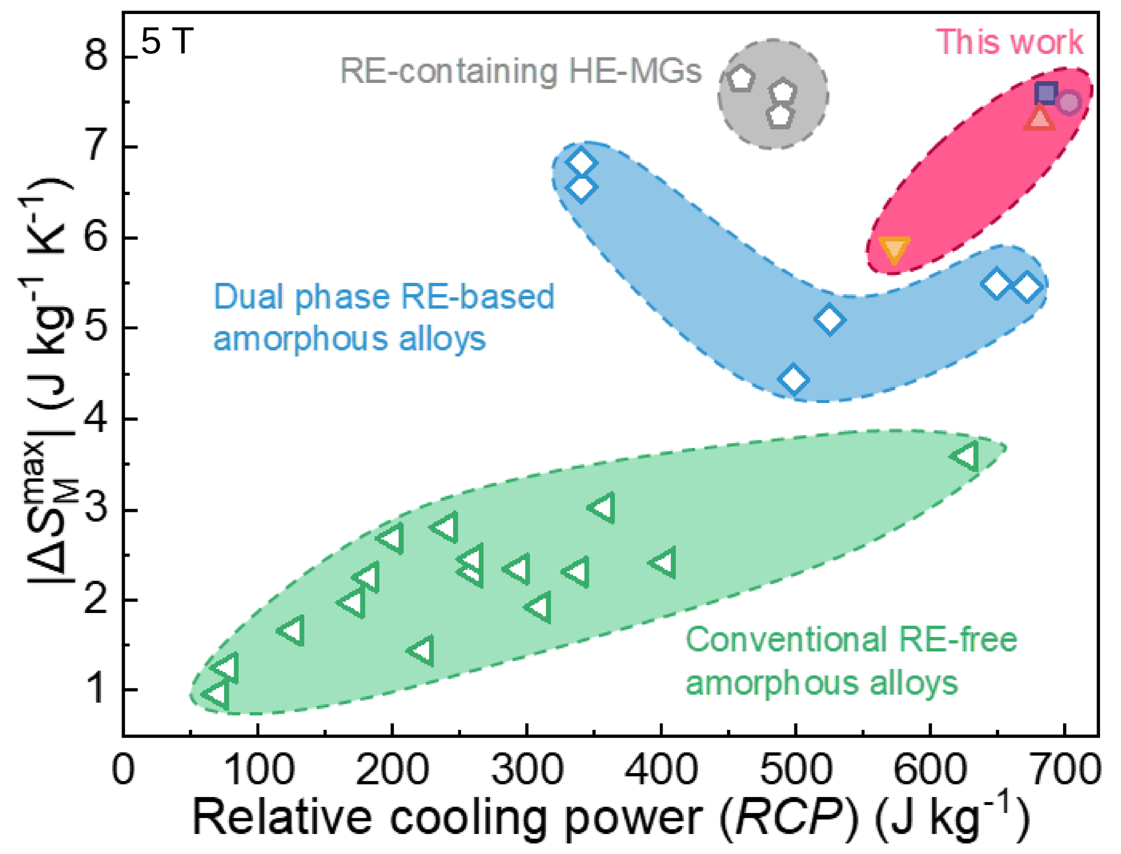

Microstructural control with current density

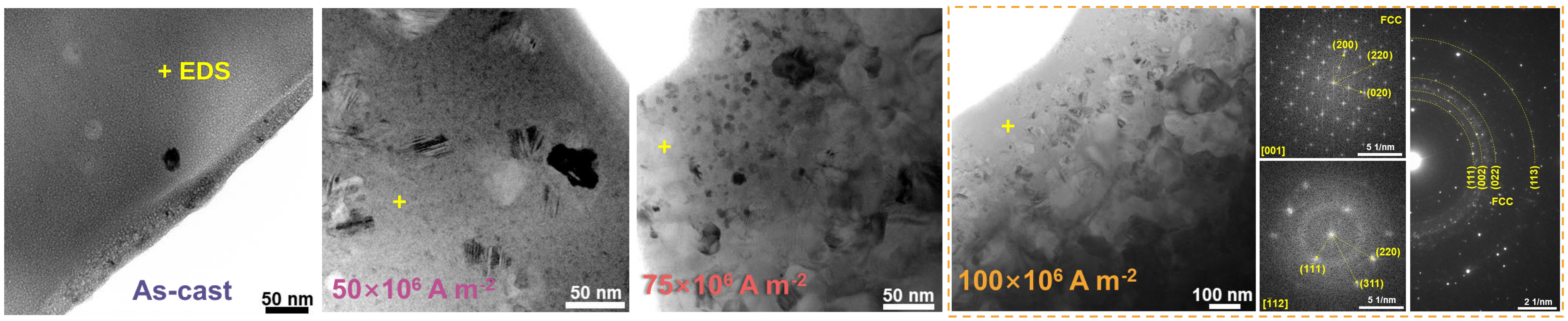

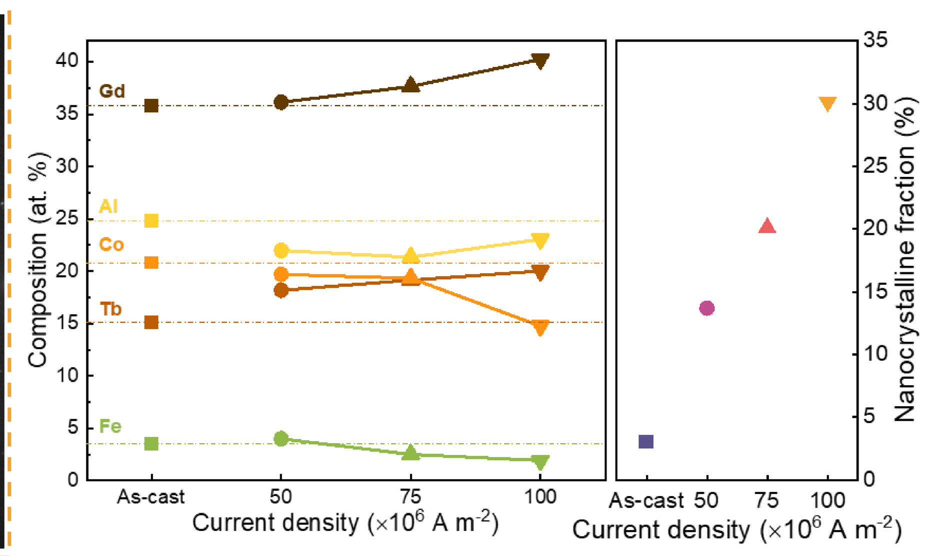

- Current annealing creates the nanocrystals within the amorphous matrix.
- The structure of the nanocrystalline phase is face-centered cubic (FCC).
- The increased current density increases the nanocrystalline fraction.
- The amorphous phase composition changes due to the change of nanocrystalline fraction.

Magnetocaloric properties

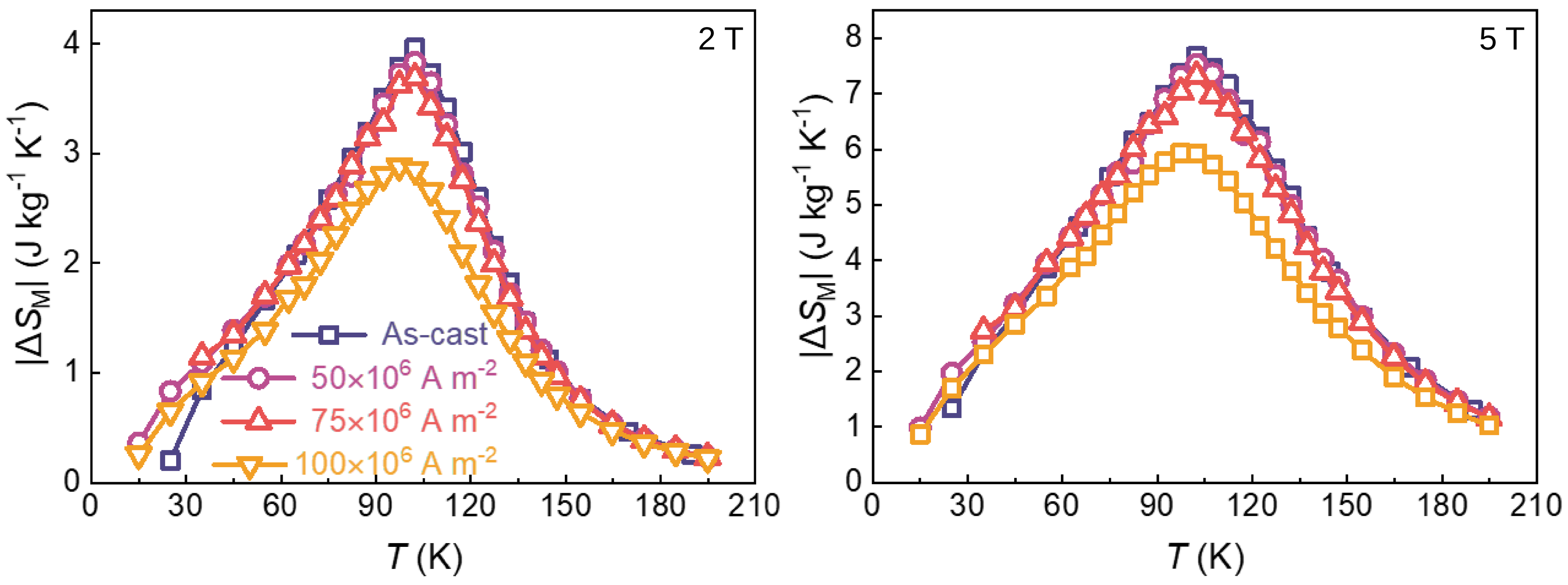

- For the annealed microwires, the magnetocaloric peak for nanocrystalline phase can be observed for low fields.
- Up to 75×10⁶ A m⁻², the annealed microwires retain the magnitude of the magnetic entropy change of the as-cast state.

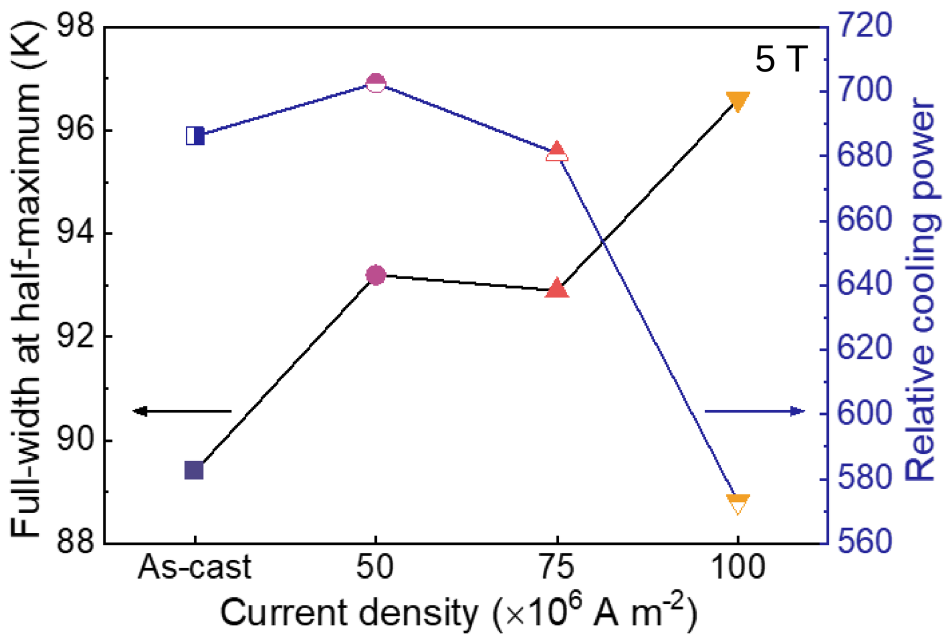

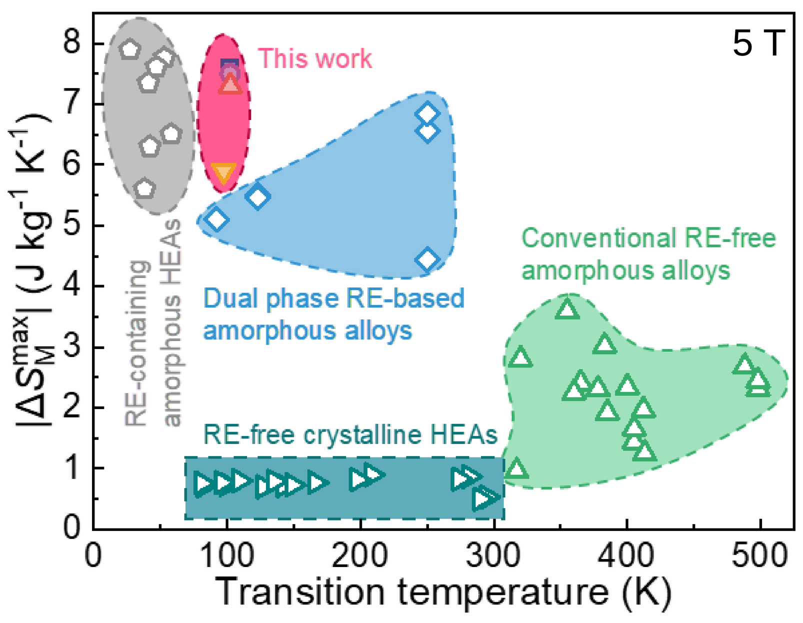

- The microwires annealed at 50×10⁶ A m⁻² show enhanced magnetocaloric response due to the composition difference between nanocrystalline and amorphous phases.
- Our work lies in the temperature range of natural gas liquefaction.

Critical behavior

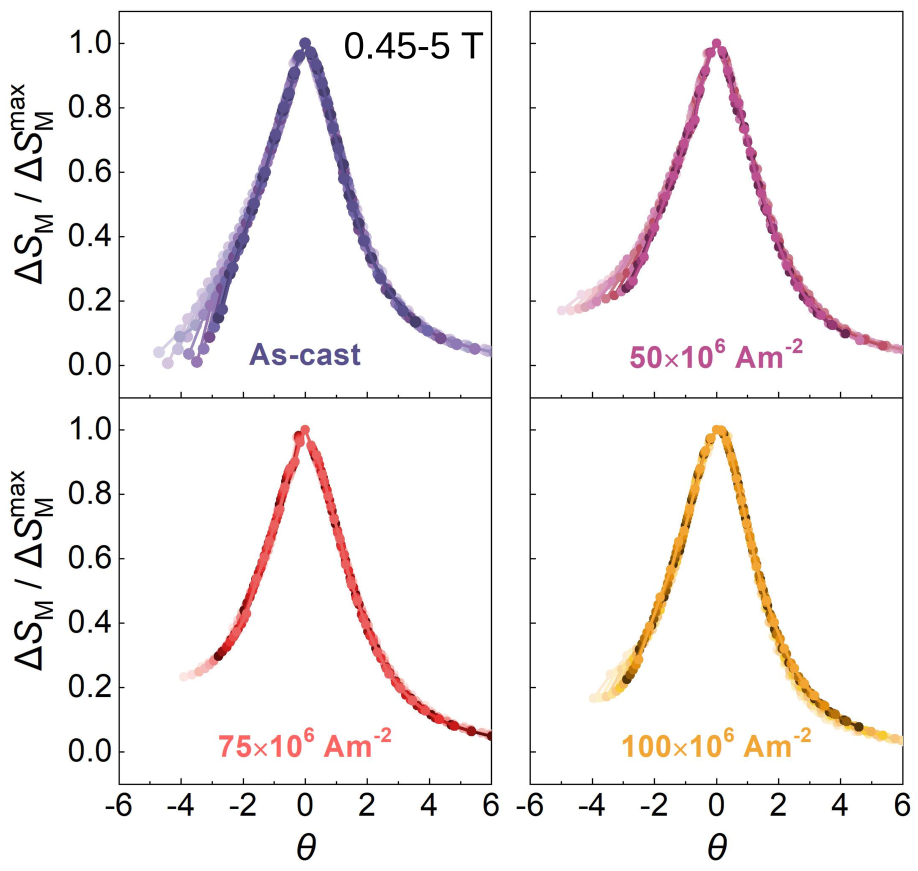

$$\theta = \begin{cases} -(T - T_{max})/(T_{r1} - T_{max}); T \le T_{max} \\ (T - T_{max})/(T_{r2} - T_{max}); T > T_{max} \end{cases}$$

- Using two reference temperatures, the challenge in rescaling the magnetocaloric curves with multiphase character is resolved.
- All microwires undergo second-order-phase-transition.

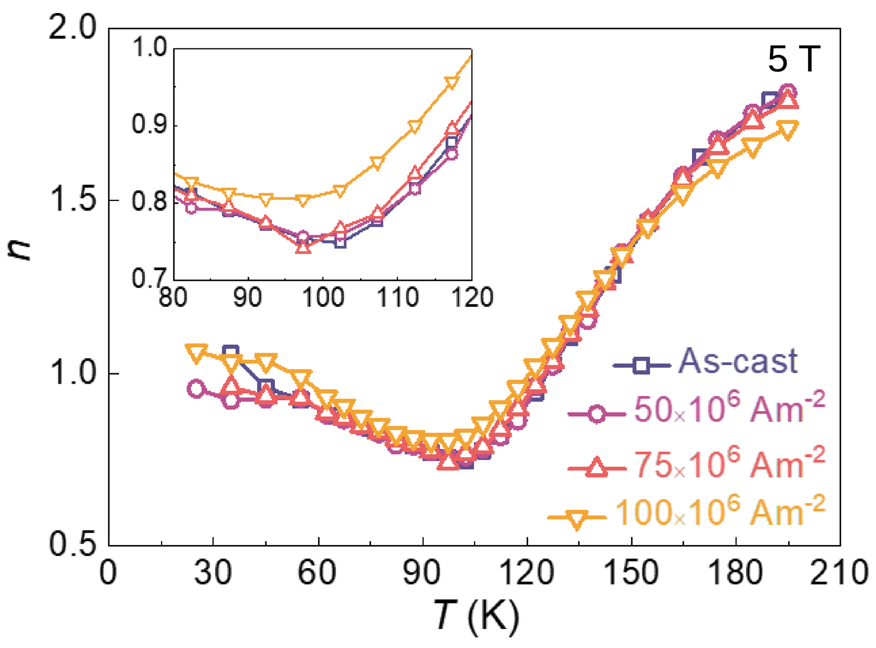

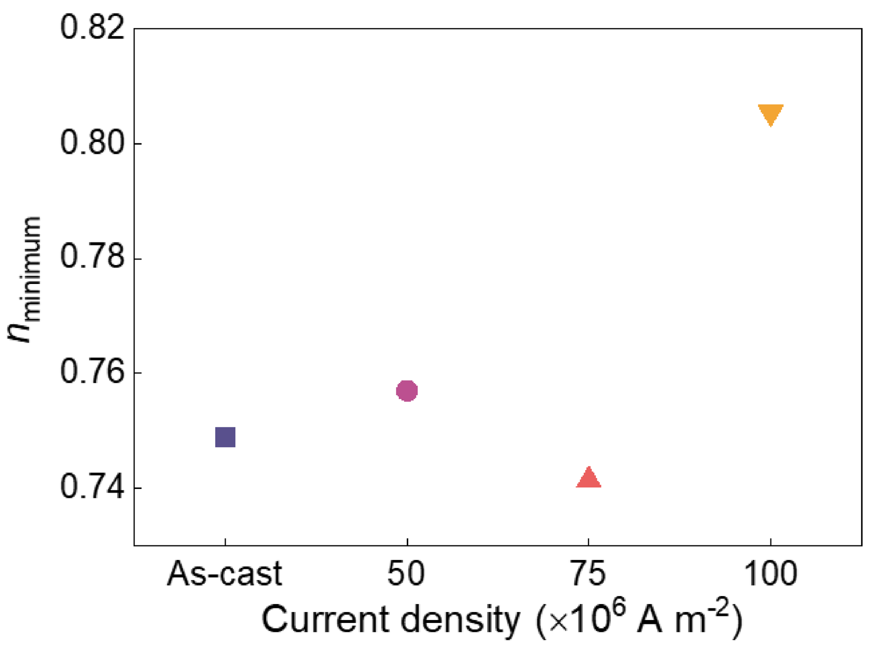

$$n = \frac{d \ln |\Delta S_M|}{d \ln |\mu_0 \Delta H|}$$

- The critical exponents for 100×10⁶ A m⁻² microwires are higher than other studied microwires, associated to a change of critical behavior.
- This is attributed to the composition change of amorphous phase by high nanocrystalline fraction.

Conclusions

- Nanocrystalline fraction is precisely tuned by current annealing.
- Annealed microwires show relatively high transition temperatures and enhanced magnetocaloric response.
- Our work demonstrates that microstructural control is a feasible way to optimize the magnetocaloric properties of HEAs.
- The critical behavior of amorphous phase is changed by high nanocrystalline fraction.

Acknowledgments

The work was supported by the financial support from the National Natural Science Foundation of China under Grant No. 51871076, 51671070, 51801044, and 51827801, and the 66th China Postdoctoral Science Foundation under Grant No. 2019M661275. V.F. and J.Y.L. acknowledge funding from AEI/FEDER-UE (grant PID2019-105720RB-I00), US/JUNTA/FEDER-UE (grant US-1260179), and Consejería de Economía, Conocimiento, Empresas y Universidad de la Junta de Andalucía (grant P18-RT-746). H.Y. acknowledges the fellowship from China Scholarship Council (CSC, No. 201906120183) for Visiting PhD Student program.

References

1. J.Y. Law, V. Franco, APL Materials, 9 (2021) 080702.
2. J.Y. Law, Á. Díaz-García, L.M. Moreno-Ramírez et al., Journal of Alloys and Compounds., 855 (2021) 157424.
3. J.Y. Law, Á. Díaz-García, L.M. Moreno-Ramírez et al., Acta Materials, 212 (2021) 116931.
4. H. Yin, J.Y. Law, Y. J. Huang et al., Materials & Design, 2021, 206: 109824.
5. H. Yin, J.Y. Law, Y. J. Huang et al., Science China Materials, Accepted (2022)

Universitat de Girona
Departament de Física

Analysis of the Effects of Chemical Composition and Manufacturing Conditions of Soft Nanocrystalline Magnetic Alloys and Composites

J. Daza[1], W. Ben Mbarek[1], L. Escoda[1], J. J. Suñol[1]

[1]*Department of Physics, Higher Polytechnic School, Campus Montilivi s/n, University of Girona, 17003, Spain*

ABSTRACT

Soft nanocrystalline alloys have been widely analysed and studied during the past few years for various applications. However, optimisation of specific chemical compositions is still being developed. The applicability of these soft nanocrystalline alloys depends mainly on the presence of nanocrystalline structures within the alloy. For this reason, manufacturing conditions of these alloys must be taken into consideration. In this study, the analysed alloys are manufactured by mechanical alloying (MA), melt spinning (MS) or the Taylor-Ulitovski method (TU). Also, composites are produced using the soft nanocrystalline alloy as the reinforcement and an epoxy resin or glass coating for the matrix (developed from metallic powders, ribbons or microwires). The principal aim of the study is to determine the effects of chemical composition and manufacturing conditions on the various soft nanocrystalline alloys. The analyses performed on the samples include a microstructural analysis, a thermomechanical analysis and a complementary functional analysis in the form of the thermomagnetic response of the various samples. The results clearly show the dependence of chemical composition on the analysed properties for the corresponding alloys. Also, manufacturing conditions have been observed to have an effect on properties such as crystal growth peak temperature.

Fe-based Alloys

Chemical Formula (at. %)	Label	Morphology/Technique
$Fe_{73.5}Si_{13.5}B_9Cu_1Nb_3$	B9-40 (40 h MA)	Powder/MA
	B9	Powder/MA
$Fe_{73.5}Si_{11.5}B_{11}Cu_1Nb_3$	B11	Powder/MA
$Fe_{73.5}Si_{9.5}B_{13}Cu_1Nb_3$	B13	Powder/MA
$Fe_{73.5}Si_{7.5}B_{15}Cu_1Nb_3$	B15	Powder/MA
$Fe_{73.5}Si_{13.5}P_9Cu_1Nb_3$	P9-40 (40 h MA)	Powder/MA
	P9	Powder/MA
$Fe_{99}Mn_1$	$Fe_{99}Mn_1$	Powder/MA
$Fe_{98}Mn_2$	$Fe_{98}Mn_2$	Powder/MA

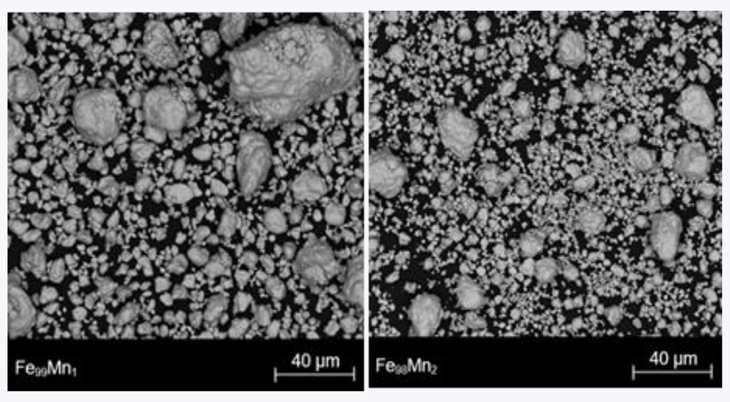

Thermal Analysis

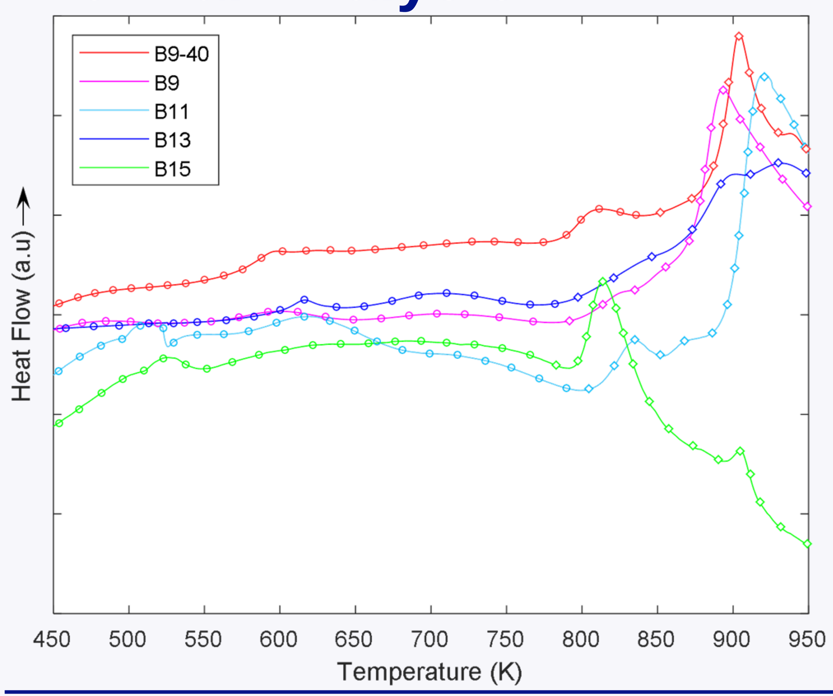

Magnetic Analysis

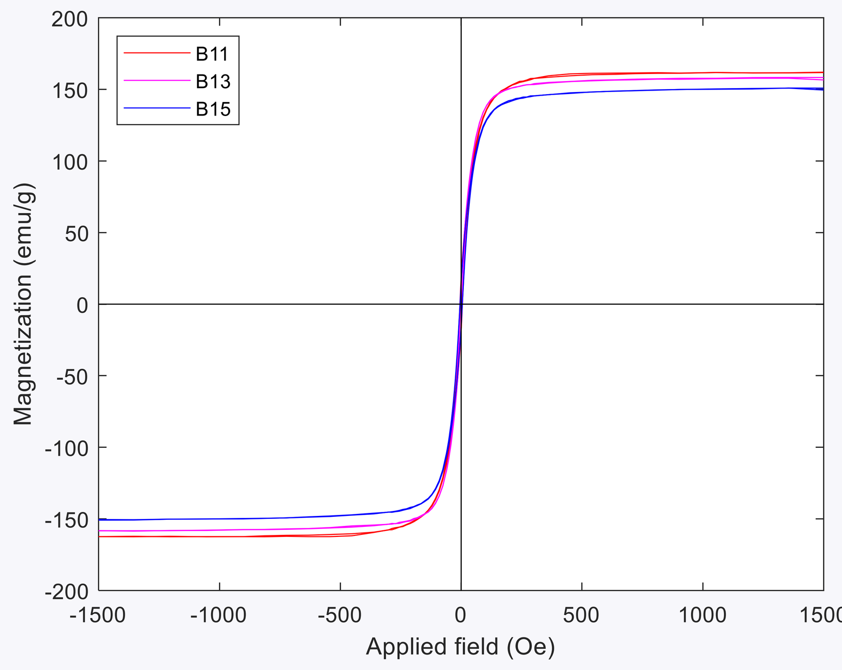

Structural Analysis

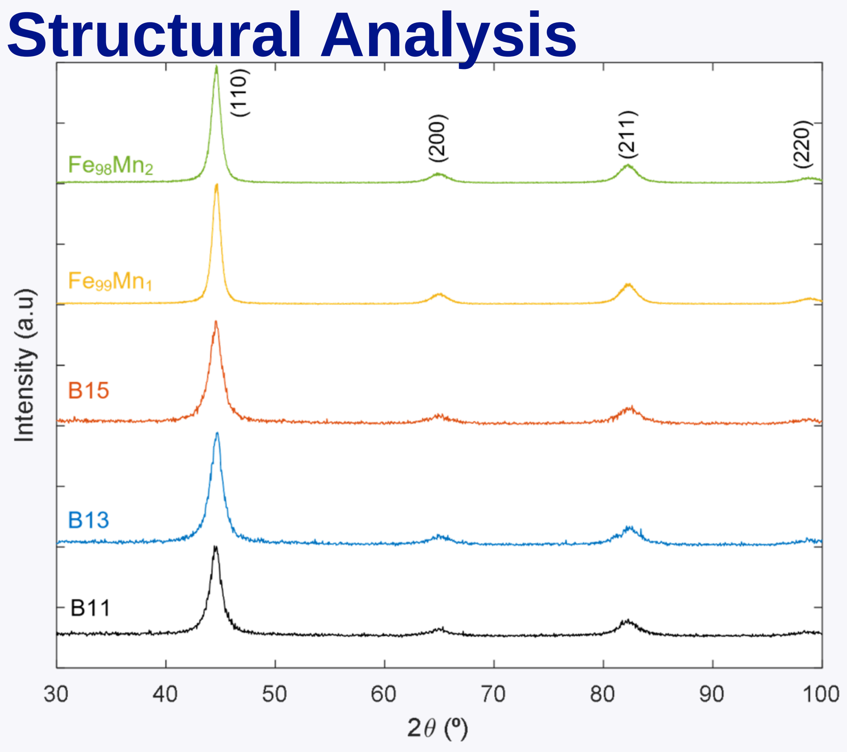

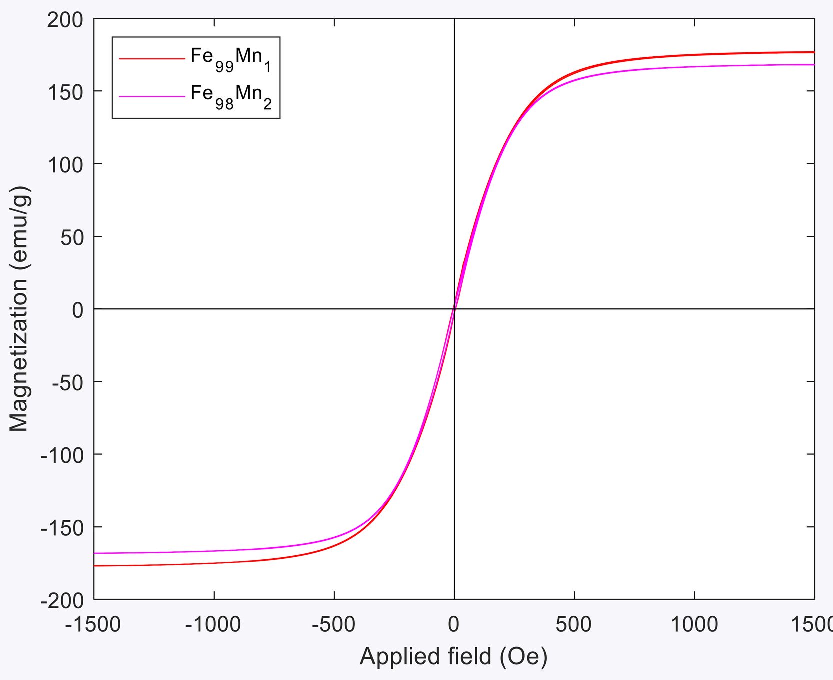

Sample	*a* (Å)	Crystal size (Å)	Microstrain index	R_{wp} (%)	R_{exp} (%)	GoF	H_c (Oe)	M_r (emu/g)	M_s (emu/g)	M_r/M_s
B11	2.867±0.001	90.3±1.3	$0.00257±9·10^{-5}$	21.072	20.802	1.013	10.0	18.0	162.5	0.1109
B13	2.866±0.001	88.7±1.2	$0.00457±1·10^{-4}$	18.808	18.477	1.018	5.6	11.7	158.3	0.0737
B15	2.864±0.001	86.6±1.1	$0.00400±2·10^{-5}$	19.233	19.055	1.009	9.4	14.8	150.9	0.0978
$Fe_{99}Mn_1$	$2.870±2·10^{-4}$	184.3±0.2	$0.00540±4·10^{-6}$	14.969	12.496	1.198	10.4	3.4	176.5	0.0193
$Fe_{98}Mn_2$	$2.871±2·10^{-4}$	168.0±1.1	$0.00529±4·10^{-5}$	14.739	12.343	1.194	7.2	2.4	168.2	0.0143

Ni-Mn-based Alloys

Chemical Formula (at. %)	Label	Morphology/Technique
$Ni_{50}Mn_{38}Sn_{12}$	$Ni_{50}Mn_{38}Sn_{12}$	Ribbon/MS
$Ni_{50}Mn_{35}In_{15}$	$Ni_{50}Mn_{35}In_{15}$	Microwire/TU

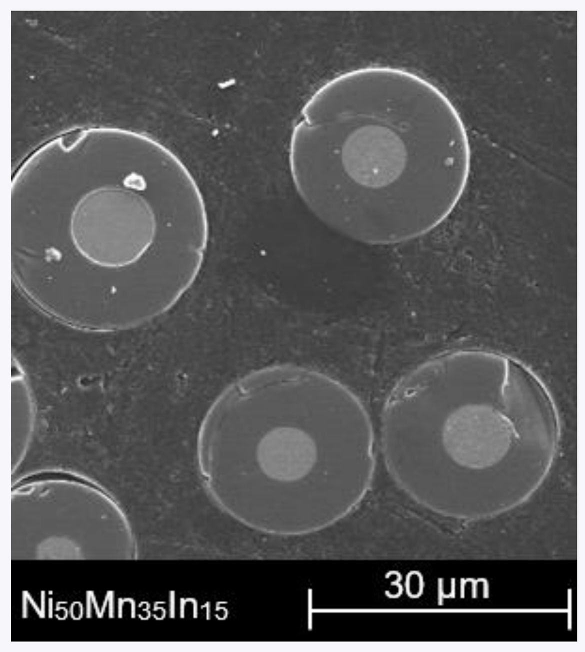

Thermal Analysis

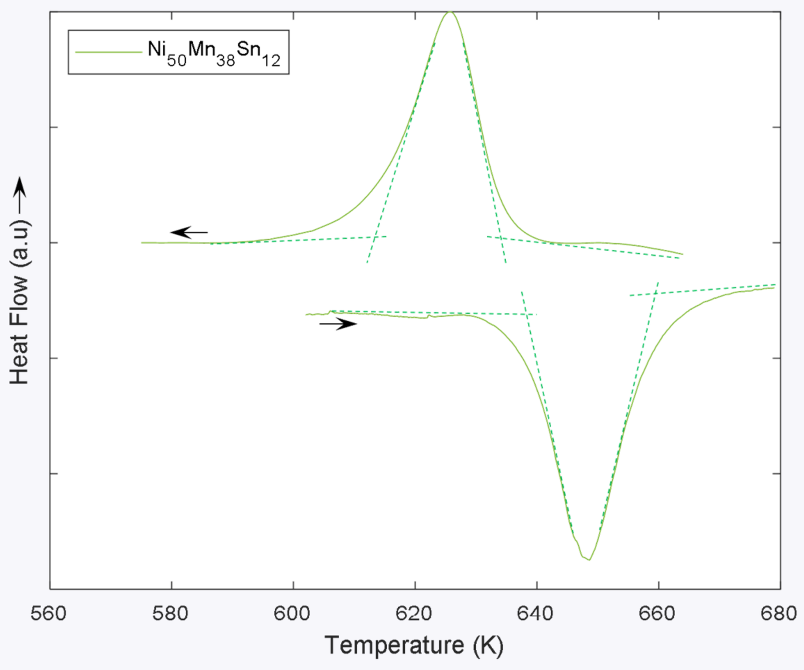

Sample	M_s (K)	M_f (K)	A_s (K)	A_f (K)
$Ni_{50}Mn_{38}Sn_{12}$	636	613	637	659

Thermomechanical Analysis

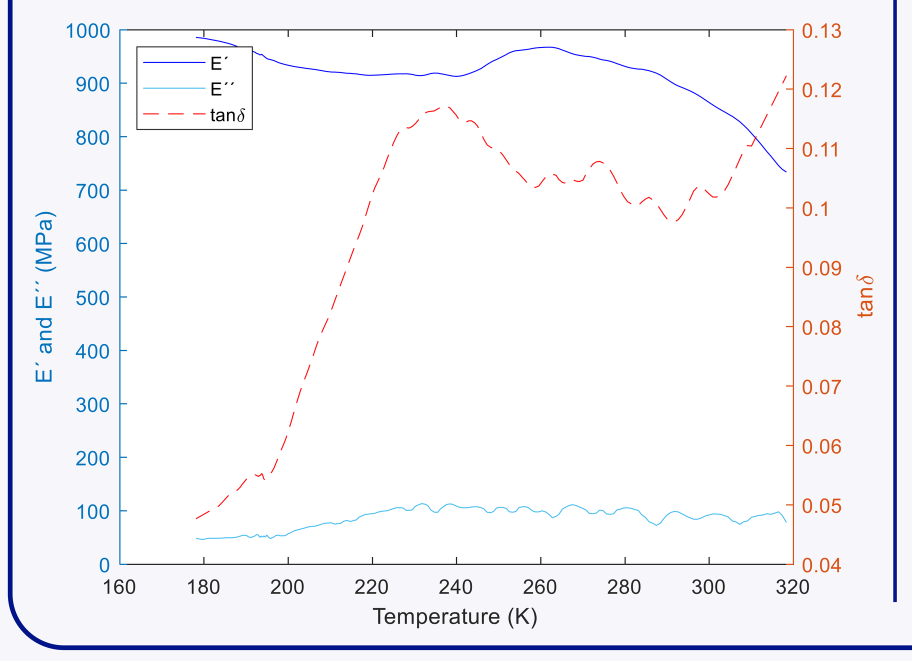

Magnetic Analysis

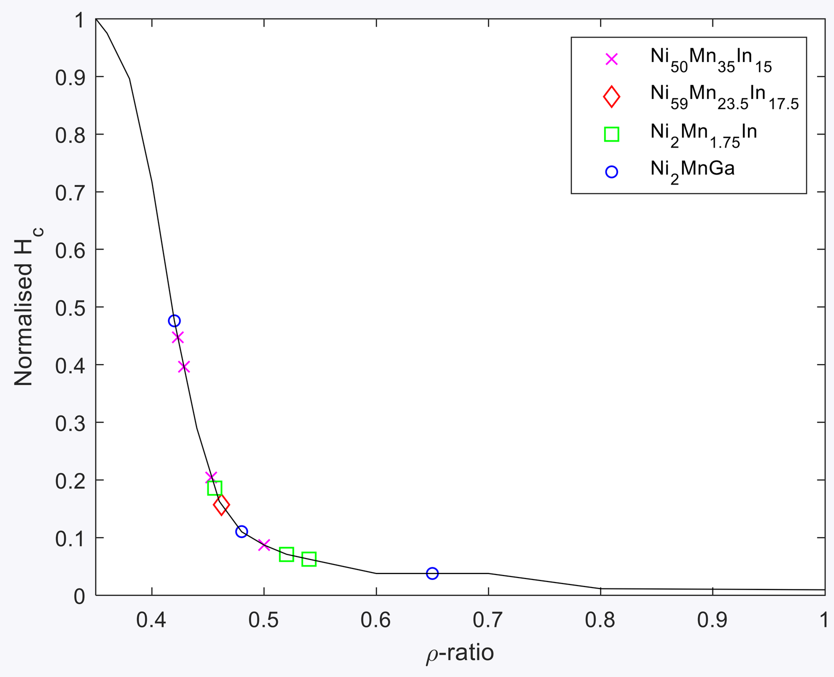

Conclusions

Fe-based Alloys

- Thermal analysis determined the effect of longer milling on crystal growth peak temperatures (longer milling, lower temperature range).
- B doping reduced thermal stability of the samples, however, it favoured lower nanocrystalline sizes. Also, with Mn doping, the same tendency was observable.
- Magnetic analysis determined that magnetic parameters of samples B11, B13 and B15 decreased as B doping increased. However, coercivity and remanent magnetization for sample B15 were higher that sample B13. This phenomenon was associated with the nanocrystalline microstructure obtained by XRD analysis.
- Mn doping decreased magnetic parameters for samples $Fe_{99}Mn_1$ and $Fe_{98}Mn_2$.

Ni-Mn-based Alloys

- Thermal analysis detected a reversible structural transformation for sample $Ni_{50}Mn_{38}Sn_{12}$.
- Thermomechanical analysis (DTMA) of the $Ni_{50}Mn_{38}Sn_{12}$ composite detected a variation in storage modulus (E') and tanδ which was associated to an energy dissipation process at the matrix-reinforcement interphase.
- Soft magnetic response of the microwires was adjusted to a curve based on the study of A. Zhukov et al. (2017) which relates the geometry of the microwire to its magnetic behaviour [4].

References

[1] R. Coll, J. Saurina, L. Escoda, J. J. Suñol, *J. Therm. Anal. Calorim.* **134** (2018) 1277-1284.

[2] D. Goswami, S. K. Anand, P. P. Jana, S. K. Ghorai, S. Chattopadhyay, J. Das, *Mater. Des.* **187** (2020) 108399.

[3] A. Carillo, J. Daza, J. Saurina, L. Escoda, J. J. Suñol, *Materials* **14** (2021) 4542.

[4] A. Zhukov, M. Ipatov, A. Talaat, J. M. Blanco, B. Hernando, L. Gonzalez-Lagarreta, J. J. Suñol, V. Zhukova, *Crystals*, **41** (2017), 7(2).

Funding - Acknowledgement

Study funded by the University of Girona PONT2020-01 and Mineco Spain PID2020-115215RB-C22 projects. We thank Prof. A. Zhukov for microwire production and supply.

instituto IMdea nanociencia

Epitaxial NdFeB films grown by molecular beam epitaxy with an Fe or V underlayer

J. Soler-Morala[1], C. Navío[1], L. Zha[2,3], J. Yang[2,3,4], A. Bollero[1]

[1] Group of Permanent Magnets and Applications, IMDEA Nanoscience, 28049, Madrid, Spain
[2] Beijing Key Laboratory for Magnetoelectric Materials and Devices, Beijing, 100871, China
[3] State Key Laboratory for Mesoscopic Physics, School of Physics, Peking University, Beijing, 100871, China
[4] Collaborative Innovation Center of Quantum Matter, Beijing,100871, China

Motivation

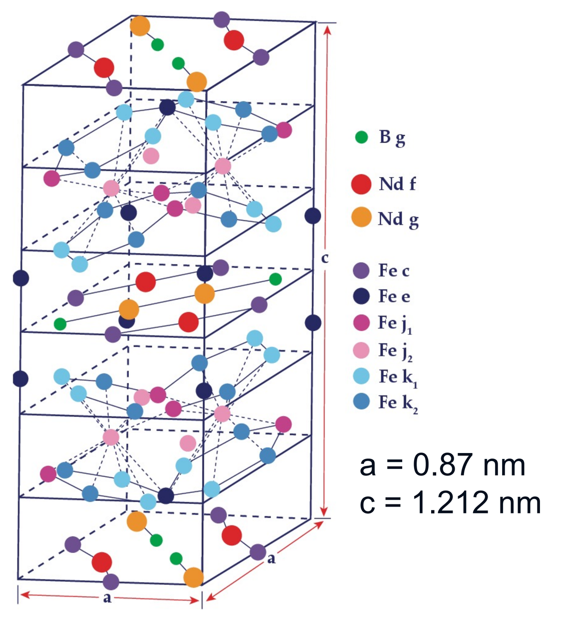

J.F. Herbst *et al*., Phys. Rev. B 29, 4176(R) (1984)

Rare-earth transition metals thin films have attracted a lot of attention due to their high magnetic anisotropy that makes them great candidates for several applications including high density magnetic recording [1-2], microelectromechanical systems and actuators [3]. Rare-earth based thin films also allow the development of novel spintronic devices [4] and they are essential materials for energy-related technologies [5]. Furthermore, the study of certain elements in these rare-earth based systems such as interfaces, grain boundaries or interstitial additions can provide a wider knowledge of their coercivity and magnetization reversal mechanisms [5-7].

The aim of this study is to analyze the first stages of the growth of NdFeB thin and ultra thin films. This range will be likely below that required to fully develop hard magnetic properties but it's extremely important to understand the initial growth stages of NdFeB when aiming at its integration in novel miniature devices [8]. NdFeB thin films up to 10 nm have been grown by Molecular Beam Epitaxy (MBE). An underlayer of 8 nm of Fe or V was previously grown in order to ensure epitaxiality. A 10 nm vanadium capping layer was deposited afterwards.

Growth and *in situ* characterization

NdFeB films by MBE on MgO (001)/Fe

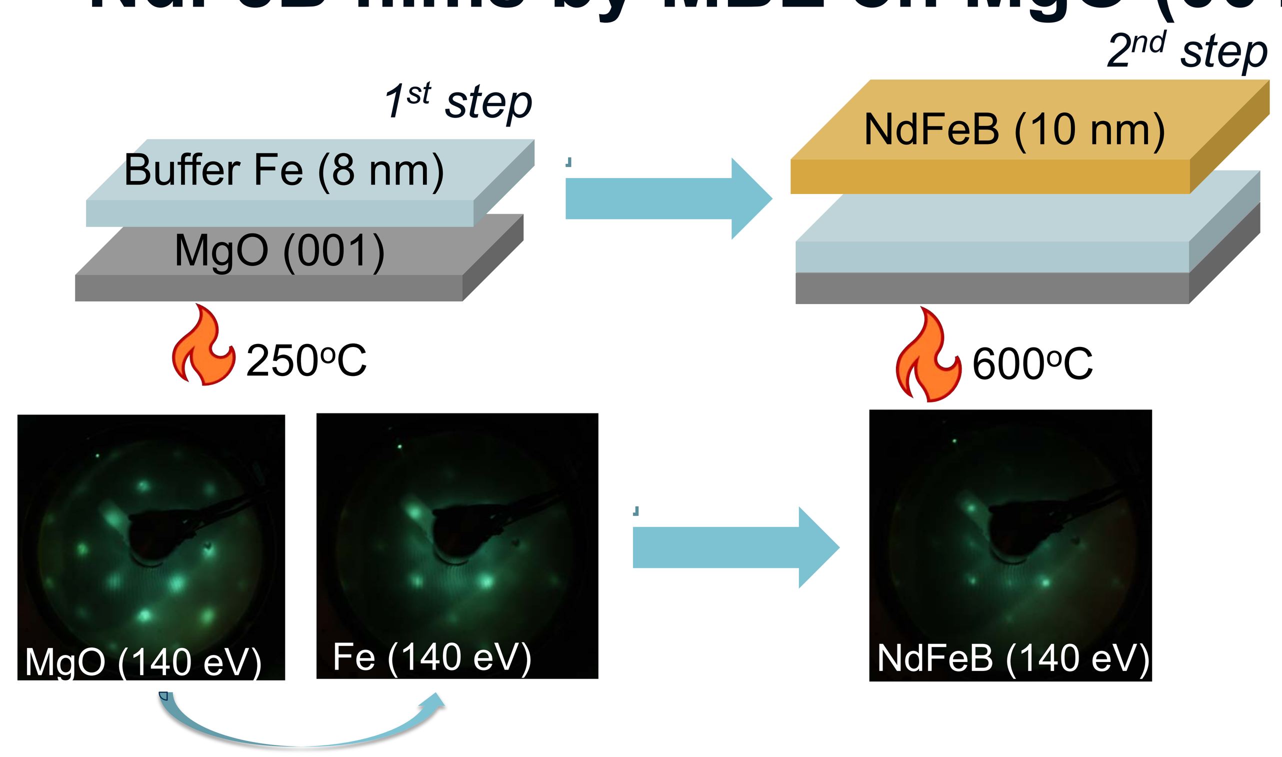

- Co-evaporation of each element (Nd, Fe and B) allows a tailored composition of the films.
- Fe underlayer and NdFeB rotated 45º with respect to the MgO substrate.
- Epitaxial growth in the same direction of the substrate and buffer.

Photoemission spectroscopy

XPS core level spectra

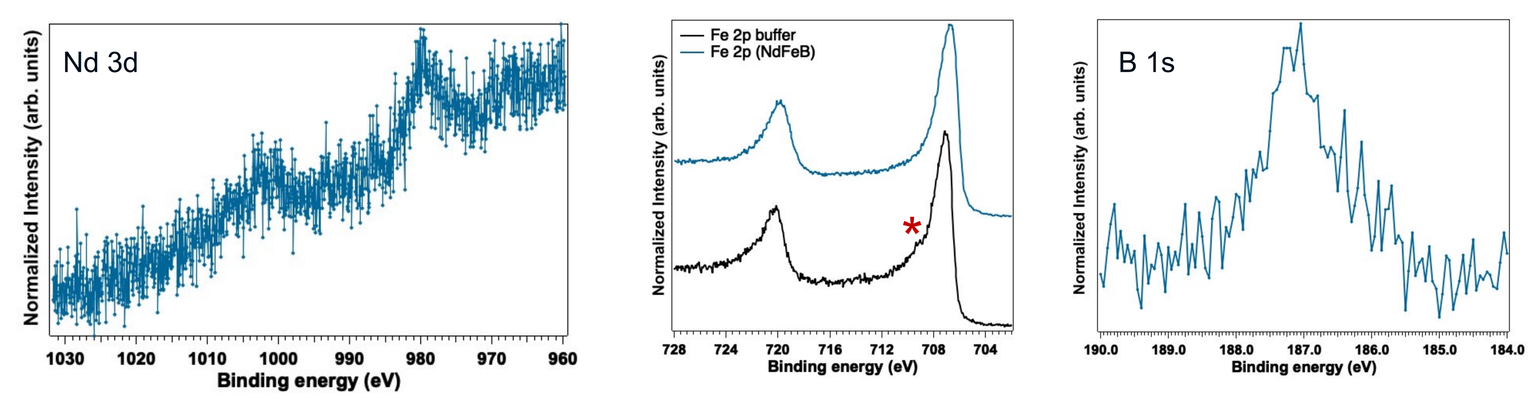

UPS He I: work function

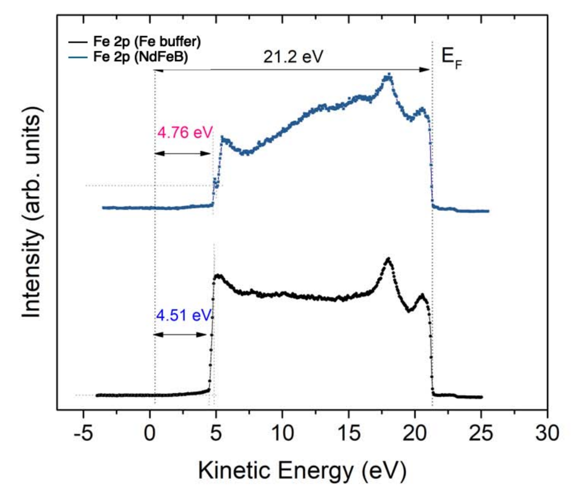

- Changes in the Fe 2p spectra: shift + change of asymmetry.
- Valence band changes. Work function measurements by applying a voltage of -5 V:

Φ_{Fe} = 4.51 eV

Φ_{NdFeB} = 4.76 eV

Magnetic and structural characterization

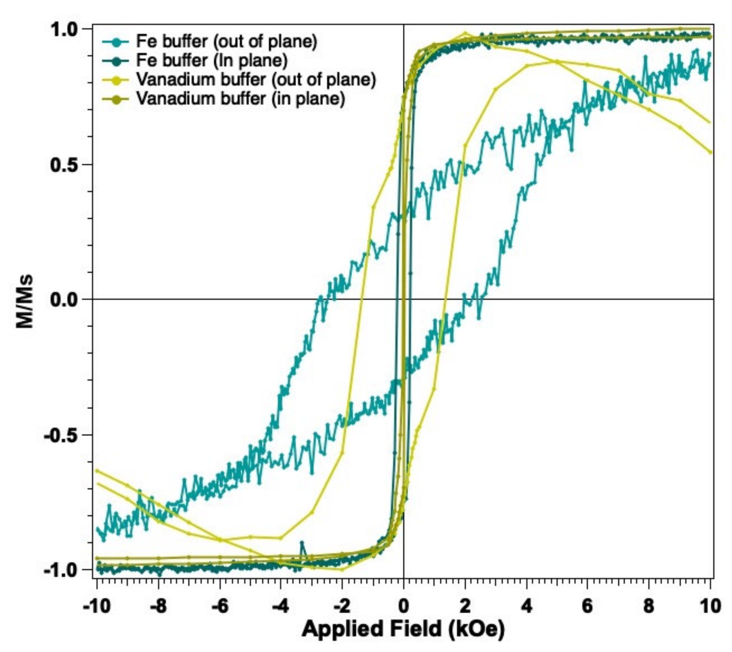

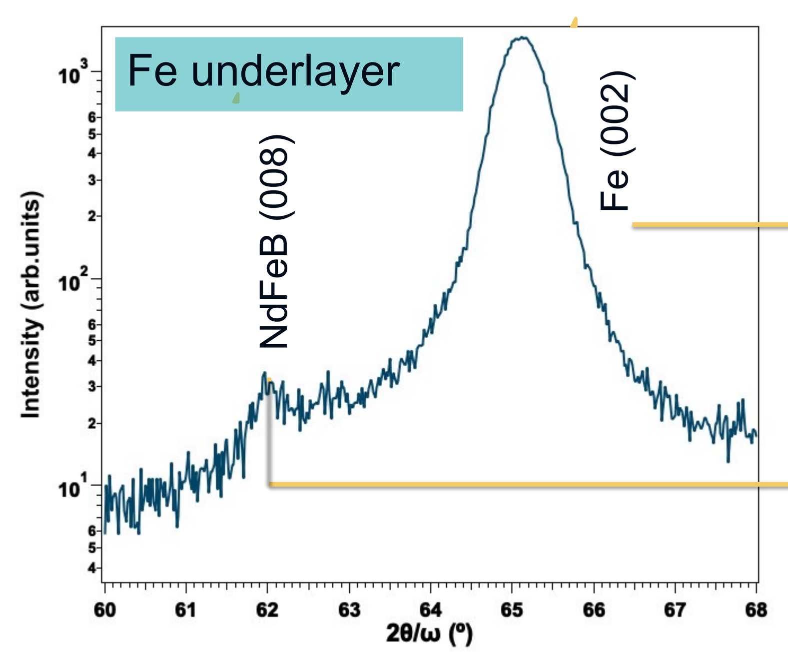

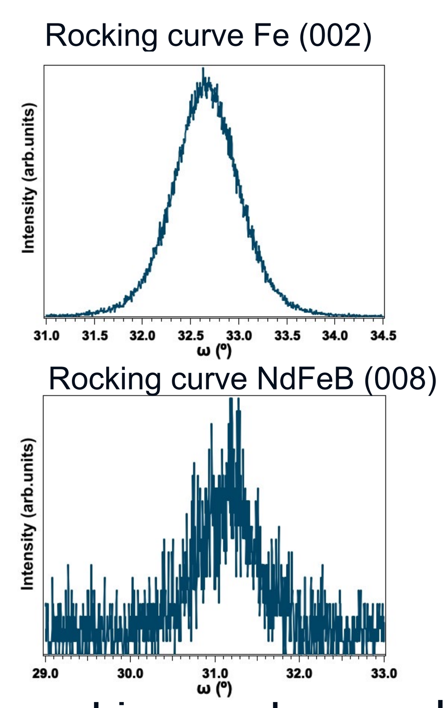

SEM image for NdFeB/Fe:

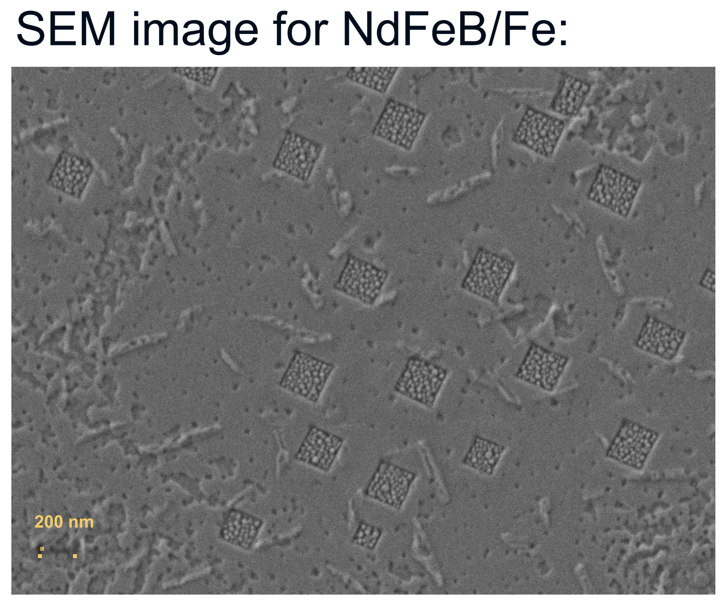

- H_c (out of plane) > 3 kOe for Fe underlayer. Strong magnetic anisotropy in both cases and in good accordance with the epitaxial growth.
- Higher coercivity for an Fe underlayer → Fe (002) and NdFeB (008) diffraction peaks are found in the XRD pattern.
- Rocking curve measurement of NdFeB (008) shows high crystallinity ($\Delta\omega$ = 0.80˚).
- Surface morphology shows square elements all of them following the same orientation.

Conclusions

- Epitaxial NdFeB films have been obtained by co-deposition of each individual element by molecular beam epitaxy.
- Work function measurements have been performed.
- Good crystallinity is obtained thanks to the high deposition temperature and the epitaxiality of the buffer layer.
- Higher coercivity obtained for an Fe underlayer.

Acknowledgements

Authors acknowledge financial support from EU through the H2020 FET Open *UWIPOM2* project (Ref. 857654). J.S.-M. acknowledges also financial support from the Regional Government of Madrid (Ref. PEJD-2019-PRE/IND-17045).

References

[1] A. Morisako *et al*., *J. Magn. Magn. Matter*. 304, 46-50 (2003)
[2] X. Liu *et al*., *J. Appl. Phys.* 97, 10K301 (2005)
[3] T.-S. Chin, *J. Magn. Magn. Matter*. 209, 75-79 (2000)
[4] A. Bollero *et al*., *Nanoscale*, 12, 1155-1163 (2020)
[5] O. Gutfleisch *et al*., *Adv. Mater.* 23, 821–842 (2011)
[6] L. Zha *et al*., *J. Magn. Magn. Matter.* 514, 167128 (2020)
[7] S. Bance *et al*., *Appl. Phys. Lett.* 104, 182408 (2014)
[8] H2020 FET-OPEN project "UWIPOM2": https://cordis.europa.eu/project/id/857654.

Oersted-field- and current- induced dynamics of a Bloch Point in a cylindrical Ni nanowire

J.A. Fernandez-Roldan[1], C. Bran[2], M. Vazquez[2] and O. Chubykalo-Fesenko[2]

[1]University of Oviedo, Oviedo, Spain

[2]Institute of Materials Science of Madrid, ICMM-CSIC, Spain

Challenges in spintronics and the Bloch Point as information carrier

- In 2021 the spintronic community has urged the investigation of magnetic recording and spin-based nanoelectronic concepts that could address the increasing demand of high storage, high speed and low consumption technologies that is demanded by industry [1].
- The 3D racetrack memory could overcome these issues by means of the control of the domain wall propagation in magnetic nanowires. [1,2].
- The Bloch Point wall in cylindrical nanowires has become an appealing domain wall since its experimental in 2014 [3].

3D racetrack memory

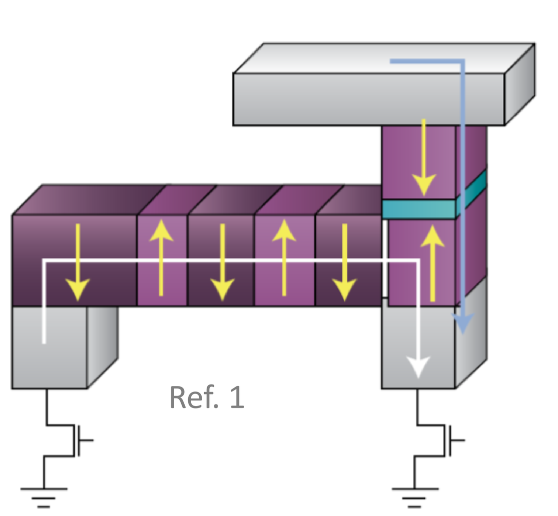

BP walls with opposite chirality propagate asymmetrically

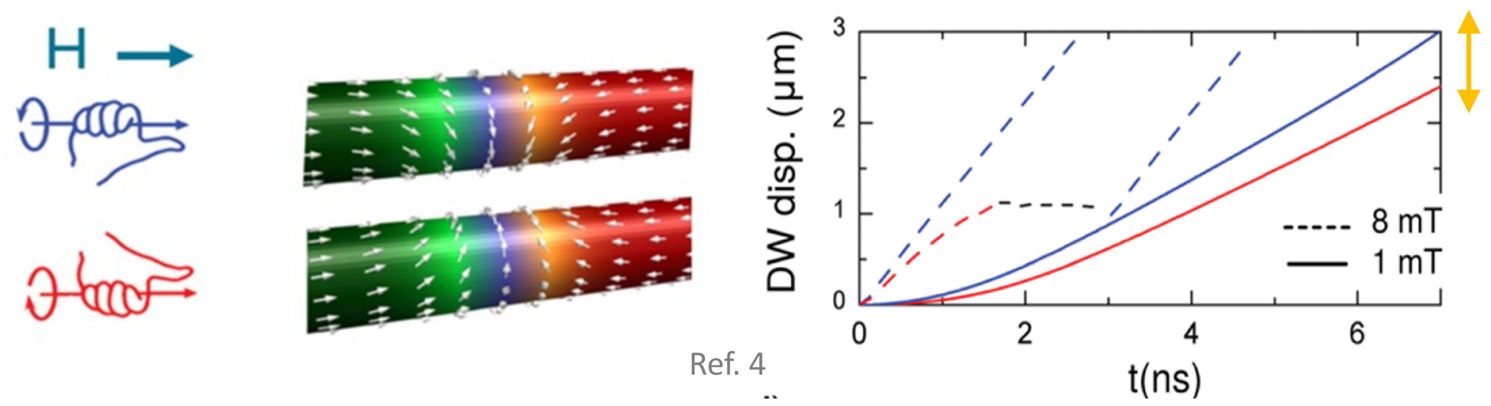

This wall carries a topological defect, the Bloch Point

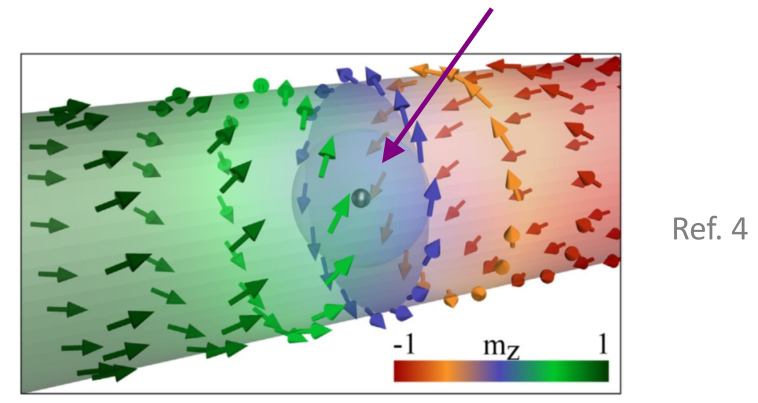

High speeds for fast devices (2 km/s)

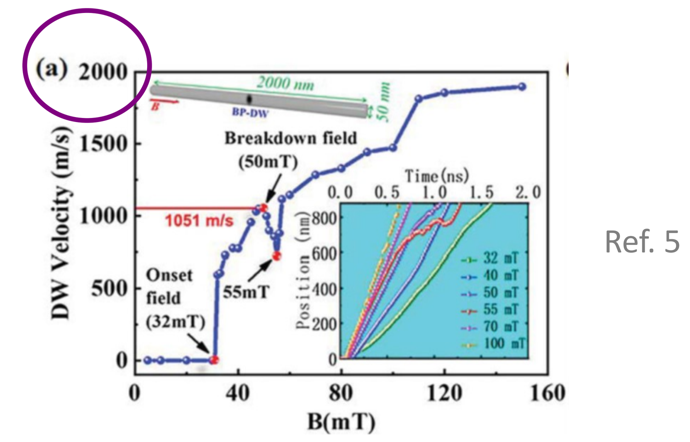

However, current-driven Bloch Points are more interesting for the development of integrated technologies with a low power consumption

Micromagnetic modelling

- We drive a prenucleated head-to-head Bloch Point Wall in a Ni nanowire (diameter 100 nm) with **spin-polarized current** via Zahn-Li spin transfer torque **and Oersted field**

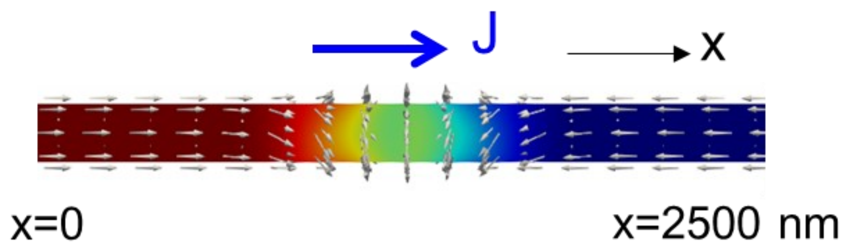

Tracking a Bloch Point

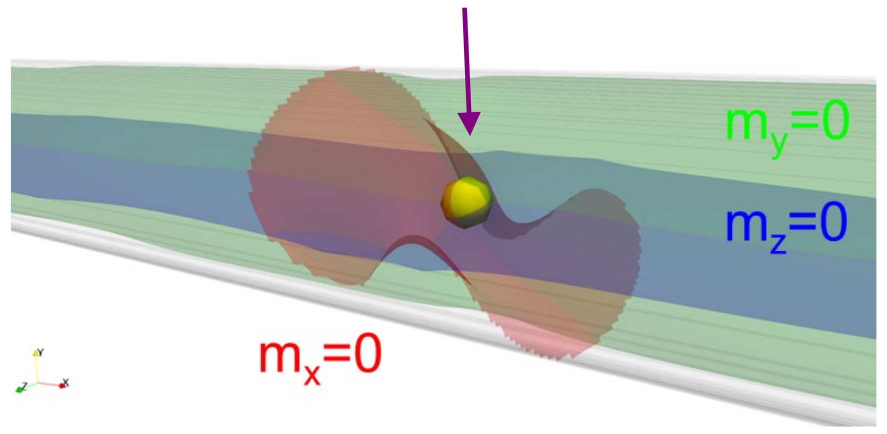

- Typical current densities J [6]: $J=10^{11}$-10^{12} Am^{-2}.
- Low J to prevent excessive Joule heating [7].

Propagation of a pre-nucleated Bloch Point with current and Oersted field

The BP with 'good' chirality propagates along the axis of the nanowire in the sense opposite to the applied current

'good' chirality = positive current

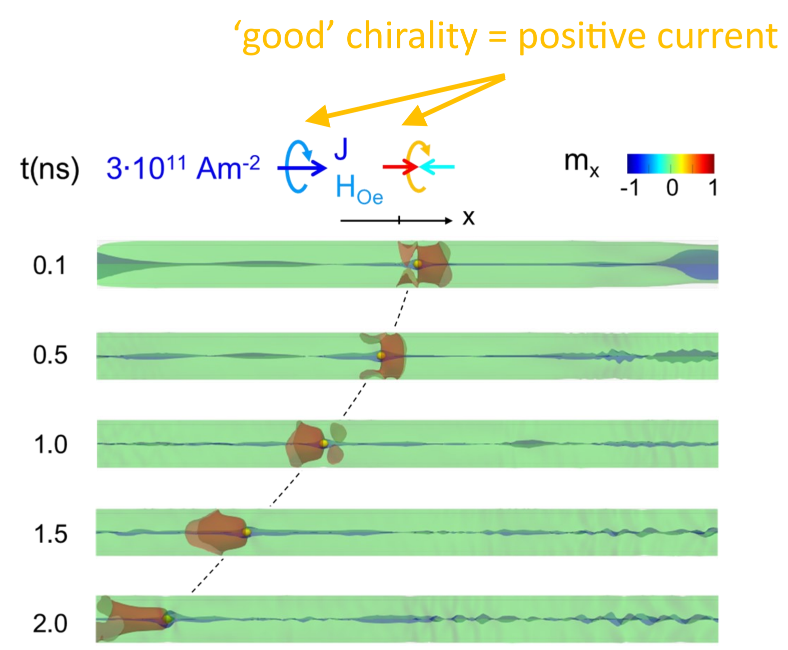

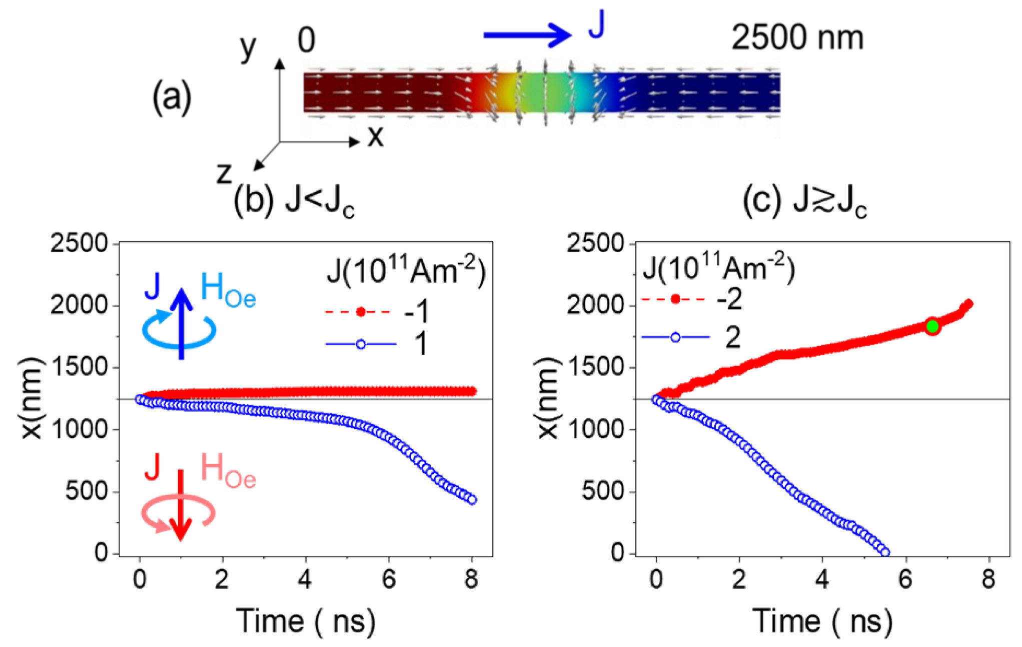

The Oersted-field-induced widening of the wall reduces the velocity of the Bloch Point

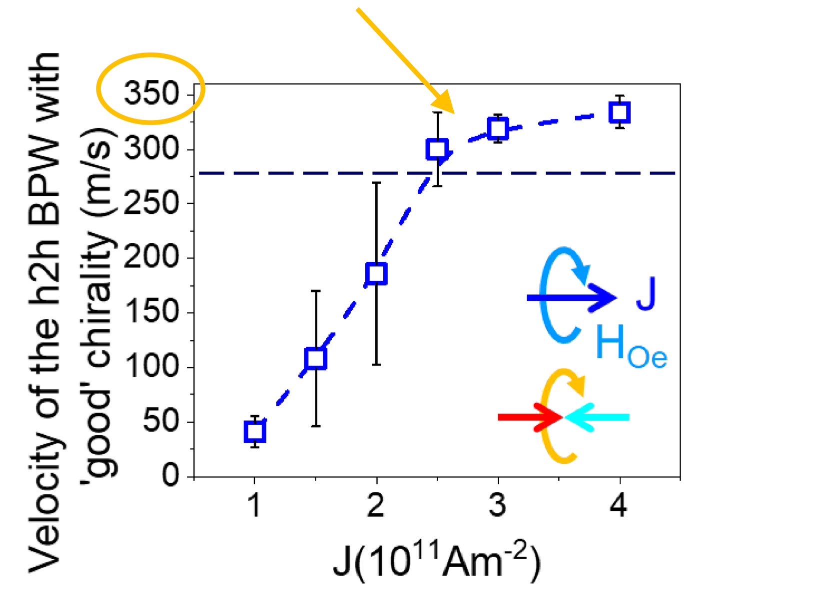

Bloch Points also nucleate from Vortex-Antivortex domain walls

This domain wall transforms into a Bloch Point under current

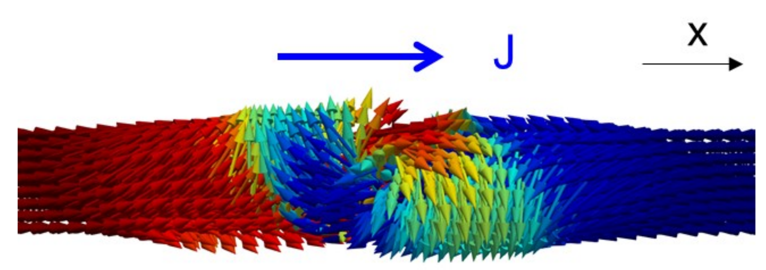

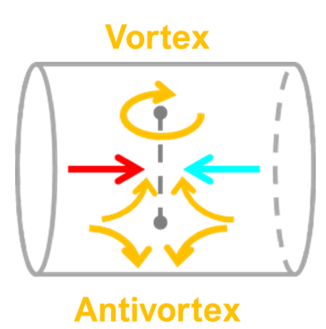

However, this Bloch Point propagates in any direction irrespectively of the current direction J !

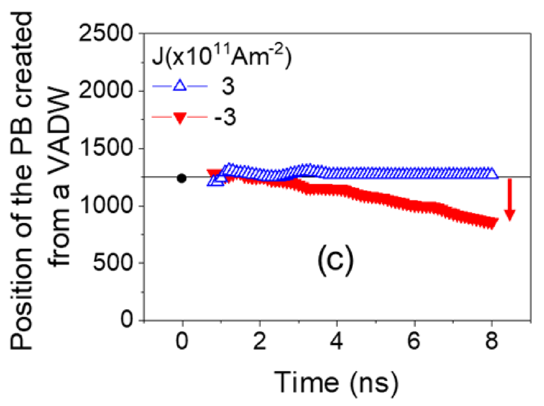

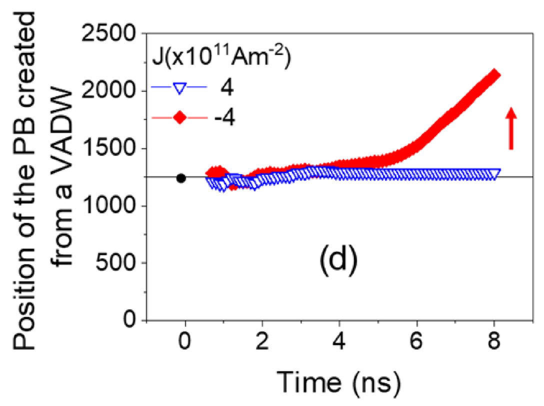

- This BP can propagate in any direction, irrespectively of the direction of the current density.
- Unlike pre-nucleated Bloch Points, this Bloch point carries an initial momentum.
- There is a previous report of inertial mass in Bloch lines [8].

Bloch Point mass in literature [8]

$$m_{Bp}=\frac{1}{\sigma_0}\left(\frac{M}{\gamma}\right)^2 l^2\int dr\left(\frac{\partial\varphi_0}{\partial z}\right)^2=\frac{\pi}{2}\frac{M}{\gamma^2 H_z'}\ln\frac{\Lambda_0}{r_m},$$

Conclusions

1. Prenucleated Bloch Points (BPs) propagate in the direction of the current with velocities close to 350 m/s . The velocitiy of the BP is suppressed by the Oersted field through the widening of the BPW width above a critical current.
2. Both, momentum and inertial mass play a major role in the dynamics of BPs that has not been envisaged up to know. Particularly, BP (inertial) mass requires a deeper investigation for precise manipulation of the BP for spintronic applications.

Acknowledgments

This work was supported by the Spanish Ministry of Science and Innovation under the grants PID2019-108075RB-C31 and PID2019-108075RB-C32-MAT.

References

1. B. Dieny *et al.*, Nat Electron 3, 446–459 (2020).
2. S. S. P. Parkin *et al.* Science 320 (2008).
3. S. Da Col, Phys. Rev. B 89, 180405(R) (2014)
4. R. Hertel *et al.*, J. Phys.: Condens. Matter **28**, 483002 (2016).
5. X.P. Ma *et al.*, Appl. Phys. Lett. 117, 062402 (2020)
6. Schöbitz *et al.* Phys. Rev. B (2021)
7. M. Proenca *et al.* Sci. Reps. 9, 17339 (2019)
8. Yu. A. Kufaev *et al.* Zh. Eksp. Teor. Fiz. 95,1523-1 529 (1989).

Differential refractometry for detection of magnetic nanoparticles

J.L. Marqués[1], J.C. Martínez-García[1], M. Salvador[1], P. Fernández-Miaja[2], J. Sebastián[2], M. Rivas[1]
[1] Department of Physics & IUTA, University of Oviedo, Gijón, Spain
[2] Department of Electrical Engineering, University of Oviedo, Gijón, Spain

Magnetic NANOTAGS

Magnetic nanoparticles (MNPs) are materials within the nanometric range (1 - 100 nm). These sizes are the same as most of the biological entities as cells, proteins, viruses, etc. Taking advantage of this, they can be used to interact with them, so they "tag" these molecules. Moreover, MNPs can also be used as transducers to profit from their magnetic signal to quantify these biomolecules.

Rapid diagnostic testing

One of the techniques used as a rapid diagnostic tool is the lateral flow immunoassays(LFIA). This type of test allows fast and low-cost detection of biomolecules. The traditional LFIA has limitations on sensitivity and reliable quantification.

To solve these limitations the usage of MNPs as NANOTAGS improves the capabilities of traditional LFIA maintaining the speed and low-cost characteristics. These are called magnetic lateral flow immunoassays. (MLFIA).

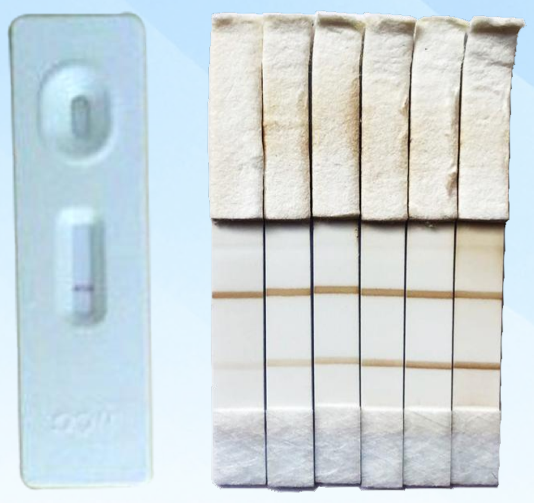

Inductive sensing

The quantification of the MNPs in the MLFIA is performed in an inductive sensor based on planar coils. The impedance variation is proportional to the presence of MNPs. The paper strip is scanned by sliding it on the detecting inductor.
This solution has adequate sensitivity however the cost and volume of the setup need to be reduced.

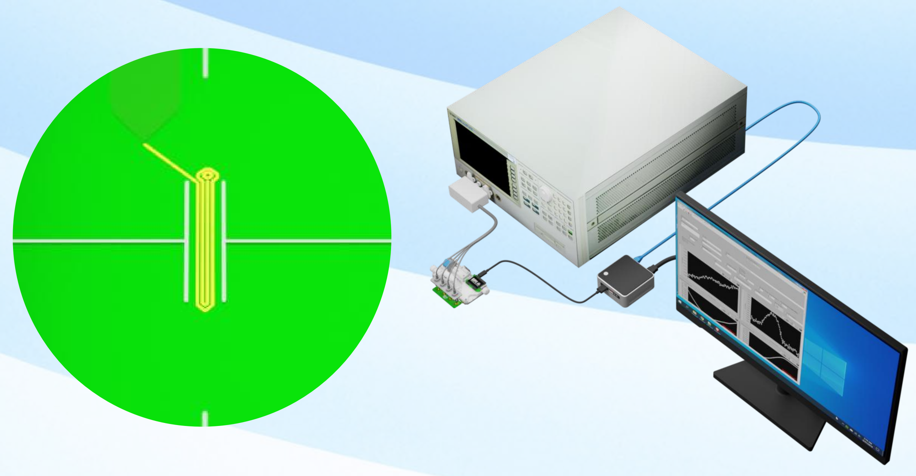

Inductor based refractometry

Refractometry at radio frequency.

A low-cost solution for the detection of MNPs is based on the measurement of the self-resonant frequency (SRF) of the sensing coil. This type of measurement can be achieved using source coupled oscillators (SCOs). Measuring the SRF obtained from the SCOs we can extract the refractive index in the proximity of our sensing inductor.

$$\mathrm{SRF} = \frac{1}{2\pi\sqrt{CL\mu'_{\mathrm{eff}}\varepsilon'_{\mathrm{eff}}}} = \frac{1}{2\pi\sqrt{CLn'_{\mathrm{eff}}}}$$

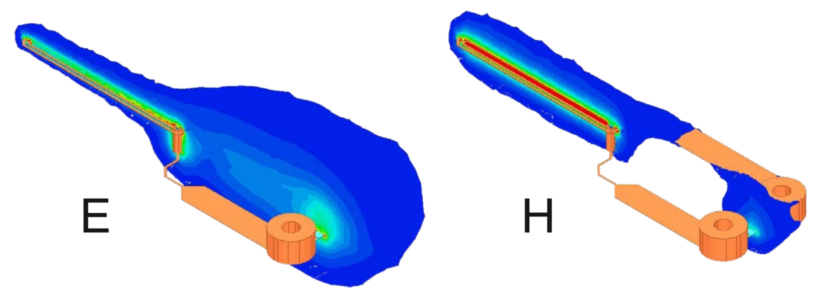

Stability compromises

The MNP quantification based on SCOs has a great sensitivity at a fraction of the cost that other solutions, however, the SRF lacks stability in large time lapses. Ambient factors as temperature, humidity, or mechanical deformations can influence the measurements.

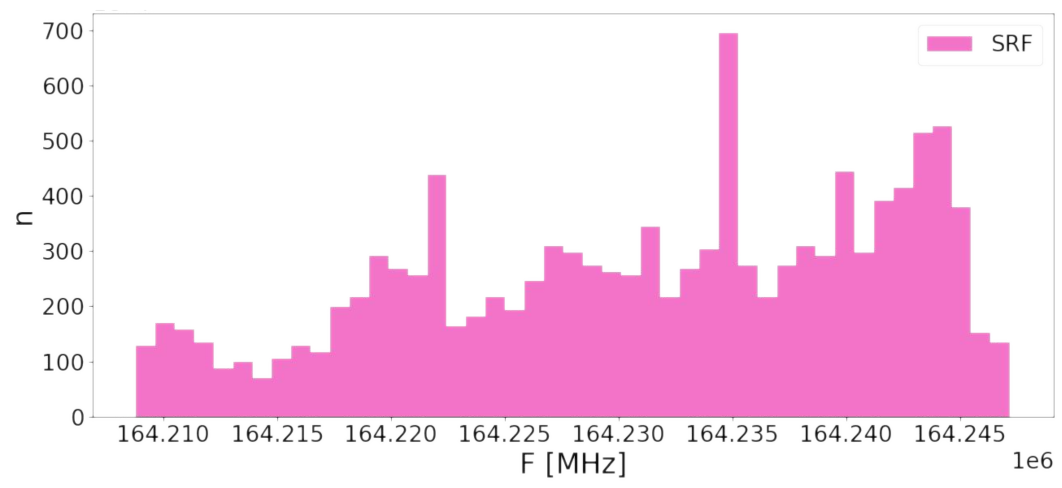

Differential refractometry architecture

To remove ambient influences we propose the usage of a differential architecture. Using a couple of identical SCOs inductive sensors, one used as a reference, we can remove the ambient influence, and eliminate the necessity of a scanning method, reducing cost, and improving stability.

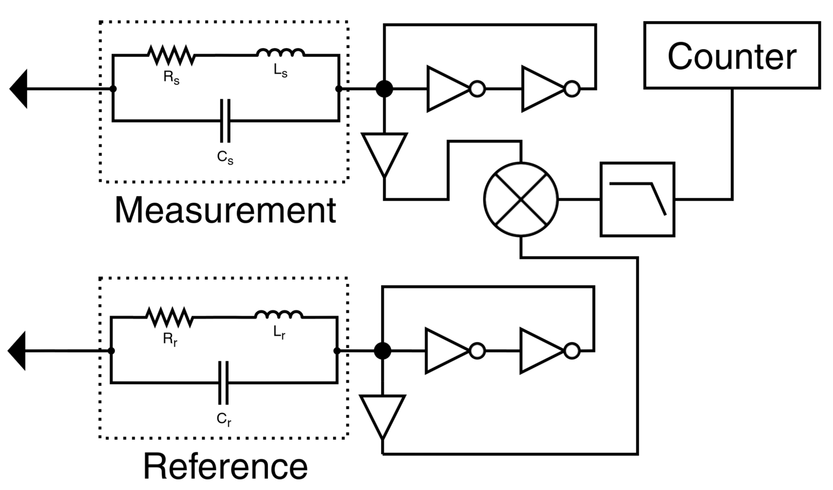

System prototype

Using previous SCOs design and in conjunction, with the proposed system architecture we have developed a differential refractometer with 8 SCOs.
With this initial device, we can prove the differential refractometry concept and test different inductor layouts to further improve stability and sensitivity.

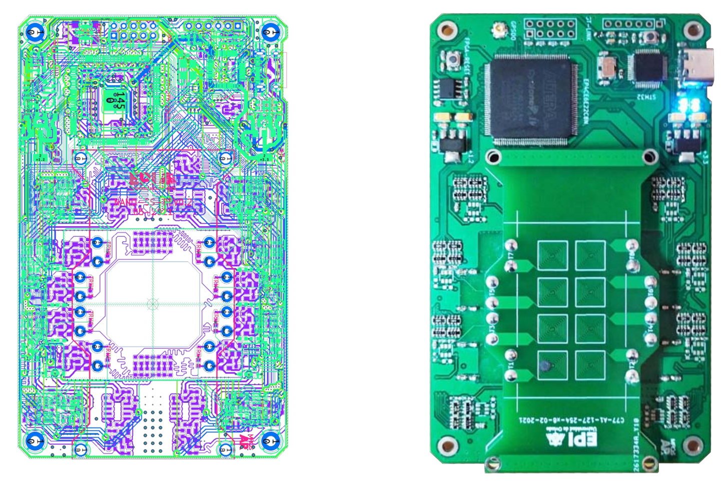

Results

Stability increase

The stability achieved by each of the SCO on the prototype has similar behavior in long time lapses to the ones observed in previous work. When the signal used is the difference between the reference SRF and the SRF of the inductor with the sample, the stability increases significantly. In this case, the long-term stability increases 4 times.
This newly achieved stability improves the repeatability of measurements and allows better comparison between multiple devices.

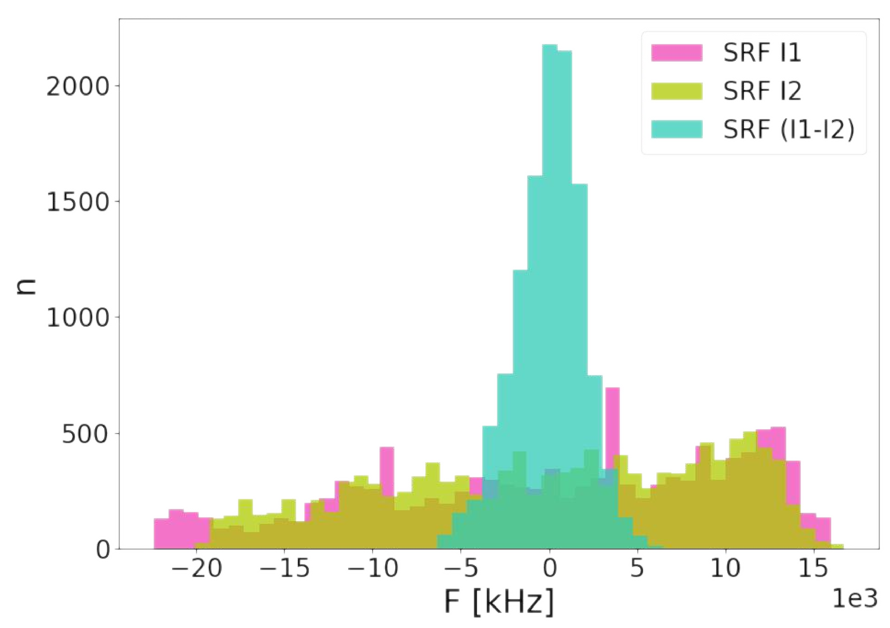

MNPs quantification

The sensitivity of the differential configuration is comparable to the sensitivity of the SCOs based detectors. However, the improved stability allows for the detection of lower masses of MNPs with greater repeatability and the measurements can be carried out for longer achieving better numerical significance.

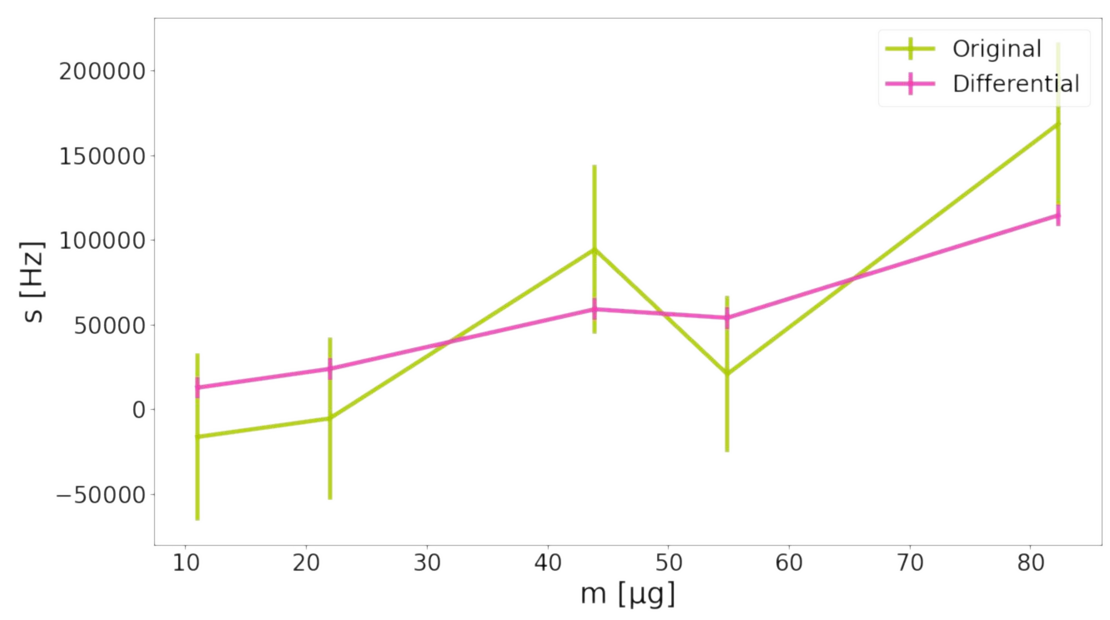

Universidad de Oviedo

https://nanobioap.org/uniovi_magnes/

@MAGNES_UniOvi

José Luis Marqués Fernández
UO254204@uniovi.es

Instituto Universitario de Tecnología Industrial de Asturias

Magnetization reversal in rhombohedral Ni nanotubes

Méndez[1] M., Fernández-Roldán[1] J.A., García[1] J., Vega[1] V., González[1] A.S., Prida[1] V. M.

[1]Departamento Física, Universidad de Oviedo, C/ Federico García Lorca 18, 33007-Oviedo, Asturias, Spain

e-mail: miguel.mendez82@gmail.com

Universidad de Oviedo
Universidá d'Uviéu
University of Oviedo

INTRODUCTION :

In this study, the magnetization reversal mechanism for nickel nanotubes having a rhombic geometry has been investigated theoretically based on previous studies [1-3]. The micromagnetic simulations were performed by means of the mumax3 program employing typical values for the magnetic parameters of the polycrystalline Ni [4], where the size of rhombic nanotubes is around 5000 nm in length, having 590 nm of major diagonal and 360 nm along the minor diagonal with a wall thickness of 44 nm for the case study. The peculiar geometry exhibited by these rhombohedral Ni nanotubes induces clear differences in the magnetization reversal processes due to their different shape when compared respect to the more usual cylindrical ones [2,3,5]. This peculiar geometry further limits the magnetic domain reversal due to sharp edge angles at the nanotube corners, which can lead to the appearance of magnetic singularities near the nanotube vertex that induce the nucleation of vortex domain wall (DW) [6].

Hysteresis loops for applied field in each direction

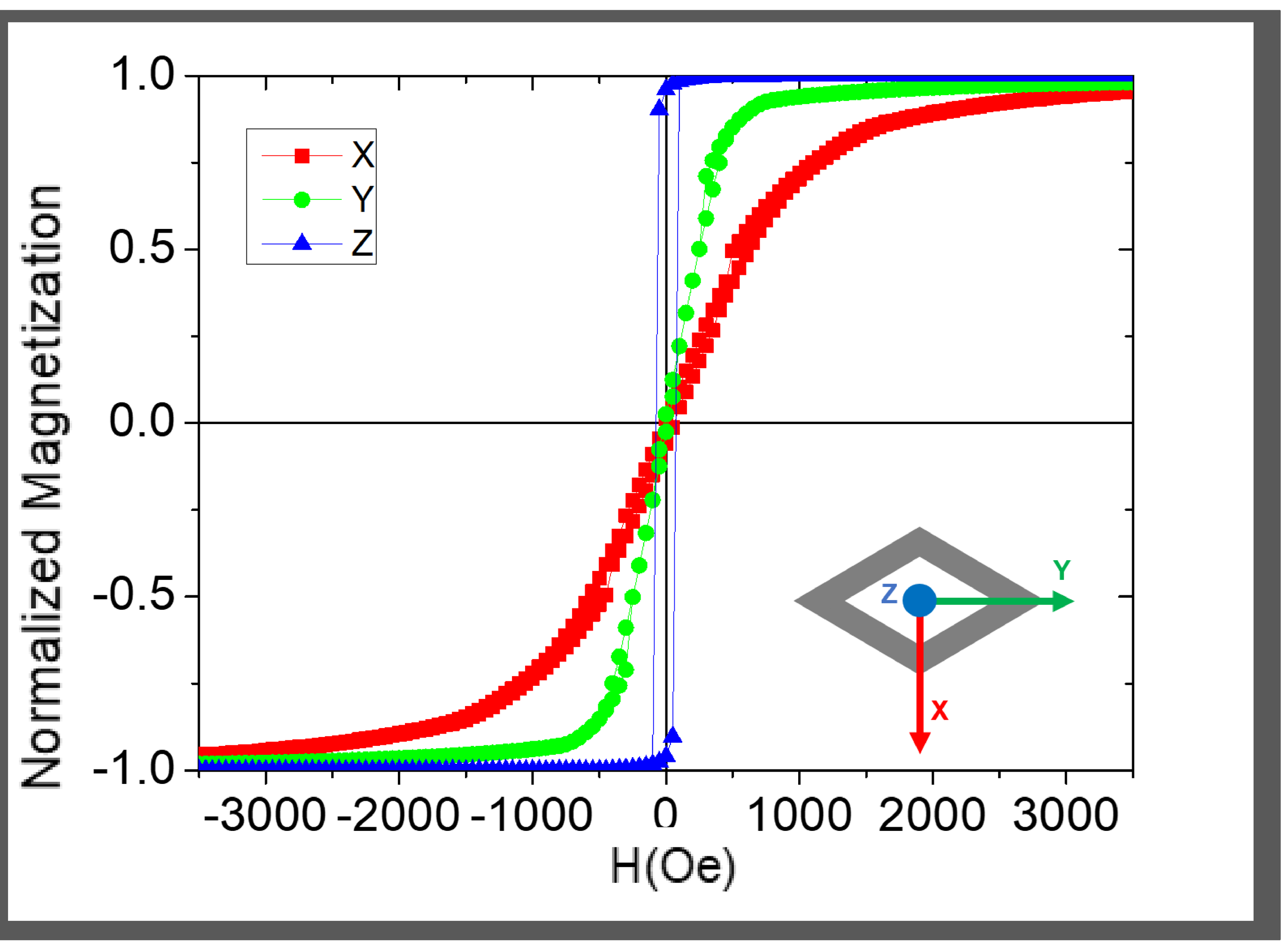

X-axis Hysteresis loop

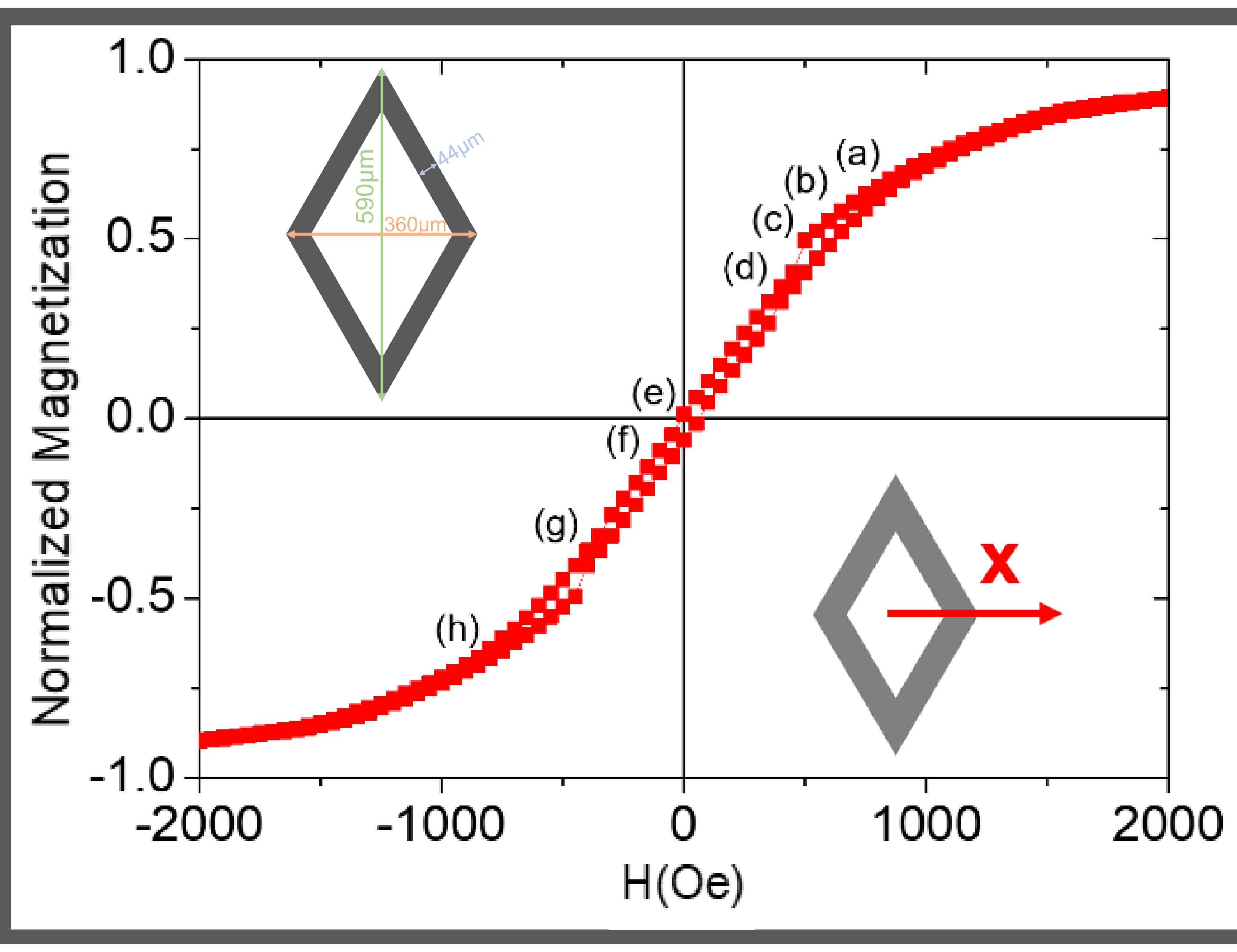

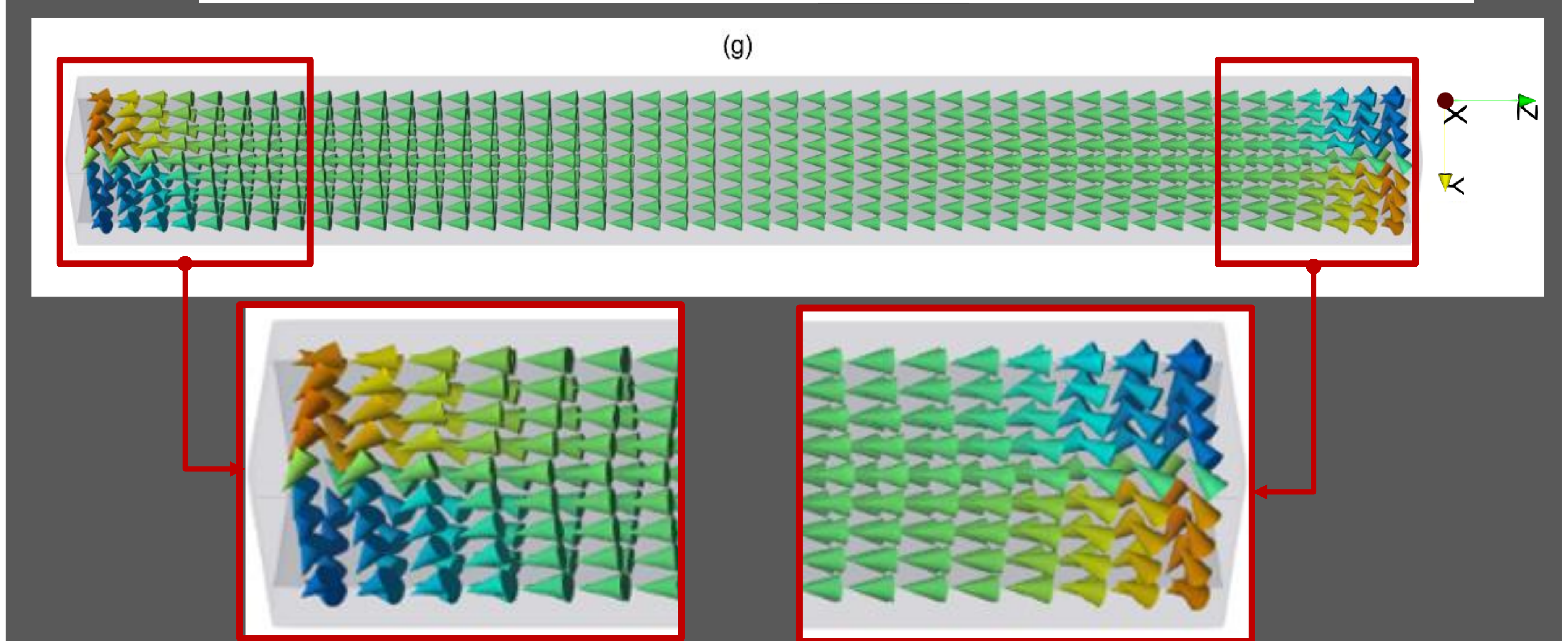

Hysteresis loop with the magnetic field applied along X-axis. C-State shown in (g) point.

Z-axis Hysteresis loop

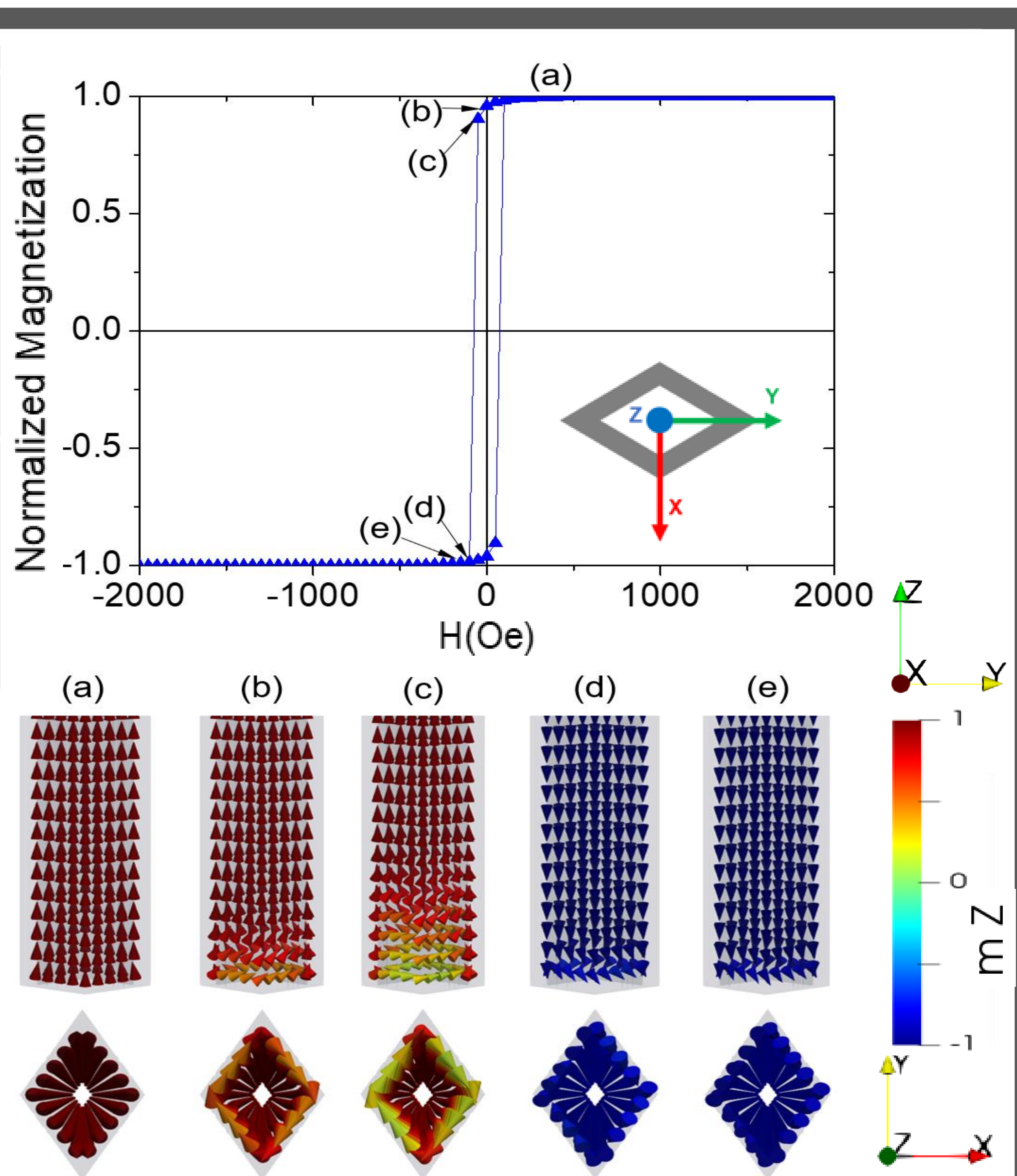

Hysteresis loop for the applied magnetic field along the Z-axis (axial direction of the rhombic nanotube), representing the magnetization reversal process along the longitudinal axis. (a) Partial Ni nanotube magnetically saturated. (b) Vortex DW appearing on edges of the nanotube. (c) Vortex DW propagating into the nanotube at remanence. (d) First step of the magnetization reversal. (e) Nanotube magnetically saturated at negative applied field values.

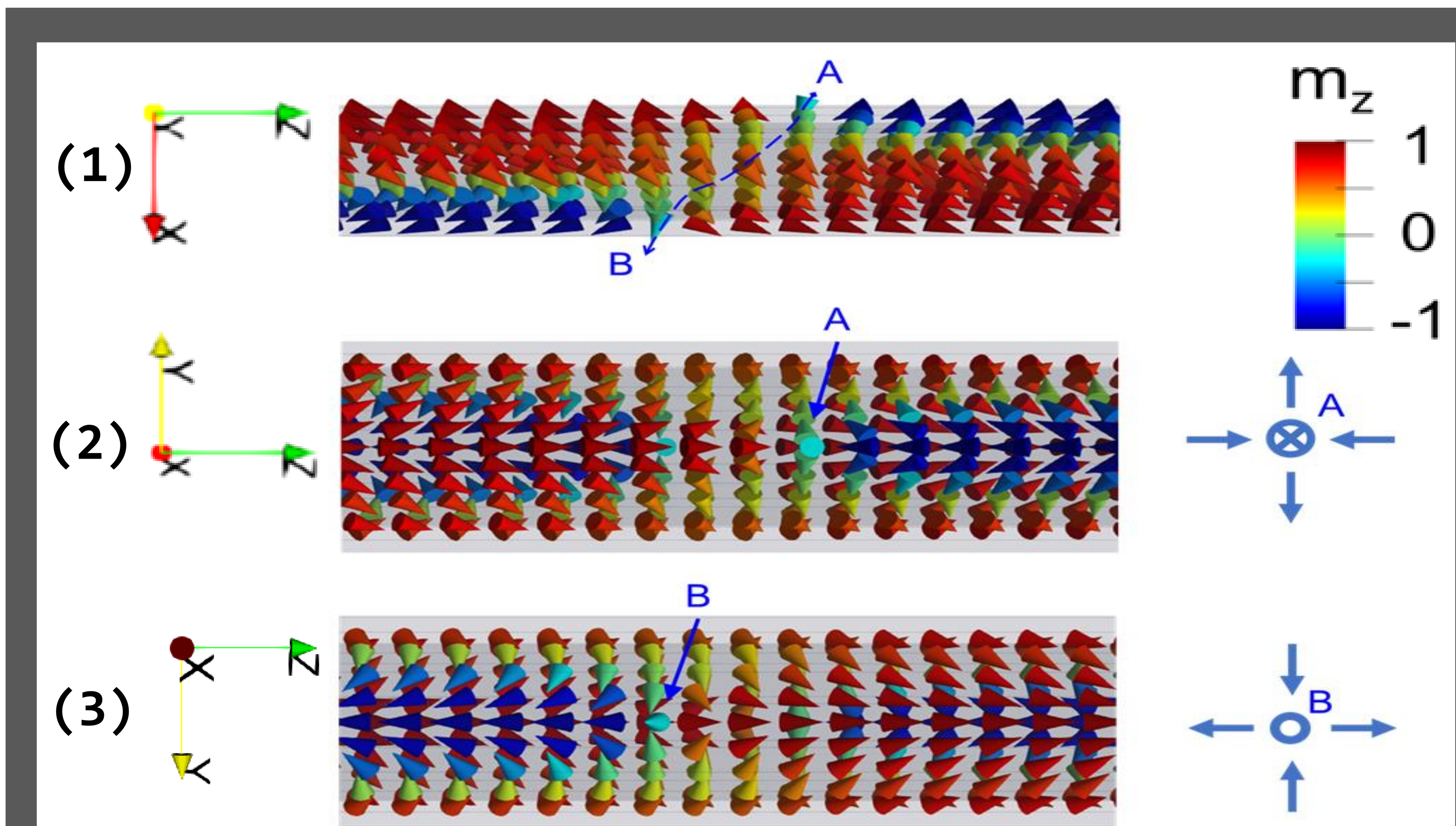

Antivortex state showing both points (1), in (2)-and-out(3), where the magnetization in points A and B follows the field lines.

References:
1. F. Muench et al., Langmuir, vol. 30, no 36, pp. 10878-10885, 2014.
2. L. Sun et al., Journal of Materials Science, vol. 35, pp. 1097-1103, 2000.
3. J. Escrig et al., Physical Review B, vol. 77, no 21, pp. 214421, 2008.
4. A. Vansteenkiste et. al, AIP Advances, vol. 4, pp. 107133, 2014.
5. J. Bachmann et al., J. Appl. Phys., vol. 105, pp. 07B521, 2009.
6. R. Wieser et al., Physical Review B, vol. 69, no 6, pp. 064401, 2004.

Acknowledgments: PID2019-108075RB-C32

Coupled micromagnetic simulations with NEGF-based coherent transport in magnetic tunnel junctions

P. Flauger[1*], C. Abert[1,2], D. Suess[1,2]

1 Faculty of Physics, University of Vienna, Austria

2 University of Vienna Research Platform MMM Mathematics - Magnetism - Materials, University of Vienna, Austria

* peter.flauger@univie.ac.at

Abstract

Spin-transfer torque driven magnetization dynamics in magnetic tunnel junctions allow for modern spintronic devices like the non-volatile and thus energy-efficient magnetoresistive random-access memory (MRAM). While coupling the Landau-Lifshitz-Gilbert (LLG) equation with the spin-drift-diffusion model allows for micromagnetic simulation of the magnetization dynamics in most GMR-based devices, the situation is more complicated in structures that exhibit coherent transport properties like magnetic tunnel junctions. This is due to the comparably high computational cost of solving the Schrödinger equation on the device region. In our work, we present an efficient solution strategy for the LLG with spin-transfer torque in magnetic tunnel junctions that takes advantage of the constant nature of the fieldlike and dampinglike torque coefficients for fixed voltages with respect to the angle between the two magnetization directions. We then compare the results to the well-known torque model of Slonczewski. In accordance with previous experimental and theoretical work, we find the dampinglike torque component to have a quadratic voltage dependence. Our coupled simulations show that this behaviour results in a non-monotone critical switching time for the antiparallel to parallel magnetization reversal direction i.e. for positive bias voltage.

Modeling of Magnetic Tunnel Junctions

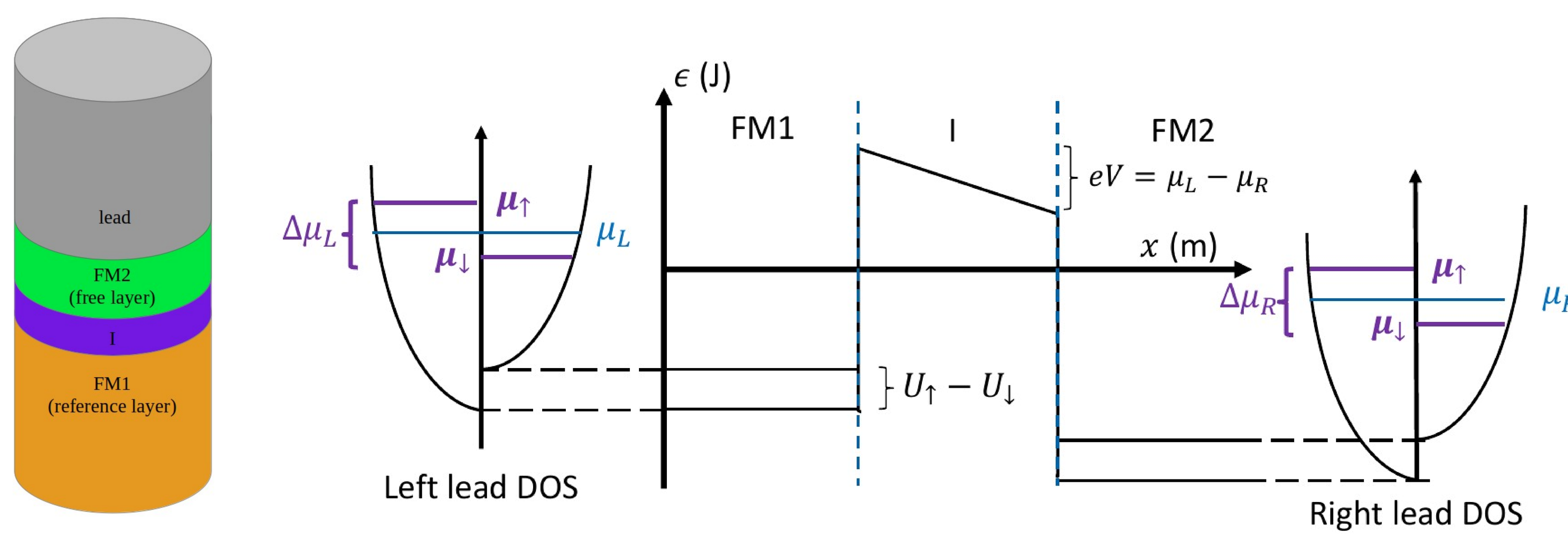

$$H(x) = -\frac{\hbar^2}{2m^*}\frac{\partial^2}{\partial x^2} + U(x) + \frac{J(x)}{2}\boldsymbol{m}\cdot\boldsymbol{\sigma}$$

$$U(x) = \frac{1}{2}\left(U_\downarrow(x) + U_\uparrow(x)\right)$$

$$J(x) = U_\downarrow(x) - U_\uparrow(x)$$

$U_\uparrow$ ... spin up potential
$U_\downarrow$ ... spin down potential
μ ... chemical potential
V ... bias voltage

Non equilibrium Green's function

To solve the Schrödinger's equation in its discretized and truncated form, one can use a Green's function approach instead of handling the rather complicated boundary conditions encountered in a direct solution strategy.

$$\mathrm{G}^R = \left[\mathbb{1}\epsilon - \mathrm{H} - \Sigma^R\right]^{-1}$$

$$\mathrm{G}^n = \mathrm{G}^R\left(\Sigma_L^{\mathrm{in}} + \Sigma_R^{\mathrm{in}}\right)\mathrm{G}^A$$

where $\mathrm{G}^A = \mathrm{G}^{R\dagger}$ and $\Sigma_k^{\mathrm{in}} = if_k(\epsilon)(\Sigma_k^R - \Sigma_k^{R\dagger})$, Σ_k^R is the open boundary condition for outgoing waves through the lead k and $f_k(\epsilon)$ is the occupation function of lead k.
The local spin accumulation components are then given by

$$s_i = \frac{\mu_B}{2\pi}\int \mathrm{Tr}\left[G^n \cdot \sigma_i\right] d\epsilon$$

Voltage dependence of dampinglike torque

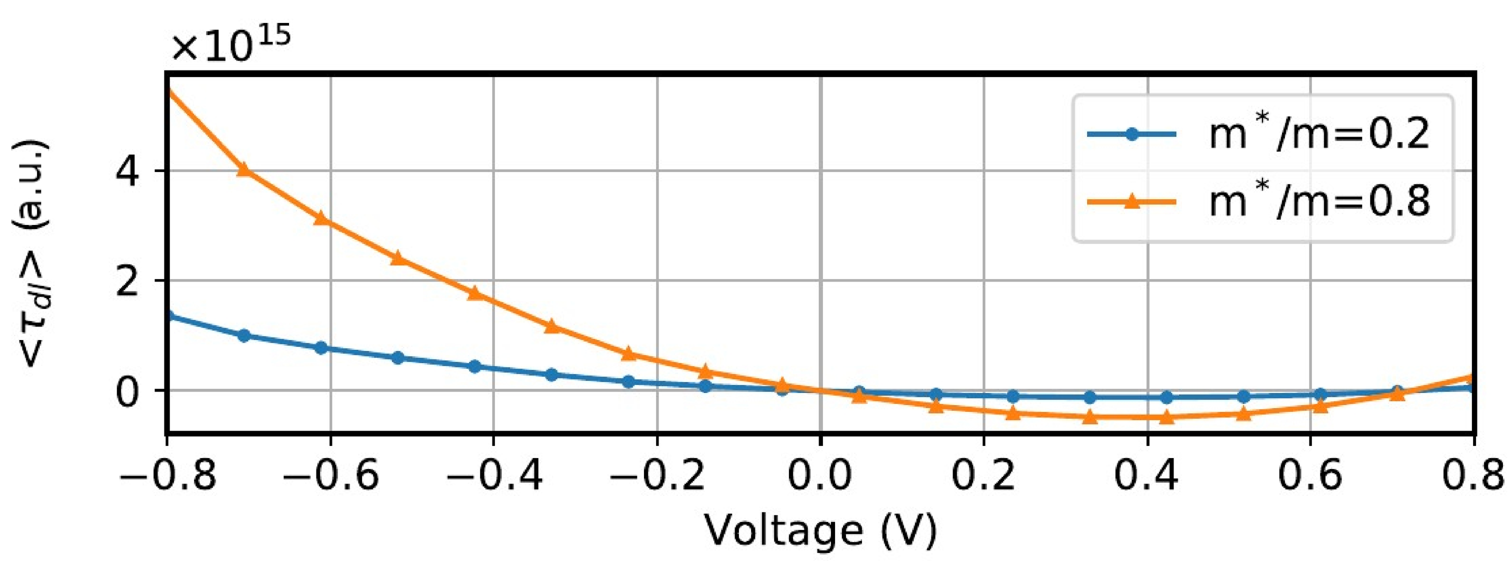

The dampinglike torque components exhibits a quadratic behavior resulting in a second sign-reversal on the positive voltage branch while it behaves monotonic for $V < 0$.

Landau-Lifshitz-Gilbert Equation

In micromagnetism, the magnetization dynamics can be described by the Landau-Lifshitz-Gilbert equation (LLG):

$$\frac{\partial \boldsymbol{m}}{\partial t} = -\gamma \boldsymbol{m} \times \boldsymbol{H}^{\mathit{eff}} + \alpha \boldsymbol{m} \times \frac{\partial \boldsymbol{m}}{\partial t} + \boldsymbol{T}$$

where $\gamma = \mu_0\gamma_e$ is the reduced gyromagnetic ratio, α is the Gilbert damping parameter and $\boldsymbol{H}^{\mathit{eff}}$ is the effective field and $\boldsymbol{m}$ is the normalized local magnetization. The torque $\boldsymbol{T}$ acting on $\boldsymbol{m}$ due to a spin accumulation $\boldsymbol{s}$ is

$$\boldsymbol{T} = \frac{J}{\hbar M_s}\boldsymbol{m} \times \boldsymbol{s}.$$

Efficient Solution Strategy

The torque can be split into two components, dampinglike and fieldlike torque. If the reference layer magnetization is denoted by $\boldsymbol{m}_{\mathrm{RL}}$ and the free layer magnetization by $\boldsymbol{m}_{\mathrm{FL}}$, then these two components acting on the free layer are

$$\boldsymbol{T}_{\text{fieldlike}} = \tau_{\mathrm{fl}}\boldsymbol{m}_{\mathrm{FL}} \times \boldsymbol{m}_{\mathrm{RL}}$$

$$\boldsymbol{T}_{\text{dampinglike}} = \tau_{\mathrm{dl}}\boldsymbol{m}_{\mathrm{FL}} \times (\boldsymbol{m}_{\mathrm{FL}} \times \boldsymbol{m}_{\mathrm{RL}})$$

Since for $\mu > \max\left[U_\uparrow, U_\downarrow\right]$ the values of τ_{fl} and τ_{dl} depend only on the applied bias voltage, one can build a lookup table of precomputed torque components and later build $\boldsymbol{T}_{\text{fieldlike}}$ and $\boldsymbol{T}_{\text{dampinglike}}$ from a dynamic basis of $\boldsymbol{m}_{\mathrm{FL}} \times \boldsymbol{m}_{\mathrm{RL}}$ and $\boldsymbol{m}_{\mathrm{FL}} \times (\boldsymbol{m}_{\mathrm{FL}} \times \boldsymbol{m}_{\mathrm{RL}})$. Since due to the matrix inversion calculating G^R is the numerically most expensive step, this strategy increases the efficiency of dramatically.

Switching Behavior

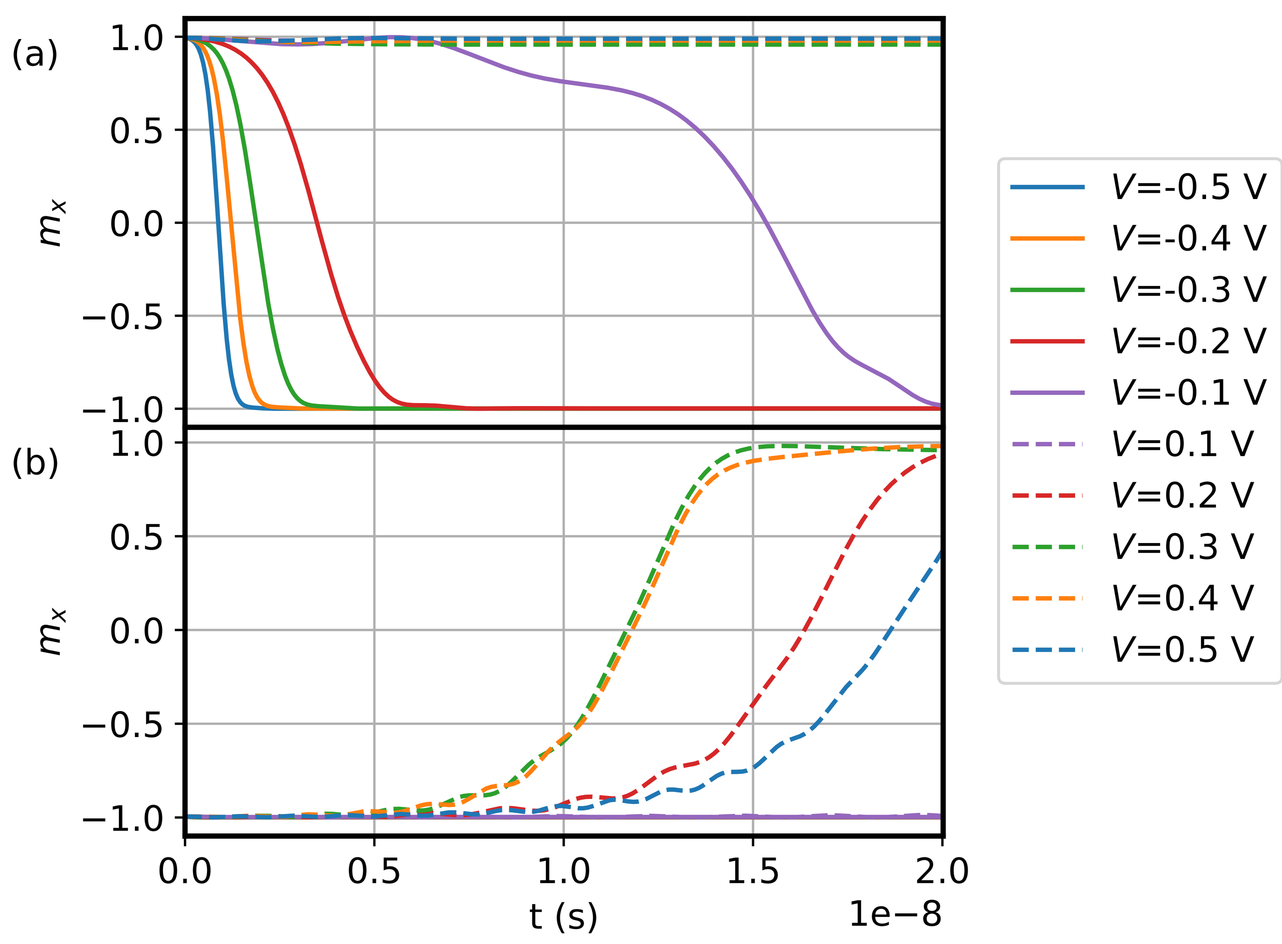

The magnetization dynamics for parallel to anti-parallel (a) and anti-parallel to parallel (b) switching. While the critical switching time decreases with higher negative bias voltage, the quadratic behavior of the dampinglike torque leads to a non-monotonic critical switching time for $V > 0$.

Structural and magnetic characterization of $CoFe_2O_4$ nanoparticles

Universidad de Oviedo

INCAR

Authors: M. González-de la Vega[1], M.P. Fernández-García[1], M. Sevilla[2], A.B. Fuertes[2], D. Martínez-Blanco[3], A. Adawi[3], P. Gorria[1] and J.A. Blanco[1]

[1]Departamento de Física, Universidad de Oviedo, 33007, Oviedo, Spain
[2]Instituto Nacional del Carbón (CSIC), 33011, Oviedo, Spain
[3]Servicios Científico-Técnicos, Universidad de Oviedo, 33006, Oviedo, Spain

OBJECTIVES

- Synthesis of $CoFe_2O_4$ NPs by pyrolysis' procedures at temperatures between 250 and 500°C.
- Control of the physicochemical properties of the NPs by varying the synthesis procedure.
- Morphological, compositional, structural, microstructural and magnetic characterization.

Experimental techniques

Scanning electron microscopy (SEM)

Thermogravimetric analysis (TGA)

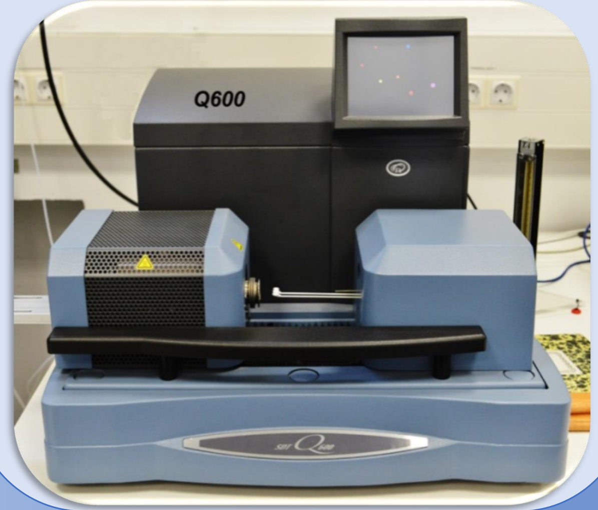

(High resolution) Transmission electron microscopy (HR-TEM)

X-ray diffraction (XRD)

Magnetometry

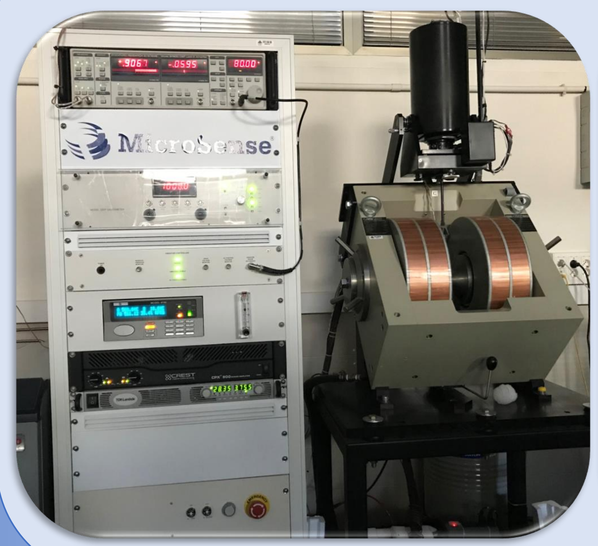

Experimental results

Morphological characterization

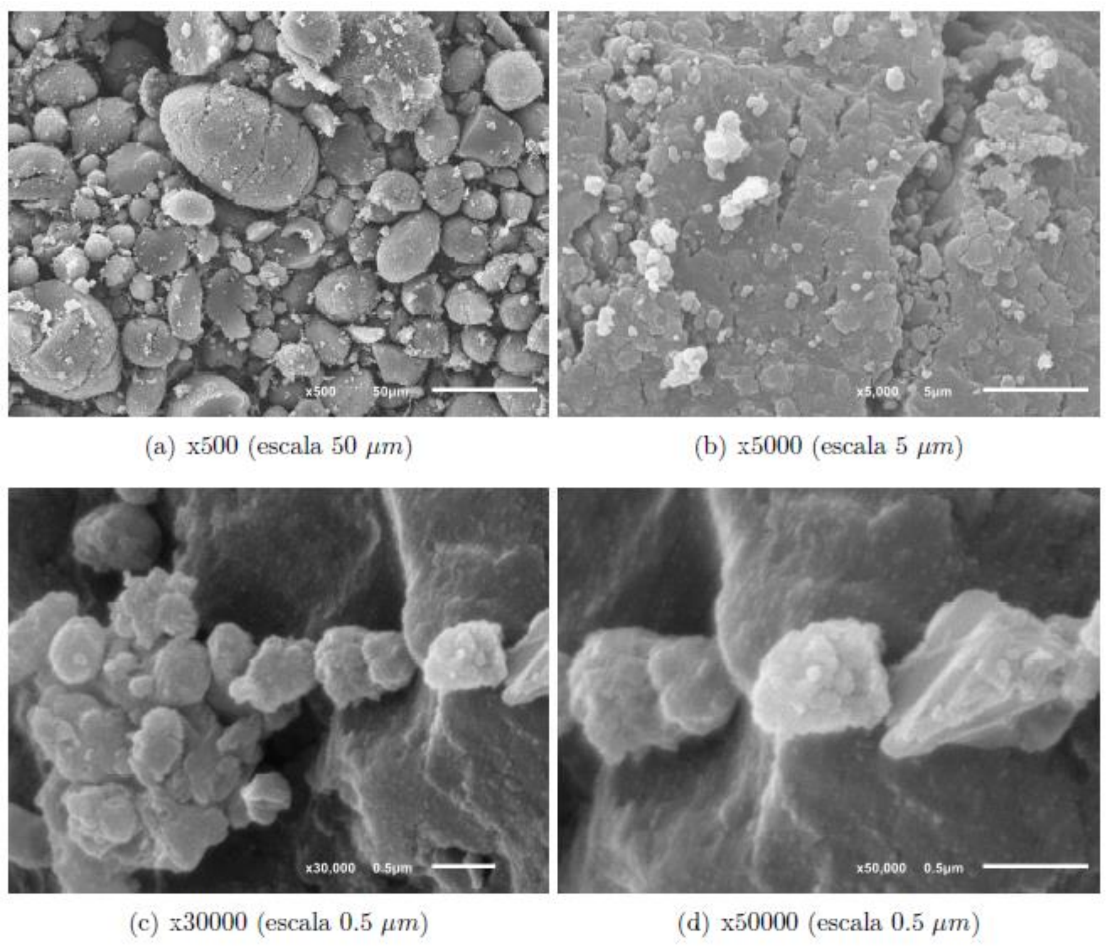

Activated carbon M30: grains of different morphology and micrometric size.

Compositional analysis

- Thermogravimetric analysis:

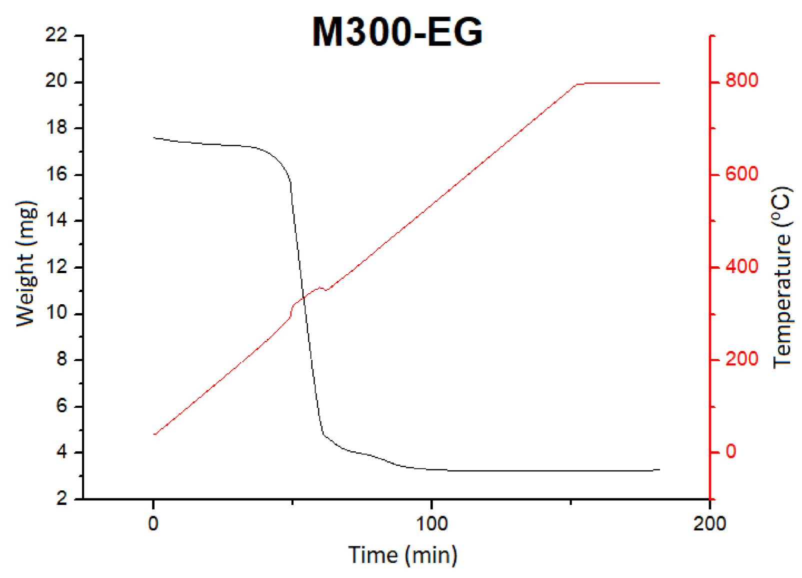

- Atomic percentages:

SAMPLE	C	O	Fe	Co	K
M250-EG	77.94	20.29	1.18	0.50	0.09
M300-EG	83.01	14.67	1.50	0.67	0.14
M350-EG	83.47	14.59	1.28	0.57	0.09
M400-EG	84.43	13.34	1.45	0.68	0.11
M450-EG	85.11	12.68	1.45	0.66	0.09
M500-EG	88.24	8.54	2.11	0.98	0.14

Metal percentage: ~ 20%

Structural and microstructural characterization

- X-ray diffraction:

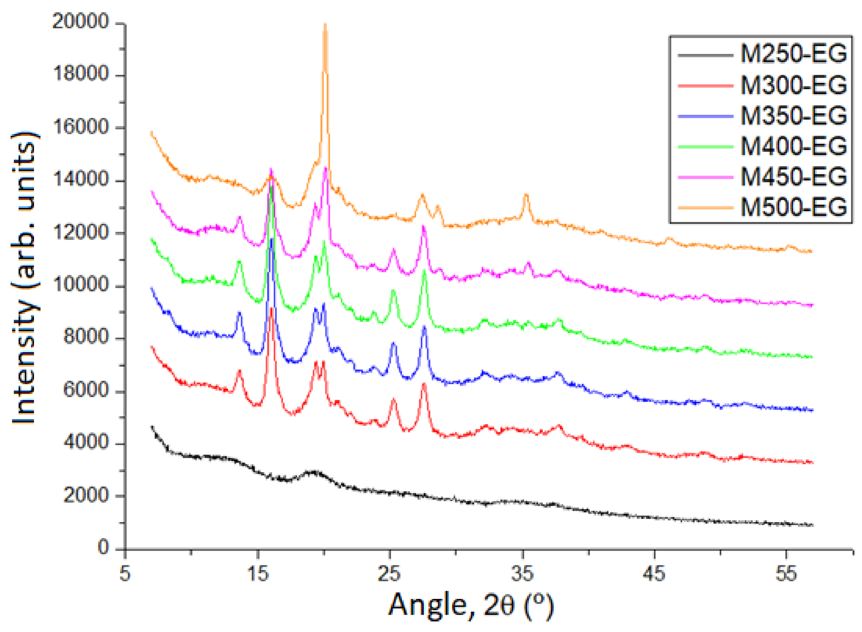

- Principal phase: $CoFe_2O_4$ cubic structure (space group $Fd\bar{3}m$)
- Broad diffraction peaks corresponding to NPs (nanometric character)

SAMPLE	χ^2	PHASES (% total intensity)				D^{DRX} (σ) [nm]	CELL PARAMETER [Å]
		CoF_2O_4	Co-hcp	Co-fcc	Fe-bcc		
M300-EG	1.75	93.04	4.66	2.31		6.692 (0.004)	8.446
M350-EG	1.49	92.54	5.46	1.99		7.687 (0.004)	8.444
M400-EG	1.74	89.12	9.24	1.64		7.871 (0.007)	8.444
M450-EG	3.12	59.06	22.16	8.81	9.97	11.481 (0.013)	8.446
M500-EG	It's not possible to fit.						

- Analysis by Rietveld refinement ⇒ Cell parameters consistent with bulk cobalt ferrite (8.391 Å).
- Mean nanoparticle dimension increase as the temperature of synthesis raises.

- Transmission electron microscopy:

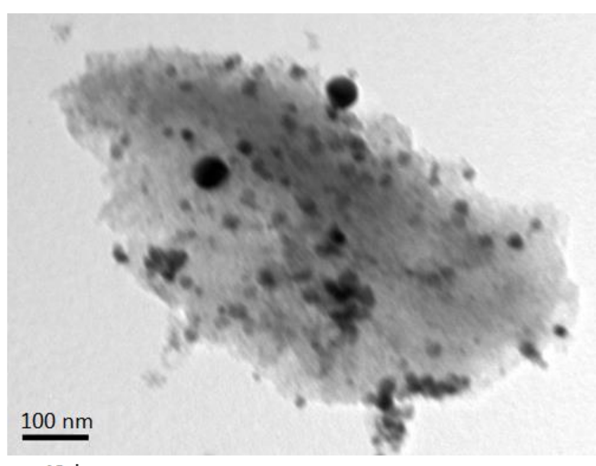

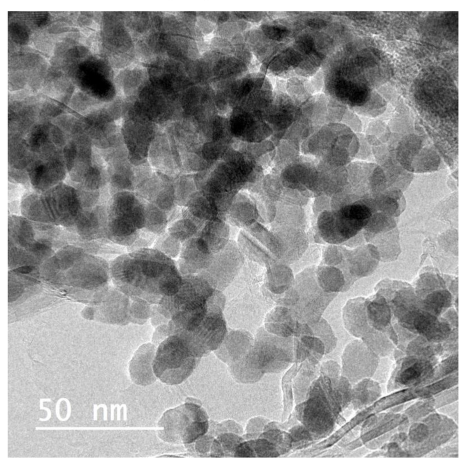

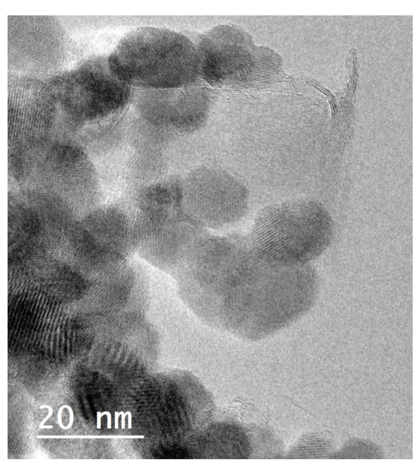

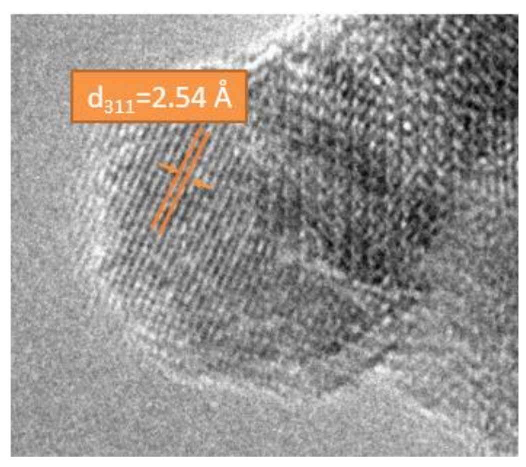

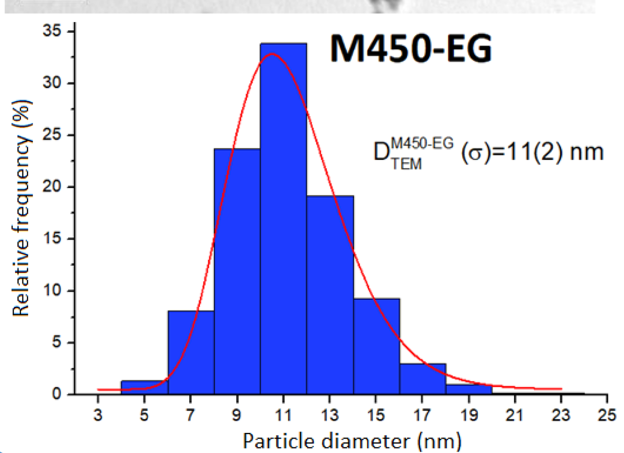

The nanoparticles (dark color) have quasi-spherical shapes and are randomly dispersed in the porous carbon matrix. The histograms of all samples reveal the presence of NPs in the range 3 and 24 nm.

∴ ⇑ Synthesis temperature ⇒ ⇑ NPs size

Magnetic characterization

- Hysteresis loops:

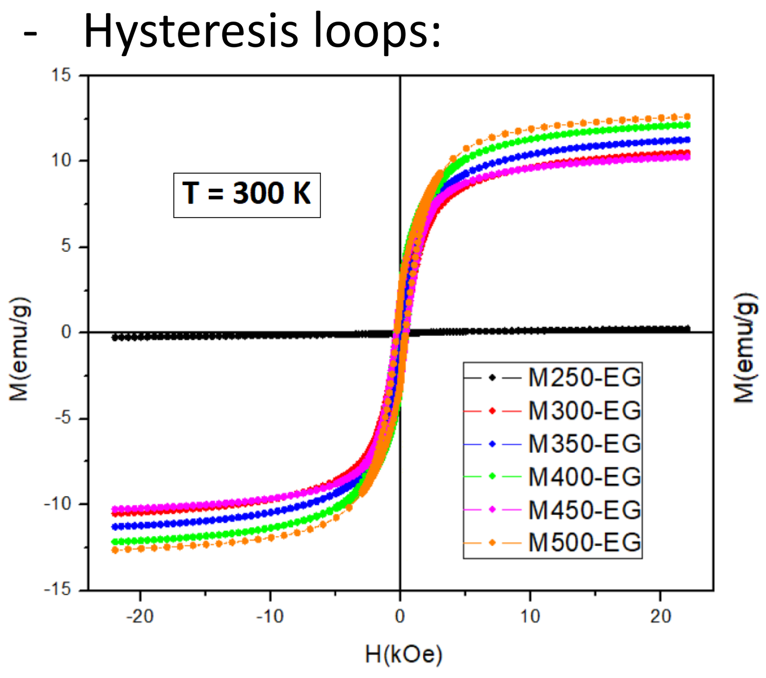

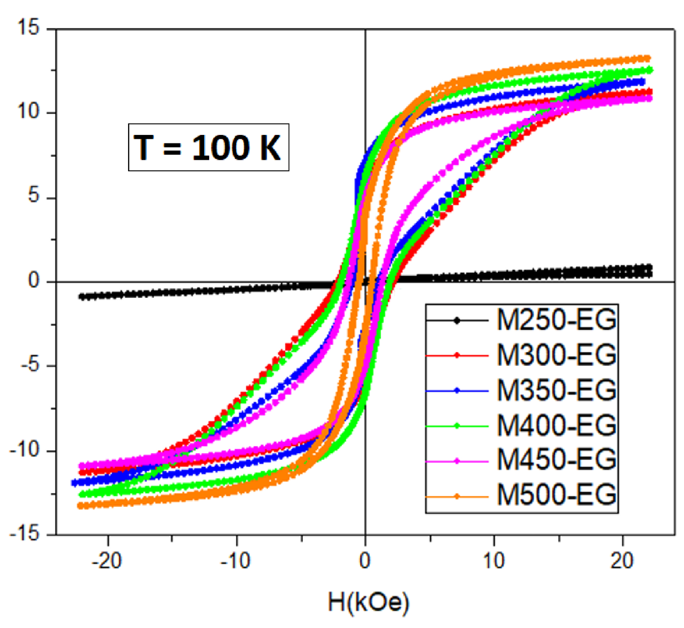

Superparamagnetic behaviour at room temperature.
⇓ Hysteresis loop's measure temperature ⇒ ⇑ Coercive field.

- ZFC-FC curves:

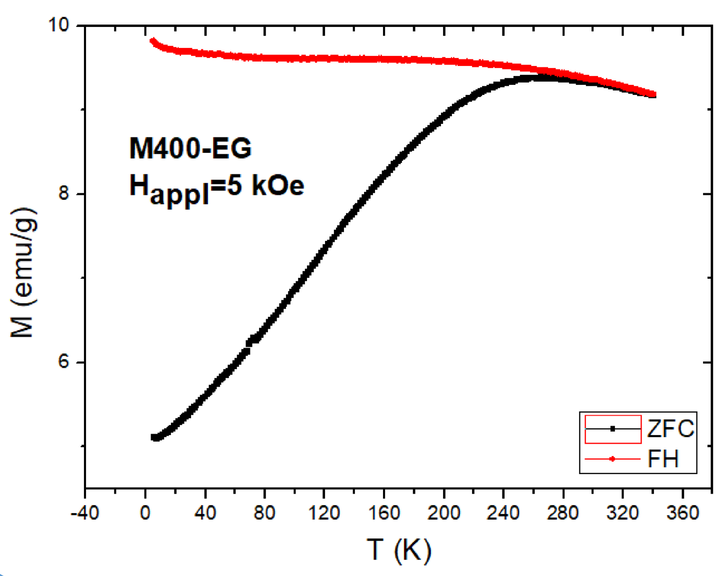

Distribution of blocking temperatures characteristic of samples with broad NPs sizes distributions.

CONCLUSIONS

- Cobalt ferrite samples were synthesized on carbon matrix following pyrolysis procedures at temperatures of 250, 300, 350, 400, 450 and 500 °C.
- Activated carbon grains have quasi-spherical morphology and sizes between 5 and 60 μm.
- The Fe:Co ratio is stoichiometry, i.e. corresponds to $CoFe_2O_4$.
- The samples present metal percentages around 20%.
- Increasing the synthesis temperature induces the reduction of the ferrite quantity and the appearance of metallic Fe and Co.
- The mean NP dimension increases as the temperature of synthesis raises.
- NPs exhibit superparamagnetic behaviour at room temperature. The coercive field increases with decreasing temperature at which the hysteresis loop is measured.
- The samples present a distribution of blocking temperatures characteristic of samples with broad NPs sizes distributions, that decreases as the applied field increases.

Acknowledgements: The authors thank Servicios Científico-Técnicos (SCTs) at the University of Oviedo for the experimental equipment provided. Also, financial support from MCIU19-RTI2018-094683-B-C52, FC-GRUPIN-IDI/2018/000185, PAPI-18-GR2010-0020 and PAPI-18-EMERG8/2018/00061008 is acknowledged.